Topics in Current Chemistry 356

Mario Barbatti
Antonio Carlos Borin
Susanne Ullrich *Editors*

Photoinduced Phenomena in Nucleic Acids II

DNA Fragments and Phenomenological Aspects

Springer

356
Topics in Current Chemistry

Aims and Scope

The series Topics in Current Chemistry presents critical reviews of the present and future trends in modern chemical research. The scope of coverage includes all areas of chemical science including the interfaces with related disciplines such as biology, medicine and materials science.

The goal of each thematic volume is to give the non-specialist reader, whether at the university or in industry, a comprehensive overview of an area where new insights are emerging that are of interest to larger scientific audience.

Thus each review within the volume critically surveys one aspect of that topic and places it within the context of the volume as a whole. The most significant developments of the last 5 to 10 years should be presented. A description of the laboratory procedures involved is often useful to the reader. The coverage should not be exhaustive in data, but should rather be conceptual, concentrating on the methodological thinking that will allow the non-specialist reader to understand the information presented.

Discussion of possible future research directions in the area is welcome.

Review articles for the individual volumes are invited by the volume editors.

Readership: research chemists at universities or in industry, graduate students.

More information about this series at
http://www.springer.com/series/128

Mario Barbatti • Antonio Carlos Borin •
Susanne Ullrich
Editors

Photoinduced Phenomena in Nucleic Acids II

DNA Fragments and Phenomenological Aspects

With contributions by

A.J.A. Aquino · P.P. Bera · J. Cadet · P. Changenet-Barret · J. Chen · T. Douki · A. Grand · D.-P. Häder · Y. Hua · K. Kawai · B. Kohler · Z. Lan · T.J. Lee · H. Lischka · Y. Lu · T. Majima · D. Markovitsi · C.K. Materese · D. Nachtigallová · M. Nuevo · F. Plasser · Richa · S.A. Sandford · R.P. Sinha · W. Thiel · Y. Zhang

Springer

Editors
Mario Barbatti
Max-Planck-Institut für Kohlenforschung
Mülheim an der Ruhr
Germany

Antonio Carlos Borin
Institute of Chemistry
University of São Paulo
São Paulo
Brazil

Susanne Ullrich
Department of Physics and Astronomy
The University of Georgia
Athens
Georgia, USA

ISSN 0340-1022 ISSN 1436-5049 (electronic)
ISBN 978-3-319-13271-6 ISBN 978-3-319-13272-3 (eBook)
DOI 10.1007/978-3-319-13272-3
Springer Cham Heidelberg New York Dordrecht London

Library of Congress Control Number: 2014957859

Printed on acid-free paper

Springer is part of Springer Science+Business Media (www.springer.com)

Preface

Photoinduced processes in nucleic acids are phenomena of fundamental importance for our biosphere. Ultraviolet solar radiation has been a continuous factor of evolutionary pressure since early biotic ages by triggering mutations, cell death, and carcinogenesis. The study of how UV radiation impacts nucleic acids has a long history, which parallels the evolution of our understanding of genetics from the beginning of the twentieth century. It has, however, been mainly in the last decade that major knowledge gaps have been filled in the field. This has been achieved thanks to the development of advanced spectroscopic techniques and computational models, which have allowed real-time observation and simulation of the evolution of electronic excitations caused by radiation.

This book embraces a broad range of topics in nucleic-acid research. It brings together leading specialists from different subfields, providing a deep overview of the current state of knowledge, including recent achievements, open problems, and comprehensive lists of references. While each chapter was developed as a thematic and self-contained text, a certain degree of overlap was maintained to interrelate individual contributions. Consequently, the chapters can be read in any order and the reader can profit from the diverse perspectives on the same subjects originating from different authors.

In the two volumes, theoretical, computational, experimental, and instrumental aspects are discussed. It is hoped, therefore, that they are of value to a wide spectrum of readers – students, scientists, and technologists. The first volume focuses (but not exclusively) on the spectroscopy and dynamics of photoexcited nucleobases and their analogues in different environments. The emphasis of the second volume is on larger fragments, from base pairs to duplexes, and on phenomenological aspects, including physiological effects, prebiotic chemistry, and charge-transport phenomena.

Editing a book of such a broad scope, involving so many different topics, sometimes felt an overwhelming experience. It began with the difficult task of selecting, among a large community composed of highly-active and successful researchers, those who would be invited to contribute a chapter. Although we had

to make some hard choices, we think that we have achieved a balanced result, with an approximately equal share of experimentalists and theorists from more than ten countries in Europe, North and South America, and Asia. Considering that the invited contributors are leaders in their fields, they were free to organize their chapters, taking only into account the broad subject area provided by us.

We are glad that, exactly as planned, the book turned out to be a very well integrated collection of independent chapters, where the focus is on reviews of particular topics rather than on the research of individual groups or the presentation of new data. Naturally, we must acknowledge all the authors for their efforts and insightful contributions. We are also grateful to all the reviewers of individual chapters, whose constructive critique was invaluable to the success of this text.

We thank Massimo Olivucci, who invited us to edit these volumes for Topics in Current Chemistry. We also express our gratitude to Arun Manoj Jayaraman from Springer, who patiently coordinated the publishing project.

For us, editing this book was a challenging task, constantly bringing us face-to-face with phenomena outside our area of expertise. We can only hope that the readers enjoy the same informative and enlightening experience.

Mario Barbatti
Antonio Carlos Borin
Susanne Ullrich

Contents

Top Curr Chem (2015) 356: 1–38
DOI: 10.1007/128_2013_517

Published online: 19 February 2014

Electronic Excitation Processes in Single-Strand and Double-Strand DNA: A Computational Approach

Felix Plasser, Adélia J.A. Aquino, Hans Lischka, and Dana Nachtigallová

Abstract Absorption of UV light by nucleic acids can lead to damaging photoreactions, which may ultimately lead to mutations of the genetic code. The complexity of the photodynamical behavior of nucleobases in the DNA double-helix provides a great challenge to both experimental and computational chemists studying these processes. Starting from the initially excited states, the main question regards the understanding of the subsequent relaxation processes, which can either utilize monomer-like deactivation pathways or lead to excitonic or charge transfer species with new relaxation dynamics. After a review of photophysical processes in single nucleobases we outline the theoretical background relevant for interacting chromophores and assess a large variety of computational approaches relevant for the understanding of the nature and dynamics of excited states of DNA. The discussion continues with the analysis of calculations on excitonic and charge transfer states followed by the presentation of the dynamics of excited-state processes in DNA. The review is concluded by topics on proton transfer in DNA and photochemical dimer formation of nucleobases.

F. Plasser
Interdisciplinary Center for Scientific Computing, Ruprecht-Karls-University, Im Neuenheimer Feld 368, 69120, Heidelberg, Germany

A.J.A. Aquino and H. Lischka (✉)
Department of Chemistry and Biochemistry, Texas Tech University, Lubbock, TX 79409-1061, USA

Institute for Theoretical Chemistry, University of Vienna, Währingerstr. 17, 1090 Vienna, Austria
e-mail: hans.lischka@univie.ac.at

D. Nachtigallová
Institute of Organic Chemistry and Biochemistry AS CR, Flemingovo nam. 2, Prague, Czech Republic
e-mail: dana.nachtigallova@uochb.cas.cz

Keywords Ab initio calculations · Charge transfer excited states · Excitonic states · Interaction of excited state nucleic acid bases · Photodynamics · UV absorption spectra

Contents

1 Introduction

Nucleic acids play a central role in biology as carriers of the genetic code. All nucleic acid bases are strongly absorbing species in the ultraviolet (UV) region and their excitation can result in production of harmful photoproducts leading to, e.g., mutations [1–3]. A well known example is the dimerization of pyrimidine type bases, i.e., formation of thymine (T<>T), cytosine (C<>C), and thymine–cytosine (C<>T) dimers [4–7]. This process is formally analogous to the dimerization of two ethylene molecules to cyclobutane, a textbook example of a reaction which is prohibited in the ground state but allowed in the excited state according to the Woodward–Hoffmann rules. Fortunately, the formation of such photoproducts occurs very rarely. The nucleic acid bases themselves show a high degree of photostability (see, e.g., [8–11]). The decay mechanisms of isolated nucleobases have been investigated by ultrafast time resolved spectroscopic techniques [11–15] and extended computational methods [16–28]. Most of the general features and many details are largely understood by now. It is well established [11, 29] that ultrafast (on the time scale of a few picoseconds) internal conversion is responsible for the relaxation of the system into the ground state without changing its chemical identity. This process occurs at structures near the crossing seam of excited-state and ground-state potential energy surfaces (PES) under conditions of a strong

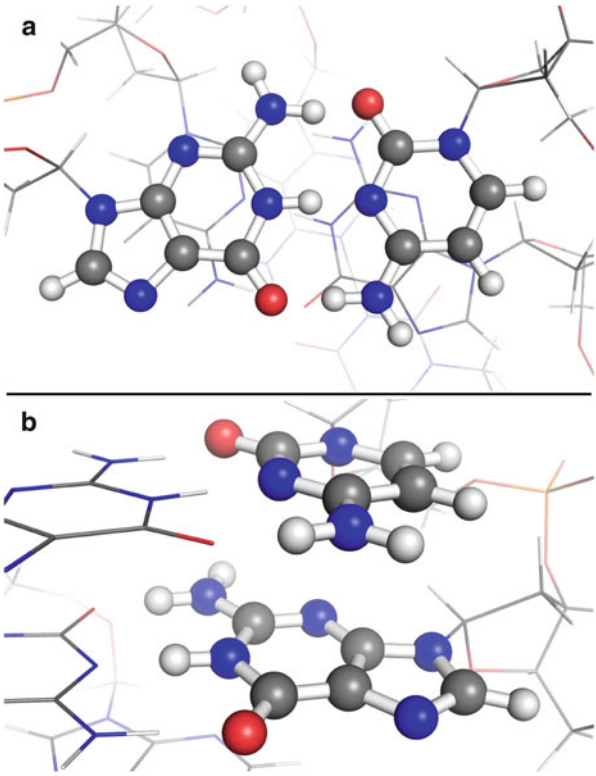

Fig. 1 Structure of Gua and Cyt allowing for inter-strand hydrogen bonding (**a**) and intra-strand stacking (**b**) interactions in the DNA double-helix

nonadiabatic coupling. Due to this mechanism nucleobases are photostable which in turn protects them against radiative damage.

The situation becomes much more complex when a nucleobase is interacting with other bases within the nucleic acid polymer. The structure of nucleic acids allows for interaction within the same strand via stacking and, in the case of double-stranded DNA, also for interactions between two strands via hydrogen bonding as illustrated in Fig. 1. These interactions are further affected by the conformation of DNA (e.g., differences can be expected in B-DNA and RNA-like A-DNA conformations) and the flexibility of the sugar–phosphate backbone which changes the mutual orientation of adjacent nucleobases and thus their interaction. This complex picture of photodynamics of nucleic acids provides a great challenge to both experimental and computational chemists.

In the present contribution the current knowledge of the photodynamics of isolated nucleobases and the survey of experimental observations and their interpretations will be provided in Sect. 1. Only a brief discussion will be given since the scope of the paper is laid on the computational approaches to the UV absorption characteristics and photodynamics of nucleic acids. The theoretical concept of electronic coupling is introduced in Sect. 2. Computational methods and their reliability for the description of excited states in DNA are discussed in Sect. 3. Section 4 discusses the interpretation of the experimentally observed absorption

Scheme 1 The numbering scheme of nucleic acid bases

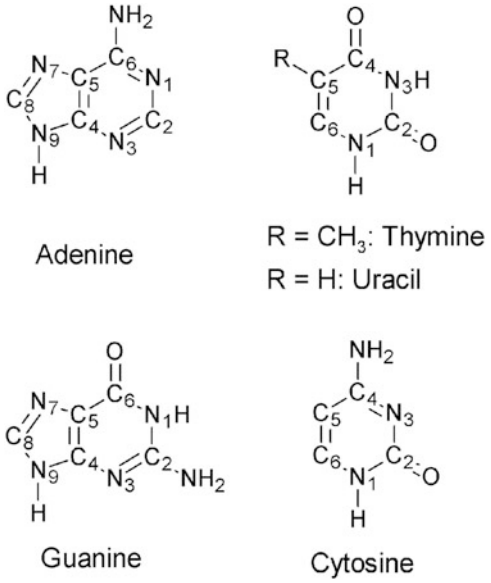

spectra of DNA and its model systems. In Sect. 5 state-of-the-art computational studies on excited states processes, including the effect of DNA environment on the photophysics of nucleobases, excimer formation, excitation energy and proton transfer, and photochemical reactions are reported. The discussion on the latter is limited to formation of cyclobutane pyrimidine dimers as the most studied process.

1.1 Ultrafast Deactivation of Single Nucleobases

The understanding of the photodeactivation mechanism of individual nucleobases is important for analysis of the more complex deactivation patterns of nucleobases embedded in DNA or RNA. It is interesting to note that all five nucleobases (adenine, guanine, thymine, cytosine, and uracil; Scheme 1) show the property of photostability due to their ultrafast, radiationless deactivation to the ground state within a few picoseconds [8, 10]. This decay provides the possibility for the nucleobase to transfer quickly the harmful excess energy accumulated by photoabsorption of UV light into heat, which further on can be dissipated to the environment. These ultrafast processes observed for all five naturally occurring nucleobases contrast with the much longer lifetimes for nucleobase analogues not found in DNA or RNA [10, 30], indicating an evolutionary pressure in early biotic ages.

The photodeactivation of nucleobases in the gas phase has been studied in detail by means of ultrafast time-resolved spectroscopy [8, 10, 11, 17]. These investigations provide the main source for relaxation times which are obtained by fitting the measured deactivation curves in terms of pump-probe delay times. Information on

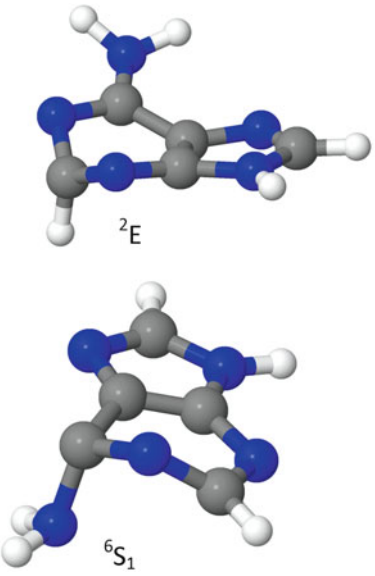

Fig. 2 Adenine structures at the conical intersections ^{2}E and ^{6}S$_1$

the structural changes responsible for the photostability are not or barely available from these data. The ultrafast and radiationless character of these processes points to internal conversion governed by conical intersections located on the crossing seam between different energy surfaces. This hypothesis has been substantiated in great detail by many theoretical investigations. Starting from the Franck–Condon (FC) region, deactivation paths have been computed leading to characteristic crossing points which are usually chosen as the minima on the intersection seam. One of the nucleobases studied extensively is adenine for which a large variety of types of intersections has been found [16, 22, 23, 31–34]. The two energetically lowest S_0–S_1 intersections show puckering at the C_2 atom and out-of-plane distortion of the NH_2 group, respectively (Fig. 2). The former structure corresponds to an S_0/π–π^* intersection characterized as envelope ^{2}E and the latter to an S_0/n–π^* intersection with a skew boat $^6S_1$ puckering following the notation of ring puckering coordinates introduced by Cremer and Pople [35]. Starting at the Franck–Condon structure, pathways connecting the bright L_a state with these intersections are supposed to have no or at most very small barriers so that both are good candidates for the explanation of the ultrafast decay of adenine. For a more detailed discussion of the outcomes of different dynamics simulations see below. In the case of the other purine base guanine, two ethylenic-type intersections (I and II) with strong out-of-plane distortion of the NH_2 group and another intersection type (denoted oop-O) with puckering at C_6 and concomitant out-of-plane motion of the oxygen atom are found [20, 28, 36–39]. The bright π–π^* state is the lowest singlet excited state in the Franck–Condon region and is connected from there via a barrierless path with the ethylenic intersections [28].

In comparison to the purine bases, the pyrimidine bases are characterized by a more complex system of conical intersections and reaction paths. In the case of cytosine, three major conical intersections have been determined. The first [25] is characterized as semi-planar. It occurs in a region of mixing of the n_O–π*, π–π* and closed shell states, which leads to a triple degeneracy as reported in [40, 41]. The second intersection leads to a puckering at N_3 connected with an out-of-plane distortion of the amino group. The third intersection involves puckering at C_6 (for more details see [42–44]). Reaction paths computed in [44] connecting the Franck–Condon region with the above-mentioned conical intersections show that these intersections are all energetically accessible and display similar qualitative features so that no a priori decision can be made concerning specific photodynamical reaction mechanisms.

Concerning theoretical investigations on the remaining nucleobases (see, e.g., [17, 21, 24, 27]), it should be mentioned at this point that not only the ring puckering motions are of relevance for the explanation of the ultrafast decay of the nucleobases but also that NH dissociation is of interest since it has been shown that this process leads to conical intersections [32] even though they are supposed to be accessible only by higher excitation energies beyond the first absorption band.

The above discussion concentrates on the singlet excited states. It should be noted that several studies discussing the triplet excited states appeared in the literature (see, e.g., [45–50]).

The large manifold of conical intersections and their reaction paths give a good picture of the different deactivation possibilities but makes conclusive predictions about the real deactivation mechanisms difficult if not impossible. Dynamics simulations have been performed to find the actual reaction paths and to obtain information about the characteristic times connected with the different processes. Owing to the strongly coupled motion involving many internal degrees of freedom, Tully surface hopping [51] and ab initio multiple spawning (AIMS) [52] appear to be methods of choice since all internal degrees of freedom are directly included in these dynamics simulations (see also [53] for a general discussion on the options and outlook of photodynamical simulations). The main bottleneck in these calculations is the necessity of performing a full quantum chemical calculation in each time step using extended methods able to describe several electronic states and their nonadiabatic coupling. Under these circumstances, mostly complete active space self-consistent field (CASSCF) or multireference configuration interaction with single excitations (MRCIS) approaches have been used [17, 19, 33, 38, 44, 54–56]. An overview of respective simulations of the photodynamics of nucleobases is available, e.g., in [18]. As an interesting alternative to the computationally expensive ab initio approaches, semi-empirical multireference methods based on the orthogonalization model 2 Hamiltonian (OM2) [34, 57, 58] and the fractional orbital occupation/AM1 model [59] have also been applied extensively in surface hopping dynamics. The performance of TDDFT using a larger variety of functionals has been investigated [60], and time-dependent tight binding density functional theory (TD-DFTB) [61] and DFTB mean field simulations [62] have been used as well. The restricted open shell Kohn–Sham (ROKS) method within the

framework of Car–Parinello dynamics [63] and quantum dynamical simulations have also been performed [64].

From this multitude of widely differing approaches, we wanted to discuss the photodynamics of adenine and cytosine in more detail. Surface hopping dynamics simulations using an MRCIS approach [33] have been performed for adenine, starting the dynamics in the L_a π–π*(S_3) state. Already after 25 fs this state is completely depopulated and practically all trajectories have arrived in the S_1 state after ~60 fs. By fitting an exponential function containing two decay constant, values of 22 and 538 fs were found, in good agreement with those of <50 and 750 fs measured by Ullrich et al. [9]. The analysis of the trajectories showed that almost exclusively the ^{2}E with puckering at C_2 was accessed. In contrast, OM2 photodynamics [34] shows a strong predominance of the NH_2 out-of-plane conical intersection ($^1S_6$). In a recent study [60] the energy profiles along the reaction coordinates leading to both mentioned intersections were computed using several methods (OM2/MRCI, MRCIS, complete active space perturbation theory to second order (CASPT2), approximate coupled cluster singles- and doubles method (CC2), and a variety of different TDDFT methods). These profiles show a preference toward the ^{2}E intersection in the case of MRCIS, CASPT2, and CC2 whereas the opposite trend is found for OM2. It was further shown that the MRCIS calculations using one lone pair (*n*) orbital in the active space were subject to a certain bias toward ^{2}E which was partially lifted by including two *n* orbitals into the active space [65]. Thus, according to current understanding, the real dynamics should still be dominated by the ^{2}E pathway but significant participation of the $^1S_6$ should be expected as well. The investigations in [60] also show a severe failure of the TDDFT and TD-DFTB approaches since an insufficient number of hoppings to the ground state were observed. Inclusion of range-separated functionals did not improve the situation significantly. For more details see [60].

In the case of cytosine, a more complex dynamics than that described for adenine is observed [18]. All three intersections described above for cytosine participate in the dynamics. Initially, cytosine relaxes along the π–π* pathway to a region of strong mixture of π–π*, *n*–π*, and closed shell character, where in a first approach about 16% of trajectories switch to the ground state with a time constant of 13 fs. It should be noted that this semi-instantaneous deactivation of cytosine through the semi-planar intersection was also found in AIMS simulations [19]. In the remaining 84% of cases, cytosine quickly relaxes to the *n*–π* state from where it either can deactivate via the semi-planar intersection to the ground state or can overcome the barrier to the π–π* state and subsequently switch to the ground state. In contrast, CASSCF(2,2) AIMS [19] and OM2 [57] simulations do not show any significant deactivation in this region. The results of surface hopping dynamics at CASSCF (12,9) level [66] are similar to those found in [18] and show predominance of the semi-planar conical intersection. Due to this complex set of events it has to be expected that even rather subtle changes in the relative positions of the energy surfaces can lead to significant modifications of the photodynamical mechanisms and all discussed results have to be regarded with care. It can be expected that

further quantitative changes will occur when more sophisticated quantum chemical methods will become available for photodynamical simulations.

Notable changes in the dynamics also have to be expected when it is performed in aqueous solution. Several computations were performed to elucidate the effect of solvent on the excited states of uracil [49, 67–78], thymine [68, 76, 77, 79, 80], guanine [81–84], cytosine [75, 77, 85, 86], and adenine and its model systems [87–89]. The aqueous solvent was shown to modify the photodynamics of nucleobases by changing relative positions of excited states of different characters in the FC region, changing the heights of reaction barriers on the paths leading to conical intersections and relative energies of excited state minima. The consequences such as a blue shift of the n–π^* states of uracil (see, e.g., [68, 70, 71, 73, 76], stabilization of a polar $S_2(\pi$–$\pi^*)$ [32] and π–σ^* [87] states of adenine, and geometry changes of excited state minima of guanine [82] on photodynamics were discussed. Dynamics studies performed on adenine [89] have shown that the out-of-plane motion of the amino group is more pronounced in water, which can explain the faster decay of the S_1 state compared to the gas phase. The overall relaxation mechanism was however the same as observed in the gas phase. This finding is in contrast to guanine [84] where the pathway via a conical intersection with out-of-plane distortion of the carbonyl oxygen becomes dominant in water solvent.

It should be noted that in extension of the above-described dynamics simulations restricted to the singlet manifold, first surface hopping dynamics simulations have been performed for cytosine combining nonadiabatic and spin-orbit effects [90, 91].

At first sight it seems that each of the nucleobases possesses its own characteristics. A general picture emerging from the dynamics simulations [18] can be given, however, by the observation that the purine bases adenine and guanine have quite a simple deactivation pattern following basically one excited state to the intersection with the ground state whereas, in the case of the pyrimidine bases cytosine, thymine, and uracil, a significantly more complex picture appears with the participation of several excited states and a significantly more complex deactivation pattern.

1.2 Survey of Experimental Studies of Interacting Nucleobases

The question of the nature of excited states of DNA was first addressed in the 1960s. Based on theoretical models, Tinoco et al. [92] invoked a delocalized character of excited states of nucleic acids in the FC region to explain the hypochromism observed in absorption spectra of polynucleotides. In contrast to this prediction, Eisinger et al. [93] proposed that the UV photon is absorbed by a single base. This prediction was made on the basis of comparison of absorption spectra of DNA with corresponding pyrimidine and purine bases. The DNA absorption spectra closely

resembled the sum of the monomer spectra and showed theoretically predicted spectral shifts and splitting of the UV band around 260 nm. A discussion on this issue based on molecular dynamics simulations and quantum chemical calculations will be given later in this chapter.

Following the prediction of the locally excited states red-shifted and broadened fluorescence spectra of di- and polynucleotides were attributed to excimers formed from these bases [5]. More pronounced occurrences of excimers observed at lower temperatures are explained by a higher degree of stacking as compared to more disordered structures at higher temperatures. Increased charge transfer (CT) contributions in these excimers were also predicted by these authors [94, 95].

In contrast to the above-discussed local character of absorption, the excitonic character in absorption spectra of di- and polynucleotides of adenine and cytosine was predicted by Kononov et al. [7], with the exciton limited to two bases. The excitonic features were, however, not observed in absorption spectra of guanine and thymine.

The experiments performed during the last two decades utilizing femtosecond time-resolved spectroscopy stimulated lively discussion on the nature of excited states of DNA. In addition to the ultrafast components decaying on the order of picoseconds, transients with lifetimes of 10–100 ps and even nanosecond time scale were observed for single- and double-stranded oligonucleotides [14, 96–103]. The existence of large decay times occurring for single-stranded oligonucleotides [98] demonstrates that stacking interactions are of primary importance for the explanation of differences in the complex decay dynamics in DNA as opposed to that observed for individual nucleic acid bases.

The interpretation of the ultrafast component observed in the experiments mentioned in the previous paragraph was based on the existence of bases undergoing monomer-like photo decay in the disordered parts of the oligo- and polymers. Different hypotheses were used to explain the slow-decay component: (1) the excitation in the FC region is localized on a single base and the interaction with an adjacent base leads to the formation of excimers [98, 101] several picoseconds after the excitation and (2) the excitation is already delocalized during the initial FC excitation, resulting in the formation of excitonic states [14, 96, 104–106]. In the latter interpretation partial emission from localized bases was suggested as well [105, 107]. Beyond the above question of the delocalization, the importance of charge transfer states is being discussed as an important issue (see, e.g., [108–113]).

A special challenge lies in interpreting and reconciling the large number of different decay times reported in the different experiments (see, e.g., [97–99, 101, 102, 114–121]). The results depend not only on the general character of the experimental technique (i.e., time-dependent absorption or emission spectroscopy) but also on the details of the preparation of the DNA samples and the base sequence, both playing an important role [118, 122]. In light of all these challenges with respect to interpreting experimental results, computational investigations play an important role in providing complementary information, shedding new light on the complex photodynamical behavior of DNA.

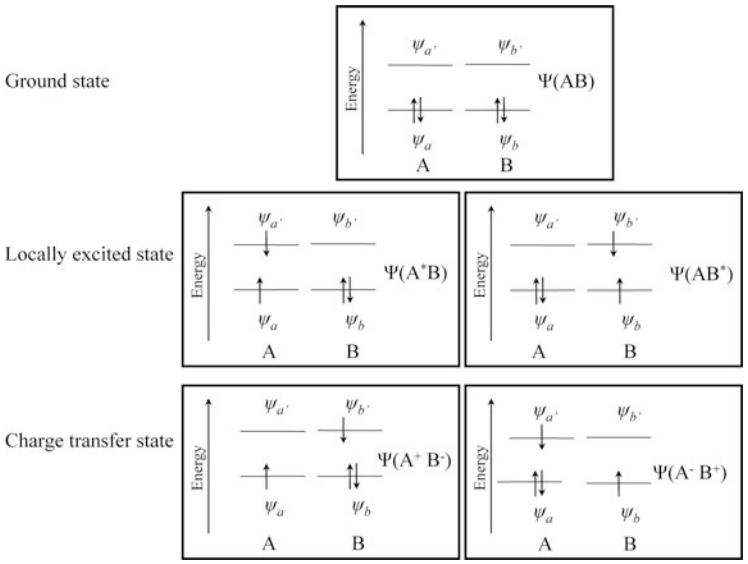

Scheme 2 Schematic illustration of the electronic interactions of identical chromophores *A* and *B* in terms of localized and charge transfer excited states

The extent of exciton delocalization is another issue discussed intensively. For example, Kadhane et al. suggested that excitons are delocalized over no more than two bases [123] and Bucharov et al. [14] suggested delocalization extending over three bases. However, delocalization over six and more bases was also considered [124]. Extended work concerning this issue is based mainly on dynamics simulations in connection with excitonic models or quantum chemical calculations, and will be discussed later in the chapter.

According to current evidence, inter-strand hydrogen bonding may also play an important role and add to the complexity of the photodynamical behavior of nucleic acids. A unique excited state behavior of Watson–Crick (WC) base pairs was shown in a resonant multi-photon ionization experiment performed in the gas phase [125]. Faster fluorescence decay of base pairs compared to isolated bases was also observed by other authors as shown in [98, 126–128]. Furthermore, interplay between intra-strand CT and inter-strand proton transfer has been suggested [128].

2 Description of Electronic Coupling

Before discussing the character of excited state interactions between nucleobases, the underlying theory will be briefly discussed. Scheme 2 describes the simplest situation of the electronic interactions of two identical chromophores (*A* and *B*) in terms of locally and charge transfer excited states. At infinite separation the locally

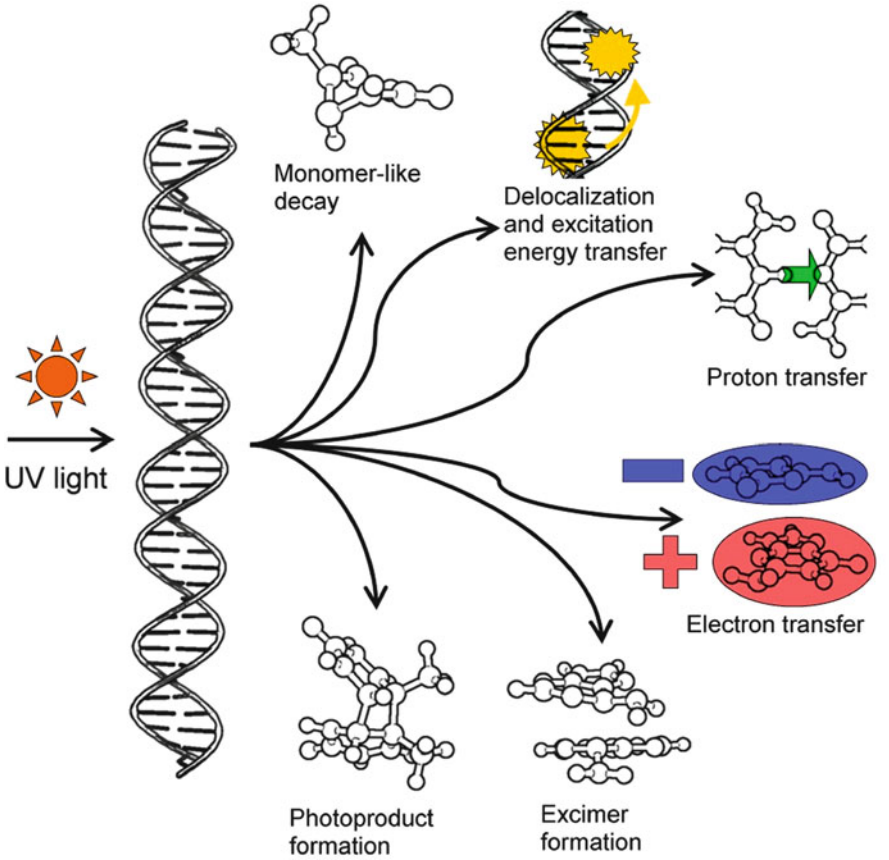

Fig. 3 Schematic representation of possible processes resulting from the interactions of nucleobases in electronically excited states

excited states (described by $\Psi(A^*B)$ and $\Psi(AB^*)$) are degenerate. At finite separation, in an adiabatic representation the degeneracy is removed and the energy splitting may be directly used to measure the excited state interaction (electronic coupling). The situation is similar for the charge transfer states described by $\Psi(A^{\cdot -}B^{\cdot +})$ and $\Psi(A^{\cdot +}B^{\cdot -})$ [129–131]. For non-symmetrical arrangements this approach is not so straightforward. Inside the polymer the environment of two bases is strongly non-symmetrical due to thermal fluctuations. In such a case the splitting will also reflect the difference in the environment of each chromophore, which causes a shift of the orbital and excitation energies that are not directly related to the electronic coupling. In the case of a stacked nucleobase pair with nucleobases mutually orientated as in a B-DNA structure, the changes in excitation energies observed during dimerization caused by non-symmetric effects are an order of magnitude larger than those caused by the 'pure' electronic interaction [132, 133].

Interaction between chromophores in electronically excited states can promote one of the following processes (Fig. 3):

1. Delocalization of the excited states which results in exciton formation.
2. Electronic excitation energy transfer.
3. Formation of a strongly interacting complex – an excimer – which results from the orbital overlap.
4. Formation of a new chemical species – a photochemical product.
5. Inter- and/or intra-strand electron or proton transfer.
6. Localization of the electronic excitation on a single base followed by a monomer-like relaxation.

The interactions during electronic excitations are governed by two main contributions: (1) Coulombic interactions which are often approximated by the interactions of transition dipole moments and higher multipole interaction terms and (2) short-range interactions, which depend on the orbital overlap between two chromophores [129–131].

While the former interactions operate over larger through-space separation R, and depend asymptotically on R^{-3}, the latter attenuate exponentially with R being unimportant for the chromophore separation larger than approximately 6 Å. Since these interactions depend on the orbital overlap they are greatly dependent on the mutual orientation of the chromophores. Thus, significantly larger short-range interactions were found for the nucleobases in the B-DNA-like orientation with almost parallel stacking as compared to A-DNA-like orientation with disordered stacking [132]. The character of the excited states also largely influences the resulting electronic interactions. For example, these interactions between the states of (n–π^*) character with negligible transition dipole moments and small orbital overlaps are much smaller in relation to states of (π–π^*) character which possess a larger transition dipole moment and a larger overlap of interacting orbitals [132].

2.1 Excimers/Exciplexes and Excitons

As already mentioned, the photoabsorption of two (or more) nucleobases within the nucleic acid structure can result in *excimers* or *exciplexes* being formed by two identical or different nucleobases, respectively. It should be emphasized that the excimers/exciplexes are not necessarily formed from one molecule in the ground state and the second from the excited state. They can be formed from different initial states, including excitons.

The wavefunction has the following general form [129, 134, 135]:

$$\mathbf{\Psi}(\text{Exciplex}) = c_1\Psi(A^*B) + c_2\Psi(AB^*) + c_3\Psi(A^{\cdot-}B^{\cdot+}) + c_4\Psi(A^{\cdot+}B^{\cdot-}), \qquad (1)$$

where $A = B$, $c_1 = c_2$, and $c_3 = c_4$ for excimers.

The first two terms correspond to locally excited states and their interaction results in exciton states (see below). At intermolecular separations below 5–6 Å, orbital interactions come into play [129, 134] mediating a mixing of the locally

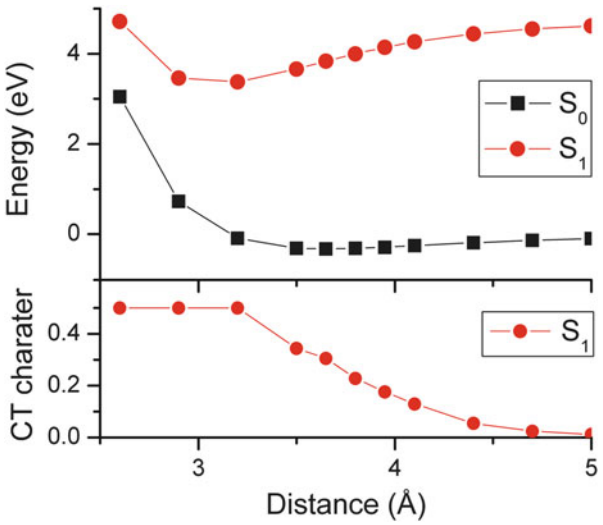

Fig. 4 Excited state energies of the S_0 and S_1 states (*top*) and charge transfer character of the S_1 state (*bottom*) of a face-to-face stacked naphthalene dimer (see [138] for details)

excited states with the charge transfer or radical-ion-pair states, described by the third and fourth terms [135]. Stabilization of the exciplex can not only occur through excitonic coupling and Coulombic interaction, which are directly derived from the excitonic and CT contributions. It has been pointed out that with decreasing separation distance a new type of strong interaction may come into play that can be identified as a quasi-bond in the geminate radical ion pair [136]. Such quasi-bonds may go along with strong structural distortions, and experimental evidence shows that electronic and steric effects play an important role [137].

In Fig. 4, excimer formation in the face-to-face stacked naphthalene dimer computed at the ab initio algebraic diagrammatic construction to second order (ADC(2)) level is illustrated as a representative example (see [138] for more details). While the ground state potential is only weakly attractive with a shallow minimum around 3.65 Å intermolecular separation, the excited state is strongly bound with a minimum at 3.2 Å and stabilization energy of 1.38 eV with respect to infinite separation. Aside from the energy, a measure for charge transfer, representing the weight of the c_3 and c_4 coefficients in the equation (1), is shown in Fig. 4 (bottom). At separations >5.0 Å the CT value is approximately zero, showing that the excited state corresponds to a pure Frenkel exciton. When the molecules are moved closer together, orbital interactions are important (cf. [129]) and the locally excited states mix with the CT states, giving a gradual increase of the CT character. At the excimer minimum the CT character reaches 50%, showing that the excited state is now an even mixture between Frenkel excitonic and charge resonance contributions. This state is accessed by a single transition between delocalized orbitals, which corresponds to the situation of a coherent homogeneous state extended over the whole complex (cf. [138, 139]).

In extended quasi-periodic systems excited states can be delocalized over a number of chromophores. Such states are usually called *excitons*. In this context it is important to distinguish whether the exciton can be described as a linear combination of locally excited states, forming a Frenkel exciton, or whether CT configurations also play a role.

The first case can be understood in terms of Frenkel exciton theory [140, 141]. In this framework a model Hamiltonian $\boldsymbol{H}$ is written as the sum of isolated chromophores H_a and a coupling term V_ab:

$$\boldsymbol{H} = \sum\nolimits_\mathrm{a} H_\mathrm{a} + \sum\nolimits_\mathrm{a} \sum\nolimits_{\mathrm{b}>\mathrm{a}} V_\mathrm{ab}. \tag{2}$$

The singly excited states are described by the term

$$\boldsymbol{\Phi}^i{}_\mathrm{a} = (-1)^\mathrm{a} \Phi^i{}_\mathrm{a} \prod\nolimits_{\mathrm{a}\neq\mathrm{b}} \Phi_\mathrm{b}, \tag{3}$$

where $\boldsymbol{\Phi}^i{}_\mathrm{a}$ corresponds to the wavefunction of the state where chromophore a is in its excited state, while others are in their-ground state. The wavefunction of the excitonic state is then written as a linear combination of the wavefunction with locally excited states:

$$\boldsymbol{\Psi}_\mathrm{k}(\mathrm{Exciton}) = \sum\nolimits_\mathrm{a} c_\mathrm{ka} \boldsymbol{\Phi}^i{}_\mathrm{a}. \tag{4}$$

The diagonal and off-diagonal terms of the exciton matrix correspond to the excitation energies of the chromophore a and the exciton coupling terms, respectively. In this picture the excitation within some energy range populates a number of excited states delocalized over several nucleobases. Furthermore, if the initial electronic wavepacket is prepared as a non-stationary starting state, such a Hamiltonian automatically leads to excitation energy transfer. If in addition vibronic contributions are considered, the system can reach the lower part of the emission band via internal conversion (intra-band scattering) [118].

When there are strong orbital interactions between the different fragments, Frenkel exciton theory is no longer sufficient and it is necessary to include explicitly charge transfer configurations into the calculation. The theoretical treatment in such a case is more involved considering that a larger number of parameters are needed [142–144]. However, the advantage of such an approach is that charge separation processes can be easily modeled.

3 Assessment of Computational Methods

A wide range of computational methods have been applied to the description of electronically excited states of DNA fragments. In this section we review these approaches shortly. Unfortunately, no perfect method exists because of the difficulties in computing excited states and the relatively large sizes of the molecular

systems involved. In the following we will characterize the main features of the individual methods, including their strong and weak points, in an attempt to aid in assessing the substantial amount of available computational literature and to explain some of the discrepancies obtained in the different studies. This section will be strongly focused on DNA fragments; for a more general overview we refer the reader to [53].

3.1 Electronic Structure Methods

In this section, the different electronic structure methods that were used to describe DNA fragments will be considered. The main focus will be laid on the computation of excited states, and additionally methods for a phenomenological analysis of excited states and the computation of interaction potentials will be discussed. The main challenge relates to the large system sizes that have to be considered. Therefore, exciton models are a logical choice and were applied by several groups [142, 145–147]. In such an approach the excited states on the different molecules and their interactions are treated by a model Hamiltonian. This Hamiltonian can be easily extended to large system sizes, allowing the study of long range effects and potentially extended delocalization. However, a major challenge in such an approach is a proper parameterization. In particular the electronic couplings are of concern and a number of different methods for estimating them were used. Usually only the Coulombic contribution is computed while the direct orbital term is assumed to be smaller. The simplest approach for the estimation of this interaction is to consider only dipole–dipole interactions. This approximation was used, e.g., by Georghiou et al. [95] and Bittner [142] to estimate the efficiency of energy transfer along the DNA helix. This approach is suitable for systems in which the separation of the two chromophores is significantly greater than the dimension of the molecule. Its validity is however questionable in the case of nucleobases, because their molecular dimension is of the same order as the intermolecular distance of a neighboring nucleobase pair. Several approximations can help to overcome this difficulty using, e.g., the atomic-transition charge distribution [148, 149] or transition-density-cube models [144]. Comparison of the electronic couplings calculated using dipole–dipole and transition-density-cube approaches show that the former significantly overestimate the interactions at shorter distances [144]. Alternatively, the hybrid-multipole model which represents a combination of a truncated-multipole and the extended-dipole model [148, 150] was used to estimate Coulombic interactions [132]. Within this hybrid model, the multipole interaction up to R^{-5} is covered exactly; all terms with higher orders are considered if they arise from the multipole expansion of the extended dipole. The Coulomb part is usually the major component of the interaction potential, but a complete description also requires consideration of the direct orbital contributions. While it was shown from explicit quantum chemical calculations that at the ground state equilibrium geometry these terms only made a small contribution ($<$100 cm) [132], the involvement of such terms could in fact be identified through a mixing of

Frenkel excitonic and CT states [113]. An ad hoc addition of orbital overlap terms in a Frenkel exciton model is difficult as it has already been pointed out that a modest additional coupling of 100 cm had a dramatic effect by doubling the delocalization length [149]. A more extended treatment of orbital overlap and resulting charge separation is possible but requires a more involved formalism and a larger number of parameters [142, 151].

Considering the structural flexibility of DNA, an atomistic description is in many cases highly desirable. As one option semi-empirical methods were used [59, 152–155]. Due to the fact that they allow an efficient description of quite large systems they were used for extended dynamics simulations, providing interesting insights. However, similar to exciton models, semi-empirical methods rely on careful parameterization, a problem which can be avoided by the use of ab initio methods. Time-dependent density functional theory (TDDFT), which offers efficient excited state computations while relying on no or relatively few empirical parameters, has been used by a number of groups [109, 110, 156]. However, a major challenge for the application of TDDFT is the overstabilization of charge transfer states occurring when local functionals are used [157]. This problem can be overcome by using range separated hybrid functionals or functionals containing an overall high amount of Hartree–Fock exchange but in such cases the energy of CT states crucially depends on the parameters determining the admixture of Hartree–Fock exchange [110, 112]. For a comparison of the performance of different density functionals when applied to DNA stacks see, e.g., [158]. Finally, a large number of wavefunction-based ab initio calculations was performed using single- and multi-reference methods. In the first case, in particular efficient second order models like the approximate coupled cluster method CC2 [159] and the algebraic diagrammatic construction ADC (2) [160] in connection with the resolution of the identity approximation [161] were applied [112, 113, 132]. However, computationally more demanding models like the equation-of-motion coupled-cluster for excitation energies (EOM-EE-CC) with double excitations and even perturbative triple excitations have also been used [162–165]. In the case of strongly distorted structures and intersections between different states, multi-reference methods are needed to provide a reliable description. For this purpose the complete-active space self-consistent field (CASSCF) method, second order perturbation theory on this reference (CASPT2) [166], and multi-reference configuration interaction with single and double excitations (MR-CISD) [167] were performed [168]. While wavefunction-based methods offer the attractive property of systematic improvability toward the exact solution, they suffer from high computational demands. Unless massively parallel computer systems are available heavy truncations have to be carried out as far as the excitation level and/or the one electron basis set are concerned. For this purpose wavefunction-based ab initio methods also require careful testing and analysis before they can be successfully applied.

After the computation of excitation energies the next decisive task is to get a maximum of information for interpretive and phenomenological models. In quantum chemical calculations on DNA fragments this task may be quite challenging in many cases due to many interacting configurations, partially

delocalized orbitals, and the presence of hidden charge resonance contributions. Several approaches have been taken to analyze the states in more detail. One useful indicator is Mulliken populations, which aside from simply quantifying charge transfer, can also be used to estimate the contribution of a given monomer to an electronic transition [169]. Furthermore, energetic criteria based on model Hamiltonians have been applied to estimate electronic couplings and to identify charge resonance states [132, 162]. A different route may be taken by considering that the transition density matrix (TDM) between the ground and excited states can be used to represent the structure of the exciton as an electron-hole pair [138, 139, 170]. By partitioning the TDM into blocks corresponding to the different fragments, locally excited, excitonic, and CT contributions can be readily identified [138]. This approach was applied to absorption spectra [113] and excimer formation [168].

Another critical problem of great importance in the description of excimers is the computation of interaction potentials. In particular, dispersion, which is the main force determining stacking interactions, is difficult to describe. In the case of non-correlated methods, dispersion is completely absent, while standard DFT functionals usually strongly underestimate it. By contrast, MP2 is known to overbind complexes [171] and from the pure ab initio methods usually only CCSD(T) with basis set extrapolation is considered to provide reliable results [172]. To obtain accurate interaction potentials a number of empirical corrections have been suggested, where in particular Grimme's dispersion correction for DFT is widely used [173]. While parameterized methods can provide very good results for standard ground state geometries, it is not clear how they perform for excited states and in particular for strongly bound exciplex structures. It has been pointed out that standard force field parameters severely exaggerate repulsion at short intermolecular separations [172], which means that attempts to use such parameters in the description of excimers may result in an underestimation of binding energies and an overestimation of binding distances. Another problem arising from short intermolecular separations is increased basis set superposition error (BSSE). It was pointed out that the counterpoise (CP) correction for BSSE may strongly affect excimer structures and binding energies [23]. However, it was later also shown that the CP correction, when applied to smaller basis sets, may significantly overshoot, thereby incorrectly destabilizing the resulting exciplexes [168].

3.2 Environmental Models, Sampling, and Dynamics

Aside from a proper description of the electronic structure, new challenges arise with respect to the description of environmental effects, proper sampling to obtain statistically significant results, and the simulation of dynamical phenomena. For representing environmental effects, continuum models as well as atomistic

descriptions have been applied. The former type of approach offers a simple well-defined way to include the main effects of environmental polarization where even a differentiation between slow and fast polarization effects is easily achieved. In particular the polarizable continuum model (PCM) [174] has been applied, e.g., in [109, 112, 175]. There are only a few adjustable parameters, most importantly the dielectric constant and the time-regime (equilibrium or non-equilibrium). However, there is some arbitrariness when choosing an effective dielectric constant to represent the effect of the heterogeneous and anisotropic surroundings (i.e., the other DNA bases, the backbone, the surrounding water molecules and counterions). To overcome this problem, quantum mechanics/molecular mechanics (QM/MM) coupling schemes for an atomistic description of the environment have been widely used [110, 113, 176, 177]. Usually the effects of the environment are considered at the level of electrostatic embedding only, and electronic polarization of the environment is neglected (see [178] for a definition of these terms). This should have an effect on vertical excitation energies, while in dynamics simulations the main solvent response can be included through orientational polarization. A critical observation, made from the PCM computations, is that the environment may have a strong impact on the stability of charge transfer states and that, aside from the time-regime (equilibrium or non-equilibrium), even the precise PCM implementation (linear-response [179] or state-specific [180]) makes a crucial difference [181]. A similar sensitivity to the environmental models is probably also present in a QM/MM framework. Thus, in summary, the importance of an accurate description of the environment should be highlighted.

The most straightforward way for sampling ground state DNA structures is by classical molecular dynamics (MD) using standard biomolecular force fields and such an approach has been taken by a number of groups [144, 149, 156, 176]. The situation becomes more complicated when effects of zero-point vibrations should also be included. For this purpose a hybrid approach based on mixed initial conditions was introduced: Large scale motions and solvent degrees of freedom are properly treated by MD while the Wigner distribution of the vibrational ground state is used to represent the central molecule of interest [182]. This approach was applied to produce initial conditions for QM/MM dynamics simulations of a DNA base [177], and a slight extension considering several active molecules was used for spectra simulations [113]. QM/MM geometry optimizations can be performed by using an averaged solvent electrostatic potential generated from MD sampling of the environmental motions [183]. This method was applied to excited state optimizations of the adenine dinucleotide [168].

To go beyond static calculations, a number of excited state dynamics studies have also been performed. A particular focus was placed on the description of non-adiabatic effects, which are essential for understanding, e.g., internal conversion, excitation energy transfer, and charge separation processes. Dynamics have been performed using exciton models [143] and wave packet propagation on parameterized surfaces [184] but in most cases on-the-fly surface hopping dynamics were applied [59, 154, 155, 176, 177]. In the latter case a QM/MM approach was often chosen to allow a real time polarization response of the environment. While

the studies presented above considered only the singlet manifold, intersystem crossings to the triplet were also already considered in surface hopping dynamics [90].

4 UV Absorption

The nature of excited states in the Franck–Condon region significantly affects the excited state behavior of nucleic acids. Thus, understanding the character of absorption spectra is crucial for the further evaluation of the photodynamics of nucleic acids. As already mentioned in the Introduction, there is still controversy as to whether during photon absorption the nucleic acids form exciton or charge transfer states or whether they remain localized. In this chapter the survey of theoretical works suggesting both possibilities of delocalization is treated separately.

4.1 Excitonic Delocalization

The concept of excitons in nucleic acids was first introduced by Tinoco et al. [92, 185] and Rhodes [186]. However, a localized character of excited states then dominated the discussions for several decades. The question of exciton character was opened again by Bouvier et al. [148]. In this work the homogeneous $(dA)_{20}.(dT)_{20}$ and alternating $(dAdT)_{10}.(dAdT)_{10}$ oligonucleotides in idealized B-DNA geometry are investigated. The two lowest excited states of adenine and one excited state of thymine are considered. The interaction between the states is described by the atomic transition charges model [187] in which the transition dipoles are decomposed onto atomic orbitals. This procedure results in transition charges located on each atom. Using this approach, delocalization of the excited states was found for both oligomers. In $(dA)_{20}.(dT)_{20}$ the intra-strand coupling dominates with a strength of about 250 cm^{-1}. In the alternating $(dAdT)_{10}.(dAdT)_{10}$ the inter-strand coupling is more important, the estimated value of the coupling being approximately 100 cm^{-1}. In the following contribution [104] the influence of structure fluctuations on the character of the Frank–Condon excited states is analyzed for oligonucleotides $(dA)_{10}.(dT)_{10}$ and $(dAdT)_5.(dAdT)_5$. A ground-state molecular dynamics simulation to scan possible DNA structures resulting from the plasticity of the sugar-phosphate helix. Importantly, the diagonal energies of monomer excited states are not affected by structural fluctuations, with the change being smaller than 10 cm^{-1}. Relatively large fluctuations of the off-diagonal terms for these structures were found, with the amplitude of the variations 35% and 45% for $(dA)_{10}.(dT)_{10}$ and $(dAdT)_5.(dAdT)_5$, respectively. The distribution of the oscillator strengths, on the other hand, is not significantly affected by the structural dynamics for the $(dA)_{10}$.

$(dT)_{10}$ oligonucleotide. In fact, 90% of the oscillator strength remains concentrated on the same eigenstates. In the case of the alternating $(dAdT)_5.(dAdT)_5$ oligonucleotide the structural disorder results in a larger spreading of the oscillator strength among eigenstates. Studies performed on $(dCdG)_5.(dCdG)_5$ [149] resulted in similar conclusions as for the afore-mentioned $(dAdT)_5.(dAdT)_5$ case: small fluctuations of monomer excitation energies, less than 15 cm^{-1}, and a large perturbation of dipolar coupling due to the structural disorder. In all the cases mentioned above a delocalization of the excited states over at least two nucleobases was observed. Delocalization over three bases was found in the calculations of the absorption spectra using the TDDFT method in combination with ground-state MD simulations for single-stranded oligomers of adenine [156] and (adenine–thymine) oligomers [188]. Formation of delocalized exciton states was further investigated in studies which combine ground-state molecular dynamics and the evaluation of the exciton model for the poly(dA).poly (dT) [143] and $(dA)_{12}.(dT)_{12}$ [144]. The lattice model and the transition density cube model, based on the transition model calculated using the TDDFT method, were used in the former and later investigations, respectively. In agreement with the work of Bouvier et al. [104] and Emanuele et al. [149], changes in electronic coupling due to structural fluctuation were found. The results indicated that during the absorption process the electronic excitation is delocalized over at least six nucleobases and localizes upon relaxation on four nucleobases. Importantly, these authors predicted the presence of charge transfer excitons in their model [144]. Charge transfer character of excitons was also suggested by Starikov et al. [189]. The character of exciton states due to structural fluctuations of B-DNA conformations was investigated in short $(dA)_n.(dT)_n$ and $(dC)_n.(dG)_n$ oligomers (with $n = 3,4$) obtained by means of ground-state molecular dynamics [152]. The effect of different conformational modes was evaluated, among which the twist is predicted as the most powerful regulator of the exciton character. It was also shown that the effect of the twist angle on the localization of electronic states is stronger in poly(dG)-poly(dC) than in poly(dA)-poly(dT) [190]. A new study based on ab initio calculations of alternating duplexes after extended sampling [113] presented a picture of rather localized states, which were situated on one or at most two bases. Considering poly(dAdT)-poly(dAdT) and poly (dGdC)-poly(dGdC) duplexes with four stacked bases in the QM region and the remaining part of the system treated at the MM level, only about a third of the states are delocalized over 1.5 bases or more. These are, however, responsible for somewhat more than 50% of the intensity at the absorption maximum due to higher than average oscillator strengths. Intramolecular vibrations were identified as the main factor responsible for spectral broadening and for causing disorder resulting in localization. This strong coupling of intramolecular modes to the excited states suggests that these are also active in the early excited state dynamics. The picture of rather localized states was also drawn from another recent study that compared measured and computed circular dichroism spectra in $(dA)_n.(dT)_n$ hairpins [147]. The TDDFT study on adenine stacks pointed out that

the A_5 spectrum is almost identical to that of A_4 [191], i.e., there are no relevant effects either of excitonic or indirect nature which go beyond four bases. While most studies focused on singlet states, triplet excitations were studied in poly (dA)-poly(dT) sequences, and it was reported that they are confined to single nucleobases [192, 193].

4.2 Charge Transfer States

Compared to the studies performed within the framework of exciton models where the charge transfer configurations are usually not included, supermolecular quantum chemical calculations automatically provide a simultaneous treatment of excitonic and the charge transfer states. The interpretation of the absorption spectra in terms of delocalized, charge transfer and localized characters of excited states became a matter of discussion due to the performance of different methods. Suitability of various methods to describe long-range charge transfer states between nucleic acids has been tested in recent years (see, for example, [108, 110–112, 169, 194–196]).

In the text below the calculations of the character of excited states observed at the ground state geometries, i.e., upon UV absorption, as affected by base pairing and stacking interactions will be reviewed with the emphasis on a formation of charge transfer states. In initial ab initio calculations the effect of base pairing was studied [42, 197–199]. Although charge transfer states were detected at higher energies when using the CIS method [197], these were the lowest in calculations at the TDDFT level employing the LDA functional [198]. Stacking interactions were considered for the first time in calculations of Varsano et al. [200]. Other calculations studying the effects of stacking on excited states formed upon UV absorption in the gas phase have been reported, e.g., in [132, 133, 162, 201–203]. The difficulties of a correct description of charge transfer states in the absorption spectra is demonstrated in the case of homologous oligomers of adenine, both single-stranded and in double stranded A–T sequences, as well as alternating A–T sequences.

Santoro et al. [109] performed the first study on the excited states of stacked nucleobases in a water environment. In this contribution the absorption spectra of the adenine dimer are studied employing TDDFT with the PBE0 functional for the $(9\text{-Met-A})_2$ and $(dA)_2$ models using a polarizable continuum model for solvent effects. The experimentally observed features when going from monomers to multimers [97, 105, 118], i.e., a blue-shift of the maximum, a red-shift of the lower-energy part, and hypochromic effect of the absorption spectra are already reproduced in the calculations of the former model. These effects reflect the coupling due to the orbital overlap in the stacking configuration of nucleobases. The symmetric combination of monomer bright transitions gives rise to the maximum of the absorption band. The character of the states responsible for low-lying energy transitions changes with the mutual orientation of the

adjacent adenines, i.e., an increasing intra-strand charge transfer character of the first excited state was found in less symmetrical arrangements in $(dA)_2$ in comparison to $(9\text{-Met-A})_2$ [109]. The same change of the maximum absorption peak, i.e., blue shift and decrease in the intensity with increasing number of stacked nucleobases, was already observed in the gas phase in calculations of Lange et al. [110] performed with a long-range-corrected PBE0 functional (LRC-ω-PBE0) on the homologous $(A)_n$ and $(T)_n$, ($n = 1$–4). In contrast to the calculations performed with a non-corrected density functional [109], charge transfer character was not observed in the states responsible for the red tail of the absorption spectra. The effect of the solvent is studied by means of a QM/MM approach with water molecules in the first solvation shell (within 2.5 Å) treated at the QM level. Depending on the solvent configuration the energies of charge transfer states span more than 1 eV and for some configurations they overlap with bright $\pi\pi^*$ states. The average stabilization of the charge transfer states by the solvent is 0.1 eV.

A blue shift of the maximum absorption band is also observed for double-stranded $(A)_2.(T)_2$ with localization on the $(A)_2$ dimer while excited states localized on the $(T)_2$ dimer are responsible for the low energy part of the spectrum [169]. The calculations performed with the M052X functional place the intra-strand (A → A) and inter-strand (A → T) charge transfer states in the range of bright excited states of the adenine dimer. Note that in the PBE0 calculations the charge transfer states are the most stable. As in the case of single-stranded oligomers, the gas phase calculations performed with the LRC-ω-PBE0 functional [110] place the intra-strand charge transfer states above the bright states. The inclusion of solvent causes a stabilization of these states by about 0.1 eV on the average.

For a single-strand with an alternating sequence of adenine and thymine studied with the LRC-ω-PBE0 functional in the gas phase, Lange et al. [110] found that, due to a mismatch of $\pi\pi^*$ state energies of these nucleobases, the intra-strand excitonic delocalization is missing and, consequently, the bright states are localized on a single base. In contrast to homologous oligomers, the CT states become resonant with the $\pi\pi^*$ states of adenine and thymine. When the second strand is included, the intra-strand CT states are placed about 0.4 eV below the bright absorption peak of adenine, while the inter-strand CT states appear about 0.7 eV above this bright peak. Note that the ADC(2) calculations performed by Aquino et al. [112] placed the lowest intra-strand CT state 0.5 and 0.3 eV above the lowest $\pi\pi^*$ states localized on adenine and thymine, respectively.

Recently Plasser et al. [113] reported the results of ADC(2) calculations of alternating oligomer duplexes in both gas phase and embedded in DNA environment employing a QM/MM scheme, together with a detailed analysis of the excited states. For both systems considered, poly(dAdT)-poly(dAdT) and poly (dGdC)-poly(dGdC), a similar picture was drawn: CT states were found energetically well above the bright states. Due to their low intensity they do not significantly contribute to the absorption spectra even when the DNA

environment is involved. A statistical treatment of the QM/MM simulations shows that only about half of the states exhibit Frenkel exciton character (a CT contribution below 0.1 e) while the remaining states show a non-negligible admixture of CT contributions, which means that they may be misrepresented in a pure Frenkel exciton model. About 15% of the states considered show significant charge separation (>0.5 e).

5 Excited State Processes

A number of factors may play a role in DNA photoactivity. These may be divided into external factors like sterical hindrances and electrostatic interactions on the one hand, and electronic interactions on the other. From a computational point of view the significance is that for the former class it may be sufficient to treat only one base at the QM level and the environment at a lower, e.g., molecular mechanics, level (QM/MM method). By contrast, for the second class it is indispensable to consider several bases simultaneously at the QM level, which imposes restrictions on the available approaches. In this chapter, studies concerned with external interactions will be reviewed first. Then direct electronic interactions will be considered, which may occur between stacked bases (leading to excitons, CT states, and exciplexes) as well as hydrogen bonded bases (where proton coupled electron transfer processes are of special interest). Finally, further reactions determining the photochemistry of DNA will be discussed.

5.1 Sterical Hindrances and Electrostatic Interactions

The calculations of the excited state relaxation of adenine [204] performed at the CASPT2/CASSCF/AMBER level assumed that the main reaction channel involves the ^{2}E conical intersection for the adenine molecule (see above, Fig. 2) in both vacuo and solvated $(dA)_{10} \cdot (dT)_{10}$ duplex. In the latter case the reaction path is flatter and features a small barrier of about 0.2 eV. These characteristics are suggested to be responsible for the slow decay component (>100 ps) observed in single and double-stranded systems with stacked adenine, thus questioning the importance of delocalized excited states. Nonadiabatic dynamics simulations employing the QM/MM method with semi-empirical treatment of the QM part (using OM2/MRCI) [58, 155] performed on an adenine molecule embedded in $(dA)_{10}$ and $(dA)_{10} \cdot (dT)_{10}$ in water predict an elongation of the excited state lifetime of adenine in comparison with the gas phase but the decay still occurs within 10 ps. In particular, decay times of 5.7 and 4.1 ps for $(dA)_{10}$ and $(dA)_{10} \cdot (dT)_{10}$, respectively, were predicted. In the single-stranded system relaxation proceeds mainly via the $^6S_1$ conical intersection but the ^{2}E pathway coexists, while in

double-stranded DNA the $^6S_1$ conical intersection is blocked due to inter-strand hydrogen bonding and only the ^2E intersection is accessed.

Surface hopping dynamics simulations using the QM/MM approach with CASSCF (cytosine) and MR-CIS (guanine) wavefunction for the QM part were performed for these two nucleobases, each embedded individually in a DNA double strand helix [177]. The restraining influence of the inter-strand hydrogen bonding on the structural deformations necessary to reach conical intersections was studied. In the case of photoexcited cytosine the isolated molecule shows relatively small puckering of the structure at the conical intersections populated during the excited state relaxation. The geometrical restrictions exerted by the hydrogen bonds of the DNA environment thus do not inhibit the photodeactivation of cytosine and consequently its excited state lifetime. In contrast to this, the isolated guanine relaxes to the ground state with strong out-of-plane motions of the NH_2 group. This motion is significantly restrained by inter-strand hydrogen bonds which results in a considerable elongation of the relaxation time.

The effect of the intra-strand interaction on the photodecay of adenine in a single-stranded DNA was studied in nonadiabatic dynamics simulations using 4-aminopyrimidine (4AP) [205] as a model for adenine. In these QM/MM calculations 4AP was treated at the CASSCF level. Comparison with the previously investigated dynamics of isolated 4AP [33] shows a very similar relaxation mechanism and only slight elongation of the excited state lifetime. During the dynamics of embedded 4AP the dynamical formation and breaking of intra-strand hydrogen bonds was observed. Interestingly, these bonds contribute to a faster decay component by enhancing the out-of-plane motion of the amino-group in relevant conical intersections.

5.2 Excimer Formation and Excitation Energy Transfer

An initial study used static calculations of stacked adenine dimers and trimers at the TDDFT/PBE0 level with PCM solvation to discuss the effect of stacking interactions on their excited state behavior [109]. This study describes a process starting from rather delocalized absorbing states, with a subsequent localization on one base on a subpicosecond time scale. After this, the system could either deactivate to the ground state or reach a low energy CT minimum on the S_1 surface, which could act as a trapping site. A quantum dynamical study performed at the same computational level indicated that charge separation could be fast and effective [108]. Subsequent studies on a number of similar cases used, aside from PBE0, the range-separated CAM-B3LYP and the M05-2X functional containing a large percentage of non-local exchange. Consideration of the $(dA)_2 \cdot (dT)_2$ system showed that the interaction between stacked bases was more important than between hydrogen bonded bases. Again, charge transfer excimers were found. A subsequent study on AG and GA stacks also emphasized the importance of charge transfer in these systems [181]. Furthermore, efficient coupling of the CT states to the locally

excited states was reported. Later, excited state relaxation in $(dA)_4$ was considered [206]. In this investigation several excited state minima were found pertaining to localized excited states, neutral excimer states, and a CT minimum. The CT minimum was identified as the most stable one. These studies used the newly implemented state-specific PCM formalism [180] to describe the solvent response to the excitation. In these calculations it was shown that this new PCM formalism led to results significantly different from the standard linear-response approach, in particular stabilizing the CT states. Similar results were also found in a more recent combined experimental and theoretical paper [191].

In contrast to the TDDFT studies, a CASPT2/CASSCF work described the formation of neutral excimers, which were especially stabilized in maximum-overlap face-to-face configurations, whereas charge transfer excimers played only a secondary role [175]. Similar to the above analysis, a bifurcation of the initial wavepacket was considered leading either to ultrafast monomer-like decay or toward the formation of excimer states. A dynamics survey using semi-empirical methods [154] described the formation of a long-lived excimer between two adenine molecules, which was structurally characterized by a short intermolecular separation of the C2 atoms (cf. Scheme 1) to an average distance of 2.2 Å. A new decay channel of this system was found, which occurred through an additional shortening of the C2–C2 distance to 1.8 Å and concurrent ring deformations. A subsequent study by this group, using dynamics at the DFTB level [207], even described the formation of a chemical bond between two adenine molecules after excitation, which was stable for about 2 ps. Whereas similar processes in pyrimidine bases can lead to photodimerization (see below), a non-reactive deactivation was observed in these dynamics investigations. Recent ab initio work using the ADC(2) and MR-CISD methods in a QM/MM framework found several minima on the S_1 surface, which possessed different degrees of delocalization and charge transfer (see Fig. 5) [168]. The lowest energy minimum was of exciplex type stabilized neither by pure excitonic interactions nor charge transfer, but by direct orbital interactions, which were mediated by a close approach of the adenine C6 atoms (down to about 2.0 Å) and a concurrent strong distortion of the molecular structures. Indications for various decay channels were found, which were related to either a further approach of the two molecules (as in [154]) or a restoration of monomer-like excited states and decay through the $^6S_1$ intersection. Partial charge transfer was observed in response to solvent polarization but it did not play a dominant role. A similar conclusion was also drawn from a recent study using the RI-CIS(D) method [208] presenting a bonded exciplex mediated by an approach of two C6 atoms. In that case no excited state minimum but only an intersection was found. However, it was pointed out that the solvent effects may destabilize this intersection. These newer results may be rationalized with the bonded exciplex model [136] (see also Sect. 2.1). Experimental evidence for this type of mechanism may be found in the unexpected fact of negative fluorescence anisotropy recorded for $(dA)_{20}$, which was taken as evidence of an out-of-plane polarization of the emitting states [191], a phenomenon which is forbidden in planar molecules by

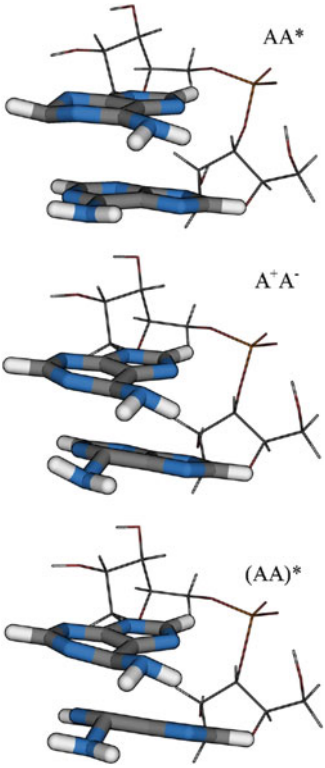

Fig. 5 Excited state minima of ApA localized on the S_1 surface: excitation localized on a single Ade (*top*), excitation from localized *n* orbital to delocalized π* orbital (*middle*), excitation from delocalized π to delocalized π* orbital (see [168] for details)

symmetry selection rules. Strong orbital overlap, combining two bases to one effective chromophore, can lift this selection rule, and a transition dipole moment with a strong out-of-plane component was indeed found for the exciplex [168].

Aside from explicit quantum chemical calculations, exciton models have also been used to describe excited state dynamics in DNA. The poly(dA).poly(dT) duplex was studied using a model considering both Frenkel excitonic and charge-transfer interactions [143]. The dynamics in this study were dominated by base-stacking whereas inter-strand interactions only played a minor role. It was found that on the adenine side the exciton remained in a cohesive bound state (i.e., no charge transfer occurred between stacked adenine molecules). By contrast, electron-hole separation into mobile charge carriers was reported on the thymine side. It was hypothesized that such charge separation and subsequent recombination could lead to triplet formation.

While the above studies considered adenine and thymine molecules, stacking interactions between two cytosine molecules were also investigated at the CASPT2 level [209] showing an attractive potential between the two cytosine molecules identified in the excited state, which could lead to red-shifted fluorescence. The strength of this interaction experienced strong dependence on BSSE. Using the CP

correction, an intermolecular separation of 3.08 Å and an excimer binding energy of 0.58 eV was obtained.

5.3 *Proton Transfer Processes*

The initial interest in the proton transfer process dates back to Watson and Crick pointing out that the occurrence of rare tautomeric forms of the nucleobases may lead to spontaneous mutations [210] and to Löwdin discussing that such tautomers may be formed through double proton tunneling in the DNA structure [211]. It has been pointed out by Guallar et al. [212] that such double proton transfer is not feasible in the ground state but that such a pathway could be accessed in the excited state. However, the computations suggested that it is unlikely that the rare tautomers would persist long enough to perturb the duplication of the genetic code [212]. Gorb et al. [213] reported that while the AT double proton transfer was completely inaccessible, the corresponding GC structure would show minimal population (with an equilibrium constant of about 10^{-6}). The same group also reported excited state investigations on the AT and GC pairs [197], as well as the AU pair [197]. In both cases the presence of locally excited states and higher lying charge transfer states was reported.

In 2004 Sobolewski and Domcke put forward the hypothesis that a proton coupled electron transfer (PCET) along the central hydrogen bond in the Watson–Crick base pair of guanine and cytosine could serve as an efficient decay channel to the ground state [42]. This hypothesis was based on CASSCF/CASPT2 calculations on structures and reaction paths optimized at the CIS level. It was found that in the vicinity of the FC region a stable charge transfer state existed, and that starting in this state a transfer of the central hydrogen bonding proton (yielding in total a PCET) could neutralize the system and stabilize this state. Potential curves revealed a weakly avoided crossing between the CT and ground states, which might provide an efficient channel for the relaxation. The study also found a locally excited path for cytosine to the ethylenic intersection, which was only later described for the isolated molecule (see, e.g., [44, 214]). An experimental work on GC dimers in the gas phase later found that the Watson–Crick bound base pair did indeed possess a much broader UV spectrum as opposed to other structures of this system [125]. These results were rationalized by computations at the CC2 level, where the three lowest energy conformers of the GC system were considered [215]. In all three cases a proton transfer path could be identified. However, this path was only favored in the WC case, whereas for the other conformers significant barriers would have to be overcome due to the fact that the CT states were higher in energy for these structures. Subsequently, time-resolved fluorescence experiments in chloroform were carried out, which supported the existence of such a decay channel by showing a short lifetime of about 0.36 ps for the GC base pair [127]. However, transient absorption experiments in chloroform in connection with TDDFT

calculations in PCM solvent contested this claim [126]. Regarding GC duplexes, it was pointed out from experiment that PCET may play a role in the case of alternating but not in homopolymeric sequences [128]. This idea was supported computationally by comparing TDDFT calculations of the GGG · CCC and GCG · CGC hexamer stacks [216].

Aside from static calculations, non-adiabatic dynamics simulations were also performed to get a deeper mechanistic insight into a potential proton transfer in GC and why it should or should not be effective. In particular, it is of interest to understand the coupling between the electronic and nuclear motion during the PCET process. In this regard the GC pair was studied by CASSCF using an approximate diabatic surface hopping method [176]. The simulations were performed in vacuo and embedded in a DNA double helix solvated in water using a QM/MM scheme. Dynamics were started in the S_1 (CT) state and the processes leading to the ground state decay were monitored. After a quick initial proton transfer, the back transfer was briefly inhibited by a diabatic trapping situation leading to several recrossings before reaching the closed shell configuration on a 100 fs time scale. This phenomenon was explained by an unusual intersection topology, possessing effectively only a one-dimensional branching space. The authors showed that the inclusion of the environment could speed up the decay through a stabilization of the charge transfer state. At this point it should be mentioned that the intersection topology described in [176] may be interpreted as a signature of an electron transfer process, which necessarily occurs when switching from the charge transfer state to the neutral state. In fact, similar surface topologies and diabatic trapping dynamics were also obtained in electron transfer model systems [217], further supporting this interpretation. The PCET deactivation process in the WC paired GC system was also studied using non-adiabatic dynamics at the restricted open shell Kohn–Sham (ROKS) level, considering the system in vacuo as well as in water solvation [218]. A steering technique was used to accelerate the forward PCET. In this study a fast deactivation on the order of 100 fs was also reported. To date, no study has been performed attempting to describe the dynamics starting from the bright $\pi\pi^*$ state to the CT state and to give a non-adiabatic description of the forward PCET process, considering that this would pose special challenges as a larger number of excited states would have to be described concurrently. However, a similar process was studied in the 2-pyridone dimer model system, using static calculations [219] and non-adiabatic dynamics, both performed at the TDDFT/BHLYP level [220] following time-resolved experiments [221]. The dynamics study highlighted that the PCET was not only governed by the energetics describing the proton transfer but also that non-adiabatic transition probabilities for the electron transfer (which were manifested by temporary hoppings into the adiabatic S_2 state) played a decisive role. This observation may provide also an explanation for the discrepancies between the dynamics studies and the above-mentioned experiments on the GC base pair [101, 126]. An efficient deactivation channel may indeed exist once the proton is transferred from G to C. However, it is not clear whether the initial proton transfer occurs after excitation into one of the bright states.

While most studies focused on the GC pair, proton transfer in the AT pair was also studied at the CC2 level [222]. Similar to [215], it was also found for AT that the WC structure possessed an efficient decay channel related to proton transfer. While the CT state was 1.5 eV above the lowest bright transition at the FC region, this state was strongly stabilized by proton transfer. Barrierless deactivation could occur through the CT state by a sequence of conical intersections. Internal conversion to the $n\pi^*$ state could serve as a competitive channel. As opposed to the WC structure no such efficient decay path was present in the most stable hydrogen bonded conformer of AT as the CT state was located at higher energy with respect to the minimum of the locally excited state. A TDDFT study of the WC bonded AT pair [223] highlighted the importance of solvent effects. In particular it was pointed out that a polar solvent could strongly stabilize the inter-strand CT state, thus disfavoring the subsequent proton transfer. The coupling via a $\pi\sigma^*$state explains the time-resolved photoionization spectroscopy of adenine and the adenine dimer. In adenine this path is not dominating although it does play a role as indicated by the H-atom detection in nanosecond spectroscopic experiments. In the adenine dimer an increased population of $\pi\sigma^*$transfer is observed. It is caused by stabilization of the relevant state in the dimer [87].

5.4 Photochemical Processes

The major photoproducts observed upon UV-irradiation of DNA include dimer or adduct formations of adjacent pyrimidine nucleobases, particularly cyclobutane pyrimidine dimers (CPDs) and the pyrimidine(6-4) pyrimidone dimers ((6-4)PP). The former products are observed more frequently (for review of experimental investigations see [224] and references therein). The dimerization proceeds via [2+2] cycloaddition of the C5–C6 double bonds of adjacent pyrimidine nucleobases and can be formed via both the singlet and triplet manifolds [224–227]. The thymine dimer (T<>T) is the major photoproduct occurring after DNA irradiation by UV light. The cytosine dimer (C<>C) on the other hand is more likely to induce mutations once it is formed [225, 228].

In the last decade, several results of experimental studies were reported, discussing the mechanism of CPD formation [226, 229–236]. For example, Schreier et al. showed that the T<>T is formed on the picosecond time scale which suggests that the formation proceeds in the singlet excited state [230]. The quantum yield of this reaction is, however, very low, of the order of 10^{-2}. Based on time-resolved femtosecond transient absorption spectroscopy, Kwok et al. [232] suggested that both pathways might simultaneously contribute to the dimerization. In this contribution the role of other excited states for this process, in particular the role of the $n\pi^*$ state, is discussed in the intersystem crossing to the triplet state.

The theoretical investigations focusing on the mechanism of the more frequently formed T<>T photoproduct considered both triplet and singlet pathways of the dimerization process. In the triplet state the stepwise mechanism was suggested

based on the results of the TDDFT [237] and CASPT2 [238] calculations. The singlet pathway was proposed to proceed via a concerted mechanism [202, 203, 236, 237, 239–241] mediated via S_1/S_0 conical intersections leading to either the original ground state or to T<>T. Blancafort and Migani [240] suggested coexistence of the alternative singlet pathway where the excitation is first localized on a single thymine with a subsequent formation of quasi-minimum of the S_1 state localized energetically above the relevant conical intersection. Based on the recently published joint experimental and theoretical investigations Banyasz et al. [236] put forward that the [2+2] cycloaddition occurs from the lowest excitonic state and follows a barrierless path. No CT states were identified in the reaction mechanism, in contrast to the formation of (6-4)PP adducts (for more detailed discussion on the mechanism of (6-4)PP formation see [242, 243]). The absence of charge transfer character in the former reaction might explain a decrease of the T<>T production in the systems with purine residues flanking the TT sequences by a formation of charge transfer purine-pyrimidine(T) exciplexes and subsequent decrease of the TT exciton population observed in the experiment [244].

Much effort has been made to explain the origin of very low quantum yield of the T<>T dimerization [229, 244–250]. It is now generally accepted that the ground state conformation of adjacent thymine controls the efficiency of this reaction with inter-molecular T...T distance and torsional angle between two double bonds (C5–C6 bond) on each thymine moiety being identified as the most important. While the agreement on the criteria for the former parameter was achieved [246–248, 250], the importance of the latter parameter is not clarified yet [246, 247]. The influence of the sugar conformation on the T<>T dimerization process was discussed as well [245, 250–252]. In a recently published contribution Improta suggested that a barrierless path from the delocalized exciton state towards T<>T is most effective when both sugars have C3-endo puckered conformation since the electronic coupling between thymines is larger compared to other sugar conformations [203].

The explanation of the experimentally observed lower yields of C<>C photoproduct as compared to T<>T [201, 239, 241, 253] has been the subject of several theoretical investigations. Results of these studies reveal a unified mechanism, i.e., concerted photocycloaddition of the BPD formation for both sequences. Possible competing reaction channels include monomer-like relaxation and excimer formation. The energy position of the conical intersection which mediates the cycloaddition (CI_{dimer} (S_0/S_1)) with respect to stable excimer structures and CI corresponding to monomer-like relaxations determines the efficiency of the BPD formation. While CI_{dimer} (S_0/S_1) is the lowest-energy structure in the case of thymine, it is comparable to the energy of the excimer in the case of cytosine and the monomer-like CI, opening other reaction funnels.

6 Conclusions

The area of light absorption by DNA and subsequent photophysical and photochemical processes is a fascinating research field with many important practical implications for everyday life. It is also an outstanding example for the interaction and influences between theory and experiment in an intensity which is very unique. In writing this chapter we have made an attempt to document the large variety of theoretical approaches and different, sometimes opposing, viewpoints to the photodynamics of DNA. Looking back on the history one can observe enormous effort and progress made in experiments and in theoretical simulations by collecting many facts and putting them in the proper perspective. However, the story is certainly not over yet and many interesting and fundamental insights are still waiting to be discovered.

Acknowledgments This work was supported by the Austrian Science Fund within the framework of the Special Research Program F41, Vienna Computational Materials Laboratory (ViCoM). We also acknowledge technical support from and computer time at the Vienna Scientific Cluster (Projects 70019 and 70151). Support was also provided by the Robert A. Welch Foundation under Grant No. D-0005. FP is a recipient of a research fellowship by the Alexander von Humboldt Foundation. This work has been supported by the grants of the Grant Agency of the Czech Republic (P208/12/1318) and the grant of the Czech Ministry of Education, Youth and Sport (LH11021). The research at IOCB was part of the project RVO:61388963.

References

1. Pfeifer GP, You YH, Besaratinia A (2005) Mutat Res Fund Mol M 571:19
2. Coulondre C, Miller JH (1977) J Mol Biol 117:577
3. Brash DE, Rudolph JA, Simon JA, Lin A, McKenna GJ, Baden HP, Halperin AJ, Ponten J (1991) Proc Natl Acad Sci U S A 88:10124
4. Becker MM, Wang Z (1989) J Mol Biol 210:429
5. Rochette PJ, Therrien JP, Drouin R, Perdiz D, Bastien N, Drobetsky EA, Sage E (2003) Nucleic Acids Res 31:2786
6. Beletskii A, Bhagwat AS (2001) J Bacteriol 183:6491
7. Douki T (2006) J Photoch Photobio B Biol 82:45
8. Ullrich S, Schultz T, Zgierski MZ, Stollow A (2004) Phys Chem Chem Phys 6:2796
9. Ullrich S, Schultz T, Zgierski MZ, Stolow A (2004) J Am Chem Soc 126:2262
10. Canuel C, Mons M, Piuzzi F, Tardivel B, Dimicoli I, Elhanine M (2005) J Chem Phys 122:074316
11. Crespo-Hernandez CE, Cohen B, Hare PM, Kohler B (2004) Chem Rev 104:1977
12. Doorley GW, McGovern DA, George MW, Towrie M, Parker AW, Kelly JM, Quinn SJ (2009) Angew Chem Int Ed 48:123
13. Peon J, Zewail AH (2001) Chem Phys Lett 348:255
14. Buchvarov I, Wang Q, Raytchev M, Trifonov A, Fiebig T (2007) Proc Natl Acad Sci U S A 104:4794
15. Markovitsi D, Sharonov A, Onidas D, Gustavsson T (2003) ChemPhysChem 4:303
16. Marian CM (2005) J Chem Phys 122:104314

17. Hudock HR, Levine BG, Thompson AL, Satzger H, Townsend D, Gador N, Ullrich S, Stolow A, Martinez TJ (2007) J Phys Chem A 111:8500
18. Barbatti M, Aquino AJA, Szymczak JJ, Nachtigallova D, Hobza P, Lischka H (2010) Proc Natl Acad Sci U S A 107:21453
19. Hudock HR, Martinez TJ (2008) ChemPhysChem 9:2486
20. Chen H, Li SH (2006) J Chem Phys 124:154315
21. Perun S, Sobolewski AL, Domcke W (2006) J Phys Chem A 110:13238
22. Perun S, Sobolewski AL, Domcke W (2005) J Am Chem Soc 127:6257
23. Serrano-Andres L, Merchan M, Borin AC (2006) Proc Natl Acad Sci U S A 103:8691
24. Matsika S (2004) J Phys Chem A 108:7584
25. Ismail N, Blancafort L, Olivucci M, Kohler B, Robb MA (2002) J Am Chem Soc 124:6818
26. Sobolewski AL, Domcke W (2002) Eur Phys J D 20:369
27. Epifanovsky E, Kowalski K, Fan PD, Valiev M, Matsika S, Krylov AI (2008) J Phys Chem A 112:9983
28. Serrano-Andres L, Merchan M, Borin AC (2008) J Am Chem Soc 130:2473
29. Hare PM, Crespo-Hernandez CE, Kohler B (2007) Proc Natl Acad Sci U S A 104:435
30. Blancafort L, Cohen B, Hare PM, Kohler B, Robb MA (2005) J Phys Chem A 109:4431
31. Chen H, Lis S (2005) J Phys Chem A 109:8443
32. Perun S, Sobolewski AL, Domcke W (2005) Chem Phys 313:107
33. Barbatti M, Lischka H (2008) J Am Chem Soc 130:6831
34. Fabiano E, Thiel W (2008) J Phys Chem A 112:6859
35. Cremer D, Pople JA (1975) J Am Chem Soc 97:1354
36. Marian CM (2007) J Phys Chem A 111:1545
37. Lan ZG, Fabiano E, Thiel W (2009) ChemPhysChem 10:1225
38. Barbatti M, Szymczak JJ, Aquino AJA, Nachtigallova D, Lischka H (2011) J Chem Phys 134:014304
39. Yamazaki S, Domcke W, Sobolewski AL (2008) J Phys Chem A 112:11965
40. Kistler KA, Matsika S (2008) J Chem Phys 128:215102
41. Blancafort L, Robb MA (2004) J Phys Chem A 108:10609
42. Sobolewski AL, Domcke W (2004) Phys Chem Chem Phys 6:2763
43. Zgierski MZ, Patchkovskii S, Fujiwara T, Lim EC (2005) J Phys Chem A 109:9384
44. Barbatti M, Aquino AJA, Szymczak JJ, Nachtigallova D, Lischka H (2011) Phys Chem Chem Phys 13:6145
45. Merchan M, Serrano-Andres L, Robb MA, Blancafort L (2005) J Am Chem Soc 127:1820
46. Gonzalez-Luque R, Climent T, Gonzalez-Ramirez I, Merchan M, Serrano-Andres L (2010) J Chem Theory Comput 6:2103
47. Etinski M, Fleig T, Marian CA (2009) J Phys Chem A 113:11809
48. Serrano-Perez JJ, Gonzalez-Luque R, Merchan M, Serrano-Andres L (2007) J Phys Chem B 111:11880
49. Marian CM, Schneider F, Kleinschmidt M, Tatchen J (2002) Eur Phys J D 20:357
50. Climent T, Gonzalez-Luque R, Merchan M, Serrano-Andres L (2007) Chem Phys Lett 441:327
51. Tully JC (1990) J Chem Phys 93:1061
52. Ben-Nun M, Martinez TJ (2002) Adv Chem Phys 121:439
53. Plasser F, Barbatti M, Aquino AJA, Lischka H (2012) Theor Chem Acc 131
54. Asturiol D, Lasorne B, Robb MA, Blancafort L (2009) J Phys Chem A 113:10211
55. Szymczak JJ, Barbatti M, Hoo JTS, Adkins JA, Windus TL, Nachtigallova D, Lischka H (2009) J Phys Chem A 113:12686
56. Nachtigallova D, Aquino AJA, Szymczak JJ, Barbatti M, Hobza P, Lischka H (2011) J Phys Chem A 115:5247
57. Lan ZG, Fabiano E, Thiel W (2009) J Phys Chem B 113:3548
58. Lu Y, Lan ZG, Thiel W (2012) J Comput Chem 33:1225
59. Alexandrova AN, Tully JC, Granucci G (2010) J Phys Chem B 114:12116

60. Barbatti M, Lan ZG, Crespo-Otero R, Szymczak JJ, Lischka H, Thiel W (2012) J Chem Phys 137:22A503
61. Mitric R, Werner U, Wohlgemuth M, Seifert G, Bonacic-Koutecky V (2009) J Phys Chem A 113:12700
62. Lei YB, Yuan SA, Dou YS, Wang YB, Wen ZY (2008) J Phys Chem A 112:8497
63. Langer H, Doltsinis NL, Marx D (2005) ChemPhysChem 6:1734
64. Picconi D, Barone V, Lami A, Santoro F, Improta R (2011) ChemPhysChem 12:1957
65. Szymczak JJ, Barbatti M, Lischka H (2011) Int J Quantum Chem 111:3307
66. Gonzalez-Vazquez J, Gonzalez L (2010) ChemPhysChem 11:3617
67. DeFusco A, Minezawa N, Slipchenko LV, Zahariev F, Gordon MS (2011) J Phys Chem Lett 2:2184
68. Gustavsson T, Banyasz A, Lazzarotto E, Markovitsi D, Scalmani G, Frisch MJ, Barone V, Improta R (2006) J Am Chem Soc 128:607
69. Gustavsson T, Sarkar N, Banyasz A, Markovitsi D, Improta R (2007) Photochem Photobiol 83:595
70. Improta R, Barone V (2004) J Am Chem Soc126:14320
71. Santoro F, Barone V, Gustavsson T, Improta R (2006) J Am Chem Soc 128:16312
72. Gustavsson T, Improta R, Markovitsi D (2010) J Phys Chem Lett 1:2025
73. Yoshikawa A, Matsika S (2008) Chem Phys 347:393
74. Mercier Y, Santoro F, Reguero M, Improta R (2008) J Phys Chem B 112:10769
75. Kistler KA, Matsika S (2009) J Phys Chem A 113:12396
76. Etinski M, Marian CM (2010) Phys Chem Chem Phys 12:4915
77. Rasmussen AM, Lind MC, Kim S, Schaefer HF (2010) J Chem Theory Comput 6:930
78. Olsen JM, Aidas K, Mikkelsen KV, Kongsted J (2010) J Chem Theory Comput 6:249
79. Nosenko Y, Kunitski M, Brutschy B (2011) J Phys Chem A 115:9429
80. Busker M, Nispel M, Haber T, Kleinermanns K, Etinski M, Fleig T (2008) ChemPhysChem 9:1570
81. Shukla MK, Leszczynski J (2008) J Phys Chem B 112:5139
82. Shukla MK, Leszczynski J (2009) Chem Phys Lett 478:254
83. Shukla MK, Leszczynski J (2010) Int J Quantum Chem 110:3027
84. Heggen B, Lan ZG, Thiel W (2012) Phys Chem Chem Phys 14:8137
85. Kistler KA, Matsika S (2010) Phys Chem Chem Phys 12:5024
86. Blancafort L, Migani A (2007) J Photochem Photobio A Chem 190:283
87. Ritze HH, Lippert H, Samoylova E, Smith VR, Hertel IV, Radloff W, Schultz T (2005) J Chem Phys 122:224320
88. Szymczak JJ, Muller T, Lischka H (2010) Chem Phys 375:110
89. Lan ZG, Lu Y, Fabiano E, Thiel W (2011) ChemPhysChem 12:1989
90. Richter M, Marquetand P, Gonzalez-Vazquez J, Sola I, Gonzalez L (2012) J Phys Chem Lett 3:3090
91. Mai S, Marquetand P, Richter M, Gonzales-Vazquez J, Gonzales L (2013) ChemPhysChem 14:1
92. Tinoco IJ (1960) J Am Chem Soc 82:4785
93. Eisinger J, Shulman RG (1968) Science 161:1311
94. Gueron M, Shulman RG, Eisinger J (1966) Proc Natl Acad Sci U S A 56:814
95. Georghiou S, Zhu S, Weidner R, Huang CR, Ge G (1990) J Biomol Struct Dyn 8:657
96. Markovitsi D, Gustavsson T, Sharonov A (2004) Photochem Photobiol 79:526
97. Crespo-Hernandez CE, Kohler B (2004) J Phys Chem B 108:11182
98. Crespo-Hernandez CE, Cohen B, Kohler B (2005) Nature 436:1141
99. Crespo-Hernandez CE, de La Harpe K, Kohler B (2008) J Am Chem Soc 130:10844
100. Kwok WM, Ma CS, Phillips DL (2006) J Am Chem Soc 128:11894
101. Middleton CT, de La Harpe K, Su C, Law YK, Crespo-Hernandez CE, Kohler B (2009) Annu Rev Phys Chem 60:217
102. Vaya I, Miannay FA, Gustavsson T, Markovitsi D (2010) ChemPhysChem 11:987

103. Plessow R, Brockhinke A, Eimer W, Kohse-Hoinghaus (2000) J Phys Chem B 104:3695
104. Bouvier B, Dognon JP, Lavery R, Markovitsi D, Millie P, Onidas D, Zakrzewska K (2003) J Phys Chem B 107:13512
105. Onidas D, Gustavsson T, Lazzarotto E, Markovitsi D (2007) J Phys Chem B 111:9644
106. Markovitsi D, Onidas D, Gustavsson T, Talbot F, Lazzarotto E (2005) J Am Chem Soc 127:17130
107. Onidas D, Gustavsson T, Lazzarotto E, Markovitsi D (2007) Phys Chem Chem Phys 9:5143
108. Santoro F, Barone V, Improta R (2009) J Am Chem Soc 131:15232
109. Santoro F, Barone V, Improta R (2007) Proc Natl Acad Sci U S A 104:9931
110. Lange AW, Herbert JM (2009) J Am Chem Soc 131:3913
111. Lange AW, Rohrdanz MA, Herbert JM (2008) J J Phys Chem B 112:6304
112. Aquino AJA, Nachtigallova D, Hobza P, Truhlar DG, Hättig C, Lischka H (2011) J Comp Chem 32:1217
113. Plasser F, Aquino AJA, Hase WL, Lischka H (2012) J Phys Chem A 116:11151
114. Crespo-Hernandez CE, Cohen B, Kohler B (2006) Nature 441:E8
115. Takaya T, Su C, de La Harpe K, Crespo-Hernandez CE, Kohler B (2008) Proc Natl Acad Sci U S A 105:10285
116. de La Harpe K, Crespo-Hernandez CE, Kohler B (2009) ChemPhysChem 10:1421
117. Vaya I, Gustavsson T, Miannay FA, Douki T, Markovitsi D (2010) J Am Chem Soc 132:11834
118. Markovitsi D, Gustavsson T, Talbot F (2007) Photochem Photobiol Sci 6:717
119. Markovitsi D, Gustavsson T, Vaya I (2010) J Phys Chem Lett 1:3271
120. Onidas D, Gustavsson T, Lazzarotto E, Markovitsi D (2007) Phys Chem Chem Phys 9:1
121. Vaya I, Changenet-Barret P, Gustavsson T, Zikich D, Kotlyar AB, Markovitsi D (2010) Photochem Photobiol Sci 9:1193
122. Schwalb NK, Temps F (2008) Science 322:243
123. Kadhane U, Holm AIS, Hoffmann SV, Nielsen SB (2008) Phys Rev E 77:021901
124. Markovitsi D, Gustavsson T, Banyasz A (2010) Mutat Res Rev Mutat 704:21
125. Abo-Riziq A, Grace L, Nir E, Kabelac M, Hobza P, de Vries MS (2005) Proc Natl Acad Sci U S A 102:20
126. Biemann L, Kovalenko SA, Kleinermanns K, Mahrwald R, Markert M, Improta R (2011) J Am Chem Soc 133:19664
127. Schwalb NK, Temps F (2007) J Am Chem Soc 129:9272
128. de La Harpe K, Crespo-Hernandez CE, Kohler B (2009) J Am Chem Soc 131:17557
129. Scholes GD, Ghiggino KP (1994) J Phys Chem 98:4580
130. Scholes GD (1996) J Phys Chem 100:18731
131. Scholes GD (1999) J Phys Chem B 103:2543
132. Nachtigallova D, Hobza P, Ritze HH (2008) Phys Chem Chem Phys 10:5689
133. Ritze HH, Hobza P, Nachtigallova D (2007) Phys Chem Chem Phys 9:1672
134. East ALL, Lim EC (2000) J Chem Phys 113:8981
135. Klessinger M, Michl J (1995) Excited states and photochemistry of organic molecules. Wiley-VCH, New York
136. Wang YS, Haze O, Dinnocenzo JP, Farid S, Farid RS, Gould IR (2007) J Org Chem 72:6970
137. Wang YS, Haze O, Dinnocenzo JP, Farid S, Farid RS, Gould IR (2008) J Phys Chem A 112:13088
138. Plasser F, Lischka H (2012) J Chem Theory Comput 8:2777
139. Tretiak S, Mukamel S (2002) Chem Rev 102:3171
140. Frenkel J (1931) Phys Rev 37:1276
141. Davydov AS (1971) Theory of molecular excitons. McGraw-Hill, New York
142. Bittner ER (2006) J Chem Phys 125:094909
143. Bittner ER (2007) J Photochem Photobio A Chem 190:328
144. Czader A, Bittner ER (2008) J Chem Phys 128:035101
145. Emanuele E, Markovitsi D, Millie P, Zakrzewska K (2005) ChemPhysChem 6:1387

146. Conwell EM, Bloch SM, McLaughlin PM, Basko DM (2007) J Am Chem Soc 129:9175
147. Patwardhan S, Tonzani S, Lewis FD, Siebbeles LDA, Schatz GC, Grozema FC (2012) J Phys Chem B 116:11447
148. Bouvier B, Gustavsson T, Markovitsi D, Millie P (2002) Chem Phys 275:75
149. Emanuele E, Zakrzewska K, Markovitsi D, Lavery R, Millie P (2005) J Phys Chem B 109:16109
150. Czikklely V, Forsterling HD, Kuhn H (1970) Chem Phys Lett 6:207
151. Conwell EM, McLaughlin PM, Bloch SM (2008) J Phys Chem B 112:2268
152. Starikov EB, Cuniberti G, Tanaka S (2009) J Phys Chem B 113:10428
153. Granucci G, Persico M (2007) J Chem Phys 126:134114
154. Zhang W, Yuan S, Whang Z, Qi Z, ZhaO J, Dou Y, Lo GV (2011) Chem Phys Lett 506:303
155. Lu Y, Lan ZG, Thiel W (2011) Angew Chem Int Ed 50:6864
156. Tonzani S, Schatz GC (2008) J Am Chem Soc 130:7607
157. Dreuw A, Weisman JL, Head-Gordon M (2003) J Chem Phys 119:2943
158. Improta R (2008) Phys Chem Chem Phys 10:2656
159. Christiansen O, Koch H, Jorgensen P (1995) Chem Phys Lett 243:409
160. Trofimov AB, Schirmer J (1995) J Phys B At Mol Opt 28:2299
161. Hattig C, Weigend F (2000) J Chem Phys 113:5154
162. Kozak CR, Kistler KA, Lu Z, Matsika S (2010) J Phys Chem B 114:1674
163. Szalay PG, Watson T, Perera A, Lotrich V, Fogarasi G, Bartlett RJ (2012) J Phys Chem A 116:8851
164. Szalay PG, Watson T, Perera A, Lotrich V, Bartlett RJ (2013) J Phys Chem A 117:3149
165. Szalay PG (2013) Int J Quantum Chem 113:1821
166. Andersson K, Malmqvist PA, Roos BO (1992) J Chem Phys 96:1218
167. Szalay PG, Muller T, Gidofalvi G, Lischka H, Shepard R (2012) Chem Rev 112:108
168. Plasser F, Lischka H (2013) Photochem Photobiol Sci 12:1440
169. Santoro F, Barone V, Improta R (2008) ChemPhysChem 9:2531
170. Luzanov AV, Zhikol OA (2010) Int J Quantum Chem 110:902
171. Riley KE, Platts JA, Rezac J, Hobza P, Hill JG (2012) J Phys Chem A 116:4159
172. Morgado CA, Jurecka P, Svozil D, Hobza P, Sponer J (2010) Phys Chem Chem Phys 12:3522
173. Grimme S (2004) J Comput Chem 25:1463
174. Cossi M, Barone V, Cammi R, Tomasi J (1996) Chem Phys Lett 255:327
175. Olaso-Gonzalez G, Merchan M, Serrano-Andres L (2009) J Am Chem Soc 131:4368
176. Groenhof G, Schafer LV, Boggio-Pasqua M, Goette M, Grubmuller H, Robb MA (2007) J Am Chem Soc 129:6812
177. Zeleny T, Ruckenbauer M, Aquino AJA, Muller T, Lankas F, Drsata T, Hase WL, Nachtigallova D, Lischka H (2012) J Am Chem Soc 134:13662
178. Bakowies D, Thiel W (1996) J Phys Chem 100:10580
179. Cossi M, Barone V (2001) J Chem Phys 115:4708
180. Improta R, Scalmani G, Frisch MJ, Barone V (2007) J Chem Phys 127
181. Santoro F, Barone V, Lami A, Improta R (2010) Phys Chem Chem Phys 12:4934
182. Ruckenbauer M, Barbatti M, Muller T, Lischka H (2010) J Phys Chem A 114:6757
183. Galvan IF, Sanchez ML, Martin ME, del Valle FJO, Aguilar MA (2003) J Chem Phys 118:255
184. Improta R, Santoro F, Barone V, Lami A (2009) J Phys Chem A 113:15346
185. Tinoco I, Bradley DF, Woody RW (1963) J Chem Phys 38:1317
186. Rhodes W (1961) J Am Chem Soc 83:3609
187. Claverie P (1978) In: Pullman B (ed) Intramolecular interactions – from diatomics to biopolymers. Wiley, New York, p 69
188. Voityuk AA (2013) Photochem Photobiol Sci 12:1303
189. Starikov EB, Lewis JP, Sankey OF (2005) Int J Mod Phys B 19:4331
190. Yamada H, Starikov EB, Hennig D, Archilla JFR (2005) Eur Phys J E 17:149

191. Banyasz A, Gustavsson T, Onidas D, Changenet-Barret P, Markovitsi D, Improta R (2013) Chem Eur J 19:3762
192. Curutchet C, Voityuk AA (2011) Chem Phys Lett 512:118
193. Curutchet C, Voityuk AA (2011) Angew Chem Int Ed 50:1820
194. Jensen L, Govind N (2009) J Phys Chem A 113:9761
195. Shukla MK, Leszczynski J (2010) Mol Phys 108:3131
196. Santoro F, Barone V, Improta R (2008) J Comput Chem 29:957
197. Shukla MK, Leszczynski J (2002) J Phys Chem A 106:1011
198. Tsokalidis A, Kaxiras E (2005) J Phys Chem A 109:2373
199. Wesolowski TA (2004) J Am Chem Soc 126:11444
200. Varsano D, Di Felice R, Marques MAL, Rubio A (2006) J Phys Chem B 110:7129
201. Roca-Sanjuan D, Olaso-Gonzalez G, Gonzalez-Ramirez I, Serrano-Andres L, Merchan M (2008) J Am Chem Soc 130:10768
202. Boggio-Pasqua M, Groenhof G, Schafer LV, Grubmuller H, Robb MA (2007) J Am Chem Soc 129:10996
203. Improta R (2012) J Phys Chem B 116:14261
204. Conti I, Altoe P, Stenta M, Garavelli M, Orlandi G (2010) Phys Chem Chem Phys 12:5016
205. Nachtigallova D, Zeleny T, Ruckenbauer M, Muller T, Barbatti M, Hobza P, Lischka H (2010) J Am Chem Soc 132:8261
206. Improta R, Barone V (2011) Angew Chem Int Ed 50:12016
207. Dou YS, Liu ZC, Yuan S, Zhang WY, Tang H, Zhao JS, Fang WH, Lo GV (2013) Int J Biol Macromol 52:358
208. Spata VA, Matsika S (2013) J Phys Chem A 117. doi:10.1021/jp4033194
209. Olaso-Gonzáles G, Roca-Sanjuán D, Serrano-Andres L, Merchan M (2006) J Chem Phys A 125:231102
210. Watson JD, Crick FHC (1953) Nature 171:737
211. Lowdin PO (1963) Rev Mod Phys 35:724
212. Guallar V, Douhal A, Moreno M, Lluch JM (1999) J Phys Chem A 103:6251
213. Gorb L, Podolyan Y, Dziekonski P, Sokalski WA, Leszczynski J (2004) J Am Chem Soc 126:10119
214. Blancafort L (2007) Photochem Photobiol 83:603
215. Sobolewski AL, Domcke W, Hattig C (2005) Proc Natl Acad Sci U S A 102:17903
216. Ko C, Hammes-Schiffer S (2013) J Phys Chem Lett 4:2540
217. Plasser F, Lischka H (2011) J Chem Phys 134:034309
218. Markwick PRL, Doltsinis NL (2007) J Chem Phys 126:175102
219. Sagvolden E, Furche F (2010) J Phys Chem A 114:6897
220. Plasser F, Granucci G, Pittner J, Barbatti M, Persico M, Lischka H (2012) J Chem Phys 137:22A514
221. Muller A, Talbot F, Leutwyler S (2002) J Chem Phys116:2836
222. Perun S, Sobolewski AL, Domcke W (2006) J Phys Chem A 110:9031
223. Dargiewicz M, Biczysko M, Improta R, Barone V (2012) Phys Chem Chem Phys 14:8981
224. Cadet J, Mouret S, Ravanat JL, Douki T (2012) Photochem Photobiol 88:1048
225. Ravanat JL, Douki T, Cadet J (2001) J Photochem Photobio B Biol 63:88
226. Cuquerella MC, Lhiaubet-Vallet V, Bosca F, Miranda MA (2011) Chem Sci 2:1219
227. Bosca F, Lhiaubet-Vallet V, Cuquerella MC, Castell JV, Miranda MA (2006) J Am Chem Soc 128:6318
228. Lee DH, Pfeifer GP (2003) J Biol Chem 278:10314
229. Schreier WJ, Schrader TE, Koller FO, Gilch P, Crespo-Hernandez CE, Swaminathan VN, Carell T, Zinth W, Kohler B (2007) Science 315:625
230. Schreier WJ, Kubon J, Regner N, Haiser K, Schrader TE, Zinth W, Clivio P, Gilch P (2009) J Am Chem Soc 131:5038
231. Marguet S, Markovitsi D (2005) J Am Chem Soc 127:5780
232. Kwok WM, Ma C, Phillips DL (2008) J Am Chem Soc 130:5131

233. Douki T, Cadet J (2003) Photochem Photobiol Sci 2:433
234. Mouret S, Philippe C, Gracia-Chantegrel J, Banyasz A, Karpati S, Markovitsi D, Douki T (2010) Org Biomol Chem 8:1706
235. Tommasi S, Denissenko MF, Pfeifer GP (1997) Cancer Res 57:4727
236. Banyasz A, Douki T, Improta R, Gustavsson T, Onidas D, Vaya I, Perron M, Markovitsi D (2012) J Am Chem Soc 134:14834
237. Zhang RB, Eriksson LA (2006) J Phys Chem B 110:7556
238. Climent T, Gonzalez-Ramirez I, Gonzalez-Luque R, Merchan M, Serrano-Andres L (2010) J Phys Chem Lett 1:2072
239. Gonzalez-Ramirez I, Roca-Sanjuan D, Climent T, Serrano-Perez JJ, Merchan M, Serrano-Andres L (2011) Theor Chem Acc 128:705
240. Blancafort L, Migani A (2007) J Am Chem Soc 129:14540
241. Serrano-Perez JJ, Gonzalez-Ramirez I, Coto PB, Merchan M, Serrano-Andres L (2008) J Phys Chem B 112:14096
242. Labet V, Jorge N, Morell C, Douki T, Grand A, Cadet J, Eriksson LA (2013) Photochem Photobiol Sci 12:1509
243. Giussani A, Serrano-Andres L, Merchan M, Roca-Sanjuan D, Garavelli M (2013) J Phys Chem B 117:1999
244. Pan ZZ, Hariharan M, Arkin JD, Jalilov AS, McCullagh M, Schatz GC, Lewis FD (2011) J Am Chem Soc 134:3611
245. Santini GPH, Pakleza C, Auffinger P, Moriou C, Favre A, Clivio P, Cognet JAH (2007) J Phys Chem B 111:9400
246. Law YK, Azadi J, Crespo-Hernandez CE, Olmon E, Kohler B (2008) Biophys J 94:3590
247. Johnson AT, Wiest O (2007) J Phys Chem B 111:14398
248. McCullagh M, Hariharan M, Lewis FD, Markovitsi D, Douki T, Schatz GC (2010) J Phys Chem B 114:5215
249. Pan Z, McCullagh M, Schatz GC, Lewis FD (2011) J Phys Chem Lett 2:1432
250. Hariharan M, McCullagh M, Schatz GC, Lewis FD (2010) J Am Chem Soc 132:12856
251. Desnous C, Babu BR, McIriou C, Mayo JUO, Favre A, Wengel J, Clivio P (2008) J Am Chem Soc 130:30
252. Ostrowski T, Maurizot JC, Adeline MT, Fourrey JL, Clivio P (2003) J Org Chem 68:6502
253. Yuan SA, Zhang WY, Liu LH, Dou YS, Fang WH, Lo GV (2011) J Phys Chem A 115:13291

Top Curr Chem (2015) 356: 39–88
DOI: 10.1007/128_2014_570

Published online: 19 October 2014

Excited States in DNA Strands Investigated by Ultrafast Laser Spectroscopy

Jinquan Chen, Yuyuan Zhang, and Bern Kohler

Abstract Ultrafast laser experiments on carefully selected DNA model compounds probe the effects of base stacking, base pairing, and structural disorder on excited electronic states formed by UV absorption in single and double DNA strands. Direct π-orbital overlap between two stacked bases in a dinucleotide or in a longer single strand creates new excited states that decay orders of magnitude more slowly than the generally subpicosecond excited states of monomeric bases. Half or more of all excited states in single strands decay in this manner. Ultrafast mid-IR transient absorption experiments reveal that the long-lived excited states in a number of model compounds are charge transfer states formed by interbase electron transfer, which subsequently decay by charge recombination. The lifetimes of the charge transfer states are surprisingly independent of how the stacked bases are oriented, but disruption of π-stacking, either by elevating temperature or by adding a denaturing co-solvent, completely eliminates this decay channel. Time-resolved emission measurements support the conclusion that these states are populated very rapidly from initial excitons. These experiments also reveal the existence of populations of emissive excited states that decay on the nanosecond time scale. The quantum yield of these states is very small for UVB/UVC excitation, but increases at UVA wavelengths. In double strands, hydrogen bonding between bases perturbs, but does not quench, the long-lived excited states. Kinetic isotope effects on the excited-state dynamics suggest that intrastrand electron transfer may couple to interstrand proton transfer. By revealing how structure and non-covalent

J. Chen
Department of Chemistry and Biochemistry, Montana State University, Bozeman, MT 59717, USA

Department of Chemistry, Emory University, Atlanta, GA 30322, USA

Y. Zhang and B. Kohler (✉)
Department of Chemistry and Biochemistry, Montana State University, Bozeman, MT 59717, USA
e-mail: kohler@chemistry.montana.edu

interactions affect excited-state dynamics, on-going experimental and theoretical studies of excited states in DNA strands can advance understanding of fundamental photophysics in other nanoscale systems.

Keywords Base pairing · Base stacking · Charge transfer state · DNA photophysics · Excimer · Excited-state dynamics · Exciton · Femtosecond transient absorption · Proton-coupled electron transfer

Contents

Abbreviations

2AP	2-Aminopurine
8-oxo-dGuo	8-Oxo-7,8-dihydro-2′-deoxyguanosine
A	Adenine
AMP	Adenosine 5′-monophosphate
ATP	Adenosine 5′-triphosphate
C	Cytosine
CASPT2	Complete active space with second-order perturbation theory
CD	Circular dichroism
CI	Conical intersection
CPD	Cyclobutane pyrimidine dimer
CR	Charge recombination
CT	Charge transfer
dAMP	2′-Deoxyadenosine 5′-monophosphate
DFT	Density functional theory
ECCD	Exciton-coupled circular dichroism
ESA	Excited-state absorption

ESPT	Excited-state proton transfer
ET	Electron transfer
FC	Franck–Condon
FTIR	Fourier-transformed infrared spectroscopy
FU	Fluorescence upconversion
G	Guanine
GSB	Ground-state bleaching
IC	Internal conversion
IET	Intermolecular energy transfer
KIE	Kinetic isotope effect
MCT	Mercury-cadmium-telluride
O	8-Oxo-7,8-dihydro-2′-deoxyguanosine (in a DNA sequence)
PCET	Proton-coupled electron transfer
PMT	Photomultiplier tube
PT	Proton transfer
QM/MM	Quantum mechanical/molecular mechanical
RI-ADC(2)	Algebraic diagrammatic construction to second-order with resolution of the identity
T	Thymine
TA	Transient absorption
TCSPC	Time-correlated single photon counting
TD-DFT	Time-dependent density functional theory
TRIR	Time-resolved infrared spectroscopy
U	Uracil
UV	Ultraviolet
VC	Vibrational cooling
VUV	Vacuum ultraviolet
WC	Watson–Crick

1 Introduction

Photodamage to the genome is initiated by excited electronic states formed in DNA by the absorption of UV photons. Although the intensity of solar UV radiation reaching the surface of earth is attenuated by stratospheric ozone, excitation of DNA is highly efficient on account of the strong $\pi^* \leftarrow \pi$ transitions of the nucleobases: adenine (A), guanine (G), cytosine (C), thymine (T), and uracil (U). In order to *minimize* photochemical damage and *maximize* the photostability of the genome, DNA excited states should decay to the electronic ground state rapidly and with high quantum efficiency. Low fluorescence quantum yields and low photoproduct quantum yields provide evidence that this is the case, but detailed understanding of the rapid nonradiative decay pathways which deactivate excited states has been the goal of many investigators during the past decade.

The excited states of the naturally occurring nucleobase monomers have been studied intensively and there is growing consensus about photophysical decay channels [1, 2]. As the understanding of excited states of single nucleobases has grown, the complex photophysics in base multimers has attracted increased attention. The trend toward studying more complex systems has been aided on the one hand by better understanding of the excited states of single bases – the building blocks of DNA and RNA strands – and on the other by advances in computing power and quantum chemical methods which enable increasingly sophisticated calculations of the electronic structure of multi-base systems. Whereas calculations of excited states of single bases were considered to be barely tractable in 2000, high-level ab initio calculations are now performed on systems containing multiple bases.

Singlet excited states of nucleobase monomers decay in hundreds of femtoseconds to the electronic ground state. Typically, a nearly barrierless pathway leads from the Franck–Condon (FC) region to S_1/S_0 conical intersections (CIs) which cause the UV-excited nucleobases to return nonradiatively to their ground states on a time scale of hundreds of femtoseconds [1–5]. Other chapters in this volume provide detailed accounts of the nonradiative decay pathways of single bases in solution and in the gas phase, but we begin with this brief generalization about the ultrashort lifetimes of single nucleobases in order to highlight the unexpectedly long lifetimes seen in DNA strands. Excited states lasting tens to hundreds of picosecond are commonplace in single- and double-stranded DNA/RNA [1, 4, 6]. Current evidence suggests that the environment in a DNA strand doesn't just prolong the lifetime of excited states localized on single bases, but instead creates new classes of excitations and new photophysical pathways not found in base monomers. A full understanding of these mechanisms is not yet available, but this chapter will emphasize growing evidence that the relevant couplings act at short distances and are the result of π–π stacking between nucleobases.

A theme of this chapter is the link between structure and excited-state dynamics. This connection reveals why interest in DNA excited states goes beyond their pertinence to photodamage. First, the non-covalent interactions which give DNA its structure are the same as those found in other supramolecular and nanoscale architectures made from smaller organic building blocks. Consequently, knowledge of how these interactions mediate energy and electron transfer (ET) in DNA may provide a better understanding of these fundamental events in other systems. Second, excited states in DNA are strongly influenced by structure, and they can thus serve as powerful probes of dynamical motions in a DNA molecule. During the short lifetimes of excited states of native bases, large-amplitude motions such as backbone torsions or rotations about glycosidic bonds are limited, and the shortest-lived excited states probe static structures, as in the case of thymine dimer photochemistry [7, 8]. A significant fraction of excited states formed in base stacks have lifetimes of up to several hundred ps [9], making them sensitive to conformational fluctuations on longer time scales. Finally, modified bases such as 2-aminopurine (2AP) have lifetimes in the nanosecond range, as monomers [10–12], and can potentially probe dynamics on still longer time scales. Comprehensive knowledge

of decay pathways of excited states of native and modified nucleobases, and of other excited state probes, is critical for extracting insights into the structural dynamics of nucleic acids from time-resolved spectroscopy.

This chapter reviews current understanding of excited states in single- and double-stranded DNA in aqueous solution obtained from ultrafast laser experiments. Although many of the model systems of greatest interest to us have been studied only by the femtosecond transient absorption (fs-TA) technique, results from time-resolved emission techniques, such as time-correlated single photon counting (TCSPC) and femtosecond fluorescence upconversion (fs-FU), will be discussed when appropriate. Comparison of results obtained from time-resolved absorption and emission experiments can bring greater insights than is possible from either technique alone. The femtosecond laser techniques used to observe excited-state dynamics in DNA model compounds are outlined in Sect. 2. The transient absorption and time-resolved emission techniques are discussed briefly with emphasis on what these techniques reveal about excited-state dynamics in DNA strands.

Section 3 discusses the three-dimensional structures adopted by the nucleic acid model compounds which have been most studied to date, including dinucleotides, and single- and double-stranded oligonucleotides. The spatial arrangement of nucleobases in DNA determines the couplings that give rise to new deactivation pathways not found in base monomers. The underlying interactions responsible for nucleic acid structure are also discussed. These are sufficiently weak that it is more accurate to consider the distribution of structures present in solution at ambient temperature than to imagine a single, well-defined structure. The relatively flat free energy landscapes governing the three-dimensional structure of nucleic acids are responsible for the structural disorder which must be carefully considered in order to interpret experimental results correctly. This section ends with an overview of excited states created by UV radiation in DNA strands.

Section 4 begins by summarizing experimental evidence that π–π stacking by nucleobases gives rise to fundamentally new decay channels. These effects are already seen in minimal π stacks of just two bases, so our discussion begins with the time-resolved spectroscopy of dinucleotides before taking up excited states in longer single strands containing more than two bases. The effects of base pairing on excited states are discussed in Sect. 5 for single base pairs in solution and for larger systems in which bases are both stacked and paired. The progression from dinucleotides to duplex DNA emphasizes how excited states in simpler model systems are influenced by the increasing complexity found in larger ones. Finally, Sect. 6 presents a summary and an outlook describing unsolved issues and promising new research directions.

2 Ultrafast Spectroscopy Techniques

The lifetimes of excited states of DNA strands are often orders of magnitude longer than those of single bases [13], as discussed in Sects. 4 and 5. These observations from time-domain spectroscopy have been a driving force for advancing understanding of DNA photophysics. Indeed, the ability to observe excited-state dynamics of DNA directly in the time domain with femtosecond time resolution has been singularly important to progress in the field. The well-known fact that the steady-state absorption spectrum of a DNA strand is very similar in appearance to the sum of the spectra of its constituent nucleotides points out the limits of relying solely on frequency-domain spectroscopy to understand excited states of DNA strands in solution.

In this section, we review the ultrafast spectroscopic techniques used to study excited-state dynamics in DNA with an emphasis on the observables and the inferences that can be obtained from them. The aim is to provide non-specialists and beginning researchers with an overview of the ultrafast laser techniques used to study DNA excited states with just enough detail so that the conclusions that practitioners of these techniques have drawn from their experiments can be better understood. Readers interested in technical details of any of the techniques may consult the cited references for more information.

Because our focus is on solution studies, we will exclude the many innovative techniques used to study DNA model compounds in the gas phase. An overview of gas-phase spectroscopic techniques is provided in Sect. 3 of [5], and descriptions of femtosecond pump-probe experiments that use sensitive photoionization detection of electrons and molecular ions to compensate for the low number densities of gas-phase species provide additional details [14–16].

Ultrafast laser techniques for studying excited states of DNA in solution can be divided into techniques that monitor absorption or techniques that monitor emission as a function of time after the sample is excited by an ultrashort (femtosecond or picosecond) laser pulse. Because nucleic acids made from the canonical bases absorb only very weakly above 300 nm, most spectroscopic studies have used UVB or UVC laser pulses, although more concentrated solutions of oligonucleotides have recently been studied using UVA excitation [17]. The third harmonic output from a titanium sapphire laser system – the nearly universal source used in femtosecond experiments – is conveniently located near 260 nm, in the vicinity of the wavelength of maximum absorption of most DNA samples. Tunable deep UV pulses can be generated from the ~800-nm fundamental using various frequency upconversion schemes and optical parametric amplification. Many modified bases [10, 11] absorb at longer wavelengths (>300 nm) than the canonical bases, making it possible to excite these chromophores selectively when they are incorporated in a DNA strand.

In the femtosecond transient absorption (fs-TA) technique, a femtosecond pump pulse creates initial excited states (thick purple arrow in Fig. 1a), which are detected through changes in the transmission of a time-delayed probe pulse (Fig. 1a–e).

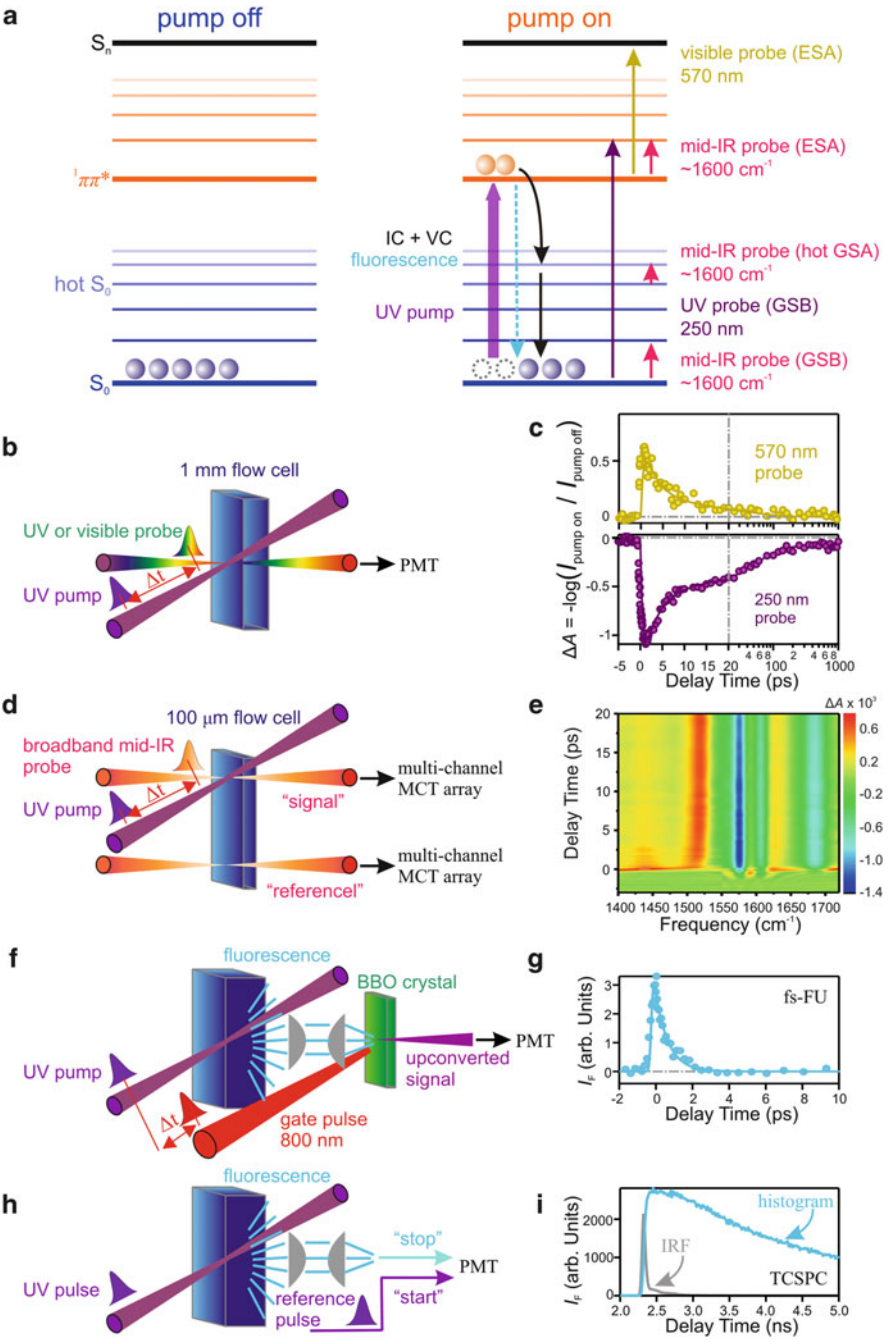

Fig. 1 (**a**) Ground- and excited-state populations in a DNA model compound before (*left*) and after (*right*) excitation by a UV pump pulse to a $^1\pi\pi^*$ state (*thick purple arrow*). After photoexcitation, the excited-state population returns to the ground state via fluorescence (*blue dashed arrow*), or ultrafast internal conversion followed by vibrational cooling (IC + VC, *black arrows*). Decay to charge transfer/excimer or other excited states is also possible, but not shown.

Many fs-TA experiments on DNA systems use UV- (long thin purple arrow in Fig. 1a) and visible-wavelength probe pulses (thin gold arrow in Fig. 1a), which monitor electronic transitions, but mid-IR probe pulses (red arrows in Fig. 1a) obtained by difference-frequency mixing of two near-IR pulses provide an alternative way to study excited states through measurement of time-dependent vibrational resonances in both ground and excited electronic states. The TA technique with mid-IR probe pulses is often referred to as time-resolved IR (TRIR) spectroscopy [18, 19]. Schematic illustrations of these TA techniques and typical signals are shown in Fig. 1b–e. Additional experimental details about these techniques can be found in the literature [18, 20–22].

In all fs-TA experiments, excited states created by the excitation or pump pulse, as well as any excited states or photoproducts populated at later times, are detected through changes in the transmission of the probe pulse. The TA signal, whether measured at a single wavelength or in broadband mode, records changes in the sample absorbance (ΔA) induced by the pump pulse and calculated as

$$\Delta A = -\log\left(\frac{I_{\text{pump on}}}{I_{\text{pump off}}}\right), \tag{1}$$

where $I_{\text{pump on}}$ and $I_{\text{pump off}}$ are the probe pulse intensities measured at the detector with and without the presence of the pump pulse, respectively. The probe beam can be split into "signal" and "reference" portions – the former is spatially overlapped with the pump pulse, while the latter is not – in order to reduce the shot-to-shot noise and improve the instrument sensitivity (Fig. 1d). In this case, ΔA is calculated using (2):

$$\Delta A = -\log\left(\frac{I_{\text{signal, pump on}} \,/\, I_{\text{reference, pump on}}}{I_{\text{signal, pump off}} \,/\, I_{\text{reference, pump off}}}\right). \tag{2}$$

TA is therefore a form of difference spectroscopy. The contribution to the TA signal from each transient species is proportional to its population multiplied by the difference between its absorption cross section and the cross section of the ground

Fig. 1 (continued) The excited-state population can be probed by visible (*gold arrow*) or mid-IR (*top red arrow*) pulses. UV (*deep purple arrow*) or mid-IR (*bottom red arrow*) pulses can be used to monitor the ground state population. Mid-IR can also probe the hot ground state absorption (*middle red arrow*). (**b–i**) Schematic illustrations of various ultrafast laser methods and representative signals. (**b**) fs-TA experiment using a single-color UV or visible probe pulse and (**c**) typical kinetic traces produced by visible probe-detected ESA (*top*) and UV-probe GSB (*bottom*). (**d**) fs-TRIR with broadband mid-IR probing showing the use of a reference beam to improve the signal-to-noise ratio. Signal and reference beams are spectrally dispersed in a spectrograph and detected by dual multi-element Mercury-Cadmium-Telluride (MCT) arrays cooled by liquid nitrogen. (**e**) Representative time- and frequency-resolved fs-TRIR data. (**f**) fs-FU technique and (**g**) a typical emission transient. (**h**) TCSPC experiment and (**i**) typical data. Note the 1,000-fold difference in time scale in (**g**) and (**i**)

state from which the transient population originated with both cross sections measured *at the probe wavelength*.

Exited-state absorption (ESA), ground-state bleaching (GSB), and stimulated emission can all contribute to TA signals. The importance of each depends on the probe wavelength chosen and the cross sections for the relevant transitions. ESA by the lowest $^1\pi\pi^*$ states of the base monomers gives rise to broad and featureless bands at visible and near UV wavelengths. For the canonical bases, a broad band occurs with λ_{max} near 600 nm, and a second, stronger, band is observed with λ_{max} below 400 nm [23, 24].

The decay of ESA at visible probe wavelengths was used to make the first accurate measurements of the $^1\pi\pi^*$ state lifetimes of DNA and RNA nucleosides in 2000 [25, 26]. The ESA cross sections of the lowest singlet excited states (S_1 states) of the various bases are very weak, and care should be taken to differentiate these signals from absorption by solvated electrons, which are easily produced by the high intensity pump pulses used in femtosecond laser experiments [26]. The detailed procedure used in our laboratory for subtracting the solvated electron signals is described in [27]. The weak ESA signals make TA studies with broadband detection difficult, and detailed comparisons of ESA spectra for the various base monomers are unavailable. Nonetheless, current information suggests that ESA spectra of the $\pi\pi^*$ singlet states of the base monomers are very similar. For example, the broadband TA spectra are remarkably similar for adenine and guanine [23, 24]. This lack of differentiation is perhaps unsurprising, given their similar ground-state absorption spectra. Too little is known about ESA spectra of base multimers to offer generalizations.

A powerful alternative to measuring excited-state lifetimes is to interrogate the repopulation of the ground state in GSB recovery experiments. In these measurements, the probe wavelength in an fs-TA experiment is tuned to a region where the ground state molecules absorb, typically in the deep UV (e.g., 250 nm) for nucleobases (thin purple arrow in Fig. 1a). The GSB signals can easily be measured because of the large ground-state absorption cross sections of the nucleobases, and GSB signals can be readily interpreted because interference from solvated electrons, which absorb negligibly at UV wavelengths [28], is greatly reduced. The obtained ΔA signal is negative, signifying the removal of ground-state population by the UV pump pulse (see (1) and (2)). As excited molecules return to the ground state, the ΔA signal approaches zero (purple trace in Fig. 1c). The observed kinetics thus measures the time for population to return to the thermally equilibrated electronic ground state. Significantly, this time can be measured without knowledge of the series of states that excited molecules pass through. Particularly when a small number of excited states or intermediates are involved, bleach-recovery TA measurements can make it possible to observe clearly the dynamics of excited states that may have weak excited-state absorption, or which may absorb at unknown wavelengths, and therefore be difficult to study. For example, bleach recovery measurements first identified a longer-lived excited state in pyrimidine nucleobases [29].

A critically important point is that whenever the time to jump from an excited state to the ground state in a nonradiative transition is short compared to the time required for solute-solvent vibrational energy transfer, the GSB kinetics are dominated by decay of vibrationally hot ground state molecules. In this case, the GSB signals measure the time for vibrational cooling (VC) and not the faster time that corresponds to the initial transition to the ground state. The ultrashort lifetimes of monomeric bases thus cause GSB signals to decay up to an order of magnitude more slowly than the disappearance of ESA at visible wavelengths. Because of its hydrogen-bonding network, VC proceeds with remarkable speed in water. Ultrafast internal conversion (IC) produces ground state molecules with an initial vibrational temperature on the order of 1,000 K. Nonetheless, this excess vibrational energy is transmitted to the solvent with a time constant of just 2 ps for adenine [30], while somewhat slower times of 5 or 6 ps have been observed for nucleobase derivatives such as caffeine which have fewer hydrogen bond donor groups [21]. In fs-TA experiments that monitor GSB kinetics, bleached ground state signals frequently exhibit a several picosecond component, and this is a valuable indicator that at least some excited states in a DNA model compound have returned via IC on a time scale that is faster than VC (i.e., faster than several picoseconds).

In fs-TA experiments, the kinetics observed at very early times, i.e., within the pulse duration of the pump and probe pulses (typically, $t < 200$ fs), are usually contaminated by signals arising from two-photon absorption [31] and/or cross phase modulation [32] from the sample (typically the solvent because of its high concentration) or the cell windows (if a static or flow cell is used). These signals, frequently called "coherent artifacts," are seen when the pump and probe pulses are temporally overlapped, and thus hinder the ability to observe extremely fast kinetics. In order to probe shorter time scales, ultrashort UV pulses produced by four-wave mixing [33] and a windowless, free-flowing liquid jet [34] can be used. Note, however, that the former increases the peak intensity of the pump pulses, while the latter usually requires solution volumes larger than are practical for DNA samples. Importantly, analysis of our fs-TA signals is restricted to delay times longer than ~200 fs to avoid these issues.

Because of inhomogeneous and homogeneous broadening, electronic transitions in DNA model compounds usually overlap strongly, making it difficult to disentangle kinetics from fs-TA experiments. fs-TRIR experiments monitor vibrational resonances (red arrows in Fig. 1a) and have the advantage that overlap between vibrational transitions can be greatly reduced, aiding kinetic interpretation. Typically, each nucleobase has one or more distinctive vibrational bands in the double-bond stretching region, where strong transitions caused by carbonyl and ring stretches are observed. These experiments are typically carried out in D_2O solution because of its greater mid-IR transmission compared to H_2O. As will be discussed below, the localized, base-specific character of vibrational modes offer an exciting, but underutilized approach to investigate excited states in multichromophoric systems.

In fs-TRIR experiments, the broad bandwidth of the mid-IR pulses (~200 cm^{-1} for a 100-fs pulse with a center wavelength of ~6 μm) is used to record ΔA signals

as a function of both time and frequency, producing two-dimensional data as in the example shown in Fig. 1e. As in the case of the fs-TA experiments that probe electronic transitions, fs-TRIR signals are composed of negative and positive signals. Negative signals arise from bleaching of ground-state vibrations, while positive signals arise from vibrations in excited electronic states and from fundamentals of highly vibrationally excited ground-state molecules. The latter species show distinctive sigmoidal signals in which the bleaching of a ground state resonance is accompanied by positive absorption on its red edge caused by anharmonicity [35]. This is the distinctive signature of VC dynamics in fs-TRIR experiments.

When excited states generated by the pump pulse can decay radiatively (blue dashed line in Fig. 1a), time-domain emission measurements are possible. Measurements can be made on ultrafast time scales using the Kerr-gated time-resolved fluorescence technique [23] or, more commonly, by fluorescence upconversion [36]. In the femtosecond fluorescence upconversion (fs-FU) technique, emission from the solution sample is typically collected using a parabolic mirror (illustrated by a lens system in Fig. 1f in order to simplify the illustration) and subsequently mixed with a time-delayed, femtosecond gate pulse in a nonlinear optical crystal to generate an upconverted signal at a higher frequency (Fig. 1f, g). Varying the arrival time of the gate pulse at the mixing crystal allows the emission decay to be recorded with subpicosecond time resolution. Importantly, fluorescence lifetimes obtained by fs-FU experiments on nucleobase monomers [36–39] are in excellent agreement with the decay time of ESA signals measured in fs-TA experiments [25, 26]. However, discrepancies between fs-TA and fs-FU measurements on DNA strands have occasionally led to confusion about excited-state decay pathways. Dynamic range limitations mean that upconversion experiments emphasize emission by brighter $^{1}\pi\pi^{*}$ states and it can be difficult to detect emission from darker states.

The extremely sensitive time-correlated single-photon counting (TCSPC) technique can detect smaller populations than can be accurately quantified in either fs-TA or fs-FU experiments. However, this method achieves sensitivity at the cost of time resolution. In TCSPC, no gate pulse is used and emission is measured directly using a fast photodetector and specialized electronics. Typically, time resolution of several tens of picoseconds is achieved using a micro-channel plate photomultiplier tube (PMT) (Fig. 1h, i). Because TCSPC measurements cannot measure the fastest emission decay components, it is necessary to combine them with fs-FU measurements to obtain a complete picture of the emission over many decades in time [40]. Notably, the high sensitivity of the TCSPC method means that the characterization of extremely weakly emitting DNA excited states could be adversely affected by impurities, and careful background correction and well-designed protocols are essential [41].

The time resolution achievable with each of the above techniques is an important experimental consideration. In all pump-probe techniques, varying the path length traversed by one of the pulses using a retroreflector mounted on a computer-controlled translation stage is used to control the delay time between pulses.

The time resolution is independent of the response time of the photodetector used, and is determined instead by the temporal widths of pump and probe pulses, which can be as short as ~10 fs. The group velocity of a femtosecond laser pulse is a function of its center wavelength. For this reason, femtosecond pulses with widely separated center wavelengths transit the solution sample at different speeds. This effect causes initially synchronized pump and probe pulses to "walk off" one another, degrading the time resolution. The walk off problem in fs-TRIR experiments is mitigated somewhat by the thinner sample path length of ~100 μm compared to the 1 mm path length which is typical of fs-TA measurements with visible and UV probe pulses. For the instrumentation in our laboratory, an instrument response function of between 100 and 200 fs is achieved for visible and UV probe experiments, while our fs-TRIR measurements have a time resolution of approximately 400 fs. Geometrical factors can smear the arrival times of emitted photons at the upconversion crystal and the time resolution of our upconversion setup is around 300 fs.

The fs-TA technique requires high intensity pulses with single-pulse energies of hundreds of nanojoules or more. These pulses are provided by a chirp-pulse amplified titanium sapphire laser system. TCSPC and fs-FU measurements do not require high pulse energies and the excitation source can be an unamplified femtosecond oscillator. The typical pulse repetition rate of an unamplified laser system of 80 MHz compared to the kilohertz repetition rate of an amplified source is a key to the high signal-to-noise ratio obtainable with TCSPC instrumentation.

3 Nucleic Acid Structure

The striking differences between excited state relaxation in single bases and in DNA and RNA strands are the result of how the bases are arranged in space. Knowledge of nucleic acid structure is thus a prerequisite for understanding nonradiative decay pathways. The spatial arrangements of the absorbing moieties in multichromophoric molecules such as DNA determine the couplings responsible for decay channels such as energy and electron transfer which are not possible in single chromophores.

The non-covalent interactions of base stacking and base pairing are responsible for DNA secondary structure and thus control the separation between coupled bases and their mutual orientations. However, it must be kept in mind that nucleic acid structures are constantly fluctuating in aqueous solution at physiological temperature – a fact which may be forgotten when one considers only the familiar yet static structures of double helical DNA obtained from X-ray crystallography. Because most nucleic acid model systems do not populate deeply trapped structures, it is vital to consider structural heterogeneity and disorder. Most di- and oligonucleotides are characterized by broad distributions of structures, which may be separated by free energy barriers that are no greater than thermal energy (k_BT). Of course, this heterogeneity fulfills a biological purpose – DNA's marginal stability enables

enzymes and other molecules to interact with, process, and alter DNA at physiological temperatures.

In this section, we emphasize the structural attributes of DNA important for interpreting photophysical experiments and provide an overview of DNA electronic structure. Here, "DNA" is shorthand for all nucleic acid model compounds, including those with RNA backbones, chosen by experimentalists for ultrafast laser experiments. The choice of compounds is driven by a reductionist philosophy and many of the systems (e.g., dinucleotides) are obviously far removed from what a biologist understands by DNA (or RNA). Nevertheless, even these "simple" model systems have considerable structural complexity that must be understood to interpret spectroscopic experiments correctly.

3.1 Base Stacking

The nucleobases are planar aromatic molecules which tend to aggregate (self-associate) in aqueous solution even when they are not covalently linked [42, 43]. This tendency is greatest for the purine bases with their larger hydrophobic surfaces, but it is also significant for the pyrimidines. The nucleobases form stacked dimers that resemble the sandwich geometries adopted by dye molecules that form H-aggregates [44]. The distinguishing feature of a base stack is that both bases lie in parallel or nearly parallel planes and are in van der Waals contact. The perpendicular distance between bases is on the order of ~3.4 Å and solvent molecules are excluded from the region of base-base overlap seen when the stack is viewed along a direction perpendicular to the base planes (Fig. 2).

The π–π stacking or base stacking geometry is a distinctive feature of DNA structure and one that accounts for most of the stabilization energy of the double helix [45]. Bases in single-stranded DNA also stack and this can be detected through both classical methods such as exciton-coupled circular dichroism (ECCD) [46–49] and UV melting (hypochromism) [45], as well as through less well-known techniques such as single-molecule stretching experiments [50, 51], velocity sedimentation analysis [52], and from the electrophoretic mobility of gapped duplexes [53].

In contrast to duplex forms, single strands melt non-cooperatively over a broad temperature range and are not amenable to study by X-ray crystallography. MD simulation can potentially provide insights into both structure and dynamics in atomistic detail, but the popular force fields used in these simulations may overstabilize base-stacked structures [54, 55]. Consequently, there is considerable uncertainty about both the distribution of structures that a single-stranded oligonucleotide can adopt in aqueous solution and the time scales for structural interconversion.

The full specification of the geometry of a stack of two bases requires some of the same coordinates used for stacked base pairs [56]. One of the bases may be

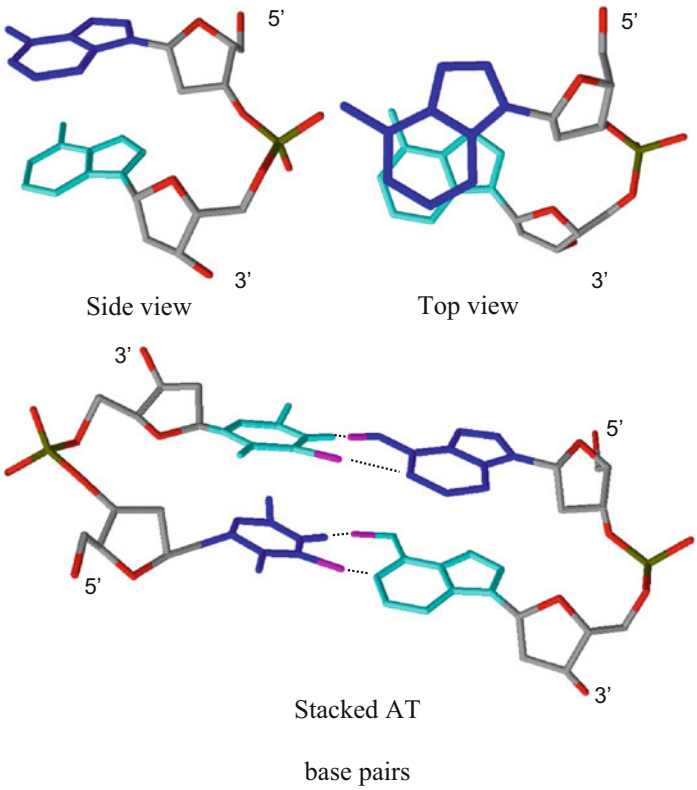

Fig. 2 *Top*: Structure of dApdA showing the face-to-back stacking motif found in the B-DNA helix. The 5′ base is shown in *dark blue*, and the 3′ base is shown in *light blue*. The *top view at right* shows that the bases form a right-handed helix (the 5′ base is on top) and illustrates the region of base-base overlap. *Bottom*: Stacked adenine and thymine base pairs with hydrogen bonds shown by *dashed lines*. Structures are illustrative and were drawn using the ACD/ChemSketch software

displaced in a direction parallel to its base plane (a parameter known as slide in double strands [56]), but the perpendicular distance between the base planes generally shows little variation for two bases in the electronic ground state and is similar to the distance of closest approach between two aromatic molecules (3.4 Å in double-stranded B-DNA). It is also necessary to specify the torsion angle between a vector lying in the plane of one base, and a second vector in the plane of the second base. This torsion angle specifies the rotational setting or 'twist' between the stacked bases.

Each nucleobase also has distinguishable faces resembling the two sides of a coin [57], and it is necessary to specify which of the two distinguishable faces of each nucleobase is oriented toward the other base. This latter information is generally overlooked because stacking in regular double-stranded DNA is face-to-back, but face-to-face and back-to-back stacking motifs are possible in aggregates and in model single strands with flexible, modified linkers [58]. Unfortunately,

the nomenclature used in the literature is frequently ambiguous or contradictory and careful inspection is needed to determine the actual structure. For example, references to face-to-face motifs in [59] are more properly described as face-to-back stacks with a fully eclipsed geometry (twist angle of 0°).

Calculations of intrinsic (gas-phase) stacking energies have considered mostly face-to-back stacks (the stacking motif found in duplex DNA) and investigators have often ignored the possibility of face-to-face stacks [60]. For example, Florián et al. in their study of nucleobase dimers only performed calculations for face-to-back dimers, and assumed that face-to-face dimers are less stable [61]. This may be incorrect for systems with modified linkers or no linkers (aggregates). In fact, a face-to-face dimer is predicted to be the global minimum energy structure for a uracil–uracil stack [60]. It is important to search for both face-to-back and face-to-face stacks and careful selection of the base stacking coordinate may help achieve this goal [62].

Base stacks in B-DNA have a right-handed twist angle (Fig. 2), but this is by no means the only possible conformation. In the gas phase, an antiparallel alignment of the permanent dipole moments of each base minimizes dipole–dipole repulsion, but in solution a parallel alignment is preferred in order to maximize the solvation energy, which varies as the square of the total dipole moment in the Onsager model [60, 61]. Overall, the electrostatic energy of two stacked bases in the gas phase is acutely sensitive to the twist angle, but solvent screening greatly reduces this sensitivity [61, 63, 64]. Calculations indicate that the interaction energy of two stacked bases in aqueous solution depends only very weakly on the twist angle between the bases as long as there is at least some overlap between their π faces [61].

Differences in stacking free energies between the gas phase and aqueous solution are a reminder that water is critically important for stabilizing base stacks. At the low concentrations (several mM) used in most ultrafast laser experiments, nucleobase monomers will aggregate or self-associate in stacks of two or more bases instead of forming hydrogen bonds with each other [65, 66]. Self-association by hydrogen bonding does occur for the guanosine mononucleotide, but only becomes important at high concentrations above 100 mM [67]. In solvent-free (gas-phase) conditions, or in low polarity solvents [68–71], bases preferentially form base pairs. In the gas phase, two adenine molecules form a hydrogen-bonded base pair [16, 72], but blocking hydrogen-bonding sites by methylation leads to base stacks [72, 73]. Interestingly, clustering with only a few water molecules is sufficient to transform the A–A base pair into a stack [16]. Hydrogen bonding between ribose groups of nucleosides in the gas phase may also favor stacking [73].

In the end, base stacking in solution results from a delicate balance of forces between the intrinsic or *in vacuo* stacking energy and hydrophobic interactions [61, 64, 74]. The interaction is enthalpy driven, yet hydrophobic [75]. Stacking is exothermic ($\Delta H < 0$) but entropically disfavored ($\Delta S < 0$) such that stacked structures are preferred at low temperature, but bases unstack as the temperature is raised. Traditionally, NMR, CD, and UV hypochromism have been used to quantify the fraction of stacked bases in dinucleotides by fitting temperature-dependent

measurements to a two-state model in which the two bases are either stacked or unstacked [76–78].

These experiments reveal that base-stacked structures of dinucleotides are only weakly stabilized near room temperature. For example, stacks formed by two adenines, the canonical base with the greatest propensity for stacking [79], are stabilized by a ΔG of only about -0.9 kcal mol^{-1}. For dApdA, the fraction of stacked dinucleotides at 25°C is approximately 80% (reviewed in [58]). The weakness of this interaction means that a distribution of stacked conformers exists in aqueous solution. Although the backbone probably influences the kinds of stacked geometries that are preferred, it does not appear to influence significantly the stability of DNA base stacks.

3.2 Base Pairing

Base pairing is the association of two nucleobases by hydrogen bonding. The familiar Watson–Crick (WC) base pairs found in double-stranded DNA are sized such that the distance between the C1′ atoms of sugars on opposite strands is the same for A·T and G·C base pairs [80]. This enables any sequence of base pairs to fit into the double helix structure without distortion. Non-WC base pairing motifs are also important, particularly in RNA. Two non-WC motifs, important in model systems which have been the subject of photophysical investigations [81–86], are shown in Fig. 3.

Although it is straightforward to study single-stranded model compounds containing only stacked bases, no model system has been found which allows single base pairs to form in water, although they can be investigated in non-aqueous solvents (see Sect. 5.1). Instead, base stacking appears to be the inevitable companion of base pairing in aqueous solution. As discussed in Sect. 5, the simultaneous presence of base stacking and base pairing interactions in aqueous solution has made it difficult to isolate effects on photophysics from interbase hydrogen bonds. One effect which has come into focus recently is VC following ultrafast IC. In a base pair, hydrogen bonds to one or more solvent molecules are replaced by hydrogen bonds which join functional groups on the two bases. Base pairing thus reduces the number of hydrogen bonds that can be formed with water molecules. As discussed in Sect. 5.2.1, this can retard the rate of VC by slowing intermolecular vibrational energy transfer from the UV-excited chromophore to the surrounding water molecules.

3.3 Structural Complexity and Disorder

Complexity and disorder are two other traits of nucleic acids in room-temperature aqueous solution. A given base in a natural DNA or RNA strand is generally flanked

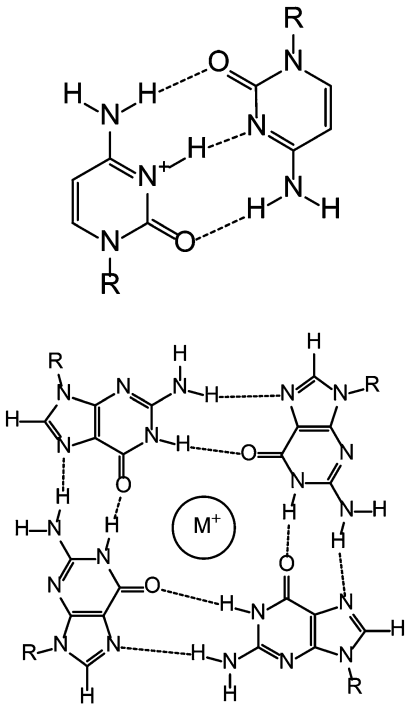

Fig. 3 Example non-WC base paired motifs found in DNA model systems that have been studied by ultrafast laser spectroscopy [81–86]. *Top*: Hemi-protonated CC base pair in which two cytosines share a single proton. *Bottom*: The G-quadruplex motif in which four guanines self-assemble around a central metal ion. *Dashed lines* indicate hydrogen bonds

by any one of four bases. The presence of minor bases such as 5-methylcytosine and 5-hydroxycytosine in DNA or any of the RNA minor bases further increases the number of possible nearest-neighbor bases. The consequences of this complexity for excited-state dynamics [87] can be explored, at least in principle, by performing (a possibly large number of) experiments on DNA oligonucleotides of appropriate sequence. More insidious is the conformational complexity which results in large numbers of structures of comparable free energy in solution – structures which may be poorly understood.

Conformational heterogeneity is manifest in different ways. In dinucleotides, stacked and unstacked bases can co-exist in equilibrium, but the stacked structures may be characterized by broad distributions of structures in which the twist angle and the stacking motif (face-to-face, face-to-back, etc.) are variables. In single strands, a wide variety of experimental techniques provide clear evidence that bases in single-stranded DNA and RNA sequences can stack with nearest neighbors [51, 88–90]. The question arises whether stacking by two bases affects the probability that a third base will stack on either end. Experimental consensus is that base stacking is mostly non-cooperative in single strands [91]. The lack of cooperativity is responsible for the broad UV melting curves observed for DNA single strands. An important consequence of non-cooperative base stacking is that the average length of stacked domains in a single-stranded oligonucleotide such as $(dA)_n$ can be quite short, even though the majority of bases are stacked with neighbors

[9, 91]. Consequently, the room-temperature structure of an oligonucleotide such as $(dA)_n$ in aqueous solution is thought to be similar to that of a rod–coil multiblock copolymer made of many short helical domains [51, 91, 92]. In Sect. 4.2.2 we argue that this stacking disorder, and not exciton delocalization, is responsible for the systematic variation in the amplitudes of fs-TA signals.

Base pairing can introduce further structural disorder. For example, base pairs near the terminus of a DNA strand open more readily than interior base pairs, an effect known as end fraying (see structure **1** in Fig. 12). Based on the rate of exchange of imino protons measured in NMR experiments, Guéron and coworkers concluded that the dissociation constant describing base pair opening of the terminal AT base pair in a self-complementary DNA octamer is 0.6 at 0°C [93]. This is higher by a factor of 40 than for a terminal GC base pair, which has three hydrogen bonds vs the two found in the AT base pair. A second kind of disorder concerns the ensemble of double-stranded structures which may be present in aqueous solution. The repetitive base sequences found in the AT-rich systems such as $(dA)_{18} \cdot (dT)_{18}$ and the alternating duplex $(dAdT)_9 \cdot (dAdT)_9$ which have been favorite systems for ultrafast laser investigations have relatively low melting temperatures and can undergo strand slippage (structure **2** in Fig. 12).

Complexity is also present in the form of structures that may not be anticipated from the secondary-structure elements found in regular B-DNA. For example, G- and C-rich sequences can spontaneously fold into G-quadruplex [94] and i-motif [95, 96] structures, respectively. The non-canonical base pairs that occur in these structures are shown in Fig. 3. Excited-state dynamics in novel DNA structures such as these will not be discussed here, but can be read about elsewhere [81–86]. Knowledge of the many ways that DNA can self-assemble into higher-order structures is clearly needed to interpret spectroscopic experiments correctly, which putatively investigate ‘standard’ single and double strands. For example, $(dG)_n$ sequences cannot be used to study G-on-G stacking in single strands because they will form G quadruplex structures in room-temperature aqueous solution [97].

3.4 Electronic Structure

Having introduced some basic structural characteristics of nucleic acids, we end this section with an overview of the types of excited electronic states found in DNA. In a multichromophoric molecule such as DNA, the singlet $\pi\pi^*$ and $n\pi^*$ states of single bases can interact to form new, delocalized excitations that span two or more bases. The electronic coupling which gives rise to these new states is sensitive to interbase separation and orientation. For this reason, spatial structure profoundly influences electronic structure in DNA.

Delocalized excitations can be approximately categorized as Frenkel excitons or charge transfer (CT) states, but mixing between these limiting cases is also possible [98, 99]. The former are neutral excited states which result from excitation resonance between degenerate or nearly degenerate transitions located on two or more

bases. When the coupled chromophores are separated by more than about 6 Å, relatively long-range electrostatic coupling between transition dipole moments of energetically similar transitions gives rise to Frenkel excitons [100–102]. At shorter intermolecular distances, there are major contributions to the electronic coupling from orbital-orbital overlap, and excimer (exciplex) states can be formed [103].

Although exciton is a general term frequently used to denote *any* excited state in a multichromophoric system, we will use exciton hereafter as a synonym for 'Frenkel exciton,' following common usage in the field. It should be kept in mind that 'excimer' (=excited dimer) and 'exciplex' (=excited complex) are similarly generic terms which in principal apply to any excited state of two chromophores with significant orbital-orbital overlap. Such states exist on a continuum running from contact ion pairs generated by the transfer of a full electron between molecules to states with strong mixing from locally excited or excitonic states [104]. Strong and short-range interactions can also lead to covalent bond formation in the excited state in both excimers and exciplexes [59, 105–108]. Clearly, anyone hoping for a completely unambiguous specification of the character of an excited state involving two chromophores will be disappointed by these terms. We will use excimer and exciplex hereafter, as they are used widely in the literature, but we shall also supplement them with terms such as 'ion pair state,' 'CT state,' and 'bonded excimer,' as appropriate, to provide additional description about an excimer state when this information is available either from experiment or calculations.

A full understanding of excited-state dynamics in DNA requires knowledge of the nature, spatial extent, lifetimes, and yields of excited states created by UV radiation. Of interest are the states reached in absorption and excited states not populated initially, but which are decay intermediates. Sections 4 and 5 explore these 'intermediate' excited states in detail. Here, we summarize briefly what is known about the excited states populated by UV absorption. Theory indicates that excitons in assemblies of bases can be delocalized over as many as two to three bases [40, 109]. They constitute a dense band of states which are affected by conformational disorder and homogeneous broadening, and which can vary widely in oscillator strength [110, 111] The strong absorption by DNA strands at UVB and especially UVC wavelengths arises overwhelmingly from bright excitonic states with little contribution from CT states on account of the low oscillator strength of the latter states [112]. Markovitsi and coworkers have argued that the very weak tail absorption by DNA oligonucleotides in the UVA spectral region is caused by direct excitation of weak CT states [17, 113]. At wavelengths longer than 320 nm, the molar absorption coefficient per base is typically not much greater than 10 M^{-1} cm^{-1}. Even though the CT states lie above the lowest energy excitons at the ground state geometry (see Sect. 4.1.5), greater inhomogeneous broadening is proposed to make them the only absorbers above 320 nm. Motivated by interest in UVA photochemistry by DNA, a few studies have appeared on the UVA spectroscopy of DNA [17, 113], but our focus in the remaining sections will be on experiments performed with UVB/UVC excitation. For such studies, the initial excited states are excitons.

4 Excited-State Dynamics in Single Strands

In this section, we consider excited states in single strands of DNA in which the nucleobases stack with one another, but lack interbase hydrogen bonds. Strikingly, a substantial fraction of excited states formed in single strands relax orders of magnitude more slowly than those of single bases (Fig. 4). These states, which appear in model compounds with two or more π-stacked bases, are referred to as long-lived excited states [1, 4, 13, 22, 23, 27, 87, 114–123] to contrast them with the subpicosecond excited states of the nucleobase monomers. Prominent long-lived signal components, with lifetimes of between a few and several hundred picoseconds, are seen in GSA and ESA signals recorded in fs-TA experiments, as discussed below. Even longer-lived states have been observed, especially using the sensitive TCSPC technique, although the quantum efficiency for reaching these states appears to be very low at UVB and UVC wavelengths. Confusingly, "long-lived" tends to mean "10–200 ps" in the literature describing fs-TA experiments (e.g., in [9]), while it generally means ">1 ns" in papers discussing fluorescence decay curves measured with the TCSPC technique (e.g., in [124]). The difference arises from the longest time scales that can be readily probed by the respective techniques. Consequently, comparisons should be made cautiously.

Long-lived excited states were first seen in fs-TA measurements on the single-stranded homopolymers poly(A) and poly(dA) [27]. This study showed that raising the temperature reduces the magnitude of the long-lived signal component (τ ~154 ps). The attenuation of the long-lived signal at high temperature was interpreted to mean that these states are formed in base stacks because base stacking is progressively disrupted at elevated temperature [125, 126].

Later experiments showed that essentially identical long-time signals are observed in the dinucleotide ApA and in the much longer homopolymer poly (A) [6], suggesting that the long-lived excited states have a spatial extent of no more than two bases. Dinucleotides (i.e., dinucleoside monophosphate compounds in which just two bases are joined by a phosphodiester linkage; see structure of dApdA in Fig. 4) are minimal-length single strands, which have taken on great importance in studies of DNA excited states. For this reason, we begin by discussing the excited-state dynamics of dinucleotides in detail, along with pertinent electronic structure calculations, before discussing excitations in single strands with more than two bases.

4.1 Dinucleotides

4.1.1 Long-Lived Excited States Form Only in Base Stacks

Compelling evidence that long-lived excited states are only formed when two bases are in van der Waals contact comes from experiments showing that these states

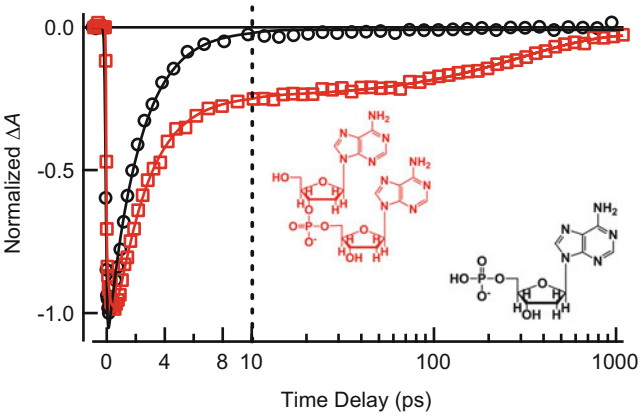

Fig. 4 fs-TA signals (266 nm pump/250 nm probe) in aqueous buffer solution: dAMP in *black* and dApdA in *red*

disappear when base stacking is eliminated. At low pH, each residue in dApdA is protonated and Coulombic repulsion completely disrupts stacking [127–129]. GSB recovery signals (pump 265 nm/probe 250 nm) show no long-lived signal for this fully unstacked structure, whereas a long-lived component with a decay time constant of ~200 ps is seen at neutral pH (Fig. 5) [9]. Protonation does not inhibit ultrafast IC, as evidenced by the identical GSB signals at pH 2 and pH 7 for dAMP [9].

Notably, long-lived excited states are still observed at low pH in poly(A) [27] and poly(dC) [81], conditions under which the polymers adopt higher-order structures which retain base stacking. This suggests that it is not protonation of the nucleobases per se that quenches long-lived excited states, but rather the loss of base stacking. This conclusion is underscored by the observation that high concentrations of methanol, a known denaturant, also causes unstacking and eliminates the long-lived excited states seen in fs-TA experiments on AA nucleobase dimers (see Sect. 4.1.6) [58].

4.1.2 Long-Lived Excited States Are Assigned to Excimers

The prominent decay components seen in fs-TA signals of $(dA)_{18}$ in aqueous solution were assigned by Crespo-Hernández et al. [13] to intrastrand excimers. Later experiments [6, 9] detected identical signals from dinucleotides and longer oligomers made of adenine (see Sect. 4.2.1), providing strong evidence that the long-lived excited states are indeed localized on just two nucleobases, as required for an excimer (=excited dimer). Time-resolved fluorescence experiments detected similar decay components in emission, both in dinucleotides [122, 130] and in longer single strands [23]. This emission is significantly red-shifted compared to that from the constituent monomers, and this observation is again consistent with

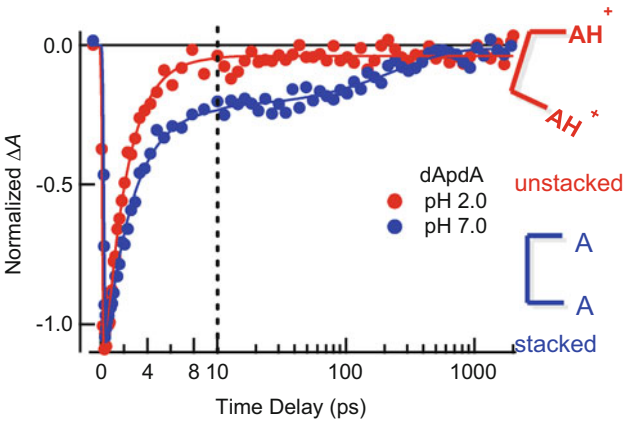

Fig. 5 fs-TA signals (266 nm pump/250 nm probe) of dApdA at pH 2 (*red*) and pH 7 (*blue*). Figure adapted from [9]

excimer formation. The finding from ultrafast laser experiments that excimers are important excited states in DNA model compounds at room temperature supports the assignment made in the 1960s of red-shifted emission seen from dinucleotides and longer DNA strands in rigid glasses at cryogenic temperatures to excimer states [131].

Alternative assignments for the long-lived excited states have been discussed [116, 132–134]. Several workers proposed that the ultrafast IC observed in the nucleobase monomers could be impeded in π-stacked systems because of steric hindrance of the out-of-plane vibrational modes that facilitate IC [116, 133–135]. However, the steric explanation is hard to reconcile with the sequence-dependent lifetimes observed in dinucleotides [6]. Presently, there is growing experimental and theoretical consensus that excited states seen in single DNA strands which decay with time constants of tens to hundreds of picoseconds are excimers [13, 23, 59, 108, 121, 122]. Evidence that these excimers have a high degree of CT character is discussed next.

4.1.3 DNA Excimers and Interbase Charge Transfer

Takaya et al. [6] reported that excimer decay rates measured by fs-TA spectroscopy in a series of RNA dinucleotides increase as the estimated energy of the radical ion pair generated by interbase electron transfer decreases. This correlation suggested that UV excitation of a stack of neutral bases produces CT states which decay by charge recombination at rates that decrease with increasing thermodynamic driving force (Marcus-inverted behavior) [6].

Very recently, direct evidence has been obtained by fs-TRIR spectroscopy that some DNA excimers exhibit the vibrational spectral features expected of radical ion pairs generated by interbase electron transfer [123, 136, 137]. By probing the

double-bond stretching region after photoexcitation of the dinucleotide dApdT, Doorley et al. [123] observed a 75-ps component with excited-state absorption features between 1,500 and 1,600 cm^{-1}. By comparing the calculated shift of the C=O stretching modes of the neutral thymine molecule and the thymine radical anion, the authors argued that this relatively broad feature can be assigned to the thymine radical anion formed by electron transfer from A to T.

Bucher et al. [136] observed slow decay components in fs-TRIR signals from di- and oligonucleotides containing 5-methylcytosine. The long-lived excited states have lifetimes of 20–300 ps and are formed in 20–40% yield. These components are furthermore absent in equimolar mixtures of the corresponding monomers. The authors assigned their mid-IR ESA bands to radical cations and anions generated by photoinduced charge separation. These assignments were supported by transient IR difference spectra of authentic radical cations of guanine and 5-methylcytosine generated by two-photon ionization. Additionally, ab initio calculations identified vibrational marker bands of the radical anions. Bucher et al. concluded that CT states formed in single strands containing more than two bases can delocalize across multiple stacked bases. This fascinating proposal will be discussed further in Sect. 4.2.2.

Finally, Zhang et al. [137] used fs-TRIR spectroscopy to study the dinucleotide d(OA) (structure shown in Fig. 6), where O stands for the modified nucleobase, 8-oxo-7,8-dihydro-2′-deoxyguanosine (8-oxo-dGuo, or O in sequences). The TRIR spectra of d(OA) at various delay times are shown in Fig. 6a. The difference spectra recorded between $30 \leq t \leq 300$ ps match the theoretical difference spectrum calculated for an ion pair consisting of an 8-oxo-dGuo radical cation and an adenine radical anion (Fig. 6b). This is a clear demonstration that an electron is transferred from the 8-oxo-dGuo residue to A, producing an exciplex best described as a strong CT state or even a contact radical ion pair. The quantum yield of forming the CT state is high and equal to 40% at 265 nm, but decreases to 10% at 295 nm, a wavelength which selectively excites 8-oxo-dGuo [137].

The potentially reactive radical ions formed in d(OA) decay to the ground state of the dinucleotide by charge recombination with a time constant of 60 ps. Ultrafast ET between π-stacked bases possibly explains how 8-oxo-dGuo can contribute to the reductive repair of thymine dimers in DNA [138] despite its ultrashort monomer lifetime [139]. The requirement that the bases must be stacked at the instant of photon absorption in order to form a radical ion pair also explains why a photoexcited purine base (A or G) cannot repair a flanking CPD when the bases are unstacked [140].

In summary, transient IR difference spectra providing direct evidence of interbase electron transfer have been measured recently in three laboratories for dinucleotides [123, 136, 137] and longer single strands [136]. It was assumed in each study that a full electron is transferred between π-stacked bases, but the question of whether an excimer with a reduced degree of CT character would have similar vibrational frequencies as a contact radical ion pair has not been explored. Also, although a crude estimate using aqueous reduction potentials suggests that ion pairs can be formed for any dimer made of the canonical

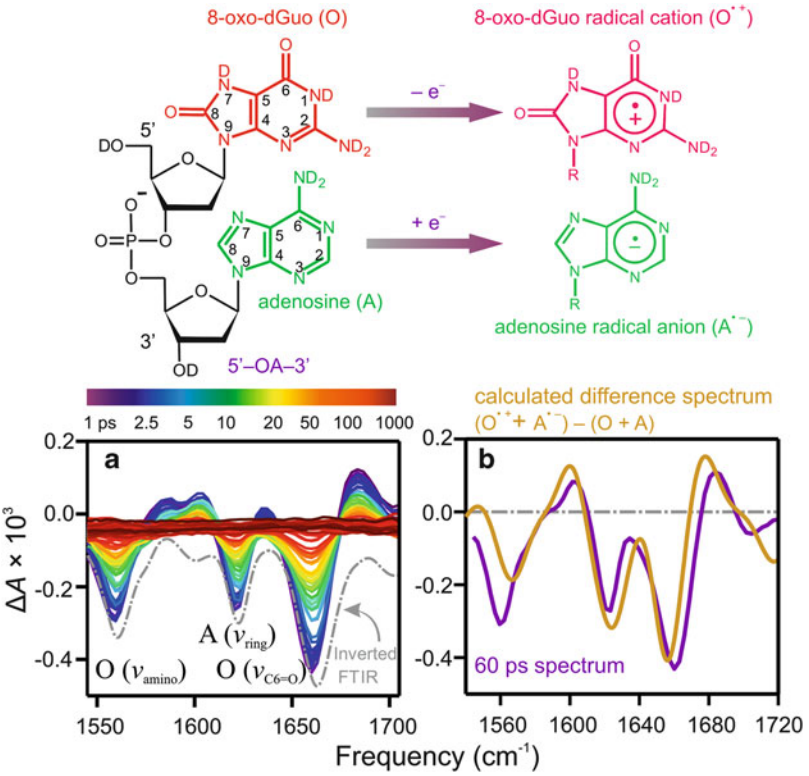

Fig. 6 (**a**) fs-TRIR spectra of d(OA) at selected pump-probe delay times (1 ps–1 ns) following 265 nm excitation. The Inverted FTIR spectrum and mode assignments are included for convenience. (**b**) The experimental difference spectrum at 60 ps (*purple line*), compared with the difference spectrum calculated as $(O^{\bullet+} + A^{\bullet-}) - (O + A)$ (*gold line*). The DFT calculations were performed at the PCM/PBE0/6-31 + G(d,p) level of theory and using the harmonic approximation for the monomeric species with 2′-deoxyribose and five explicit D_2O molecules included. The structures of d(OA), $O^{\bullet+}$ and $A^{\bullet-}$ are also shown. Figure adapted from [137]

nucleobases [137], it is unknown whether full electron transfer occurs in homodimers such as $(dA)_2$, or whether these form excimers with a reduced degree of CT character. Calculations discussed in Sect. 4.1.5 have predicted the existence of both types of excimers in AA stacks.

4.1.4 Initial Excitons Decay to Excimers

An important observation from fs-TA and TRIR experiments is that a large fraction of all initial excited states decay to excimers [9, 13, 136, 137]. An analysis of GSB signals recorded with 266-nm pump pulses found that ~30% of all excited states in $(dA)_2$ in room-temperature aqueous solution decay to excimers [9]. Bucher et al. [136] concluded that 25% of excited states in the dinucleotide d(^{5m}CA),

where ^{5m}C is 5-methylcytosine, decay to excimers. Considering that unstacked conformations cannot form excimers (Sect. 4.1.1), the probability of excimer/exciplex formation is even higher for excitations in base stacks.

The observation of high excimer yields has important implications regarding their nature. If the excimers were as bright in emission as the $^1\pi\pi^*$ states of the mononucleotides, then the high yields and long lifetimes of the excimers would cause the fluorescence quantum yields of the dinucleotides to increase by orders of magnitude, but this is not observed. For example, the AA excimer, which may be one of the brightest of DNA excimers, causes the fluorescence quantum yield of $(dA)_{20}$ ($\phi_f = 6 \times 10^{-4}$ [17]) to increase by just an order of magnitude compared to dAMP ($\phi_f = 6.8 \times 10^{-5}$ [141]), even though the oligomer lifetime is ~1,000 times longer. This comparison and the very weak nature of the long-time emission [23, 122, 130] – a circumstance that made it difficult to even detect long-lived excited states by the fs-FU technique at first (see discussion in [4]) – indicates that the long-lived excited states are comparatively dark, and have lower radiative transition rates than the bright $\pi\pi^*$ states of the monomers. This is fully consistent with the strong CT character described in the previous section. It is important to note that the excimer states are not completely dark, as decay components are observed in time-resolved fluorescence experiments closely matching those found in fs-TA experiments in dinucleotides [122, 130] and longer single strands [23].

A variety of experiments suggest that excimers or CT states are populated in less than 1 ps from the initial excitons [6, 13]. For example, Zhang et al. [137] observed that the CT state yield in d(OA) is four times higher at 265 nm than at 295 nm. This suggests that there is greater coupling between the initial excitonic state and the CT state at 265 nm and ultrafast transfer from the former to the latter. In addition, the excimers emit at wavelengths to the red of the base monomers, but rising emission signals have not been observed at these longer wavelengths (or at any emission wavelength) in fs-FU experiments [122, 130]. The paradigm in which excitons decay on an ultrafast time scale to excimer or CT states is also supported by computational studies [108, 142]. For example, quantum dynamical calculations predict that IC from excitonic to CT states can occur in less than 100 fs in adenine single strands containing between two and ten bases [143].

4.1.5 Computational Predictions and Multiple Excimers

The principal findings from calculations of excited states of π-stacked nucleobase dimers are briefly reviewed in this section, focusing on the A–A dimer, the most studied system and one of special relevance to fs-TA experiments on single strands. These calculations provide insight into the exciton-to-excimer decay mechanism introduced above. Considerable computational effort has been devoted to locating the vertical energies of CT states within the manifold of excited states, and here we present a small number of conclusions from only a few representative studies. Accurate ab initio prediction of excited state energies is enormously challenging because of the large number of atoms and the desire to include realistic solvation

models. System size frequently makes it prohibitively expensive to use higher levels of theory. Because of their efficiency, DFT calculations are popular, but this method can predict spuriously low energies for CT states [144] unless suitable long-range corrected functionals are used [145, 146].

TD-DFT studies of the π-stacked adenine dimer by Lange and Herbert using long-range corrected functionals [147], of stacked adenine–guanine systems by Santoro et al. [117], and a study of adenine multimers with the ribose-phosphate backbone included by Improta and Barone [108] predict that the CT states lie within about 0.3 eV of the bright excitonic states at the geometry of the electronic ground state. These TD-DFT results are roughly in line with ab initio CASPT2 calculations performed on the π-stacked adenine dimer, which predict that the CT states are 0.1–0.3 eV above the lowest lying excitonic state [59]. Plasser and Lischka computed the excited-state properties of a stacked adenine dimer using the RI-ADC(2) method [120]. These supermolecule ab initio calculations, which treat CT and excitonic states on an equal footing, revealed that CT states lie 0.6–0.8 eV above the bright excitonic states. Accurate equation of motion coupled-cluster calculations have since narrowed the gap somewhat between the bright ππ* states and the lowest CT state [148].

Although the CT excited state for AA lies vertically above the lowest energy excitons, what counts is whether there is an accessible pathway leading from the Franck–Condon region to the CT state. Computational studies which performed excited-state geometry optimization confirm that such paths exist [107, 108]. A recent quantum dynamical investigation furthermore suggests that this interconversion can occur on an ultrafast time scale [143]. In summary, a growing number of computational studies support the concept that decay of single strand excitons to excimers is energetically feasible and occurs on an ultrafast time scale.

An important contribution from theory is the location of more than one type of excimer minimum on the potential energy hypersurface of AA stacks [59, 108, 121]. The suggestion that two excimers are formed in UV-excited $(dA)_{20}$ was originally made by Kwok et al. [23]. Ab initio calculations of excited states of stacked adenine dimers identified a neutral excimer with an eclipsed geometry (twist angle of 0°), which is characterized by short C4–C4′ and C5–C5′ distances [59, 108]. Plasser and Lischka [120] also describe a geometry-optimized excimer state (termed an exciplex state in [120]) with a very short distance of 2.00 Å between the C6 atoms of each adenine. The resulting strong orbital interaction between the two adenines yields an excited state very different compared to the Franck–Condon state and it has character intermediate between a Frenkel exciton and a charge resonance state [120]. It will be important to see whether these predictions for adenine dimers extend to dinucleotides containing two different bases.

Large-scale backbone motions are required to bring two bases in B-form DNA into an eclipsed conformation. For this reason, it may be impossible to reach a fully eclipsed conformation in actual di- and oligonucleotides because of backbone constraints, and excimers having larger twist angles have been predicted

[108, 121]. Banyasz et al. [121] suggested that two different excimers can explain the trends in steady-state and time-resolved fluorescence spectra from adenine homo-oligonucleotides. In particular, they argued from their TCSPC experiments on $(dA)_{20}$ that the subnanosecond emission (λ_{em} ~360 nm) should be assigned to the "neutral excimer" (a bonded excimer), while nanosecond time scale and longer wavelength emission arises from an AA CT state which, in its energy-minimized geometry, has a stacking distance similar to that in the electronic ground state of the oligomer [121].

To support their assignment, Banyasz et al. [121] pointed out that the emission band at 360 nm seen for $(dA)_{20}$ is missing in the fluorescence spectrum of the $(dA)_{20}{\cdot}(dT)_{20}$ duplex. They proposed that the neutral excimer responsible for the subnanosecond emission decay in $(dA)_{20}$ is unable to form in duplex $(dA)_{20}{\cdot}(dT)_{20}$ because base pairing prevents the required torsional motions [121]. This explains the absence of any significant picosecond time scale emission from AT homoduplexes as reported in [40, 149], but this model leaves unresolved the nature of the excited states seen in fs-TA experiments for $(dA)_{18}{\cdot}(dT)_{18}$ and related homoduplexes that decay with a lifetime of ~70 ps (see Sect. 5.2.1).

Temps and coworkers [130] invoked the fully eclipsed excimer geometry calculated by Olaso-González et al. [59] to interpret the ~5 and ~280 ps decay components observed in their fs-FU experiments on the dinucleotide d(pApA). They proposed that an initial excimer is formed with a twist angle of ~36° between the bases (corresponding to the initial geometry in the B-DNA helix), which decays in 5 ps to a more stable, eclipsed (twist = 0°) excimer. They assigned the 280-ps lifetime to the latter species. A similar model was discussed in a later study of d(ApG) [122]. In that study, a ~6-ps component was again observed at red-shifted wavelengths in the fluorescence signal. Its absence in a GSB recovery measurement is consistent with a model in which less stable excimers decay to more stable ones as bases undergo large amplitude motions.

However, proof is lacking that the minimum energy excimer or exciplex actually corresponds to a structure with zero twist. In addition, it has not been demonstrated that the requisite large-amplitude twisting motions can actually be completed on a 5–6 ps time scale. After all, reorientational diffusion of a single adenosine molecule occurs more slowly. An alternative explanation is that the energy of the emitting excimer state is progressively lowered by changes in the environment. This possibility is suggested by spectral changes seen in the emission spectrum of $(dA)_{20}$ [130] which could be described as a continuous red shifting on the few picosecond time scale. Although solvation dynamics in neat water are largely complete in less than 1 ps [150], significantly slower solvation times have been reported for chromophores embedded in DNA [151, 152].

4.1.6 Excimer Lifetimes and Stacking Geometry

Several diadenosine compounds (Fig. 7) were studied by fs-TA and steady-state (UV/vis, CD) spectroscopy in order to explore the effects of (1) temperature,

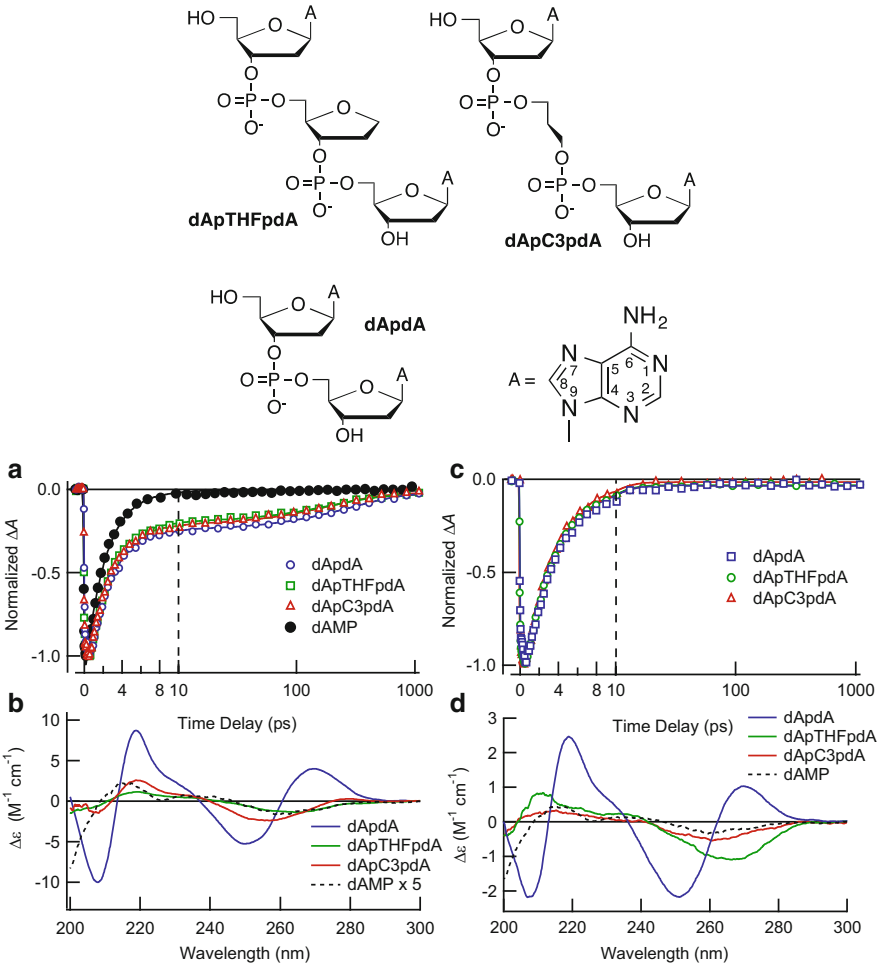

Fig. 7 *Top*: Structures of the 2′-deoxyadenosine dimers studied. *Bottom*: fs-TA signals (266 nm pump/250 nm probe) and CD spectra in buffered aqueous solution (**a**, **b**) and in 80 vol% methanol:20 vol% buffer (**c**, **d**)

(2) solvent composition, and (3) the nature of the covalent linker joining the nucleobases on excited-state dynamics [58]. Dimers of (2′-deoxy)adenosine were chosen because of adenine's high stacking propensity in aqueous solution [43, 153, 154]. A pronounced long-lived component is observed in all three 2′-deoxyadenosine dimers which is not seen in the pump-probe signal of the monomer dAMP (Fig. 7a). This signal component vanishes completely in 80 vol% methanol/20 vol% water (Fig. 7c). Methanol was used in this study as a denaturing co-solvent to disrupt π–π stacking of the adenine moieties. The exciton-coupled circular dichroism (ECCD) spectra indicate that the 2′-deoxyadenosine

units remain stacked most of the time in aqueous solution (Fig. 7b), while few, if any, stacked structures are present in aqueous methanol (Fig. 7d).

When two 2′-deoxyadenosines are separated by an abasic site (dApTHFpdA and dApC3pdA in Fig. 7), the bases stack just as readily as when they are nearest neighbors, yet these compounds show no ECCD signals (Fig. 7b). Low barriers to helix inversion for diadenosines joined by longer linkers may produce a racemic ensemble in which left- and right-handed helical conformations are in dynamic equilibrium [58]. These results caution that a CD spectrum resembling that of a monomer (i.e., one that lacks excitonic interactions) is not a foolproof indicator of unstacked conformations [58].

Even though the bases in dApdA adopt an extended conformation in 80% methanol, as indicated by the lack of a long-lived component in the fs-TA signal (Fig. 7c), the ECCD signal is not fully eliminated (Fig. 7d). This indicates that an ECCD signal does not always imply base stacking. In their computational study of ECCD by the RNA dinucleotide ApA, Johnson et al. [155] identified a conformation with perpendicularly oriented base planes for which the calculated CD signal was only 20% as intense, but otherwise had the same spectral shape as the calculated CD spectrum of a co-facially stacked conformer with B-DNA geometry. An open conformation with intervening solvent molecules can thus lack the orbital-orbital overlap necessary for excimer formation, but still yield an ECCD spectrum, perhaps because the short phosphodiester linker constrains the two bases in dApdA to adopt unstacked conformations that are predominantly chiral.

The absence of base stacking in aqueous methanol is a reminder that hydrophobic interactions are critically important for stabilizing base stacks [154, 156]. In most nonaqueous solvents, dinucleotides adopt unfolded conformations in which the bases have no overlap between their π orbitals and are separated by solvent molecules. Interestingly, extended, unstacked conformations were not observed in a molecular dynamics (MD) simulation of ApA in methanol [157]. This discrepancy with experiment adds to evidence that the empirical force fields used in MD simulations overstabilize base stacking in single-stranded systems [54, 55, 158].

High concentrations of methanol disrupt base stacking more effectively than high temperature conditions (Fig. 8). Increasing the percentage of methanol causes the signature of the excimer state in the fs-TA signals from dApdA to decrease in amplitude, and eventually disappear above 50% methanol concentration (Fig. 8b). Increasing temperature in aqueous solution also leads to attenuation of the slow decay component, but the fs-TA signal recorded at the highest temperature still exhibits a long-lived decay (Fig. 8a). The detection of excimers in dApdA at 75°C confirms that there is still substantial AA base stacking at high temperature. Earlier, Davis and Tinoco concluded from NMR measurements that the two bases in ApA remain close to each other with no solvent molecules in between most of the time, even at 90°C [159].

Two 5′,5′-linked diadenosine oligophosphates P^1,P^4-di(adenosine-5′) tetraphosphate (Ap_4A) and P^1,P^5-di(adenosine-5′)pentaphosphate (Ap_5A) were also studied by fs-TA and CD (Fig. 9). Previous studies suggested that these compounds adopt non-face-to-back stacking motifs [160, 161]. The long-

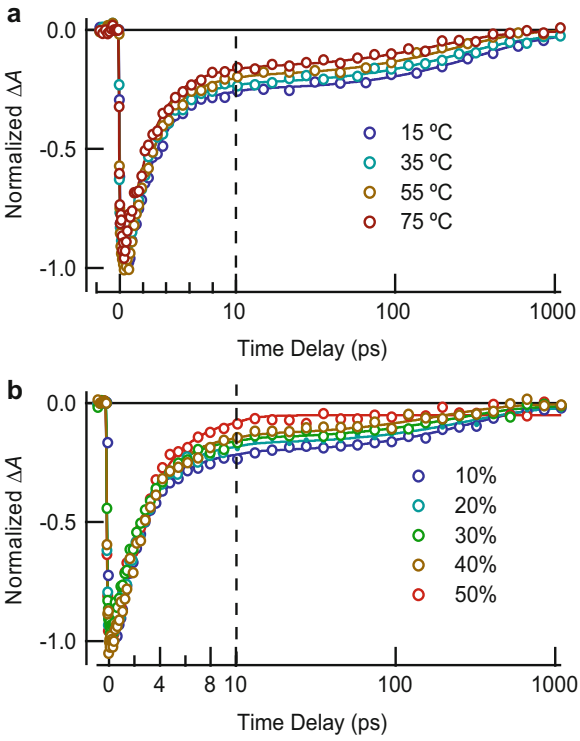

Fig. 8 fs-TA signals (266 nm/250 nm) from (**a**) dApdA at the indicated temperatures in aqueous buffer solution, and (**b**) in methanol–water solutions as a function of the percent methanol by volume

wavelength couplet seen in the ECCD spectra of Ap_4A and Ap_5A (Fig. 9b) is opposite in sign to the one seen in dApdA (Fig. 7b). This and other characteristics of the CD spectra are best explained by a face-to-face stacking motif. Interestingly, the fs-TA GSB signals (266 nm/250 nm) for these two dimers reveal that excimers are formed which have lifetimes similar to those seen in the 2′-deoxyadenosine dimers.

The main messages of the work described in [58] is that AA stacks form readily in substrates having very different backbones and excimers form in high yields in these stacks, despite the different distributions of ground-state conformations. The disappearance of long-lived fs-TA signals under conditions that still produce ECCD signals is evidence that the interactions between bases leading to excimer states are short-ranged [58]. The steep distance dependence that characterizes excimer formation is furthermore consistent with interbase electron transfer (see Sect. 4.1.3). It is well known that electron transfer rates decrease exponentially with donor–acceptor distance [162]. Excimer formation thus requires π−π stacking between nucleobases because this organization positions an electron donor and acceptor base close enough to make electron transfer competitive with the very high rate ($\sim 10^{13}$ s^{-1}) of IC observed in base monomers.

The very different ECCD spectra in Figs. 7 and 9 indicate that twist angles and stacking motifs (face-to-back, face-to-face, etc.) differ in these five adenine dimers with their different linkers. In spite of this variation, excimers are formed in all,

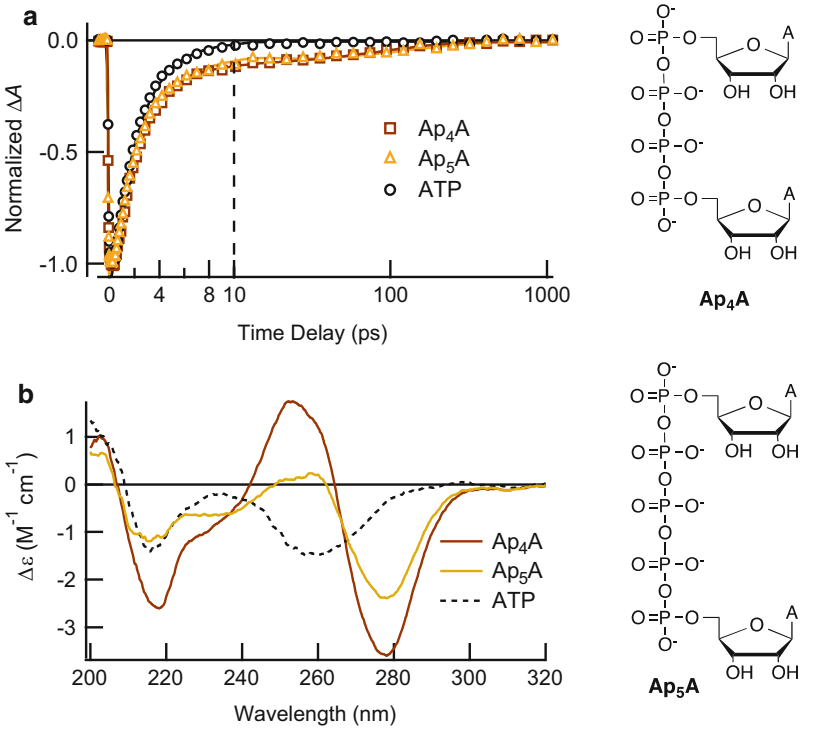

Fig. 9 (**a**) fs-TA signals (266 nm pump/250 nm probe) and (**b**) CD spectra in buffer solution of adenosine 5′-triphosphate (ATP), Ap_4A, and Ap_5A (structures shown at *right*)

which decay with remarkably similar, if not identical, lifetimes [58]. This could be because motions needed to reach a lowest energy excimer are largely complete in ~10 ps, the earliest time at which the AA excimer can be observed without interference from hot-ground state absorption following ultrafast IC by shorter-lived excited states [58].

It is, however, important to note that face-to-face (AA dimers in Fig. 9) and face-to-back stacks (AA dimers in Fig. 7) cannot achieve identical geometries without flipping over one of the bases, a motion thought to occur on subnanosecond time scales. This could indicate that the excimer state formed in high yield is not a neutral or bonded excimer [59, 107, 108, 163, 164], the energy and lifetime of which might be expected to depend sensitively on geometry. Instead, an excimer which is essentially a contact radical ion pair similar to those observed in d(OA) and other base heterodimers (Sect. 4.1.2) may be responsible. The energy of such an excimer could depend more weakly on twist angle and stacking motif.

4.2 Single-Stranded Oligonucleotides

An important observation from ultrafast laser experiments is that long-lived states are ubiquitous in DNA single strands, regardless of length. Comparison of dinucleotide signals with those from longer oligomers provides insight into the nature of the excited states and can be used to draw conclusions about excited-state localization.

4.2.1 Excimer Dynamics in Oligonucleotides

Experimental results from many laboratories have detected excimers in DNA oligonucleotides containing more than two bases. Experiments performed using the fs-TA technique on $(dA)_{18}$ [27], poly(A), and poly(dA) [13] all revealed a slow decay component of between 100 and 200 ps. Buchvarov et al. [132] observed long-lived excited states in a series of single-stranded homo-adenine oligomers in fs-TA experiments. Su et al. [9] also investigated variable-length dA homo-oligonucleotides using the UV pump/UV probe fs-TA technique. Their measured GSB signals (Fig. 10) show that long-lived excimers are formed in all oligonucleotides, regardless of length. Earlier, Takaya et al. [6] had observed that the RNA dinucleotide ApA and its corresponding homopolymer poly(A) have identical long-time signals in GSB experiments. The constancy of the long lifetime on going from $(dA)_2$ to $(dA)_{18}$ strongly suggests that the excitations probed in all strands are delocalized over no more than two π-stacked neighbors, consistent with excimer formation.

Time-resolved fluorescence experiments provide a slightly different perspective on the dynamics of the optically prepared exciton states. The emission anisotropy measured in fs-FU experiments decays on the femtosecond time scale for many single and double strands [124]. Markovitsi and coworkers assign this decay to IC ("energy transfer" or "intraband scattering") among excitonic states [124, 165]. However, the proposal from fs-TA experiments that excitons decay in $<$100 fs to excimer/exciplex states (Sect. 4.1.4) is a possible additional mechanism for the rapid anisotropy decay. The transition dipole moments of DNA excimers can be oriented out of the plane of the bases in contrast to the in-plane excitonic transition moments [120, 166]. Thus, femtosecond evolution from an exciton to an excimer state would lead to a rapid change in polarization anisotropy.

4.2.2 Exciton and Excimer Delocalization in Single-Stranded DNA

Using a novel approach, Buchvarov et al. [132] estimated the spatial extent of DNA excitons using fs-TA signal amplitudes recorded from variable-length adenine homo-oligonucleotides. By fitting the amplitudes as a function of the strand length, the authors estimated a "1/e delocalization length" of 3.3 ± 0.5 bases in $(dA)_n$

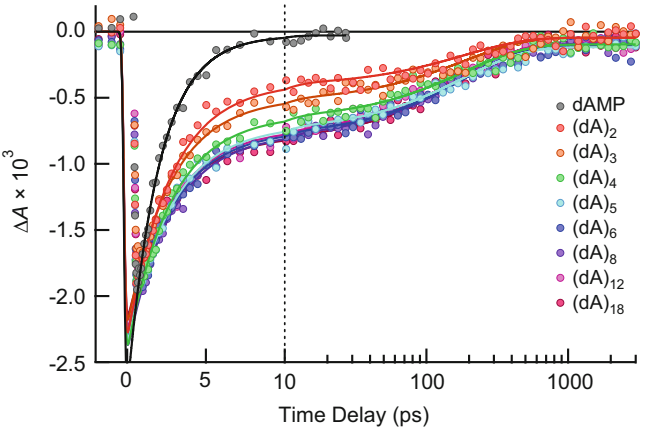

Fig. 10 fs-TA signals (266 nm pump/250 nm probe) of dAMP and adenine homo-oligonucleotides with 2 to 18 bases obtained with consecutive scans. Figure reused with permission from [9], copyright (2012) American Chemical Society

sequences, a result that implies greater exciton delocalization in the longer strands [132]. Interestingly, CD experiments also suggest that excitons can span more than two bases, but in a manner that depends on excitation wavelength. Nielsen and co-workers concluded that excitons prepared by photons with wavelengths above 220 nm extend over just two bases, while excitons prepared by VUV photons were suggested to spread over up to eight bases [167]. The compact, lower energy excitons are more relevant to the excitation conditions in the ultrafast laser experiments. In a computational study, Tonzani and Schatz [168] predicted a delocalization length of approximately three residues for single-stranded $(dA)_n$ oligomers containing between 7 and 11 bases.

Su et al. [9] reinvestigated $(dA)_n$ oligonucleotides by the fs-TA technique and showed that the GSB signals could be fitted to the same time constants regardless of length, and only the relative *amplitude* of the slow signal component increased with increasing strand length (Fig. 10) [9]. They argued that long-lived excitations in single strand adenine tracts are already fully localized excimers no later than 1 ps after excitation, and cast doubt on the possibility of using fs-TA signals recorded several picoseconds after excitation to reach conclusions about exciton delocalization, as was done in [132].

Su et al. [9] emphasized that structural disorder, specifically, the variation in the fraction of stacked bases with length, provides a better explanation of the amplitude variation seen in Fig. 10. They pointed out that the average length of stacked domains in ss DNAs is generally much less than the strand length [91]. In fact, these authors estimated that the average stacked domain in $(dA)_{18}$ is only 1.8 bases long, assuming that 69% of all bases in $(dA)_{18}$ are stacked near room temperature.

An interesting variation on the concept of delocalized excitons is the idea that CT (or excimer) states can delocalize across multiple stacked bases. Such states have been observed in calculations of double strands [147], and they are familiar

from work on DNA charge transport [169]. Bucher et al. [136] concluded from their fs-TRIR studies of DNA single strands that one or both of the radical ions produced by UV excitation can delocalize across multiple stacked bases. This conclusion is based on experiments in which 5-methylcytosine was selectively excited in a single strand that also contained an adenine positioned a variable distance away by intervening uracil bases. The observed bleaching of ground-state IR fundamentals of both the U and A bases led the authors to conclude that charge separation can extend over distances of 10 Å [136].

The identical GSB recovery dynamics observed by Su et al. [9] for $(dA)_2$ and $(dA)_{18}$ are difficult to reconcile with the notion of delocalized radical ions. If the electron or hole in the AA excimer in a $(dA)_n$ sequence were delocalized, then this would probably affect the rate of charge recombination in the longer oligomers. However, if the average stacked domain is really only on the order of two bases in both $(dA)_2$ and $(dA)_{18}$, then radical ion delocalization may not be relevant to the experiments of Su et al. [9]. By the same token, the possibility that domains of three or more stacked bases are improbable would contradict the assumption by Bucher et al. [136] that the bases in their single strands are well stacked. It should also be noted that uracil has a low propensity for stacking [127, 170]. In any event, the very stimulating proposal that radical ions could be spatially delocalized in DNA invites further study.

5 Excited-State Dynamics in Base Pairs and in Double-Stranded DNA

The precise effects of base pairing on excited-state dynamics in nucleobase multimers are still uncertain and considerable effort is currently focused on this topic. Although the photophysics of base stacks can be studied in the absence of base pairing interactions using the dinucleotide and single-stranded model systems described in Sect. 4, study of base pairs in aqueous solution in the absence of base stacking is problematic. In water, bases will stack rather than form hydrogen bonds with one another, as demonstrated by self-association studies of base monomers [42, 43]. Consequently, a model system has not yet been found for preparing a single base pair in aqueous solution that is not simultaneously π-stacked with other bases as mentioned in Sect. 3.2.

The shortage of model systems for single base pairs in aqueous solution has not led to a shortage of hypotheses. One with a long history is the idea that UV excitation induces one or more protons in hydrogen bonds to move from one nucleobase to its base-paired partner [171]. Double proton transfer in two hydrogen bonds is illustrated for AT and GC base pairs in Fig. 11. By altering the tautomeric forms of the bases on both strands, UV-induced interstrand proton transfer (PT) would be mutagenic, if back PT to reform the starting bases were to be frustrated [171]. The lifetimes of $^1\pi\pi^*$ states of monomeric bases are virtually the

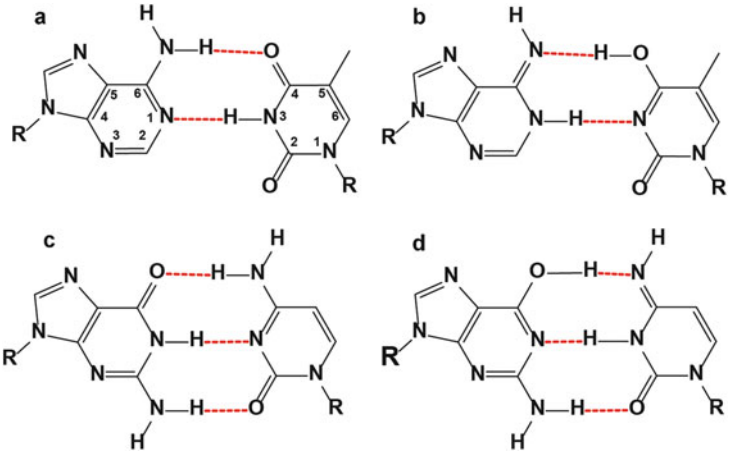

Fig. 11 A Watson–Crick AT base pair (**a**) before and (**b**) after double proton transfer (DPT). A Watson–Crick GC base pair (**c**) before and (**d**) after DPT

same in water and in aprotic solvents [172–174], indicating that deactivation does not involve excited-state proton transfer (ESPT). However, most of the canonical bases are stronger bases than water, and PT could be more favorable within a base pair than between a base and a solvent molecule.

The fundamental and as yet unanswered question is whether base pairing introduces new excited-state deactivation channels such as ESPT or the aborted hydrogen atom transfer mechanism suggested by Domcke and Sobolewski [175] (see below), or whether base pairing simply perturbs decay channels already operative in single bases and single strands. The latter possibility could reflect structural or steric constraints imposed by paired bases, or it could be a consequence of an altered dielectric environment caused by the exclusion of water molecules from the hydrogen bonding faces of the bases. This section reviews selected studies which address the above question. After discussing experiments on single base pairs in environments where they can be formed (i.e., in the gas phase and in low polarity solvents such as $CHCl_3$), results on double-stranded oligonucleotides made from stacked base pairs will be presented.

5.1 Single Base Pairs

A highly influential computational study by Sobolewski and Domcke considered excited state deactivation pathways in a single GC base pair [175]. This study introduced the stimulating proposal that aborted transfer of a hydrogen atom in a hydrogen bond joining the two bases mediates ultrafast decay to the electronic ground state. In particular, photoexcitation is proposed to populate a CT state in which an electron is transferred from G to C accompanied by motion of the N_1

proton along the middle of the three GC hydrogen bonds (the WC GC pair is illustrated in Fig. 11c). According to the calculations, proton transfer, driven by interstrand CT, leads to a CI with the ground state that is responsible for ultrafast deactivation. A similar paradigm was presented soon afterwards for a single AT base pair [176]. The Sobolewski and Domcke mechanism was invoked to explain the broad spectra observed for single WC GC base pairs in a supersonic jet using the IR-UV hole-burning technique by Abo-Riziq et al. [177]. Narrow spectra were observed for non-WC forms of the GC base pair, and the authors suggested that the special electronic structure of the WC pair leads to rapid excited-state quenching.

Although single base pairs will not form in aqueous solution, they can be prepared in nonpolar solvents, especially with suitably derivatized nucleobases. Schwalb and Temps [70] studied a modified GC base pair in chloroform using the fs-FU technique. They measured a fluorescence lifetime of 0.355 ps for the WC base pair, which is modestly shorter than the lifetimes of the separate G and C derivatives in the same solvent. Schwalb and Temps suggested that ultrafast PT in a GC base pair, perhaps taking place as suggested by Domcke and Sobolewski [175], could explain their observations.

More recent experiments on single base pairs in chloroform have revealed dynamics resembling those of a monomer and failed to document ultrafast PT [70, 178, 179]. TD-DFT calculations also indicate that even a weakly polar solvent can dramatically alter the energetics of the relevant excited states, leading to a barrier to PT not seen in the gas-phase calculations [178]. Significantly, long-lived excited states with lifetimes of ~20 ps are readily observed in a variety of duplexes formed from GC base pairs [180]. This is strong evidence that ultrafast excited-state decay is not the exclusive decay channel, or may not take place at all. Finally, a study of the planar A-A base pair in the gas phase by femtosecond time-resolved photoelectron spectroscopy showed only lifetimes resembling those of a monomer with no evidence of excimer states and no suggestion of PT [16].

5.2 Double-Stranded Oligonucleotides

A central message from Sect. 4 of this review is that excited-state delocalization in single strands depends strongly on whether or not the absorbing bases are present in stacked domains. In double strands, a high fraction of all bases are expected to be stacked compared to the more disordered single strands (see Sect. 3.3). The consequences of a greater degree of structural order on dynamics have been studied using both TA and time-resolved emission techniques [22, 118, 124, 181].

5.2.1 Long-Lived Excited States Are Observed in Stacked Base Pairs

An important generalization, first reported in 2005 [13], is that base pairing does not lead to strong quenching of the long-lived excited states seen in single-stranded

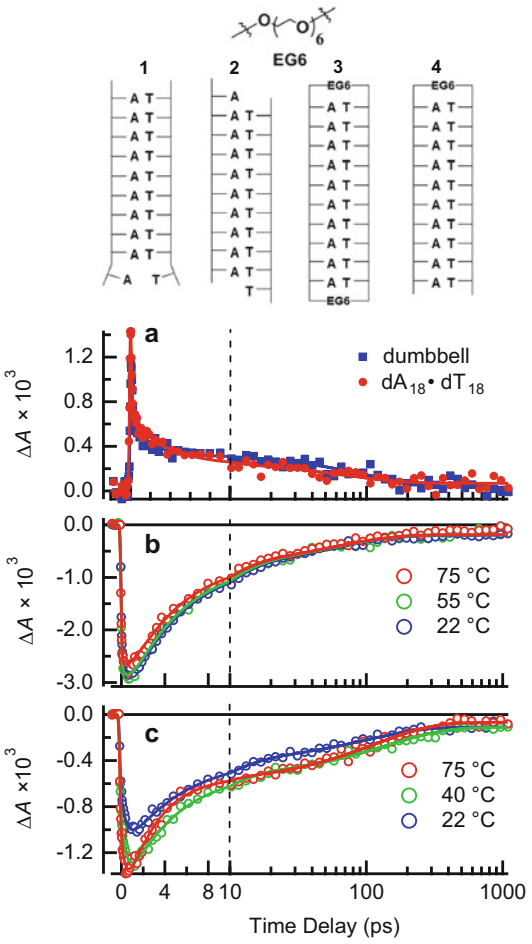

Fig. 12 *Top*: AT DNA homoduplexes with stacking and pairing defects (**1**, **2**) that are eliminated in the EG6-linked dumbbell (**3**) and hairpin (**4**) structures. fs-TA signals (pump 265 nm) (**a**) at room temperature from (3) and from duplex $dA_{18}{\cdot}dT_{18}$ at 350 nm, (**b**) from (3), and (**c**) from $dA_{18}{\cdot}dT_{18}$ at the indicated temperatures. The probe wavelength in panels b and c is 250 nm

nucleic acids. Crespo-Hernández et al. [13] reported that long-lived excited states in duplex $(dA)_{18} \cdot (dT)_{18}$ have similar decay kinetics compared with single-stranded $(dA)_{18}$, suggesting that AT base pairing neither inhibits the formation of, nor accelerates the decay of, excimers in the adenine strand.

Important new insights into the photophysics of double-stranded DNA were obtained from a study of DNA dumbbell and hairpin conjugates made up of AT base pairs (**3** and **4** in Fig. 12) [22]. The non-chromophoric hexa(ethylene glycol) linkers used in these AT conjugates increase the melting temperature by approximately 40°C compared to unlinked homo-duplexes with the same number of base pairs. These covalent linkers largely eliminate the slipped and frayed structures present in solution for low-melting $(dA)_n \cdot (dT)_n$ duplexes (**1** and **2** in Fig. 12), allowing the excited-state dynamics of stacked A · T base pairs to be observed without interference from structures with stacking or pairing defects.

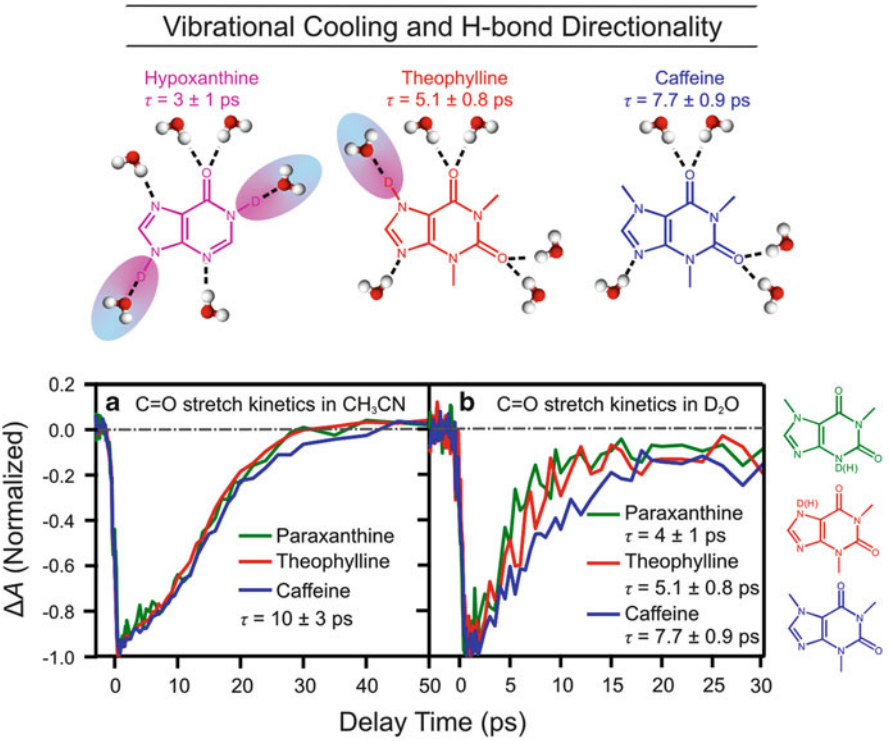

Fig. 13 *Top*: Vibrational cooling (VC) time constants in D_2O and H-bond donors; (*bottom*) bleach recovery kinetics for the carbonyl stretch ($\nu_{C=O}$) of several xanthines in (*a*) acetonitrile at 1,665 cm^{-1}, and (*b*) D_2O solution at 1,640 cm^{-1}. Figure adapted from [21]

UV pump/UV probe fs-TA signals for the dumbbell and hairpin structures decay on two widely separated time scales [22]. Results for the dumbbell are shown in Fig. 12b). A fast component of 4.7 ps is observed along with a slower component of ~70 ps. The fast component is assigned to VC following ultrafast IC – the latter process is seen in the subpicosecond decay of the excited-state absorption seen at 350 nm (Fig. 12a). The slow component of 4.7 ps is the slowest VC lifetime ever observed in double-stranded DNA made only of AT base pairs. For comparison, the VC lifetime of AMP is 2.3 ps [30]. A study [21] of VC by monomeric xanthine derivatives, which demonstrated a correlation between the count of solute hydrogen bond donor groups and VC rates (Fig. 13), provided the key to interpreting this surprising finding. In an AT base pair, two N-H bonds are formed with hydrogen bond acceptors on the complementary base, eliminating two hydrogen bonds with solvent molecules. Because the N–H modes are no longer in resonance with solvent OH stretches, VC occurs more slowly for structures with WC base pairs than for monomeric bases or single-stranded DNA.

Chen et al. recognized that the 70 ps lifetime measured for dumbbell **3** is substantially shorter than the lifetime reported in 2005 for the similar $(dA)_{18} \cdot (dT)_{18}$

duplex by Crespo-Hernández et al. [13]. A reinvestigation of the latter sample (see Fig. 12c) determined that the dynamics are in fact nearly identical to the dumbbell. Chen et al. concluded that the earlier results were obtained at an elevated temperature at which the duplex was substantially denatured [22]. The culprit was the spinning cell used in the 2005 study, which had a very small working volume. The slow (diffusion-limited) exchange between pumped and non-pumped volumes of the solution and the high efficiency of nonradiative decay by DNA resulted in a sample temperature of between 40°C and 50°C which denatured the low-melting AT homo-duplex discussed in the 2005 paper [13]. The use of a flow cell by Chen et al. in the 2013 study [22] completely eliminated laser-induced melting, and the authors were able to record accurately the excited-state dynamics of AT base pairs by the fs-TA technique for the first time (Fig. 12c).

The results in Fig. 12 establish that the long-lived excited states in both the dumbbell and in $(dA)_{18} \cdot (dT)_{18}$ decay somewhat more rapidly than excitations in single-stranded $(dA)_n$ sequences (70 vs 180 ps [9]). There is some quenching caused by base pairing, but this quenching occurs at a modest rate compared to the ultrafast deactivation predicted for GC base pairs [175]. The ~70-ps decay is essentially independent of temperature between 22°C and 75°C (Fig. 12b). This confirms that changes in excited-state dynamics seen in single-stranded and duplex DNAs without linkers at elevated temperatures are caused mainly by thermal disordering. On-going fs-TRIR experiments in Montana seek to understand the nature of this quenching.

A notable result from this study is the simultaneous presence in the fs-TA signals of a subpicosecond decay and the ~70 ps channel for the dumbbell. In the dumbbell, structural disorder is minimized and virtually all bases are stacked and paired. This is strong experimental evidence that ultrafast IC remains a significant decay channel in an A · T-DNA duplex system in which virtually all bases occur in stacked base pairs. The observation of fast and slow decay components in DNA single strands (Fig. 4) does not prove this because of the possibility that the fast component is caused by excitations localized on unstacked bases. Ultrafast IC in base stacks has been predicted theoretically [59, 108, 115, 182, 183].

The reduction in lifetime in the dumbbell (70 ps [22]) compared to dA_{18} (~180 ps [9]) is also not necessarily the result of modifications to electronic structure from base pairing. Recognizing that there are many stacking defects in single strands, one side effect of double strand formation is an increase in the average number of bases that are intimately stacked, and this could affect excimer-state dynamics. However, it would seem more reasonable to observe longer, and not shorter, lifetimes in longer stacks, if longer stacks facilitate escape by the radical ions formed by charge separation. It is possible that the fast decay channel seen in the dumbbell is caused after all by deactivation of at least some excited states by base pair-specific interactions. This observation pinpoints one of the current challenges to interpreting the biphasic dynamics seen in single- and double-stranded oligonucleotides: are the experiments observing the same decay channels in both systems or are the dynamics fortuitously similar even though fundamentally different excited states and decay channels are involved?

5.2.2 Long-Lived Excited States and Helix Conformation

AT base pairing measurably affects nonradiative decay rates in AT duplexes, but other experiments have shown that excimer lifetimes are insensitive to base-pairing motif and helix conformation [184]. de La Harpe et al. studied a $d(GC)_9 \cdot d(GC)_9$ duplex by fs-TA spectroscopy [184]. This self-complementary DNA duplex adopts different conformations in solution depending on the ionic strength and pH, allowing the effect of different base stacking motifs on excited-state dynamics to be studied in a system of constant base sequence.

In low salt conditions, $d(GC)_9 \cdot d(GC)_9$ adopts a typical B-form helix, but in high salt conditions the sequence undergoes a structural transition to the left-handed Z-form. Despite the starkly different base stacking geometries between the two conformations, nearly identical signals were observed for the B- and Z-conformations. The lifetime of the Z-form was measured to be 7.6 ± 0.8 ps at 250 nm probe in agreement with the 6.3 ± 0.6 ps lifetime measured for the B-form duplex within experimental uncertainty. TRIR experiments on poly(dGdC)·poly (dGdC) by Doorley et al. [185] revealed some differences in dynamics between B- and Z-form helices, but the authors commented that the relaxation occurs on similar time scales despite the considerable structural changes. Recently, GC hairpins with hexa(ethylene glycol) linkers were studied in TCSPC emission experiments by Brazard et al. [181]. The authors concluded that more ordered helices have measurable effects on the complex mix of emissive excited states.

A further result of interest with the alternating GC duplex follows from a comparison of fs-TA and TCSPC emission measurements. Bleach recovery signals measured in fs-TA experiments suggest that the vast majority of excitations (perhaps more than 95%) return to the electronic ground state in tens to hundreds of picoseconds when DNA strands are excited at UVB or UVC wavelengths. In contrast, sensitive TCSPC measurements have detected much longer-lived excited states which decay on the nanosecond time scale [121, 186]. Markovitsi et al. [124] estimated that 20% of excited states in alternating GC duplex polymers emit on the nanosecond time scale [124], yet GSB recovery signals measured for $d(GC)_9 \cdot d(GC)_9$ show that nearly all excited states decay within the first 100 ps after excitation [187]. Nanosecond emission components were also reported for $(dA)_{20}$ [121, 149]. Kwok and Phillips [23], who studied emission from the same substrate with lower time resolution, argued that any nanosecond time scale emission must be extremely weak. This is consistent with fs-TA GSB signals at both UV and mid-IR wavelengths, which show that excited states with nanosecond lifetimes in DNA single and double strands are formed in very low quantum yields under UVB/UVC excitation.

5.2.3 Proton-Coupled Electron Transfer in DNA

As discussed in Sect. 4, intrastrand CT or excimer/exciplex states are ubiquitous whenever bases are stacked in DNA. This suggests that charge separation along a strand could be coupled to proton transfer within a base pair (Fig. 14). This is a proton-coupled electron transfer (PCET) process initiated in DNA by UV radiation [187]. It differs from predicted PCET within a single base pair [175, 188] by proposing that 'vertical' ET (i.e., between stacked bases) triggers 'horizontal' PT (i.e., within a base pair). Calculations predict that barriers to PT are dramatically lower in singly oxidized and reduced base pairs [189–193].

Solvent kinetic isotope effects (KIEs) on the lifetimes of excited states have been observed in fs-TA experiments on double-stranded DNA model systems, especially in double strands with an alternating base sequence (e.g., GCGC...) in each strand [13, 187]. These experiments reveal coupling to proton coordinates but it is unclear whether the KIEs are a consequence of proton transfer or just represent a general solvent KIE on the rate of decay of an intrastrand CT state. For example, a pronounced solvent KIE is observed in fs-TA signals from $d(GC)_9.d(GC)_9$ in D_2O [187]. Compared with H_2O, the initial decay component remained the same, but a long-lived 22 ± 6 ps component with approximately half of the amplitude of the maximum ground-state bleach was observed in D_2O. Meanwhile, the same isotope effect was not observed in signals from the non-alternating d(C4G4)·d(C4G4) duplex.

A modified $d[(GX)_9GC]$ sequence, where X is 3-methylcytidine, was also studied by de La Harpe et al. [187]. The presence of the methyl group interferes with hydrogen bonding, causing this sequence to form a stacked single strand. The KIE observed in this case is very similar to the modest effect seen in an equimolar solution of C and G and is assigned to slower VC in D_2O vs H_2O for those excitations that decay via ultrafast IC to the electronic ground state. Thus, the absence of a strong KIE in the single-stranded $d[(GX)_9GC]$ sequence suggests that base pairing is responsible for the KIE seen in the $d(GC)_9.d(GC)_9$ double strand.

Computational studies have provided an additional perspective on PT in GC base pairs. Li et al. calculated that PT is energetically favorable for the GC radical anion base pair with a free-energy change of -3 kcal mol^{-1} [192]. Kumar and Sevilla found that proton transfer is favorable if water molecules are included to mimic the hydration environment in DNA. The free energy change was predicted to be -0.65 kcal mol^{-1} with an activation energy of 1.42 kcal mol^{-1} [195]. Ko and Hammes-Schiffer studied both intra- and interstrand CT states of model duplex structures with alternating and non-alternating GC base pairs [196]. The energy of the interstrand CT state decreases when the proton is displaced from G to C and a barrier may appear during this process. Meanwhile, the intrastrand CT states are less sensitive to proton displacement. These researchers also found that photoexcitation of the alternating duplex could lead to an intrastrand CT state, which could undergo a nonadiabatic transition to an interstrand CT state via proton transfer. Because of the relatively high energies of the intrastrand CT states, this pathway

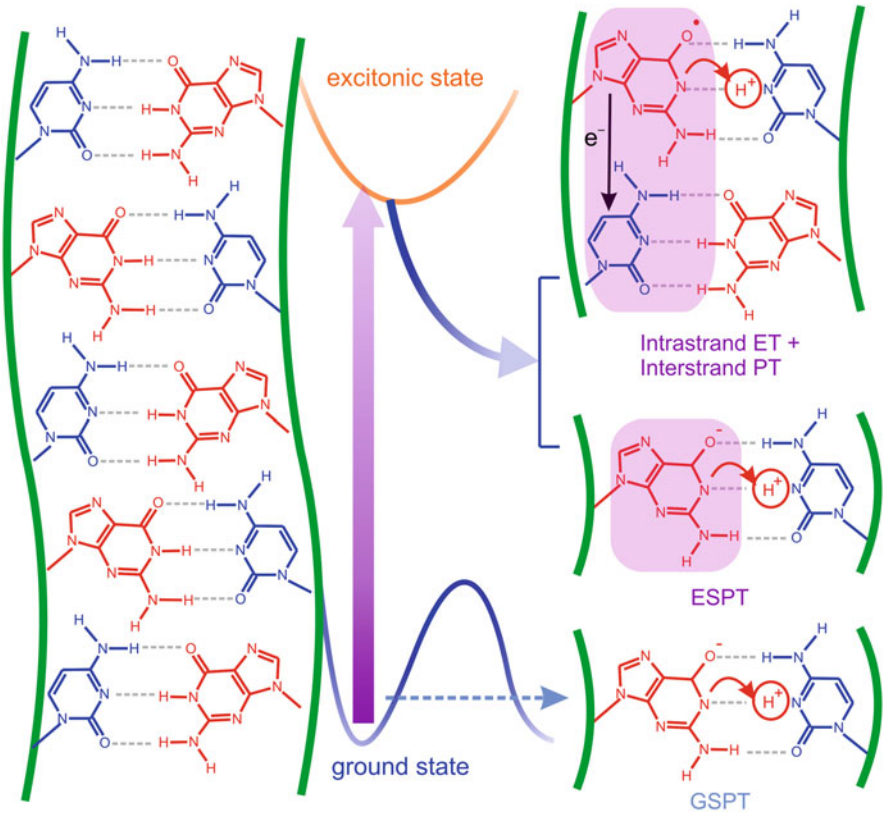

Fig. 14 Illustration of possible proton transfer and proton-coupled electron transfer events in an alternating GC duplex. GSPT: ground-state proton transfer. This single PT requires overcoming a calculated barrier of ~15 kcal mol^{-1} [191]. ESPT: excited-state proton transfer. Locally excited G transfers a proton to its base paired partner. The barrier to single PT is similar in the excited state as in the ground electronic state [194], but simultaneous transfer of an electron and a proton may be barrierless [175]. Intrastrand ET + Interstrand PT: photoexcitation transfers an electron from G to C on the same strand, followed by spontaneous interstrand PT from $G^{\bullet+}$ to C

was suggested to be isotopically sensitive and unavailable in the non-alternating sequences in support of the experimental results in [187].

6 Summary and Outlook

The reductionist approach to studying excited states in single and double strands of nucleic acids through carefully selected model systems has led to dramatic advances during the past decade. It is increasingly clear that interbase electron transfer is a major decay channel for excited states of DNA strands – a process that

requires π−π stacking of the bases. In stacked domains it has been shown that half or more of all excitations populate charge separated states that subsequently undergo charge recombination on time scales of tens to hundreds of picoseconds [136, 137]. Even the relatively long time constant of ~200 ps measured for the excimer lifetime in a dA-dA stack [9, 23, 27, 58, 132] appears to be faster than the time needed for the radical ions to diffuse away from one another or for photochemical reactions to take place.

Growing evidence that CT states are formed in DNA strands whenever bases are stacked has important consequences for understanding DNA photodamage. It will be important to determine whether nucleobase radical ion pairs produced by UV excitation can undergo subsequent chemical reactions prior to their recombination by back electron transfer. One possible outcome of photoinduced ET in DNA is repair of the cyclobutane pyrimidine dimer (CPD), the most ubiquitous photoproduct formed in DNA by UV light. There is keen interest in the possibility that UV light can repair a CPD by photoinduced ET from a more easily oxidized base [140, 197–199]. Nguyen and Burrows recently demonstrated that UV-B irradiation of 8-oxo-dGuo, a signature product of oxidatively damaged DNA, can repair CPDs in double-stranded DNA [138]. They attributed repair to ET from an excited electronic state of 8-oxo-dGuo to the CPD. The proposed pathway is reminiscent of how the flavin in photolyase repairs CPDs by photoinduced electron transfer [200, 201]. The ability of a damaged base to act in the same way as a repair enzyme has exciting implications for the early evolution of DNA.

Given the multiple classes of excited states created when DNA absorbs UV radiation – states populated either directly by absorption, or indirectly as intermediates along relaxation pathways back to the electronic ground state – an essential aim is to describe the lifetimes and yields of the various states. Understanding the nature of the emissive states with nanosecond lifetimes, which are formed in low yields (Sect. 5.2.2), and their relation to the much greater populations of excited states which decay on much faster time scales is an important future challenge. The proposal by Vayá et al. [186] that radical ions may occasionally escape to form free ions which contribute to the long-time emission merits study, especially because of the role that free ions could play in DNA photodamage.

The key structural motif that enables interbase electron transfer is base stacking, and experiments indicate that disrupting orbital-orbital overlap between stacked bases either by raising temperature or adding a denaturant completely eliminates this channel. These observations delineate important opportunities for electronic structure theorists to fill knowledge gaps surrounding fundamental nonradiative processes of electron and energy transfer in stacks of aromatic organic molecules. Adding base pairing interactions does not eliminate the CT states seen in single strands of stacked bases. It is an open question whether interstrand PT is an important deactivation mechanism for excited states in DNA [193, 202–205].

Nonetheless, differences are observed in double vs single strands such as slightly faster rates of decay and modest solvent kinetic isotope effects. These observations hint that intrastrand CT is coupled to proton coordinates. There have, however, been no direct observations to date of PT dynamics, either in the gas phase or in

solution, although this remains an important objective of on-going fs-TRIR experiments. Very recently, Hunger et al. [85] detected guanine radicals formed in H-bonded aggregates of guanine following UV excitation. However, PT was postulated to take place from a slowly formed triplet CT state, and the rate of PT was not determined [85]. There does not appear to be evidence from time-resolved spectroscopy that UV excitation induces proton transfer on a subnanosecond time scale in *any* DNA system. The notion that UV light initiates proton-coupled electron transfer in DNA also illuminates new frontiers for future experimental and theoretical investigation. *The gulf between theoretical predictions of PT in base pairs and the paucity of experimental evidence for this phenomenon* poses an engaging future challenge for experimentalists and theoreticians.

On the other hand, how these CT states, which do not appear to be directly populated by UV absorption, are reached from the initially populated excited states is uncertain, but evidence suggests that they are formed on an ultrafast time scale which is faster than the typical instrument response time of fs-TA and fs-FU instrumentation. Furthermore, recent evidence indicates that the efficiency of reaching the CT state is wavelength dependent: UVC excitation populates the CT state in higher yield than does UVB. This striking observation may provide valuable information on how the CT state is reached from an initial exciton.

The observation of length-independent excited-state dynamics for single-stranded A tracts, combined with the rapid and efficient formation of the CT state in minimal stacks with only two nucleobases, indicates that the excitation energy provided by the UV photon is delocalized over no more than two residues. This short delocalization length is a direct result of the marginally stable DNA single strands, where stacked bases are randomly distributed along the stack and are usually flanked by unstacked bases. Understanding the behavior of excitations in longer stacked domains such as those in duplex DNAs is an important future challenge.

As the nature of the states formed by UV excitation of DNA comes into sharper focus, more work is needed to understand how the non-covalent interactions found in DNA (base stacking and base pairing) control the dynamics of these states. Because these same motifs occur in other supramolecular architectures, efforts to understand photophysical decay channels in DNA can deliver fundamental insights applicable to understanding electron and energy transfer in diverse structures formed from organic building blocks. Future work targeting improved understanding of the feedbacks between electronic structure and conformational dynamics will play a central role. These challenging topics have been studied separately for many years, but spectroscopic and computational advances in the field of DNA photophysics, many of which are described in this volume, are now in place to explore fruitfully their overlap. Full understanding of the nature of excited states and their deactivation pathways will enable time-resolved spectroscopy to be an increasingly precise probe of conformational dynamics in nucleic acid molecules, eventually providing an experimental check on the molecular dynamics simulations used to predict structural dynamics on nanosecond and faster time scales [206].

Acknowledgments This work has been supported by grants from the Chemical Structure, Dynamics and Mechanisms Program of the National Science Foundation and from the NASA Astrobiology Program. Many current and former students, postdoctoral researchers, and collaborators have contributed to this work over the past 15 years. Their efforts, which are documented in the papers cited in this chapter, have been indispensible to the success of this work.

References

1. Kohler B (2010) J Phys Chem Lett 1:2047
2. Gustavsson T, Improta R, Markovitsi D (2010) J Phys Chem Lett 1:2025
3. Crespo-Hernández CE, Cohen B, Hare PM, Kohler B (2004) Chem Rev 104:1977
4. Middleton CT, de La Harpe K, Su C, Law YK, Crespo-Hernández CE, Kohler B (2009) Annu Rev Phys Chem 60:217
5. Kleinermanns K, Nachtigallova D, de Vries MS (2013) Int Rev Phys Chem 32:308
6. Takaya T, Su C, de La Harpe K, Crespo-Hernández CE, Kohler B (2008) Proc Natl Acad Sci USA 105:10285
7. Schreier WJ, Schrader TE, Koller FO, Gilch P, Crespo-Hernández CE, Swaminathan VN, Carell T, Zinth W, Kohler B (2007) Science 315:625
8. Schreier WJ, Kubon J, Regner N, Haiser K, Schrader TE, Zinth W, Clivio P, Gilch P (2009) J Am Chem Soc 131:5038
9. Su C, Middleton CT, Kohler B (2012) J Phys Chem B 116:10266
10. Ward DC, Reich E, Stryer L (1969) J Biol Chem 244:1228
11. Rist MJ, Marino JP (2002) Curr Org Chem 6:775
12. Thompson KC, Miyake N (2005) J Phys Chem B 109:6012
13. Crespo-Hernández CE, Cohen B, Kohler B (2005) Nature 436:1141
14. Kang H, Lee KT, Jung B, Ko YJ, Kim SK (2002) J Am Chem Soc 124:12958
15. Ullrich S, Schultz T, Zgierski MZ, Stolow A (2004) J Am Chem Soc 126:2262
16. Smith VR, Samoylova E, Ritze HH, Radloff W, Schultz T (2010) Phys Chem Chem Phys 12:9632
17. Banyasz A, Vayá I, Changenet-Barret P, Gustavsson T, Douki T, Markovitsi D (2011) J Am Chem Soc 133:5163
18. Towrie M, Grills DC, Dyer J, Weinstein JA, Matousek P, Barton R, Bailey PD, Subramaniam N, Kwok WM, Ma CS, Phillips D, Parker AW, George MW (2003) Appl Spectrosc 57:367
19. Towrie M, Doorley GW, George MW, Parker AW, Quinn SJ, Kelly JM (2009) Analyst 134:1265
20. Oliver TAA, Zhang Y, Ashfold MNR, Bradforth SE (2011) Faraday Discuss 150:439
21. Zhang Y, Chen J, Kohler B (2013) J Phys Chem A 117:6771
22. Chen J, Thazhathveetil AK, Lewis FD, Kohler B (2013) J Am Chem Soc 135:10290
23. Kwok W-M, Ma C, Phillips DL (2006) J Am Chem Soc 128:11894
24. Karunakaran V, Kleinermanns K, Improta R, Kovalenko SA (2009) J Am Chem Soc 131:5839
25. Pecourt J-ML, Peon J, Kohler B (2000) J Am Chem Soc 122:9348
26. Pecourt J-ML, Peon J, Kohler B (2001) J Am Chem Soc 123:10370
27. Crespo-Hernández CE, Kohler B (2004) J Phys Chem B 108:11182
28. Jou F-Y, Freeman GR (1979) J Phys Chem 83:2383
29. Hare PM, Crespo-Hernández CE, Kohler B (2007) Proc Natl Acad Sci U S A 104:435
30. Middleton CT, Cohen B, Kohler B (2007) J Phys Chem A 111:10460
31. Elles CG, Rivera CA, Zhang Y, Pieniazek PA, Bradforth SE (2009) J Chem Phys 130:13
32. Kovalenko SA, Dobryakov AL, Ruthmann J, Ernsting NP (1999) Phys Rev A 59:2369

33. Jailaubekov AE, Bradforth SE (2005) Appl Phys Lett 87
34. Tauber MJ, Mathies RA, Chen XY, Bradforth SE (2003) Rev Sci Instrum 74:4958
35. Zhang Y, Improta R, Kohler B (2014) Phys Chem Chem Phys 16:1487
36. Gustavsson T, Sharonov A, Markovitsi D (2002) Chem Phys Lett 351:195
37. Peon J, Zewail AH (2001) Chem Phys Lett 348:255
38. Gustavsson T, Sharonov A, Onidas D, Markovitsi D (2002) Chem Phys Lett 356:49
39. Pancur T, Schwalb NK, Renth F, Temps F (2005) Chem Phys 313:199
40. Markovitsi D, Gustavsson T, Talbot F (2007) Photochem Photobiol Sci 6:717
41. Markovitsi D, Onidas D, Talbot F, Marguet S, Gustavsson T, Lazzarotto E (2006) J Photochem Photobiol. A 183:1
42. Schweizer MP, Broom AD, Ts'o POP, Hollis DP (1968) J Am Chem Soc 90:1042
43. Broom AD, Schweizer MP, Ts'o POP (1967) J Am Chem Soc 89:3612
44. Valdes-Aguilera O, Neckers DC (1989) Acc Chem Res 22:171
45. Bloomfield VA, Crothers DM, Tinoco I Jr (1974) Physical chemistry of nucleic acids. Harper & Row, New York
46. Gray DM, Ratliff RL, Vaughan MR (1992) Methods Enzymol 211:389
47. Woody RW (1995) Biochem Spectroscopy 246:34
48. Berova N, Di Bari L, Pescitelli G (2007) Chem Soc Rev 36:914
49. Kypr J, Kejnovska I, Renciuk D, Vorlickova M (2009) Nucleic Acids Res 37:1713
50. Ke C, Humeniuk M, S-Gracz H, Marszalek PE (2007) Phys Rev Lett 99:018302
51. Seol Y, Skinner GM, Visscher K, Buhot A, Halperin A (2007) Phys Rev Lett 98:158103
52. Hatters DM, Wilson L, Atcliffe BW, Mulhern TD, Guzzo-Pernell N, Howlett GJ (2001) Biophys J 81:371
53. Mills JB, Vacano E, Hagerman PJ (1999) J Mol Biol 285:245
54. Banáš P, Mládek A, Otyepka M, Zgarbová M, Jurečka P, Svozil D, Lankaš F, Šponer J (2012) J Chem Theory Comput 8:2448
55. Chen AA, García AE (2013) Proc Natl Acad Sci U S A 110:16820
56. Olson WK, Bansal M, Burley SK, Dickerson RE, Gerstein M, Harvey SC, Heinemann U, Lu X-J, Neidle S, Shakked Z, Sklenar H, Suzuki M, Tung C-S, Westhof E, Wolberger C, Berman HM (2001) J Mol Biol 313:229
57. Rose IA, Hanson KR, Wilkinson KD, Wimmer MJ (1980) Proc Natl Acad Sci U S A 77:2439
58. Chen J, Kohler B (2014) J Am Chem Soc 136:6362
59. Olaso-González G, Merchán M, Serrano-Andrés L (2009) J Am Chem Soc 131:4368
60. Hunter RS, van Mourik T (2012) J Comput Chem 33:2161
61. Florián J, Šponer J, Warshel A (1999) J Phys Chem B 103:884
62. Jafilan S, Klein L, Hyun C, Florián J (2012) J Phys Chem B 116:3613
63. Šponer J, Leszczyński J, Hobza P (1996) J Phys Chem 100:5590
64. Šponer J, Šponer JE, Mládek A, Jurečka P, Bánaš P, Otyepka M (2013) Biopolymers 99:978
65. Ts'o POP, Melvin IS, Olson AC (1963) J Am Chem Soc 85:1289
66. Ts'o POP, Chan SI (1964) J Am Chem Soc 86:4176
67. Eimer W, Dorfmuller T (1992) J Phys Chem 96:6790
68. Hamlin RM Jr, Lord RC, Rich A (1965) Science (Washington, DC, USA) 148:1734
69. Kyogoku Y, Lord RC, Rich A (1967) J Am Chem Soc 89:496
70. Schwalb NK, Temps F (2007) J Am Chem Soc 129:9272
71. Schwalb NK, Michalak T, Temps F (2009) J Phys Chem B 113:16365
72. Plützer C, Hunig I, Kleinermanns K (2003) Phys Chem Chem Phys 5:1158
73. Asami H, Yagi K, Ohba M, Urashima S, Saigusa H (2013) Chem Phys 419:84
74. Šponer J, Jurečka P, Marchan I, Luque FJ, Orozco M, Hobza P (2006) Chem Eur J 12:2854
75. Lowe MJ, Schellman JA (1972) J Mol Biol 65:91
76. Brahms J, Michelson AM, van Holde KE (1966) J Mol Biol 15:467
77. Powell JT, Richards EG, Gratzer WB (1972) Biopolymers 11:235
78. Olsthoorn CSM, Bostelaar LJ, De Rooij JFM, Van Boom JH, Altona C (1981) Eur J Biochem 115:309

79. Buhot A, Halperin A (2004) Phys Rev E 70:020902
80. Donohue J, Trueblood KN (1960) J Mol Biol 2:363
81. Cohen B, Larson MH, Kohler B (2008) Chem Phys 350:165
82. Schwalb NK, Temps F (2009) J Photochem Photobiol. A 208:164
83. Miannay FA, Banyasz A, Gustavsson T, Markovitsi D (2009) J Phys Chem C 113:11760
84. Nguyen Thuan D, Haselsberger R, Michel-Beyerle M-E, Anh Tuan P (2013) ChemPhysChem 14:2667
85. Hunger K, Buschhaus L, Biemann L, Braun M, Kovalenko S, Improta R, Kleinermanns K (2013) Chem Eur J 19:5425
86. Changenet-Barret P, Hua Y, Markovitsi D (2014) Electronic excitations in guanine quadruplexes. Springer, Berlin Heidelberg, p 1
87. Schwalb NK, Temps F (2008) Science 322:243
88. Brahms J, Mommaerts WFH (1964) J Mol Biol 10:73
89. Cassani GR, Bollum FJ (1969) Biochemistry 8:3928
90. Ke CH, Loksztejn A, Jiang Y, Kim M, Humeniuk M, Rabbi M, Marszalek PE (2009) Biophys J 96:2918
91. Applequist J, Damle V (1966) J Am Chem Soc 88:3895
92. Luzzati V, Mathis A, Masson F, Witz J (1964) J Mol Biol 10:28
93. Nonin S, Leroy J-L, Gueron M (1995) Biochemistry 34:10652
94. Davis JT (2004) Angew Chem Int Ed 43:668
95. Gehring K, Leroy JL, Guéron M (1993) Nature 363:561
96. Leroy JL, Gueron M, Mergny JL, Helene C (1994) Nucleic Acids Res 22:1600
97. Holm AIS, Kohler B, Hoffmann SV, Nielsen SB (2010) Biopolymers 93:429
98. Plasser F, Lischka H (2012) J Chem Theory Comput 8:2777
99. Blancafort L, Voityuk AA (2014) J Chem Phys 140:8
100. Kasha M (1963) Radiat Res 20:55
101. Bouvier B, Gustavsson T, Markovitsi D, Millié P (2002) Chem Phys 275:75
102. Czader A, Bittner ER (2008) J Chem Phys 128:035101
103. Scholes GD, Ghiggino KP (1994) J Phys Chem 98:4580
104. Gould IR, Young RH, Mueller LJ, Albrecht AC, Farid S (1994) J Am Chem Soc 116:8188
105. Wang YS, Haze O, Dinnocenzo JP, Farid S, Farid RS, Gould IR (2007) J Org Chem 72:6970
106. Wang YS, Haze O, Dinnocenzo JP, Farid S, Farid RS, Gould IR (2008) J Phys Chem A 112:13088
107. Spata VA, Matsika S (2013) J Phys Chem A 117:8718
108. Improta R, Barone V (2011) Angew Chem Int Ed 50:12016
109. Voityuk AA (2013) Photochem Photobiol Sci 12:1303
110. Bouvier B, Dognon J-P, Lavery R, Markovitsi D, Millié P, Onidas D, Zakrzewska K (2003) J Phys Chem B 107:13512
111. Emanuele E, Markovitsi D, Millie P, Zakrzewska K (2005) ChemPhysChem 6:1387
112. Plasser F, Aquino AJA, Hase WL, Lischka H (2012) J Phys Chem A 116:11151
113. Mouret S, Philippe C, Gracia-Chantegrel J, Banyasz A, Karpati S, Markovitsi D, Douki T (2010) Org Biomol Chem 8:1706
114. Ritze HH, Hobza P, Nachtigallova D (2007) Phys Chem Chem Phys 9:1672
115. Santoro F, Barone V, Improta R (2009) J Am Chem Soc 131:15232
116. Conti I, Altoè P, Stenta M, Garavelli M, Orlandi G (2010) Phys Chem Chem Phys 12:5016
117. Santoro F, Barone V, Lami A, Improta R (2010) Phys Chem Chem Phys 12:4934
118. de La Harpe K, Kohler B (2011) J Phys Chem Lett 2:133
119. Zeleny T, Ruckenbauer M, Aquino AJA, Muller T, Lankas F, Drsata T, Hase WL, Nachtigallova D, Lischka H (2012) J Am Chem Soc 134:13662
120. Plasser F, Lischka H (2013) Photochem Photobiol Sci 12:1440
121. Banyasz A, Gustavsson T, Onidas D, Changenet-Barret P, Markovitsi D, Improta R (2013) Chem Eur J 19:3762
122. Stuhldreier MC, Temps F (2013) Faraday Discuss 163:173

123. Doorley GW, Wojdyla M, Watson GW, Towrie M, Parker AW, Kelly JM, Quinn SJ (2013) J Phys Chem Lett 4:2739
124. Markovitsi D, Gustavsson T, Vaya I (2010) J Phys Chem Lett 1:3271
125. Holcomb DN, Tinoco I Jr (1965) Biopolymers 3:121
126. Eisenberg H, Felsenfeld G (1967) J Mol Biol 30:17
127. Warshaw MM, Tinoco I Jr (1965) J Mol Biol 13:54
128. Ogasawara N, Inoue Y (1976) J Am Chem Soc 98:7048
129. Dolinnaya NG, Fresco JR (1992) Proc Natl Acad Sci USA 89:9242
130. Stuhldreier MC, Schüler C, Kleber J, Temps F (2011) In: Chergui M, Jonas D, Riedle E, Schoenlein R, Taylor A (eds) Ultrafast phenomena XVII proceedings of the 17th international conference, Snowmass, Colorado, USA, July 18–23, 2010 Oxford University Press, New York, p 553
131. Eisinger J, Guéron M, Shulman RG, Yamane T (1966) Proc Natl Acad Sci U S A 55:1015
132. Buchvarov I, Wang Q, Raytchev M, Trifonov A, Fiebig T (2007) Proc Natl Acad Sci U S A 104:4794
133. Lu Y, Lan ZG, Thiel W (2011) Angew Chem Int Ed 50:6864
134. Lu Y, Lan ZG, Thiel W (2012) J Comput Chem 33:1225
135. Onidas D, Gustavsson T, Lazzarotto E, Markovitsi D (2007) J Phys Chem B 111:9644
136. Bucher DB, Pilles BM, Carell T, Zinth W (2014) Proc Natl Acad Sci U S A 111:4369
137. Zhang Y, Dood J, Beckstead AA, Li X-B, Nguyen KV, Burrows CJ, Improta R, Kohler B (2014) Proc Natl Acad Sci U S A 111:11612
138. Nguyen KV, Burrows CJ (2011) J Am Chem Soc 133:14586
139. Zhang Y, Dood J, Beckstead A, Chen J, Li X-B, Burrows CJ, Lu Z, Matsika S, Kohler B (2013) J Phys Chem A 117:12851
140. Pan ZZ, Chen JQ, Schreier WJ, Kohler B, Lewis FD (2012) J Phys Chem B 116:698
141. Onidas D, Markovitsi D, Marguet S, Sharonov A, Gustavsson T (2002) J Phys Chem B 106:11367
142. Improta R, Santoro F, Barone V, Lami A (2009) J Phys Chem A 113:15346
143. Santoro F, Improta R, Avila F, Segado M, Lami A (2013) Photochem Photobiol Sci 12:1527
144. Dreuw A, Weisman JL, Head-Gordon M (2003) J Chem Phys 119:2943
145. Lange AW, Rohrdanz MA, Herbert JM (2008) J Phys Chem B 112:6304
146. Improta R (2008) Phys Chem Chem Phys 10:2656
147. Lange AW, Herbert JM (2009) J Am Chem Soc 131:3913
148. Szalay PG, Watson T, Perera A, Lotrich V, Bartlett RJ (2013) J Phys Chem A 117:3149
149. Markovitsi D, Talbot F, Gustavsson T, Onidas D, Lazzarotto E, Marguet S (2006) Nature 441:E7
150. Jimenez R, Fleming GR, Kumar PV, Maroncelli M (1994) Nature 369:471
151. Andreatta D, Lustres JLP, Kovalenko SA, Ernsting NP, Murphy CJ, Coleman RS, Berg MA (2005) J Am Chem Soc 127:7270
152. Furse KE, Corcelli SA (2010) J Phys Chem Lett 1:1813
153. Tazawa S, Tazawa I, Tso POP, Alderfer JL (1972) Biochemistry 11:3544
154. Guckian KM, Schweitzer BA, Ren RXF, Sheils CJ, Tahmassebi DC, Kool ET (2000) J Am Chem Soc 122:2213
155. Johnson WC Jr, Itzkowitz MS, Tinoco I Jr (1972) Biopolymers 11:225
156. Šponer J, Riley KE, Hobza P (2008) Phys Chem Chem Phys 10:2595
157. Norberg J, Nilsson L (1998) Biophys J 74:394
158. Murata K, Sugita Y, Okamoto Y (2004) Chem Phys Lett 385:1
159. Davis RC, Tinoco I Jr (1968) Biopolymers 6:223
160. Scott JF, Zamecnik PC (1969) Proc Natl Acad Sci U S A 64:1308
161. Stern N, Major DT, Gottlieb HE, Weizman D, Fischer B (2010) Org Biomol Chem 8:4637
162. Moser CC, Keske JM, Warncke K, Farid RS, Dutton PL (1992) Nature 355:796
163. Zhang WY, Yuan SA, Wang ZJ, Qi ZM, Zhao JS, Dou YS, Lo GV (2011) Chem Phys Lett 506:303

164. Dou YS, Liu ZC, Yuan S, Zhang WY, Tang H, Zhao JS, Fang WH, Lo GV (2013) Int J Biol Macromol 52:358
165. Markovitsi D, Onidas D, Gustavsson T, Talbot F, Lazzarotto E (2005) J Am Chem Soc 127:17130
166. Wilson RW, Callis PR (1976) J Phys Chem 80:2280
167. Nielsen LM, Hoffmann SV, Nielsen SB (2013) Photochem Photobiol Sci 12:1273
168. Tonzani S, Schatz GC (2008) J Am Chem Soc 130:7607
169. Shao F, Augustyn K, Barton JK (2005) J Am Chem Soc 127:17445
170. Simpkins H, Richards EG (1967) J Mol Biol 29:349
171. Löwdin PO (1963) Rev Mod Phys 35:724
172. Cohen B, Hare PM, Kohler B (2003) J Am Chem Soc 125:13594
173. Gustavsson T, Sarkar N, Lazzarotto E, Markovitsi D, Improta R (2006) Chem Phys Lett 429:551
174. Gustavsson T, Banyasz A, Sarkar N, Markovitsi D, Improta R (2008) Chem Phys 350:186
175. Sobolewski AL, Domcke W (2004) Phys Chem Chem Phys 6:2763
176. Perun S, Sobolewski AL, Domcke W (2006) J Phys Chem A 110:9031
177. Abo-Riziq A, Grace L, Nir E, Kabelac M, Hobza P, de Vries MS (2005) Proc Natl Acad Sci U S A 102:20
178. Biemann L, Kovalenko SA, Kleinermanns K, Mahrwald R, Markert M, Improta R (2011) J Am Chem Soc 133:19664
179. Roettger K, Soennichsen FD, Temps F (2013) Photochem Photobiol Sci 12:1466
180. Crespo-Hernández CE, de La Harpe K, Kohler B (2008) J Am Chem Soc 130:10844
181. Brazard J, Thazhathveetil AK, Vaya I, Lewis FD, Gustavsson T, Markovitsi D (2013) Photochem Photobiol Sci 12:1453
182. Santoro F, Barone V, Improta R (2007) Proc Natl Acad Sci U S A 104:9931
183. Improta R (2012) J Phys Chem B 116:14261
184. de La Harpe K, Crespo-Hernández CE, Kohler B (2009) ChemPhysChem 10:1421
185. Doorley GW, McGovern DA, George MW, Towrie M, Parker AW, Kelly JM, Quinn SJ (2009) Angew Chem Int Ed 48:123
186. Vayá I, Gustavsson T, Miannay FA, Douki T, Markovitsi D (2010) J Am Chem Soc 132:11834
187. de La Harpe K, Crespo-Hernández CE, Kohler B (2009) J Am Chem Soc 131:17557
188. Kumar A, Sevilla MD (2013) Photochem Photobiol Sci 12:1328
189. Colson AO, Besler B, Sevilla MD (1992) J Phys Chem 96:9787
190. Colson A-O, Besler B, Close DM, Sevilla MD (1992) J Phys Chem 96:661
191. Bertran J, Oliva A, Rodríguez-Santiago L, Sodupe M (1998) J Am Chem Soc 120:8159
192. Li X, Cai Z, Sevilla MD (2001) J Phys Chem B 105:10115
193. Kumar A, Sevilla MD (2010) Chem Rev 110:7002
194. Guallar V, Douhal A, Moreno M, Lluch JM (1999) J Phys Chem A 103:6251
195. Kumar A, Sevilla MD (2009) J Phys Chem B 113:11359
196. Ko C, Hammes-Schiffer S (2013) J Phys Chem Lett 4:2540
197. Chinnapen DJF, Sen D (2004) Proc Natl Acad Sci U S A 101:65
198. Holman MR, Ito T, Rokita SE (2007) J Am Chem Soc 129:6
199. Law YK, Forties RA, Liu X, Poirier MG, Kohler B (2013) Photochem Photobiol Sci 12:1431
200. Kao YT, Saxena C, Wang LJ, Sancar A, Zhong DP (2005) Proc Natl Acad Sci U S A 102:16128
201. Jorns MS (1987) J Am Chem Soc 109:3133
202. Shafirovich V, Dourandin A, Geacintov NE (2001) J Phys Chem B 105:8431
203. Shafirovich V, Dourandin A, Luneva NP, Geacintov NE (2000) J Phys Chem B 104:137
204. Shafirovich V, Dourandin A, Huang W, Luneva NP, Geacintov NE (1999) J Phys Chem B 103:10924
205. Shafirovich VY, Courtney SH, Ya N, Geacintov NE (1995) J Am Chem Soc 117:4920
206. Spoerlein S, Carstens H, Satzger H, Renner C, Behrendt R, Morader L, Tavan P, Zinth W, Wachtveitl J (2002) Proc Natl Acad Sci U S A 99:7998

Top Curr Chem (2015) 356: 89–122
DOI: 10.1007/128_2014_533

Published online: 20 March 2014

Computational Modeling of Photoexcitation in DNA Single and Double Strands

You Lu, Zhenggang Lan, and Walter Thiel

Abstract The photoexcitation of DNA strands triggers extremely complex photo-induced processes, which cannot be understood solely on the basis of the behavior of the nucleobase building blocks. Decisive factors in DNA oligomers and polymers include collective electronic effects, excitonic coupling, hydrogen-bonding interactions, local steric hindrance, charge transfer, and environmental and solvent effects. This chapter surveys recent theoretical and computational efforts to model real-world excited-state DNA strands using a variety of established and emerging theoretical methods. One central issue is the role of localized vs delocalized excitations and the extent to which they determine the nature and the temporal evolution of the initial photoexcitation in DNA strands.

Keywords Base pairing · Base stacking · Charge transfer · Delocalized state · DNA strand · Exciton · Hydrogen bond · Nonadiabatic dynamics · Photoexcitation · QM/MM

Y. Lu
Scientific Computing and Modeling NV, Vrije Universiteit, De Boelelaan 1083, 1081HV, Amsterdam, The Netherlands

Z. Lan (✉)
Key Laboratory of Biobased Materials, Qingdao Institute of Bioenergy and Bioprocess Technology, Chinese Academy of Sciences, 189 Songling Road, Qingdao 266101, Shandong, P. R. China

The Qingdao Key Laboratory of Solar Energy Utilization and Energy Storage Technology, QIBEBT-CAS, 189 Songling Road, Qingdao 266101, Shandong, P. R. China
e-mail: lanzg@qibebt.ac.cn

W. Thiel (✉)
Max-Planck-Institut für Kohlenforschung, Kaiser-Wilhelm-Platz 1, 45470 Mülheim an der Ruhr, Germany
e-mail: thiel@kofo.mpg.de

Contents

Abbreviations

A	Adenine derivatives
ADC	Algebraic diagrammatic construction
Ade	9*H*-Adenine
AM1	Austin model 1
C	Cytosine derivatives
CASPT2	Complete active space second-order perturbation theory
CASSCF	Complete active space self-consistent field
CC	Coupled cluster
CC2	Second-order coupled cluster
CCSD	Coupled cluster singles and doubles
CI	Configuration interaction
CIS	Configuration interaction singles
CISD	Configuration interaction singles and doubles
CMP	Cytidine monophosphate
CPD	Cyclobutane pyrimidine dimer
CT	Charge transfer
Cyt	Cytosine
dA	Deoxyadenosine monophosphate (or dAMP)
dAdo	Deoxyadenosine
dC	Deoxycytidine monophosphate (or dCMP)
DFT	Density functional theory
dG	Deoxyguanosine monophosphate (or dGMP)
DNA	Deoxyribonucleic acid
dT	Deoxythymidine monophosphate (or dGMP)
dThd	Deoxythymidine
FAD	Flavin adenine dinucleotide
G	Guanine derivatives
GMP	Guanosine monophosphate

Gua	9*H*-Guanine
HF	Hartree–Fock
KS	Kohn–Sham
LIIC	Linear interpolation in internal coordinates
LRC-TDDFT	Long-range-corrected time-dependent density functional theory
LR-TDDFT	Linear response time-dependent density functional theory
m^1T	1-Methylthymine
m^9A	9-Methyladenine
MCSCF	Multi-configurational self-consistent field
MD	Molecular dynamics
MNDO	Modified neglect of diatomic overlap
MO	Molecular orbital
MP2	Second-order Møller–Plesset perturbation
MRCI	Multi-reference configuration interaction
NDDO	Neglect of diatomic differential overlap
OM2	Orthogonalization model 2
PCM	Polarizable continuum model
PES	Potential energy surface
PM3	Parameterized model 3
QM/MM	Quantum mechanics/molecular mechanics
RNA	Ribonucleic acid
RPA	Random phase approximation
T	Thymine derivatives
TDA	Tamm–Dancoff approximation
TDDFT	Time-dependent density functional theory
TDHF	Time-dependent Hartree–Fock
Thy	Thymine
TSH	Trajectory surface hopping
UV	Ultraviolet
ZDO	Zero overlap differential
ZINDO	Zerner's intermediate neglect of differential overlap
ZINDO/S	Zerner's intermediate neglect of differential overlap for spectra

1 Introduction

In the fields of photophysics, photochemistry, and photobiology, one essential goal is to understand the photoinduced reactions of deoxyribonucleic acid (DNA) and ribonucleic acid (RNA) that are crucial for the photostability of the genetic material. In the past decades, thanks to the rapid development of spectroscopic techniques, numerous advanced experiments have provided detailed information on DNA excited-state processes [1–11]. Even so, it is rather difficult for experimental work alone to identify the roles of the many different mechanisms that are entangled with each other during DNA photoreactions. Therefore, theoretical studies have become

valuable as guides and supplements to experimental studies [12–14]. However, the theoretical treatment of complex excited-state DNA systems is clearly still very challenging [12, 14, 15].

All photoinduced processes of DNA start with an initial photoexcitation. The building blocks of DNA and RNA – adenine (A), thymine (T), guanine (G), cytosine (C), and uracil (U)[1] [16, 17] – contain five- and/or six-membered aromatic rings, which show strong absorption in the ultraviolet (UV) between 4–6 eV [1, 18, 19]. The absorption (and emission) spectra of DNA strands are not simply a superposition of the corresponding spectra of the individual nucleobases (or nucleosides/nucleotides). Instead, excitations on individual bases may couple to each other such that the overall excitation becomes delocalized over multiple bases [4–6, 9, 10]. If this is the case, an *excimer/exciplex* (an excited-state dimer/excited-state complex) will be formed [5], which is called a *Frenkel exciton* if the promoted electron is still tightly bound to the generated "hole" through Coulomb interactions [4, 5, 10, 20]. The formation mechanism of delocalized states in DNA strands is still debated, especially with regard to the size of the delocalized domain [5].

Studying DNA excited-state dynamics is even more challenging due to the existence of many possible reaction channels. Time-resolved spectroscopic experiments show that the UV absorption of DNA is followed by an ultrafast decay of the excited states [5, 21]. This indicates the existence of nonadiabatic processes, i.e., transitions from one electronic state to another through efficient nonradiative internal-conversion channels that allow the system to repopulate the electronic ground state [2, 5]. Such processes have drawn much recent interest, since they are believed to be dominant in many excited-state phenomena, such as the internal conversion of nucleobase monomers, hydrogen transfer between adjacent paired bases, and the nonradiative decay of stacked bases through delocalized pathways [5]. Proper modeling of such dynamical processes requires descriptions that take into account the breakdown of the *Born–Oppenheimer approximation* and the coupling of electronic and nuclear motion during internal conversion [22, 23].

Nonadiabatic processes are capable of dissipating the excess energy brought by photons before further photochemical reactions take place. This prevents organisms from being damaged by photoreactions and thus provides *photostability* [24]. It is conceivable that photostability is an outcome of natural selection during evolution [25]. In organisms, more than 99.9% of photon energy is dissipated through photoprotection mechanisms [26], with the remainder ($<0.1\%$) being responsible for sunburn and some skin cancers [27, 28]. In the latter case, photolesion occurs as DNA strands undergo complicated photochemical reactions. Dimerization of two stacked pyrimidines is commonly perceived as the mechanism of photolesion [5, 29]. However, on the theoretical side, there are still open points in the modeling of pyrimidine dimerization that need to be clarified [5], since it is difficult to set up

[1] We use the IUB 1984 one-letter abbreviations [16] for the associated DNA strand building blocks, while we specify the variants of nucleobase, nucleoside, or nucleotide with the IUPAC-IUB 1970 three-letter abbreviations [17] (throughout the chapter unless otherwise stated).

reasonable models for the potential influence of the photoinactive sugar-phosphate backbones and the biological/solvent environments while balancing computational accuracy and efficiency [30, 31].

Much recent research has been devoted to the mechanisms of the various photoinduced processes that occur in DNA strands after UV excitation [5, 8, 32–37]. In this chapter, we outline recent progress in computational studies on the photoexcitation of DNA strands. Given the limited space, we do not aim for a comprehensive account of all published work, but rather for a general overview. We highlight the most important experimental advances in this field only briefly, since they have been presented in recent reviews [2–11] and in other chapters of this book. Likewise, we cover the excited-state features of small DNA units, such as single nucleobases and hydrogen-bonded base pairs, only to the extent needed for the discussion of the DNA strands, without going into much detail. This chapter is structured as follows. Section 2 introduces the theoretical models and computational techniques often applied to excited-state DNA systems. Section 3 first summarizes the experimental results (Sect. 3.1) and then reviews theoretical studies on DNA excited states (Sect. 3.2) at different stages of modeling – from isolated nucleobases via single nucleobases in DNA strands and stacked nucleobases to solvated DNA single and double strands. In Sects. 3.3 and 3.4 we discuss the effects of base stacking and pairing on the photoinduced processes of DNA strands, as well as the influence of the DNA biological/solvent environment and the formation of excitons and excimers/exciplexes. Finally, we address the photodamage caused by dimerization (Sect. 3.5) and the photoexcitation of modified and other helical conformations of DNA strands (Sect. 3.6).

2 Theoretical Background

2.1 Excited-State Electronic Structure Methods

The past few decades have witnessed the development of a hierarchy of quantum-chemical methods that can be used to investigate the structures and properties of molecules and solids [38, 39]. Nowadays, properties and reactions in the electronic ground state can be studied routinely by computation. High-level ab initio methods, such as coupled cluster theory [40] and Møller–Plesset perturbation theory [41], give accurate predictions for ground-state properties. Because of its favorable cost-performance ratio, density functional theory (DFT) is used widely and successfully in studies of chemical reactions [42], both in organic and transition metal chemistry. Moreover, there are fast semiempirical approaches for treating large systems [43, 44]. One of the central tasks in this field is to develop efficient high-level correlated methods to deal with large systems without losing much accuracy [38, 39].

Concerning excited states, electronic-structure calculations provide information on various kinds of spectra (including absorption, emission, electronic energy loss,

and circular dichroism spectra), on excited-state potential energy surfaces (PESs) and reaction pathways, and on the geometries of excited-state minima, *conical intersections*, and intermediates [14, 15, 45–49]. Generally speaking, the modeling is more demanding for excited states than for the ground state, and many different approaches are in use [14, 15]. However, unlike in the case of the ground state, there is no "standard" approach to excited-state electronic-structure problems in general. The existing excited-state electronic-structure methods all have their merits and shortcomings – with regard to accuracy, general applicability, and computational demand [50–55]. One should thus carefully examine the suitability of the available methods before making a specific choice for a given application [14, 15]. In the following, we give a brief overview of some of the mainstream theories for calculating the electronic structure of excited states.

2.1.1 Configuration Interaction

The configuration interaction (CI) ansatz [50, 56, 57] describes the electronic wavefunction as a linear combination of configuration state functions (in the simplest case: Slater determinants). The CI eigenvalues and eigenvectors are determined by a variational calculation [56, 57]. In the standard single-reference CI treatment, all excited configurations are generated from just one reference configuration. In most cases, the ground-state Slater determinant obtained from Hartree–Fock (HF) theory is taken as the reference, and the excited configurations are derived by exciting electrons from the occupied HF molecular orbitals (MOs) to the virtual MOs. Inclusion of all possible excited configurations leads to full CI (FCI) treatment, which yields the exact results for the given basis set. However, even for small compounds, FCI is extremely expensive [56, 57]. Thus, in practice, approximations are adopted to reduce the number of configurations in the CI expansion, typically by truncating at a certain excitation level. Inclusion of only single or only single and double excitations results in the popular CIS and CISD methods, respectively. The efficient CIS approach can easily be applied to medium-sized systems such as the DNA nucleobases [58–61]. CIS will give a qualitatively reasonable description if the problem under study happens to involve just single excitations. Still, the accuracy of CIS is often unsatisfactory, as there can be errors in the computed vertical excitation energies of more than 1.5 eV in some cases [14]. The deviations may become even larger when doubly excited or charge-transfer excited states are involved [62].

2.1.2 Coupled Cluster Theory

Among the single-reference methods, coupled cluster (CC) theory provides some of the most accurate models for excited states [51, 53, 54]. They are size-consistent and size-extensive by design. The coupled-cluster expansion [40] automatically includes the contributions of many higher-order excitations (i.e., those that can be

constructed from the lower-order terms via the exponential cluster ansatz). Most widely used is the coupled cluster method with single and double excitations (CCSD). Inclusion of a perturbational estimate of the contributions from the triple excitations leads to the CCSD(T) method that is currently considered as the "gold standard" for ground-state calculations [63]. For electronically excited states, approximate CC treatments can be formulated in the framework of linear response theory, for example CC2 (second order) or CC3 (third order) [64]. CC2 is quite efficient and fairly accurate for excited states that are dominated by single excitations [51, 54]. An alternative is the equation-of-motion coupled cluster (EOM-CC) method [65–68] which has been implemented at the EOM-CCSD and higher levels, also on massively parallel computers [69]. The EOM-CC approaches are computationally very demanding, but also very accurate. In benchmarks by Szalay and coworkers, they were shown to be capable of describing excited-state DNA building blocks most accurately [68, 70–72]. CC-based methods have been applied successfully to study the excited states of DNA nucleobase/strand systems, for example in [67, 73–76].

2.1.3 Multi-configuration and Multi-reference Treatments

Sometimes the HF determinant does not provide a qualitatively adequate zero-order description of the electronic structure, for example in quasi-degenerate states as encountered near conical intersections. Such situations can be handled by the multi-configurational self-consistent-field (MCSCF) method. In this ansatz, the wavefunction is expanded in terms of a set of predefined configurations, and both the MO and CI coefficients are optimized [77–81]. The MCSCF theory is thus fully variational with respect to the MO and CI vectors. A systematic approach is to define an *active space* including a limited number of MOs and to perform an FCI treatment within the active space – this is the complete active space self-consistent-field (CASSCF) method [77, 80]. A simplified variant is the restricted active space self-consistent-field (RASSCF) method [82, 83], in which the active space is partitioned and CI excitations are truncated for certain parts of the active space. CASSCF and RASSCF can describe quasi-degenerate electronic states in a qualitatively correct manner, and they are therefore well suited for exploring the topology of excited-state potential surfaces. Being popular tools in theoretical studies of excited states, they have been used for constructing nucleobase photoreaction paths and for simulating nucleobase photodynamics, for example, in [73, 84–87]. However, because of limitations in the size of the active space, CASSCF misses much of the dynamic electron correlation, which may cause large errors in the computed excitation energies. A remedy is to apply second-order perturbation theory on top of CASSCF [88, 89]. The resulting CASPT2 treatment generally gives excellent excitation energies [51, 55, 88, 89] for the valence excited states of organic molecules. The computational cost of the CAS methods grows dramatically with the active space size. In practice, active spaces with 14–18 orbitals/electrons can typically be handled with currently available computational resources, which are just about sufficient for

an appropriate description of nucleobases and base pairs. The proper choice of the active space is crucial in CAS methods, because missing relevant orbitals may lead to unsafe results, even for vertical excitation energies [51, 55]. An alternative to CASPT2 is to perform multi-reference configuration interaction (MRCI) calculations based on CASSCF orbitals [81]. For example, selected CASSCF solutions can be used as references on which the CI expansion is built, typically by considering single and double excitations. In this manner, one may construct small CI expansions that yield reasonable results with affordable computational cost [81]

2.1.4 Semiempirical Methods

In the ab initio Hartree–Fock approach, the construction of the Fock matrix requires evaluation of a large number of multicenter two-electron integrals over the atomic orbitals. This step can be rather time-consuming for large systems. In semiempirical methods, many of these integrals are neglected, and the remaining ones are usually represented by expressions containing parameters that are adjusted against experimental reference data. There are several levels of approximation that result in different semiempirical models [43, 44]. Popular semiempirical MO methods include AM1 (Austin model 1) [90], PMx (parameterized models, $x = 3$–7) [91–96], and OMx (orthogonalization models, $x = 1$–3) [97–101]. Any type of semiempirical Hamiltonian can be integrated into CI approaches to describe excited states. Early attempts were the development of ZINDO/S [102, 103] and AM1/CI [104]. It was pointed out that ZINDO/S outperforms other semiempirical methods in the description of the DNA charge-transfer electronic coupling [105]. The AM1/CI and PM3/CI methods were recently shown to be capable of modeling semiclassical nonadiabatic dynamics of DNA fragments [106, 107].

Most semiempirical models rely on the zero differential overlap (ZDO) approximation and thus tend to fail in properly predicting MO energy gaps [100] and excitation energies. Carrying out a targeted reparameterization can partly make up for this deficiency – for example, ZINDO/S was especially parameterized to reproduce electronic spectra [108]. An alternative is to include orthogonalization corrections into the semiempirical Fock matrix as done in the OMx methods. This leads to an asymmetric splitting of bonding and antibonding orbitals, with the latter being destabilized more than the former are stabilized (as in the ab initio case and hence superior to the symmetric splitting in standard ZDO-based methods). The OMx MOs thus provide a reasonable starting point for an MRCI treatment of electronically excited states. Conceptually, dynamic electron correlation is effectively incorporated in the semiempirical Hamiltonian, and it is thus generally sufficient to perform OMx/MRCI calculations with a small (minimum) number of reference configurations and a rather small active space (typically including only single and double excitations). Benchmark calculations show that the OM2/MRCI approach gives rather reliable results for the excited states of many organic molecules [109]. For example, the overall mean absolute deviation of (singlet and

triplet) vertical excitation energies is about 0.4–0.5 eV [109]. OM2/MRCI was successfully employed in a series of studies on both the static excited-state properties and the nonadiabatic dynamics of DNA base/strand systems [110–116].

2.1.5 Density Functional Theory

Density functional theory (DFT) is currently the workhorse for most ground-state calculations, thanks to its reliability and high efficiency [42]. Its time-dependent version (TDDFT) [50, 117] is designed to compute excited-state properties. In most cases, TDDFT calculations evaluate the linear response (LR) of the time-dependent Kohn–Sham (KS) density to the perturbing external potential. This LR-TDDFT approach has become the standard TDDFT implementation [50, 117]. Since it is computationally efficient and appears like a "black-box" method, TDDFT is currently the most popular single-determinant method for treating excited states [117]. However, it should be applied with caution, because it is not a genuine "black-box" method and has prominent limitations [14, 50]. TDDFT generally describes valence excited states quite well, with absolute mean deviations of about 0.3–0.5 eV for excitation energies (compared with accurate ab initio results) [52]; however, when charge-transfer excitations are involved, TDDFT with standard functionals is erratic and yields severely underestimated excitation energies [14, 50, 118]. Moreover, doubly-excited states cannot be handled unless one resorts to special treatments [119]. Range-separated hybrid functionals were developed to overcome the charge-transfer problems, by introducing different weights of HF exchange for short-range and long-range interactions. Validations of long-range-corrected (LRC) TDDFT methods [120] for charge-transfer states of π-stacked adenines showed that their performance can be tuned well by introducing an adjustable length-scale parameter [60, 121]. In comparisons [122] of three recent LRC functionals, namely BNL [123, 124], CAM-B3LYP [125], and LC-PBE0 [126, 127], it was found that only CAM-B3LYP gave reasonable energies for the interbase charge-transfer excited states of the hydrogen-bonded Watson–Crick A·T and G·C base pairs. There are also indications that the meta-hybrid M06-HF [128] and M06-2X [129] functionals may be adequate to treat the photoexcitation of nucleobase monomers and oligomers [130]. However, in a systematic excited-state dynamics study of 9*H*-adenine (Ade), the experimentally observed ultrafast decay was not reproduced in TDDFT-based surface hopping simulations with any of the six tested functionals (PBE, B3LYP, PBE0, CAM-B3LYP, BHLYP, and M06-HF) whereas reasonable decay times were obtained at the ab initio MRCIS and the semiempirical OM2/MRCI levels [131]. TDDFT is widely applied to construct delocalized exciton-type Hamiltonians for DNA strands consisting of stacked nucleobases (see Sect. 2.1.7).

As a single-reference method, canonical TDDFT encounters severe difficulties around conical intersections. The Tamm–Dancoff approximation (TDA) [50] is presumed to alleviate the problems associated with nearly degenerate states [132–134],

but its performance still needs to be examined carefully. An alternative promising approach to handle such situations is provided by multi-reference DFT-based methods such as DFT/MRCI [135].

2.1.6 Polarization Propagator Methods

Response theory can be applied not only to KS-DFT but also to other theoretical schemes. In this framework, one computes the frequency-dependent polarizability (i.e., the response to the incoming light) and determines the excitation energies from the poles of this function. This approach is called polarization propagator [136] because of its relation to the many-body Green's function propagator theory. Popular response methods for excited-state calculations are time-dependent HF (TDHF) theory and the random phase approximation (RPA), with the latter providing results of similar quality as CIS [50]. A perturbative expansion [137] can be applied to the polarization propagator using the algebraic diagrammatic construction (ADC) [138]. Expansion up to second and third order leads to the ADC(2) and ADC(3) methods, respectively. Loosely speaking, ADC(2) can be considered as an MP2 variant for excited states. It often provides excellent accuracy, particularly for charge-transfer states that are problematic in TDDFT. ADC methods have been applied successfully to simulate a DNA double-stranded system [76] (see Sect. 3.3).

2.1.7 Excitons

The electronic transition triggered by photoexcitation may lead to charge separation between the electron being excited (e^-) and the remaining hole (h^+). The term "exciton" denotes a bound state that is supported by the Coulomb attraction between this electron and the hole. This concept is borrowed from solid-state physics: when the e^-/h^+ pair is separated by a sufficiently large distance, there is a completely delocalized Wannier–Mott exciton that is often encountered in metals and semiconductors [139]; when the distance is not large enough, a Frenkel exciton [20] is formed with a relatively localized excitation that may, however, still be delocalized over several chromophore units. Excitons may thus be formed by or after photoexcitation in complex systems with multiple similar chromophores, such as for instance in DNA strands [5].

In quantum chemistry, the extent of localization/delocalization of a Frenkel exciton can be assessed through the coupling between the excitations on different individual chromophores. As an example, we briefly outline a typical procedure used for constructing an excitonic model of DNA strands [140, 141]. First, a ground-state molecular dynamics (MD) simulation was run to get a few snapshots with different conformations of DNA strands. For each of them, the low-lying excited states of the individual bases were then calculated at the quantum level, including the electrostatic interactions with the other bases in the strand and with

the solvent environment, which defined the diagonal terms of the excitonic Hamiltonian. The off-diagonal terms (i.e., the electronic couplings between different chromophore units) were evaluated from the dipole–dipole interactions. The electronic states of the DNA strands were then obtained by diagonalizing the excitonic Hamiltonian. The energies, couplings, and eigenstates of the chromophore units showed some fluctuation among the MD snapshots.

2.2 Hybrid QM/MM Methods

The theoretical description of the excited states of solvated DNA bases/oligomers/polymers (with thousands of atoms) is challenging because of the high computational demands of the electronic-structure calculations. Fortunately, photoinduced processes usually take place within a relatively small part of the whole system, and the remaining thousands of atoms have only an indirect influence, mainly through steric and electrostatic interactions. In such a situation, it is reasonable to apply the hybrid quantum mechanics/molecular mechanics (QM/MM) method [142, 143] which divides the system into (at least) two subdomains: the QM region is the photoactive part that is treated at a suitable level of quantum mechanics; the MM region, containing the remaining part of the whole system including solvent, is mimicked by a molecular mechanics method (normally an additive force field). The electrostatic interactions between the QM and MM parts can be treated at different levels of approximation. As the name suggests, mechanical embedding completely neglects polarization effects between the QM and MM regions so that the MM environment only affords steric effects. By contrast, electronic embedding considers the QM region as being immersed in a background of MM point charges (effective force-field charges), which leads to electronic QM polarization in response to the MM environment. Electronic QM/MM embedding was shown to be indispensable for correctly representing excited-state DNA systems, as it strikingly modulates the excited-state dynamics [76, 114, 115, 144].

Some QM-only investigations on DNA excited states have employed implicit solvent models [145, 146], e.g., the polarizable continuum model (PCM) [147–158]. Since these models do not consider the explicit atomic surrounding of the investigated DNA chromophores, they simplify the complex biomolecular environment in DNA by treating it as a homogeneous solvent with an effective dielectricity constant.

2.3 Nonadiabatic Dynamics

Compared with the ground state, the PES topology is usually far more complicated in excited states. Photoexcitation may trigger a number of complex photoinduced processes including reactions on a single excited-state PES as well as transitions between different electronic states, the PESs of which may approach or even cross each other. One type of surface crossing is a conical intersection [45, 47–49]

between two electronic states with the same multiplicity. In the vicinity of conical intersections, strong interstate couplings (nonadiabatic vibronic couplings) induce ultrafast transitions between the states. The theoretical description of such internal conversion processes must go beyond the Born–Oppenheimer approximation and account for the coupled electron-nuclear motion [23]. A second type of crossing is due to the spin-orbit coupling between states of different multiplicities; such intersystem crossings may also be involved in some photoprocesses of DNA [159–163], as discussed, for example, in [5]. However, internal conversion is generally considered to be the mechanism that dominates the photoinduced processes in DNA systems [5, 18, 19].

For a detailed understanding of DNA photoreactions, it is essential to run nonadiabatic excited-state dynamics to determine the branching ratios of possible reaction channels, the lifetimes of excited-state species, and time-resolved spectra. This is challenging given both the size and complexity of DNA and the need for a self-consistent treatment of the electronic and nuclear degrees of freedom. Among the various available dynamics methods [22, 48, 49, 164–166], the trajectory surface hopping (TSH) approach is one of the most popular [15]. TSH propagates the nuclear motion along a classical trajectory on a single adiabatic PES, while computing the electronic wavefunction at each step on the fly. Nonadiabatic transitions are modeled as instantaneous hops between different adiabatic PESs. There are different approaches to determine the hopping probability, with the fewest-switches algorithm [167] being most widely used. Due to its simplicity, TSH can be easily performed at different theoretical levels, both QM-only and QM/MM [14, 15]. In the TSH framework, the photodynamic behavior remains fully governed by the PESs, but pre-construction of high-dimensional PESs is avoided. TSH is commonly considered as a most practical tool for efficient nonadiabatic dynamics simulations in large systems like DNA strands. Successful TSH studies on DNA photodynamics will be presented in Sect. 3.

Other nonadiabatic dynamics methods include multi-configuration time-dependent Hartree [164, 168], ab initio multiple spawning [165, 166], mean-field Ehrenfest dynamics [169], coherent switching with decay of mixing [170], and quantum-classical Liouville [169] approaches. Some of these are very expensive and not yet applicable to DNA systems, while others have been employed to study DNA photochemistry. For example, a recently developed method called semiclassical electron-radiation-ion dynamics, a kind of real-time electrodynamics starting from the Ehrenfest theorem, was reported to give reasonable results for excited-state DNA bases [171].

3 Photoexcitation of DNA Strands

Various theoretical approaches (see the preceding section) have been applied to model virtually every aspect of DNA photoexcitation, including energetics [122, 172], base-pairing and electronic coupling [173], damage and repair reactions

[174, 175], π-stacking and excited-state delocalization (charge transfer, excimers/exciplexes, and excitons) [140, 176–178], and excited-state dynamics [144]. In this section we overview recent results of computational efforts directed toward understanding the photoexcitation in DNA strands. None of the currently available theoretical approaches is yet quantitatively reliable in modeling a system as large as solvated DNA strands. Simulation of the excited-state dynamics in the condensed phase is especially challenging because of the need to describe realistically both the electronic structure of all relevant electronic states under the influence of the environment and the dynamics of the entire system. A single nucleobase embedded in DNA strands (Sect. 3.2) serves as a starting point to approach real DNA systems. Stacked base oligomers (Sect. 3.3) and base pairs (Sect. 3.4) have been studied as simple models of DNA strands. The mechanisms of DNA photodamage are discussed in Sect. 3.5. The photoexcitation of other types of DNA strands is reviewed briefly in Sect. 3.6.

3.1 Summary of Experimental Results

Numerous experimental studies employing several time-resolved spectroscopic techniques have been reported on solvated DNA models in the past decade. The simplest models in the condensed phase are single nucleobases (or single nucleosides/nucleotides), e.g., 9*H*-adenine [or 9-methyladenine (m^9A)/deoxyadenosine (dAdo)], which were found to exhibit decay time constants of 180–670 fs in water, slightly shorter than in the gas phase [113]. Regarding the more complicated photophysics and photochemistry of DNA, the spectroscopists have reported multiexponential decay behavior with time constants ranging from hundreds of femtoseconds to hundreds of picoseconds [5]. To rationalize the much longer components compared to isolated (gas-phase or solvated) nucleobases, it was suggested that the photodynamics in DNA may be composed of multiple decay channels involving localized and/or delocalized states and processes. A variety of decay models have been proposed to explain the puzzling observations. Comprehensive surveys of the massive amounts of experimental spectroscopic results are given in the reviews and perspectives about DNA excitation by Kohler, Markovitsi, and others [3, 5, 7, 9–11, 179]. The A/T and G/C strands show generally similar behavior upon photoexcitation, so we take the A/T strands as an example and highlight the primary hypotheses as follows:

- The Kohler group [5, 7, 180, 181] investigated $(dA)_{18}$ and $(dA)_{18}{\cdot}(dT)_{18}$ (where we use a middle dot "·" to denote the hydrogen-bonded base paring from here on; dA is deoxyadenosine monophosphate and dT is deoxythymidine monophosphate, as depicted in Fig. 1). They concluded that singlet excited states of single or poorly stacked bases relax to the hot ground state by ultrafast internal conversion within 1 ps, while initial excitons delocalized over several bases rapidly (sub-picosecond) evolve into localized excimers or charge-transfer (CT) states that survive longer than 100 ps, independent of the strand length.

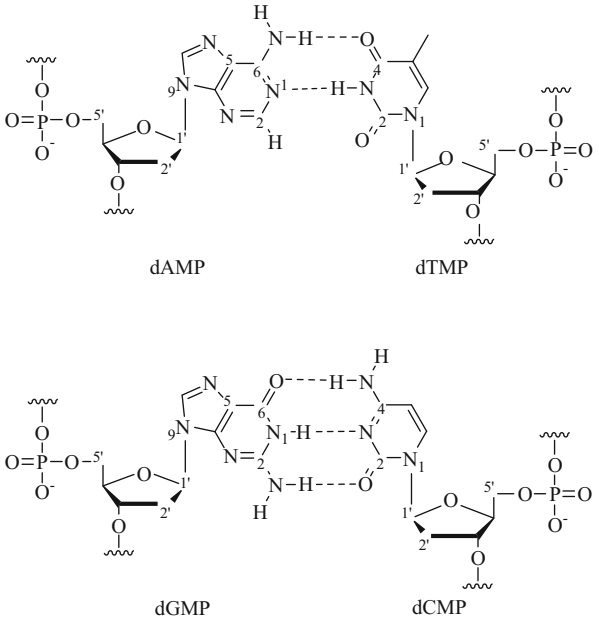

Fig. 1 Chemical structures and Watson–Crick base pairs of deoxyadenosine monophosphate (dA or dAMP), deoxythymidine monophosphate (dT or dTMP), deoxyguanosine monophosphate (dG or dGMP), and deoxycytidine monophosphate (dC or dCMP) that occur as building blocks in DNA strands

- The Fiebig group [182, 183] studied $(dA)_{2-18}$ and $(dA)_{12/18}{\cdot}(dT)_{12/18}$. Their fits gave a monoexponential time constant of ~8 ps, which was ascribed to electronically relaxed excitons that were initially formed upon UV absorption. They conjectured an excitonic delocalization over at least three bases.
- Markovitsi and coworkers [4, 9, 184–186] measured $(dA)_{20}$, $(dA)_{20}{\cdot}(dT)_{20}$, and double-stranded polymers $(dA)_n{\cdot}(dT)_n$. They also detected multiexponential decay components of 0.3–0.85 ps, 1.6–3.9 ps, and up to 187 ps. They interpreted their findings as Frenkel and/or CT excitons [20, 187, 188] extending over several bases, which were proposed to give rise to the longer components after ultrafast (<100 fs) intraband scattering. They suggested that the decay of $^1\pi \rightarrow \pi^*$ and/or $^1n \rightarrow \pi^*$ states of unstacked thymine/adenine bases corresponds to the faster components.
- Markovitsi and coworkers [154, 189] recently proposed a general diagram for the excited-state processes in natural calf thymus DNA: the optically bright excitonic states first decay to charge-transfer and/or charge-separated states (the distinction being whether donor D^+ and acceptor A^- are close to or far away from each other); $^1\pi \rightarrow \pi^*$ states that cause the delayed fluorescent emission are then accessed through charge recombination, intraband scattering, and excitonic localization, while the ground state is primarily repopulated by charge recombination.
- Using a triexponential decay function, Schwalb and Temps [190] reported similar fitting results with time constants of 0.52–0.63, 2.6–5.8, and 16.2–97.0 ps for their up-conversion experiments on $(dA)_{20}$ and $(dA)_{20}{\cdot}(dT)_{20}$.

- Phillips and coworkers [191] proposed a decay mechanism of $(dA)_{20}$, in which all components originate from monomeric adenine excitations, which then embark on different decay paths including radiationless internal conversion (~0.39 ps) and the formation of two excimers (~4.3 and ~182 ps).

Moreover, a series of circular dichroism experiments [37, 192, 193] showed that the initial excitation in DNA homopolymers (adenine, thymine, and cytosine) generates excitons limited to only two bases, while the exciton extends over more bases in RNA homopolymers (adenine). It is noteworthy that the simple dinucleotide 2′-deoxyadenylyl(3′ → 5′)-thymidine (dApdT), which easily becomes unstacked in aqueous solution, also exhibits long-lived (~5 and ~75 ps) excited-state dynamics [194]. This implies that π-stacking of multiple nucleobases may not necessarily be the only origin of the long-lived species in DNA strands. Hence, although a number of interpretations have emerged to rationalize the experimental observations, there is still a long way to go before arriving at a consensus on all aspects of DNA photoexcitation. Controversial issues include the localized and/or delocalized character of the excited states and the effects of the environment (solvent and DNA backbone), which call for computational studies.

3.2 Single Bases in DNA Strands

The enigma of DNA photochemistry has aroused much interest on the theoretical side. There have been many theoretical efforts to establish sound models for DNA photochemistry and to explain the experimental observations. It is logical to study the complicated photoinduced processes of DNA by starting from the basics – single nucleobases [19, 21]. For example, 9*H*-adenine is one of the most studied nucleobases, and its excited state properties are rather well known [19]. The absorption maximum of 9*H*-adenine at 252 nm (4.92 eV) is assigned to two close-lying $^1\pi \rightarrow \pi^*$ states, which are labeled L_a and L_b [19]. Another singlet state of $^1n \rightarrow \pi^*$ character, located only 0.073 eV below the $^1\pi \rightarrow \pi^*$ state, may be involved in the photoexcitation as a dark state [195]. Biexponential fitting of the time-resolved spectra in the gas phase gives time constants of 40–100 fs and 0.75–1 ps for the short and long components, respectively [196–201]. These sub-picosecond time scales are considered to be fingerprints of intrabase internal conversions [19]. A number of computational investigations on 9*H*-adenine have been conducted, and several minimum-energy crossing points or conical intersections connecting the PESs of the low-lying singlet states have been located [84, 87, 110, 202–205]. Two conical intersections, labeled ^2E and $^6S_1$ following the Cremer-Pople-Boeyens classification [206, 207], are energetically favorable. They are characterized by strong out-of-plane deformations at the C2–H2 and C6–N6 moieties, respectively [84, 87, 110, 202–205]. On the basis of these computational results, several principal reaction paths in the gas phase have been suggested. For example, based on linear interpolation in internal coordinates (LIIC) at the

CASPT2//CASSCF level, Barbatti and Lischka [87] found barrierless paths to both ^2E and $^6S_1$ conical intersections. Their findings agree with the report by Perun et al. at a similar theoretical level [84, 208]. Hassan et al. [209] reported MRCI//CASSCF calculations giving an ultrafast conversion from L_a to $^1n \rightarrow \pi^*$ that was followed by a steep LIIC path down to the $^6S_1$ conical intersection, whereas the route toward the ^2E conical intersection required an activation energy of 0.21 eV. By contrast, Conti et al. [210] found the $^6S_1$ conical intersection to lie 0.42 eV above the $^1n \rightarrow \pi^*$ minimum at the CASPT2//CASSCF level. Semiempirical MRCI surface-hopping dynamics simulations by Fabiano and Thiel [110] indicated a two-step nonadiabatic relaxation with an initial ~15-fs $S_2 \rightarrow S_1$ deactivation and a subsequent ~560-fs exponential decay to the ground state (S_0), fairly analogous to the ab initio MRCIS excited-state dynamics [87] except that the second step mainly proceeded via the $^6S_1$ channel (OM2/MRCI) rather than the ^2E channel (MRCIS). To summarize, these studies of gas-phase 9*H*-adenine agree on some general qualitative features, for example, the presence of three closely coupling excited states around 5 eV ($^1n \rightarrow \pi^*$, L_a $^1\pi \rightarrow \pi^*$, and L_b $^1\pi \rightarrow \pi^*$), the existence of several competing nonradiative decay channels (e.g., $^6S_1$ vs ^2E), and the distorted geometries at the corresponding conical intersections, while differing in mechanistic details. These investigations have laid the foundation for the subsequent exploration of real DNA systems. For further details regarding the excited-state properties and dynamics of the five nucleobases, see the recent review article by Kleinermanns et al. [19]. Most recently, Tuna et al. [211] reported that intramolecular proton transfer from the ribose 5′-OH group to the adenine N3 atom (see Fig. 1) is possibly responsible for the much shorter observed lifetime of adenosine compared with 9*H*-adenine [212].

Many experimental studies have reported distinct spectral shifts of isolated nucleobases when going from the gas phase to aqueous solution: e.g., red shifts of 9*H*-adenine and 9-methyladenine by 0.15–0.21 eV and blue shifts of 3*H*-cytosine and 3-methylcytosine by 0.30–0.38 eV [5, 213–215]. When going from solvated nucleobases to the corresponding DNA strands, there are only slight shifts. For example, the aqueous absorption maximum is found at 4.73 eV for the dA/dT mixture, at 4.78 eV for $(dA)_{20}\cdot(dT)_{20}$, and at 4.72 eV for $(dAdT)_{10}\cdot(dTdA)_{10}$ [184]; the absorption maximum of adenosine is measured at 4.77 eV in aqueous solution while it is at 4.82 eV for $(dA)_{20}$ [216]. These *solvatochromic* shifts are induced by the complex electrostatic and steric environment in the condensed phase. Valiev and Kowalski [67, 74] computed the steady-state photoexcitation for a single cytosine in the native DNA environment at the QM/MM level using EOM-CCSD(T) for the QM part. They reported pronounced blue shifts of the two lowest singlet excited states, $^1\pi \rightarrow \pi^*$ at 5.01 eV and $^1n \rightarrow \pi^*$ at 5.79 eV on average, compared to the gas-phase values of 4.76 and 5.24 eV for a single cytosine, respectively. Correspondingly, the ionization potentials of all four DNA nucleobases also increase in solvated QM/MM DNA models compared with the gas phase [217]. Thiel and coworkers [113–115] reported a small steady-state blue shift (0.09–0.17 eV) for a single adenine embedded in $(dA)_{10}$ and $(dA)_{10}\cdot(dT)_{10}$ relative to the absorption energy of aqueous 9*H*-adenine. Although these QM/MM

results reflect the solvent and environmental effects in a qualitatively correct manner, they should not be directly compared to the experimental spectra, because the calculations took into account only a single QM nucleobase (neglecting other bases as well as QM interbase interactions).

Lu et al. [114, 115] carried out QM/MM nonadiabatic dynamics simulations for a single adenine embedded in single- and double-stranded oligomers $(dA)_{10}$ and $(dA)_{10} \cdot (dT)_{10}$, treating the QM adenine with the semiempirical OM2/MRCI approach. They found that the $^6S_1$ and ^2E conical intersections (see above) remain the dominating decay channels, but the computed time constants for the monomeric excited-state decay increase dramatically, roughly by an order of magnitude compared with the gas or aqueous phase (~4.1–5.7 vs ~0.4–0.6 ps at the same level of QM theory, see above). They identified the main reason for the much slower internal conversion as a strong lowering of the interstate coupling caused by the electrostatic environment of the DNA strands. They simulated the time-dependent fluorescence spectrum of single adenine in $(dA)_{10}$ (by considering the time-dependent population of excited adenine during the dynamics run), which reproduced the temporal behavior of the experimental spectra in a qualitatively reasonable manner [191]. Lischka and coworkers also performed QM/MM surface-hopping studies on a single nucleobase (or its derivatives) in DNA strands [144, 218]. In their latest study [218] they employed ab initio MRCIS surfaces for a single guanine base in DNA; they observed that less than 9% of the guanine population decayed to the ground state within the simulation time (0.5 ps), which also implies a much longer time constant in DNA compared to that for isolated guanine (~0.22 ps). On the other hand, a single cytosine (treated with CASSCF) was reported to exhibit a slightly faster decay (~0.48 ps [218]) when embedded in DNA than in vacuo (~0.69 ps [219]), because of energetic factors. It should be emphasized that these monomeric models provide reasonable explanations for some experimental observations in DNA strands, but they cannot be considered conclusive because they ignore multiple-base mechanisms (see below).

Most of the published computational studies address single nucleobases without the sugar-phosphate backbone. A recent LRC-TDDFT study [220] stressed that the involvement of backbone MOs in the photoexcitation of DNA strands should not simply be neglected. It is well known that electron attachment may induce DNA bond breaking which normally happens at the sugar (C5′–O5′, C3′–O3′) and the glycosidic (N9–C1′) σ bonds (see Fig. 1) [32, 33, 59]. Theoretical modeling of this bond breaking has usually been carried out in the electronic ground state. However, according to Kumar and Sevilla [221, 222], the bond-breaking reactions could be activated in dark $^1\pi \rightarrow \sigma^*$ excited states that are indirectly populated through vibronic coupling with optically bright $^1\pi \rightarrow \pi^*$ states. If so, it would clearly be crucial also to reckon with backbone contributions to the photoexcitation of DNA strands.

3.3 Base Stacking in DNA Strands

We now shift the focus toward models containing more than one nucleobase. A large number of theoretical studies have been carried out on the excitation of stacked bases (in vacuo, water, or solvated DNA) using various theoretical methods [223]. First of all, one should note that different base sequences give different results. Matsika and coworkers [61] compared the performance of different methods (including CIS, TDDFT, CASSCF, and CC) in the description of excited-state π-stacked nucleobases. A benchmark study by Aquino et al. [130] reported stable interbase charge-transfer states for stacked adenine-thymine and stacked guanine-cytosine, the simplest stacked base pairs. However, the nature, and especially the delocalization degree, of the initially populated excited states in real DNA systems remains a puzzle [37]. The available computational results on the localization/delocalization degree seem to be highly dependent on the stacked base sequences, configurational fluctuations, and the chosen theoretical methods (see below for detailed discussions).

Using the CIS approach, Matsika and coworkers [224, 225] studied the quenching of fluorescence in stacked 2-aminopurine-pyrimidine complexes and stacked 2-aminopurine dimers in the gas phase, as models of stacked base pairs in natural DNA. They discovered that conical intersections with interbase bonding interactions can induce some of the stacked bases to decay from charge-transfer excimers. This suggests a possible dimer mechanism of radiationless decay that might contribute to the very low fluorescence quantum yield of natural DNA.

Since electronic-structure calculations are still not practical for describing highly delocalized states in complexes containing several stacked nucleobases, the exciton model is often used for modeling the bound excitation and excited-state energy transfer of natural DNA [226] (see Sect. 2.1.7). Applying Frenkel exciton theory to gas-phase $(dA)_{20}{\cdot}(dT)_{20}$ and $(dAdT)_{10}{\cdot}(dTdA)_{10}$, Bouvier et al. inferred in an early study [184] that dipolar coupling alone may induce delocalization after photoexcitation. In their excitonic model, the excitation energies of individual nucleobase monomers (i.e., the diagonal terms in the excitonic Hamiltonian matrix) were derived from experimental parameters and considered insensitive to the local environment. Further investigations [140, 141] on the duplexes $(dA)_{10}{\cdot}(dT)_{10}$ and $(dGdC)_5{\cdot}(dCdG)_5$ in the aqueous phase (with QM/MM) employed the same excitonic approach, which gave only a slight blue shift in the simulated absorption spectra – consistent with experimental observations that the DNA UV spectra resemble the superposition of the spectra of the monomeric bases [227]. Charge-transfer states were not included in their exciton model since only dipolar couplings (without interbase orbital overlap) were included when computing the electronic couplings (i.e., the off-diagonal terms of the excitonic Hamiltonian). Hu et al. [216] built a similar excitonic model with dipolar interactions and characterized the π-stacked adenines as *hypsochromic aggregates* (H-aggregates) [228] that display a blue shift of the absorption maxima.

Based on their TDDFT calculations of stacked 9-methyladenine (m^9A) dimers and trimers in water (described with PCM), Improta and coworkers [147] interpreted the experimentally observed subpicosecond components (see Sect. 3.1) as ultrafast decay of the bright delocalized states, proceeding either via a localized monomeric pathway or via a pathway involving dark interbase charge-transfer excimers. Their theoretical calculations reproduced a typical signature of excimers, namely the slight blue shift and the decrease in oscillator strength compared with the monomers. The authors speculated that the decay components longer than 100 ps could be related to full geometric relaxation of the charge-transfer state. Using an excitonic model, Improta et al. [150] pointed out in particular that there is a fast and effective transfer in stacked adenines between bright excitonic states and dark charge-transfer states, because of their strong coupling. Recent theoretical studies [153, 157] on $(dA)_4$ and $(m^9A)_n$ ($n = 1$–5) at the PCM/TDDFT level, combined with spectroscopy experiments on $(dA)_{20}$, enriched the proposed scenario: the absorbing states of stacked adenines are bright excitonic states delocalized over up to four bases; they may rapidly localize to bright excited states on base monomers, or evolve into darker $^1\pi \rightarrow \pi^*$ excimers and/or charge-transfer excimers/exciplexes. Remarkably, these features were generally found to be independent of the number of stacked adenines. According to the proposed scenario, the multiexponential UV absorption spectra can be interpreted in terms of excitons (picosecond components), neutral excimers (sub-nanosecond components), and charge-transfer states (nanosecond components). Quantum dynamics simulations (without nuclear relaxation) at the PCM/TDDFT level indicated that charge-transfer states arise from the initial excitonic states within a few femtoseconds and survive for at least ~1 ps [158].

Bittner [176] proposed a novel excitonic Hamiltonian for poly(dA)·poly(dT) on the basis of the lattice fermion model, which includes all *intrastrand* and *interstrand* excitonic coupling terms. Taking both orbital overlap and dipolar couplings into consideration, Bittner [176, 229] computed the electronic dynamics (with fixed nuclear coordinates) in vacuo and showed that delocalized excitonic states with weak interstrand coupling immediately decay into non-excitonic charge-separated states (e^-/h^+ pairs) in the deoxythymidine (dThd) strand, but remain unchanged for several hundred femtoseconds in the deoxyadenosine (dAdo) strand. Based on INDO/S calculations and MD simulations, Voityuk [230] arrived at a similar conclusion, namely that singlet excitation energy transfer in poly(dA)·poly(dT) is prevailing in the dT strand. However, Lange and Herbert [60] suggested a contradictory picture on the basis of LRC-TDDFT calculations on Ade_3·Thy_3 (Thy = thymine) in aqueous solution, which gave optically bright excitonic states that are almost localized on the adenine strand. Furthermore, averaging the excitonic states over conformations obtained from ground-state MD simulations yielded blue-shifted absorption spectra (compared with those of the base monomers) [231]. Notably, Voityuk's QM/MM-based exciton model for poly(dA)·poly(dT) [232] predicts direct population of intrastrand (rather than interstrand) charge-separated states upon UV absorption, whereas both intrastrand and

interstrand charge-transfer states are important in the LRC-TDDFT modeling of Lange and Herbert [60].

In the QM/MM exciton model for $(dA)_{10}\cdot(dT)_{10}$ and $(dGdC)_5\cdot(dCdG)_5$ developed by the Markovitsi group [140, 141], the delocalization extends over at least two nucleobases. This agrees with experimental evidence that the delocalization involves more than three or four bases [182]. Coincidentally, in Bittner's model [231], the excitons delocalize over at least six nucleobases. In simulations by Voityuk [232], the bright excitons spread over almost all intrastrand nucleobases in an ideal B-DNA strand [$(dA)_n\cdot(dT)_n$ (n = 1–8)], while thermal fluctuations and vibronic interactions induced significant localization and reduced the average length of the excitons to around three nucleobases. By contrast, Plasser et al. [76] concluded from their QM/MM [QM = ADC(2)] calculations on aqueous $(dAdT)_6\cdot(dTdA)_6$ and $(dGdC)_6\cdot(dCdG)_6$ that most excitonic and charge-transfer excited states are delocalized over at most two bases in these oligomers.

The well-known *hyperchromism* in DNA (i.e., the experimentally observed increase of photoabsorbance with DNA denaturation, for example through melting caused by heating) has been related to a presence of excitonic states by D'Abramo et al. [233]. These authors evaluated excitonic interactions with the perturbed matrix method (PMM) at the CASPT2//CASSCF level. Their computed (QM/MM) absorption spectra of nucleobases embedded in poly(dA) and poly (dT) show ~30% greater absorbance and a slight red shift of the absorption maximum compared with poly(dA)·poly(dT), well matching the experimental observations. They explained this phenomenon by the higher delocalization of excitonic states in single strands than in the duplex. According to TDDFT calculations by Varsano et al. [234], π-stacking causes more significant hyperchromism than hydrogen bonding.

Over the past decade, the electronic coupling in e^-/h^+ pairs and the energy transfer along π-stacking DNA strands was systematically investigated by Rösch, Voityuk, and others [235–259]. The e^-/h^+ transfer in DNA strands was found to be sensitive to the base sequence and the strand conformation [260]. It was predicted that solvent effects could confine the charge delocalization to a single base pair in double-stranded (9*H*-guanine)$_n$·(cytosine)$_n$ ($Gua_n\cdot Cyt_n$, n = 2–9) [247] and that excess charges could also be localized on a single base in π-stacked radical-cation single strands [251, 261]. Voityuk and Davis [249] showed how DNA-protein contacts may directly affect the stability of a guanine radical cation (h^+) in the dynamics of long-range hole transport. In contrast to electron transfer, the triplet-triplet energy transfer in DNA strands was found to occur on the nanosecond timescale [262] (which might be associated with the very long-lived species observed experimentally) and to be less influenced by the environment [263]. A molecular switch driven by photoexcitation was designed by utilizing the charge-transfer features in DNA strands [264]. Further models for charge transfer/transport in DNA strands have been extensively discussed by several theoretical groups, for example, in [265–298]. For more detailed information, we refer the reader to some excellent reviews on these topics [299–304].

3.4 Base Pairing in DNA Strands

The pairing structure of DNA double helices is maintained by the hydrogen bonds between purines and pyrimidines. Calculations at the CC2 level of the Ade·Thy Watson–Crick base pair in the gas phase by Perun et al. [73] revealed that the hydrogen bonds also enhance the photostability of DNA. According to their results, after photoexcitation to the bright localized $^1\pi \rightarrow \pi^*$ state [$^1\pi \rightarrow \pi^*$ (LE)], the base pair can easily access the dark intermolecular charge-transfer state $^1\pi \rightarrow \pi^*$ [$^1\pi \rightarrow \pi^*$ (CT)] through a conical intersection close to the Franck–Condon region. The charge separation in the $^1\pi \rightarrow \pi^*$ (CT) state triggers a hydrogen-bond-mediated proton transfer from adenine to thymine that balances out the charges and leads to a minimum with biradical character. Thereafter, the base pair returns to the ground state (S_0) through the conical intersection connecting the S_0 and $^1\pi \rightarrow \pi^*$ (CT) states, which is found to be lower in energy than the minima of the bright states. Starikov et al. [305] calculated possible conformations of DNA duplexes $(dA)_n{\cdot}(dT)_n$ and $(dG)_n{\cdot}(dC)_n$ ($n = 3, 4$) at the ZINDO level and reported that their excitation energy and the contribution of the charge-transfer transition (charge-transfer exciton) are highly conformation-dependent. Taking solvent effects into account at the PCM/TDDFT level, Improta and coworkers [151] drew a different conclusion for their (9-methyladenine)$_2$·(1-methylthymine)$_2$ [$(m^9A)_2{\cdot}(m^1T)_2$] tetramer model. They asserted that the bright states are delocalized over the adenine-thymine pair and that the initial excitation is followed by ultrafast localization to a single base. They did not find proton transfer to play a key role in the deexcitation of their model. A recent time-resolved experiment [306] detected species in $(dA)_n{\cdot}(dT)_n$ double strands (~70 ps) that are shorter-lived than those for single-stranded $(dA)_n$ (~100–200 ps) [307]. This suggests that base pairing may have significant impact on the excitation behavior of double strands, which still lacks a clear theoretical explanation.

Likewise, there is experimental and computational evidence that the photodynamics of an isolated Gua·Cyt base pair is closely related to interbase proton transfer [308–310]. The conformation of the Watson–Crick base pair was found to be the key to the photostability of Gua·Cyt [311], which may even involve double proton transfer in the gas phase [312]. There are also experiments supporting a proton-transfer mechanism in alternating G/C double strands [e.g., $(dGdC)_n{\cdot}(dCdG)_n$], which, however, strongly depends on the base sequence [313]. For a Watson–Crick guanine·cytosine (G·C) base pair embedded in native B-DNA, CASSCF/MM surface-hopping dynamics simulations by Groenhof et al. [314] suggested that the primary radiationless decay channel is a single proton transfer from 9*H*-guanine to cytosine followed by efficient internal conversion. Moreover, double proton transfer (originating from the guanine N1 and the cytosine N4 atoms) was also observed in the simulations as a minor channel. Another mechanistic option is the so-called proton-coupled electron transfer (PCET) – proton transfer accompanied by transfer of an electron in the same direction but generally not at the same time [315], which effectively results in the transfer of a

neutral hydrogen atom. At the CASPT2//CASSCF level, stepwise double hydrogen transfer was calculated to be the most favorable decay pathway for Gua·Cyt in vacuo, among the three possible proton/hydrogen-transfer processes [315]. When embedded in a DNA duplex using the QM/MM method, the Gua·Cyt pair was still found to decay via the same pathway, with an estimated lifetime of ~50 fs [315]. However, these calculations did not explain the experimental fact that the ground-state recovery in G/C duplexes [$(dGdC)_9$·$(dCdG)_9$, (dG_4dC_4)·(dC_4dG_4), and $(dG_5dA_4dG_5)$·$(dC_5dT_4dC_5)$] is much slower than in a mixture of CMP and GMP [316].

According to CASPT2//CASSCF studies of gas-phase 9*H*-adenine by Perun et al. [84, 208], the $^6S_1$ decay channel with an out-of-plane amino group (see Sect. 3.2) may be suppressed when the base is paired with thymine (or uracil in RNA) through Watson–Crick hydrogen bonds. This prediction was confirmed in the QM/MM surface-hopping studies of a single adenine in $(dA)_{10}$·$(dT)_{10}$ by Lu et al. [114, 115]. Unlike the single-stranded $(dA)_{10}$, the monomeric $^6S_1$ channel in the double strand is completely locked, and the ^2E channel becomes dominant, since it does not require geometric deformations that perturb hydrogen bonds. Similar restraints by hydrogen bonding were found for guanine in a DNA duplex in QM/MM surface-hopping simulations by Zelený et al. [218]. However, hydrogen bonding is not the reason for the slower monomeric decay in the DNA strands compared with the gas or aqueous phase (see Sect. 3.2). We note again that the QM regions were confined to single bases in these QM/MM studies, which thus disregarded mechanisms involving more than one base (e.g., proton transfer, intermolecular charge transfer, and exciton formation).

Additionally, Rak, Voityuk, and coworkers [317, 318] suggested that proton transfer and base pairing could be associated with the electronic coupling in π-stacked DNA. The coupled effects of base pairing and base stacking in water were carefully examined for Gua_3·Cyt_3 and (GuaCytGua)·(CytGuaCyt) by Ko and Hammes-Schiffer [319] by means of QM/MM (QM = TDDFT) calculations: in both cases, proton transfer was found to stabilize the interstrand charge-transfer state, and in (GuaCytGua)·(CytGuaCyt) it helped facilitate the nonadiabatic decay from the intrastrand to the interstrand charge-transfer state [35, 36].

3.5 Pyrimidine Dimerization

One of the most important DNA photochemical reactions is the photolesion due to UV excitation. Pyrimidine dimerization is considered to be the major cause of photolesion [5]. The main photoproducts are cyclobutane pyrimidine dimers (CPDs), and the end result may be mutagenesis, cell death, or even skin cancer. CPDs are formed by [2 + 2]-cycloaddition linking two C5=C6 double bonds of two neighboring pyrimidine bases (see Fig. 2) [5, 320, 321]. There is considerable debate about the mechanism of this cyclization reaction – one core issue is the multiplicity. For instance, based on time-resolved fluorescence and absorption

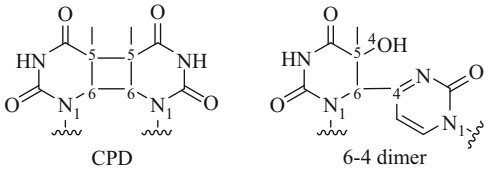

Fig. 2 *Left*: cyclobutane pyrimidine dimer (CPD); *right*: 6-4 photoproduct

spectroscopy, Kwok et al. [322] proposed for $(dT)_{20}$ that formation of the photoproduct takes ~140 ps and is mediated by a biradical intermediate through self-quenching of the T_1 state, which is accessed (~1.7 fs) by an ultrafast singlet-triplet intersystem crossing. In contrast, time-resolved infrared (IR) spectroscopic experiments [180] provided strong evidence in support of the direct formation of the dimer in a singlet $\pi \rightarrow \pi^*$ state, within only ~1 ps after excitation. Single nucleobases were also reported to undergo an ultrafast direct dimerization in a resonance Raman study by Loppnow and coworkers [323, 324].

Robb and coworkers [325] compared two possible [2+2]-cycloaddition pathways of a stacked thymine dimer in the gas phase at the CASPT2//CASSCF level. The first one was a stepwise thermal reaction in the electronic ground state (S_0) via two biradical transition states with activation energies of about 60 kcal/mol; the second one involved excitation to a singlet excited state (S_1), which cyclizes via a barrierless concerted mechanism and returns to S_0 by an ultrafast internal conversion at the S_0/S_1 conical intersection. It is obvious that the latter pathway is favored, which is analogous to nonadiabatic cyclization reactions of stacked ethylenes. Based on similar CASPT2//CASSCF calculations in vacuo, Blancafort and Migani [326] realized that the reactive excimer in the B-DNA conformation is a dark state possessing little oscillator strength. Although the excimer is accessible when conformational and environmental effects are taken into account in the aqueous phase, the authors proposed another possible mechanism: an unreactive localized excited state is initially populated and then decays to the reactive state through avoided crossings. A PCM/TDDFT study [155] reported a barrierless [2 + 2]-dimerization originating from bright $^1\pi \rightarrow \pi^*$ excitons and a less favorable 6-4 dimerization (see Fig. 2) involving a barrier and charge transfer from the 5′-end to the 3′-end, without excluding monomeric decay pathways in loosely stacked bases. Dou and coworkers [327] observed in their semiclassical dynamics simulations that cyclization takes place after the excimer decays to the ground state through the S_0/S_1 conical intersection and that the two cyclobutane bonds (C5–C5′ and C6–C6′) between two stacked thymines are then formed one by one within ~110 fs.

Using CASPT2 calculations, Merchán, Serrano-Andrés, and coworkers [175, 328] rationalized the lower dimerization yield of cytosine compared with thymine: the former has a stable singlet excimer that needs to overcome a barrier (though small) to reach the S_0/S_1 conical intersection, while this process is downhill in the latter. The authors also proposed a barrierless non-concerted dimerization mechanism in the triplet manifold, the efficiency of which relies on the ease of the S_0/T_1 intersystem crossing [175, 328]. Overall, in real systems, these two mechanisms

will be modulated by many factors such as DNA sequence, aggregation, and solvent.

Besides CPDs, 6-4 dimers (see Fig. 2) can also be found in the photoproducts as the result of nucleophilic attack, but their yield is smaller than that of CPDs by an order of magnitude [329]. These 6-4 photoproducts have also drawn much attention because they are even more mutagenic than CPDs [330]. CASPT2//CASSCF calculations by Blancafort and Migani [326] suggested that the reaction involves an oxetane-type precursor generated via a charge-transfer excited state. There is evidence [154, 329, 331] from time-resolved spectra of $(dT)_{20}$ and from theoretical calculations on thymine dinucleotide (TpT) that this charge-transfer state, which could be directly populated by optical excitation, is stabilized in solution compared to the gas phase [326], owing to the stabilizing interactions with the solvent and the sugar-phosphate backbone. The fact that the 6-4 addition reaction only plays a secondary role was explained with a significant energy barrier, which is also induced by dynamical solvent effects [154].

The conformational control of pyrimidine dimerization in DNA strands was widely discussed in theoretical investigations, for example in [320, 331, 332]. The probability of dimerization is highly dependent on the distance and the dihedral angle between the C5=C6 double bonds [320, 333]. Lewis and coworkers [331, 332] addressed the conformational fluctuations by taking snapshots from ground-state MD simulations for $(dT)_{20}$ and $(dT)_{20}{\cdot}(dA)_{20}$, which indicated that the mid-point distance d between the two approaching C5=C6 double bonds (see Fig. 2) plays a more important role for the dimerization than the dihedral angle. By fitting to experimental data, they found the proportion of MD snapshots with $d < 3.52$ Å to be equal to the quantum yield of the [2+2] cycloaddition. Similarly, they concluded that the 6-4 dimerization occurs when the distance between the C5 and O4 atoms (see Fig. 2) is smaller than 2.87 Å. Combined experimental and theoretical investigations by Lewis and coworkers [332, 334, 335] indicated that flanking purine bases (for example, in a local sequence consisting of a purine-pyrimidine-pyrimidine motif such as G-T-T) modulate the dimerization efficiency of stacked pyrimidines mainly by affecting their ground-state conformations (rather than by energy or charge transfer). Generally speaking, the quantum yield of dimerization depends on many factors, such as the kind of adjacent nucleobases [336], excited-state dimer repair [337], quenching of dimerization [338], and ground-state donor-acceptor interactions between π-stacked bases [334].

Organisms have developed a defense mechanism against photolesion caused by pyrimidine dimerization. For example, in the human body, photoinduced DNA damage is fixed by photolyases – a class of repair enzymes [292, 339–344]. The repair mechanism has been the subject of several theoretical studies that arrived at the following scenario: a reduced flavin adenine dinucleotide ($FADH^-$) transfers one electron (e^-) to the thymine–thymine dimer, the anion formed reverts back to normal thymine bases by ring opening via a radical intermediate, and the electron then returns again to FADH [342, 345–349]. For further information on this topic, we refer the reader to reviews such as [29] and [344].

3.6 *Other Helical Conformations and Modified Strands*

Besides the standard DNA strands discussed above, there are other uncommon helix conformations such as A-DNA and Z-DNA. The Quinn group [350] reported that the nonradiative decay takes longer for the Z-form than for the B-form of poly (dCdG)·poly(dGdC), with experimental monoexponential time constants of 16–20 ps. By contrast, the Kohler group [351] reported that the experimentally observed nonradiative decay lifetime of $(dCdG)_9 \cdot (dGdC)_9$ is independent of the helix conformation (also in the region of several picoseconds). These findings call for theoretical studies on Z-DNA to check whether the established theoretical explanations for B-DNA photodynamics carry over to the more loosely stacked Z-DNA strands. In a different context, the photoexcited Z-DNA double strands were modeled in a study of their circular dichroism spectra using the high-level symmetry-adapted cluster CI method [352].

There is also interesting research on nonstandard DNA strands. For example, DNA strands modified with tethered chromophores (e.g., ethidium [353]) and DNA assemblies containing nucleobase-like chromophores (e.g., deazaguanine and inosine [354, 355]) were widely used to probe the DNA e^-/h^+ transport processes (see Sect. 3.3). Photoinduced electron transfer in a synthetic artificial mimic of DNA strands – peptide nucleic acid – was studied computationally, since it may play a key role in the evolution of life [282, 356]. Making use of the excited-state properties of DNA strands, theoretical chemists have attempted to design photodriven molecular motors [357, 358].

4 Conclusion and Outlook

In this chapter we have presented a broad overview of computational studies on photoexcitation in DNA single and double strands. A wide range of excited-state theoretical models and computational techniques are available for computational chemists to simulate DNA strands in excited states. High-level ab initio quantum methods are still too expensive to model systems as complex as solvated DNA strands unless approximations are made and accuracy is sacrificed. The hybrid QM/MM approach offers a viable alternative by considering just the photoactive center at an expensive and accurate QM level, while using a simple MM force-field description for the DNA and solvent environment that may play an essential role in the photoexcitation. Semiempirical CI methods are a promising tool for the modeling of rather large photoexcited systems, after proper validation against experiments or high-level calculations. TDDFT can often be employed successfully to investigate the delocalized excitonic coupling in DNA strands, in spite of its deficiencies for charge-transfer and near-degenerate states. Static calculations can thus yield a wealth of theoretical information on DNA electronically excited states, both on spectra and excited-state potential energy surfaces. In addition,

nonadiabatic dynamics simulations can provide a rich and detailed picture of photoinduced processes in DNA strands – including mechanisms, deactivation pathways, lifetimes, branching ratios, and time-resolved absorption and emission spectra.

However, a full understanding of the extremely complex photophysics and photochemistry in DNA strands is still an elusive goal for computational studies. There is a logical road map to proceed from simple models toward fully atomistic simulations of DNA by consecutively addressing (1) a single nucleobase in vacuo/water, (2) a single nucleobase embedded in DNA strands, (3) multiple interacting nucleobases embedded in DNA strands, and (4) complete solvated DNA strands. At present, efforts on step (1) have established a solid understanding of isolated nucleobases in the gas phase and in water, and the research in this field has thus been moving rapidly toward steps (2) and (3) in recent years. The dramatic slowdown of the nonradiative decay in DNA strands, as observed in several time-resolved spectroscopic studies, has been rationalized both by a monomeric mechanism and by invoking delocalized excitonic states. Proton and/or hydrogen transfers through base pairing have been proposed to play an important role in the photoinduced processes of DNA, but their overall significance is still debated. Studies of base stacking have uncovered a number of potentially important effects, including excitonic delocalization, charge transfer, and charge/energy transport, but there is still considerable controversy concerning the nature of the initially generated excited state (electronic configuration and delocalization degree) and its evolution over time. Photoinduced damage to DNA is generally attributed to pyrimidine dimerization by [2+2]-cycloaddition, but there is still discussion about the detailed mechanism and alternative pathways, combined with the challenge to contribute theoretically to the design of an improved photoprotection strategy. Electronically excited states in uncommon DNA helix conformations and modified DNA strands constitute another important area of theoretical DNA research. When studying all these topics, a realistic computational modeling will not only strive for an accurate treatment of the photoactive region, but also carefully reckon with the complex chemical/biological environment including the sugar-phosphate backbone and the solvent. Progress toward a more complete understanding of DNA photochemistry seems most likely through joint efforts both from the experimental and computational sides.

Acknowledgement Z. L. is grateful for support from the CAS 100 Talent Project and from NSFC projects (Grant No. 21103213 and 91233106).

References

1. Callis PR (1983) Annu Rev Phys Chem 34:329
2. Crespo-Hernández CE, Cohen B, Hare PM, Kohler B (2004) Chem Rev 104:1977
3. Kohler B (2007) Photochem Photobiol 83:592

4. Markovitsi D, Gustavsson T, Talbot F (2007) Photochem Photobiol Sci 6:717
5. Middleton CT, de La Harpe K, Su C, Law YK, Crespo-Hernández CE, Kohler B (2009) Annu Rev Phys Chem 60:217
6. Markovitsi D (2009) Pure Appl Chem 81:1635
7. Kohler B (2010) J Phys Chem Lett 1:2047
8. Gustavsson T, Improta R, Markovitsi D (2010) J Phys Chem Lett 1:2025
9. Markovitsi D, Gustavsson T, Banyasz A (2010) Mutat Res 704:21
10. Markovitsi D, Gustavsson T, Vayá I (2010) J Phys Chem Lett 1:3271
11. Markovitsi D, Sage E, Lewis FD, Davies J (2013) Photochem Photobiol Sci 12:1256
12. Garavelli M (2006) Theor Chem Acc 116:87
13. Shukla MK, Leszczynski J (2007) J Biomol Struct Dyn 25:93
14. González L, Escudero D, Serrano-Andrés L (2012) ChemPhysChem 13:28
15. Plasser F, Barbatti M, Aquino AJA, Lischka H (2012) Theor Chem Acc 131:1073
16. Cornish-Bowden A (1985) Nucleic Acids Res 13:3021
17. IUPAC-IUB Commission (1970) Eur J Biochem 15:203
18. de Vries MS, Hobza P (2007) Annu Rev Phys Chem 58:585
19. Kleinermanns K, Nachtigallová D, de Vries MS (2013) Int Rev Phys Chem 32:308
20. Frenkel J (1931) Phys Rev 37:1276
21. Saigusa H (2006) J Photochem Photobiol C 7:197
22. Yarkony DR (2011) Chem Rev 112:481
23. Fabiano E, Lan Z, Lu Y, Thiel W (2011) In: Domcke W, Yarkony DR, Köppel H (eds) Conical intersections II: theory, computation and experiment, vol 17, Advanced series in physical chemistry. World Scientific, Singapore, p 463
24. Abramczyk H (2012) Vib Spectrosc 58:1
25. Serrano-Andrés L, Merchán M (2009) J Photochem Photobiol C 10:21
26. Volkovova K, Bilanicova D, Bartonova A, Letašiová S, Dusinska M (2012) Environ Health 11:S12
27. Wondrak GT (2007) Curr Opin Investig Drugs 8:390
28. Hruza LL, Pentland AP (1993) J Invest Dermatol 100:S35
29. Cadet J, Mouret S, Ravanat JL, Douki T (2012) Photochem Photobiol 88:1048
30. Rossle SC, Frank I (2009) Front Biosci 14:4862
31. Virshup AM, Punwong C, Pogorelov TV, Lindquist BA, Ko C, Martínez TJ (2008) J Phys Chem B 113:3280
32. Simons J (2006) Acc Chem Res 39:772
33. Kumar A, Sevilla MD (2010) Chem Rev 110:7002
34. Vayá I, Gustavsson T, Miannay F-A, Douki T, Markovitsi D (2010) J Am Chem Soc 132:11834
35. Genereux JC, Barton JK (2010) Chem Rev 110:1642
36. Teo YN, Kool ET (2012) Chem Rev 112:4221
37. Nielsen LM, Hoffmann SV, Nielsen SB (2013) Photochem Photobiol Sci 12:1273
38. Pyykkö P, Stanton JF (2012) Chem Rev 112:1
39. Thiel W (2011) Angew Chem Int Ed 50:9216
40. Lyakh DI, Musiał M, Lotrich VF, Bartlett RJ (2012) Chem Rev 112:182
41. Cremer D (2011) WIREs Comput Mol Sci 1:509
42. Cohen AJ, Mori-Sánchez P, Yang W (2012) Chem Rev 112:289
43. Thiel W (1996) In: Prigogine I, Rice SA (eds) New methods in computational quantum mechanics, vol 93, Advances in chemical physics. Wiley, New York, p 703
44. Thiel W (2014) WIREs Comput Mol Sci 4:145
45. Yarkony DR (1996) Rev Mod Phys 68:985
46. Bernardi F, Olivucci M, Robb MA (1996) Chem Soc Rev 25:321
47. Yarkony DR (1998) Acc Chem Res 31:511

48. Domcke W, Yarkony DR, Köppel H (eds) (2004) Conical intersections I: electronic structure, dynamics and spectroscopy, vol 15, Advanced series in physical chemistry. World Scientific, Singapore
49. Domcke W, Yarkony DR, Köppel H (eds) (2011) Conical intersections II: theory, computation and experiment, vol 17, Advanced series in physical chemistry. World Scientific, Singapore
50. Dreuw A, Head-Gordon M (2005) Chem Rev 105:4009
51. Schreiber M, Silva-Junior MR, Sauer SPA, Thiel W (2008) J Chem Phys 128:134110
52. Silva-Junior MR, Schreiber M, Sauer SPA, Thiel W (2008) J Chem Phys 129:104103
53. Sauer SPA, Schreiber M, Silva-Junior MR, Thiel W (2009) J Chem Theory Comput 5:555
54. Silva-Junior MR, Sauer SPA, Schreiber M, Thiel W (2010) Mol Phys 108:453
55. Silva-Junior MR, Schreiber M, Sauer SPA, Thiel W (2010) J Chem Phys 133:174318
56. Shavitt I (1977) In: Schaefer HF III (ed) Methods of electronic structure theory, vol 3, Modern theoretical chemistry. Plenum, New York, p 189
57. Sherrill CD, Schaefer HF III (1999) In: Löwdin P-O, Sabin JR, Zerner MC, Brändas E (eds) Advanced quantum chemistry, vol 34. Academic Press, San Diego, p 143
58. Shukla MK, Leszczynski J (eds) (2008) Radition induced molecular phenomena in nucleic acids, vol 5, Challenges and advances in computational chemistry and physics. Springer, Amsterdam
59. Gu J, Leszczynski J, Schaefer HF III (2012) Chem Rev 112:5603
60. Lange AW, Herbert JM (2009) J Am Chem Soc 131:3913
61. Kozak CR, Kistler KA, Lu Z, Matsika S (2010) J Phys Chem B 114:1674
62. Subotnik JE (2011) J Chem Phys 135:071104
63. Riley KE, Pitonák M, Jurecka P, Hobza P (2010) Chem Rev 110:5023
64. Christiansen O, Koch H, Jørgensen P (1995) Chem Phys Lett 243:409
65. Stanton JF, Bartlett RJ (1993) J Chem Phys 98:7029
66. Kowalski K, Valiev M (2008) Int J Quantum Chem 108:2178
67. Kowalski K, Valiev M (2008) J Phys Chem A 112:5538
68. Szalay PG (2013) Int J Quantum Chem 113:1821
69. Fan PD, Valiev M, Kowalski K (2008) Chem Phys Lett 458:205
70. Szalay PG, Watson T, Perera A, Lotrich VF, Bartlett RJ (2012) J Phys Chem A 116:6702
71. Szalay PG, Watson T, Perera A, Lotrich V, Fogarasi G, Bartlett RJ (2012) J Phys Chem A 116:8851
72. Szalay PG, Watson T, Perera A, Lotrich V, Bartlett RJ (2013) J Phys Chem A 117:3149
73. Perun S, Sobolewski AL, Domcke W (2006) J Phys Chem A 110:13238
74. Valiev M, Kowalski K (2006) J Chem Phys 125:211101
75. Epifanovsky E, Kowalski K, Fan PD, Valiev M, Matsika S, Krylov AI (2008) J Phys Chem A 112:9983
76. Plasser F, Aquino AJA, Hase WL, Lischka H (2012) J Phys Chem A 116:11151
77. Roos BO (1980) Int J Quantum Chem 17:175
78. Knowles PJ, Werner H-J (1985) Chem Phys Lett 115:259
79. Werner H-J, Knowles PJ (1985) J Chem Phys 82:5053
80. Roos BO (2007) In: Lawley KP (ed) Ab initio methods in quantum chemistry II, vol 69, Advances in chemical physics. Wiley, Chichester, p 399
81. Szalay PG, Müller T, Gidofalvi G, Lischka H, Shepard R (2012) Chem Rev 112:108
82. Malmqvist P-Å, Rendell A, Roos BO (1990) J Phys Chem 94:5477
83. Bearpark MJ, Ogliaro F, Vreven T, Boggio-Pasqua M, Frisch MJ, Larkin SM, Morrison M, Robb MA (2007) J Photochem Photobiol. A 190:207
84. Perun S, Sobolewski AL, Domcke W (2005) J Am Chem Soc 127:6257
85. Yamazaki S, Domcke W (2008) J Phys Chem A 112:7090
86. Yamazaki S, Domcke W, Sobolewski AL (2008) J Phys Chem A 112:11965
87. Barbatti M, Lischka H (2008) J Am Chem Soc 130:6831
88. Andersson K, Malmqvist P-Å, Roos BO, Sadlej AJ, Wolinski K (1990) J Phys Chem 94:5483
89. Andersson K, Malmqvist P-Å, Roos BO (1992) J Chem Phys 96:1218
90. Dewar MJS, Zoebisch EG, Healy EF, Stewart JJP (1985) J Am Chem Soc 107:3902

91. Stewart JJP (1989) J Comput Chem 10:209
92. Stewart JJP (1989) J Comput Chem 10:221
93. Stewart JJP (1991) J Comput Chem 12:320
94. Stewart JJP (2004) J Mol Model 10:155
95. Stewart JJP (2007) J Mol Model 13:1173
96. Stewart JJP (2013) J Mol Model 19:1
97. Kolb M (1991) Ph.D. Thesis, Universität Wuppertal
98. Kolb M, Thiel W (1993) J Comput Chem 14:775
99. Weber W (1996) Ph.D. Thesis, Universität Zürich
100. Weber W, Thiel W (2000) Theor Chem Acc 103:495
101. Scholten M (2003) Ph.D. Thesis, Heinrich-Heine-Universität Düsseldorf
102. Ridley J, Zerner M (1973) Theor Chim Act 32:111
103. Ridley JE, Zerner MC (1976) Theor Chim Act 42:223
104. Granucci G, Toniolo A (2000) Chem Phys Lett 325:79
105. Voityuk AA (2006) Chem Phys Lett 427:177
106. Granucci G, Persico M, Toniolo A (2001) J Chem Phys 114:10608
107. Alexandrova AN, Tully JC, Granucci G (2010) J Phys Chem B 114:12116
108. Voityuk AA (2013) WIREs Comput Mol Sci 3:515
109. Silva-Junior MR, Thiel W (2010) J Chem Theory Comput 6:1546
110. Fabiano E, Thiel W (2008) J Phys Chem A 112:6859
111. Lan Z, Fabiano E, Thiel W (2009) ChemPhysChem 10:1225
112. Lan Z, Fabiano E, Thiel W (2009) J Phys Chem B 113:3548
113. Lan Z, Lu Y, Fabiano E, Thiel W (2011) ChemPhysChem 12:1989
114. Lu Y, Lan ZG, Thiel W (2011) Angew Chem Int Ed 50:6864
115. Lu Y, Lan Z, Thiel W (2012) J Comput Chem 33:1225
116. Heggen B, Lan Z, Thiel W (2012) Phys Chem Chem Phys 14:8137
117. Casida ME, Huix-Rotllant M (2012) Annu Rev Phys Chem 63:287
118. Dreuw A, Head-Gordon M (2004) J Am Chem Soc 126:4007
119. Levine BG, Ko C, Quenneville J, Martínez TJ (2006) Mol Phys 104:1039
120. Baer R, Livshits E, Salzner U (2010) Annu Rev Phys Chem 61:85
121. Jacquemin D, Wathelet V, Perpète EA, Adamo C (2009) J Chem Theory Comput 5:2420
122. Jensen L, Govind N (2009) J Phys Chem A 113:9761
123. Baer R, Neuhauser D (2005) Phys Rev Lett 94:043002
124. Livshits E, Baer R (2007) Phys Chem Chem Phys 9:2932
125. Yanai T, Tew DP, Handy NC (2004) Chem Phys Lett 393:51
126. Adamo C, Scuseria GE, Barone V (1999) J Chem Phys 111:2889
127. Adamo C, Barone V (1999) J Chem Phys 110:6158
128. Zhao Y, Truhlar DG (2006) J Phys Chem A 110:13126
129. Zhao Y, Truhlar D (2008) Theor Chem Acc 120:215
130. Aquino AJ, Nachtigallová D, Hobza P, Truhlar DG, Hättig C, Lischka H (2011) J Comput Chem 32:1217
131. Barbatti M, Lan Z, Crespo-Otero R, Szymczak JJ, Lischka H, Thiel W (2012) J Chem Phys 137:22A503
132. Tavernelli I, Curchod BFE, Rothlisberger U (2009) J Chem Phys 131:196101
133. Tapavicza E, Tavernelli I, Rothlisberger U, Filippi C, Casida ME (2008) J Chem Phys 129:124108
134. Tavernelli I, Tapavicza E, Rothlisberger U (2009) J Mol Struc Theochem 914:22
135. Grimme S, Waletzke M (1999) J Chem Phys 111:5645
136. Schirmer J (1982) Phys Rev A 26:2395
137. Trofimov AB, Stelter G, Schirmer J (2002) J Chem Phys 117:6402
138. Trofimov AB, Krivdina IL, Weller J, Schirmer J (2006) Chem Phys 329:1
139. Wannier GH (1937) Phys Rev 52:191
140. Emanuele E, Markovitsi D, Millié P, Zakrzewska K (2005) ChemPhysChem 6:1387
141. Emanuele E, Zakrzewska K, Markovitsi D, Lavery R, Millié P (2005) J Phys Chem B 109:16109

142. Senn HM, Thiel W (2007) In: Reiher M (ed) Atomistic approaches in modern biology, vol 268, Topics in current chemistry. Springer, Berlin, p 173
143. Senn HM, Thiel W (2009) Angew Chem Int Ed 48:1198
144. Nachtigallová D, Zelený T, Ruckenbauer M, Müller T, Barbatti M, Hobza P, Lischka H (2010) J Am Chem Soc 132:8261
145. Cramer CJ, Truhlar DG (1999) Chem Rev 99:2161
146. Orozco M, Luque FJ (2000) Chem Rev 100:4187
147. Santoro F, Barone V, Improta R (2007) Proc Natl Acad Sci USA 104:9931
148. Improta R (2008) Phys Chem Chem Phys 10:2656
149. Santoro F, Barone V, Improta R (2008) ChemPhysChem 9:2531
150. Improta R, Santoro F, Barone V, Lami A (2009) J Phys Chem A 113:15346
151. Santoro F, Barone V, Improta R (2009) J Am Chem Soc 131:15232
152. Santoro F, Barone V, Lami A, Improta R (2010) Phys Chem Chem Phys 12:4934
153. Improta R, Barone V (2011) Angew Chem Int Ed 50:12016
154. Banyasz A, Douki T, Improta R, Gustavsson T, Onidas D, Vayá I, Perron M, Markovitsi D (2012) J Am Chem Soc 134:14834
155. Improta R (2012) J Phys Chem B 116:14261
156. Dargiewicz M, Biczysko M, Improta R, Barone V (2012) Phys Chem Chem Phys 14:8981
157. Banyasz A, Gustavsson T, Onidas D, Changenet-Barret P, Markovitsi D, Improta R (2013) Chem Eur J 19:3762
158. Santoro F, Improta R, Avila F, Segado M, Lami A (2013) Photochem Photobiol Sci 12:1527
159. Kamiya M (1978) Biochim Biophys Acta 517:527
160. Marian CM, Schneider F, Kleinschmidt M, Tatchen J (2002) Eur Phys J D 20:357
161. Marian CM, Kleinschmidt M, Tatchen J (2008) Chem Phys 347:346
162. González-Luque R, Climent T, González-Ramírez I, Merchán M, Serrano-Andrés L (2010) J Chem Theory Comput 6:2103
163. Richter M, Marquetand P, González-Vázquez J, Sola I, González L (2012) J Phys Chem Lett 3:3090
164. Worth GA, Cederbaum LS (2004) Annu Rev Phys Chem 55:127
165. Ben-Nun M, Martínez TJ (2002) In: Prigogine I, Rice SA (eds) Advances in chemical physics, vol 121. Wiley, New York, p 439
166. Levine BG, Martínez TJ (2007) Annu Rev Phys Chem 58:613
167. Tully JC (1990) J Chem Phys 93:1061
168. Wang H, Thoss M (2003) J Chem Phys 119:1289
169. Stock G, Thoss M (2005) In: Rice SA (ed) Advances in chemical physics, vol 131. Wiley, New York, p 243
170. Jasper AW, Nangia S, Zhu C, Truhlar DG (2006) Acc Chem Res 39:101
171. Dou Y, Liu Z, Yuan S, Zhang W, Tang H, Zhao J, Fang W, Lo GV (2013) Int J Biol Macromol 52:358
172. Chung WC, Lan Z, Ohtsuki Y, Shimakura N, Domcke W, Fujimura Y (2007) Phys Chem Chem Phys 9:2075
173. Nachtigallová D, Hobza P, Ritze H-H (2008) Phys Chem Chem Phys 10:5689
174. Tachikawa H, Kawabata H (2008) Chem Phys Lett 462:321
175. Serrano-Pérez JJ, González-Ramírez I, Coto PB, Merchán M, Serrano-Andrés L (2008) J Phys Chem B 112:14096
176. Bittner ER (2006) J Chem Phys 125:094909
177. Tonzani S, Schatz GC (2008) J Am Chem Soc 130:7607
178. Olaso-González G, Merchán M, Serrano-Andrés L (2009) J Am Chem Soc 131:4368
179. Gustavsson T, Sharonov A, Onidas D, Markovitsi D (2002) Chem Phys Lett 356:49
180. Crespo-Hernández CE, Cohen B, Kohler B (2005) Nature 436:1141
181. Wagner OI, Esposito A, Köhler B, Chen C-W, Shen C-P, Wu G-H, Butkevich E, Mandalapu S, Wenzel D, Wouters FS, Klopfenstein DR (2009) Proc Natl Acad Sci USA 106:19605

182. Buchvarov I, Wang Q, Raytchev M, Trifonov A, Fiebig T (2007) Proc Natl Acad Sci USA 104:4794
183. Fiebig T (2009) J Phys Chem B 113:9348
184. Bouvier B, Dognon J-P, Lavery R, Markovitsi D, Millié P, Onidas D, Zakrzewska K (2003) J Phys Chem B 107:13512
185. Onidas D, Gustavsson T, Lazzarotto E, Markovitsi D (2007) Phys Chem Chem Phys 9:5143
186. Onidas D, Gustavsson T, Lazzarotto E, Markovitsi D (2007) J Phys Chem B 111:9644
187. Rashbah EI, Sturge MD (1982) Excitons. North-Holland, Amsterdam
188. Davydov AS (1971) Theory of molecular excitons. Plenum Press, New York
189. Vayá I, Gustavsson T, Douki T, Berlin Y, Markovitsi D (2012) J Am Chem Soc 134:11366
190. Schwalb NK, Temps F (2008) Science 322:243
191. Kwok W-M, Ma C, Phillips DL (2006) J Am Chem Soc 128:11894
192. Holm AIS, Nielsen LM, Kohler B, Hoffmann SV, Nielsen SB (2010) Phys Chem Chem Phys 12:3426
193. Nielsen LM, Hoffmann SV, Nielsen SB (2012) Chem Commun 48:10425
194. Doorley GW, Wojdyla M, Watson GW, Towrie M, Parker AW, Kelly JM, Quinn SJ (2013) J Phys Chem Lett 4:2739
195. Fucaloro AF, Forster LS (1971) J Am Chem Soc 93:6443
196. Ullrich S, Schultz T, Zgierski MZ, Stolow A (2004) J Am Chem Soc 126:2262
197. Ullrich S, Schultz T, Zgierski MZ, Stolow A (2004) Phys Chem Chem Phys 6:2796
198. Canuel C, Mons M, Piuzzi F, Tardivel B, Dimicoli I, Elhanine M (2005) J Chem Phys 122:074316
199. Ritze H-H, Lippert H, Samoylova E, Smith VR, Hertel IV, Radloff W, Schultz T (2005) J Chem Phys 122:224320
200. Satzger H, Townsend D, Zgierski MZ, Patchkovskii S, Ullrich S, Stolow A (2006) Proc Natl Acad Sci USA 103:10196
201. Samoylova E, Lippert H, Ullrich S, Hertel IV, Radloff W, Schultz T (2005) J Am Chem Soc 127:1782
202. Barbatti M, Lischka H (2007) J Phys Chem A 111:2852
203. Serrano-Andrés L, Merchán M, Borin AC (2006) Chem Eur J 12:6559
204. Serrano-Andrés L, Merchán M, Borin AC (2006) Proc Natl Acad Sci USA 103:8691
205. Marian CM (2005) J Chem Phys 122:104314
206. Cremer D, Pople JA (1975) J Am Chem Soc 97:1354
207. Boeyens JCA (1978) J Cryst Mol Struct 8:317
208. Perun S, Sobolewski AL, Domcke W (2005) Chem Phys 313:107
209. Hassan WMI, Chung WC, Shimakura N, Koseki S, Kono H, Fujimura Y (2010) Phys Chem Chem Phys 12:5317
210. Conti I, Garavelli M, Orlandi G (2009) J Am Chem Soc 131:16108
211. Tuna D, Sobolewski AL, Domcke W (2014) J Phys Chem A 118:122
212. Asami H, Yagi K, Ohba M, Urashima S, Saigusa H (2013) Chem Phys 419:84
213. Clark LB, Peschel GG, Tinoco I (1965) J Phys Chem 69:3615
214. Li L, Lubman DM (1987) Anal Chem 59:2538
215. Du H, Fuh R-CA, Li J, Corkan LA, Lindsey JS (1998) Photochem Photobiol 68:141
216. Hu L, Zhao Y, Wang F, Chen G, Ma C, Kwok W-M, Phillips DL (2007) J Phys Chem B 111:11812
217. Cauët E, Valiev M, Weare JH (2010) J Phys Chem B 114:5886
218. Zelený T, Ruckenbauer M, Aquino AJA, Müller T, Lankaš F, Dršata T, Hase WL, Nachtigallová D, Lischka H (2012) J Am Chem Soc 134:13662
219. Barbatti M, Aquino AJA, Szymczak JJ, Nachtigallová D, Lischka H (2011) Phys Chem Chem Phys 13:6145
220. Li JH, Chai JD, Guo GY, Hayashi M (2012) Phys Chem Chem Phys 14:9092
221. Kumar A, Sevilla MD (2008) J Am Chem Soc 130:2130
222. Kumar A, Sevilla MD (2009) ChemPhysChem 10:1426

223. Šponer J, Šponer JE, Mládek A, Jurečka P, Banáš P, Otyepka M (2013) Biopolymers 99:978
224. Liang J, Nguyen QL, Matsika S (2013) Photochem Photobiol Sci 12:1387
225. Liang J, Matsika S (2011) J Am Chem Soc 133:6799
226. Markovitsi D, Small G (2002) Chem Phys 275:VII
227. Eisinger J, Shulman RG (1968) Science 161:1311
228. Kasha M, Rawls HR, El-Bayoumi MA (1965) Pure Appl Chem 11:371
229. Bittner ER (2007) J Photochem Photobiol A 190:328
230. Voityuk AA (2010) Phys Chem Chem Phys 12:7403
231. Czader A, Bittner ER (2008) J Chem Phys 128:035101
232. Voityuk AA (2013) Photochem Photobiol Sci 12:1303
233. D'Abramo M, Castellazzi CL, Orozco M, Amadei A (2013) J Phys Chem B 117:8697
234. Varsano D, Di Felice R, Marques MAL, Rubio A (2006) J Phys Chem B 110:7129
235. Voityuk AA, Rösch N, Bixon M, Jortner J (2000) J Phys Chem B 104:9740
236. Voityuk AA, Jortner J, Bixon M, Rösch N (2000) Chem Phys Lett 324:430
237. Voityuk AA, Siriwong K, Rösch N (2001) Phys Chem Chem Phys 3:5421
238. Voityuk AA, Jortner J, Bixon M, Rösch N (2001) J Chem Phys 114:5614
239. Voityuk AA, Rösch N (2002) J Chem Phys 117:5607
240. Jortner J, Bixon M, Voityuk AA, Rösch N (2002) J Phys Chem A 106:7599
241. Voityuk AA, Rösch N (2002) J Phys Chem B 106:3013
242. Rak J, Voityuk AA, Marquez A, Rösch N (2002) J Phys Chem B 106:7919
243. Siriwong K, Voityuk AA, Newton MD, Rösch N (2003) J Phys Chem B 107:2595
244. Voityuk AA, Siriwong K, Rösch N (2004) Angew Chem Int Ed 43:624
245. Voityuk AA (2005) J Phys Chem B 109:17917
246. Voityuk AA (2005) J Chem Phys 123:034903
247. Voityuk AA (2005) J Chem Phys 122:204904
248. Voityuk AA (2007) Chem Phys Lett 439:162
249. Voityuk AA, Davis WB (2007) J Phys Chem B 111:2976
250. Voityuk AA (2007) J Phys Chem C 111:7207
251. Blancafort L, Voityuk AA (2007) J Phys Chem A 111:4714
252. Voityuk AA, Duran M (2008) J Phys Chem C 112:1672
253. Voityuk AA (2008) J Chem Phys 128:115101
254. Félix M, Voityuk AA (2008) J Phys Chem A 112:9043
255. Siriwong K, Voityuk AA (2008) J Phys Chem B 112:8181
256. Voityuk AA (2008) Chem Phys Lett 451:153
257. Voityuk AA (2009) J Phys Chem B 113:14365
258. Voityuk AA (2009) Phys Chem Chem Phys 11:10608
259. Félix M, Voityuk AA (2011) Int J Quantum Chem 111:191
260. Migliore A, Corni S, Varsano D, Klein ML, Di Felice R (2009) J Phys Chem B 113:9402
261. Blancafort L, Voityuk AA (2006) J Phys Chem A 110:6426
262. Curutchet C, Voityuk AA (2011) Angew Chem Int Ed 50:1820
263. Curutchet C, Voityuk AA (2011) Chem Phys Lett 512:118
264. Řeha D, Voityuk AA, Harris SA (2010) ACS Nano 4:5737
265. Berlin YA, Burin AL, Ratner MA (2000) Superlattices Microstruct 28:241
266. Berlin YA, Burin AL, Ratner MA (2000) J Phys Chem A 104:443
267. Dekker C, Ratner MA (2001) Phys World 14:29
268. Berlin YA, Burin AL, Ratner MA (2001) J Am Chem Soc 123:260
269. Kurnikov IV, Tong GSM, Madrid M, Beratan DN (2002) J Phys Chem B 106:7
270. Tong GSM, Kurnikov IV, Beratan DN (2002) J Phys Chem B 106:2381
271. Berlin YA, Burin AL, Ratner MA (2002) Chem Phys 275:61
272. Grozema FC, Siebbeles LDA, Berlin YA, Ratner MA (2002) ChemPhysChem 3:536
273. Beljonne D, Pourtois G, Ratner MA, Brédas JL (2003) J Am Chem Soc 125:14510
274. LeBard DN, Lilichenko M, Matyushov DV, Berlin YA, Ratner MA (2003) J Phys Chem B 107:14509

275. Starikov EB (2004) Mod Phys Lett B 18:825
276. Hennig D, Starikov EB, Archilla JFR, Palmero F (2004) J Biol Phys 30:227
277. Yamada H, Starikov EB, Hennig D, Archilla JF (2005) Eur Phys J E 17:149
278. Senthilkumar K, Grozema FC, Guerra CF, Bickelhaupt FM, Lewis FD, Berlin YA, Ratner MA, Siebbeles LDA (2005) J Am Chem Soc 127:14894
279. Starikov EB, Fujita T, Watanabe H, Sengoku Y, Tanaka S, Wenzel W (2006) Mol Sim 32:759
280. Prytkova TR, Beratan DN, Skourtis SS (2007) Proc Natl Acad Sci USA 104:802
281. Yamada H, Starikov EB, Hennig D (2007) Eur Phys J B 59:185
282. Hatcher E, Balaeff A, Keinan S, Venkatramani R, Beratan DN (2008) J Am Chem Soc 130:11752
283. Grozema FC, Tonzani S, Berlin YA, Schatz GC, Siebbeles LDA, Ratner MA (2008) J Am Chem Soc 130:5157
284. Kubař T, Elstner M (2008) J Phys Chem B 112:8788
285. Kubař T, Woiczikowski PB, Cuniberti G, Elstner M (2008) J Phys Chem B 112:7937
286. Grozema FC, Tonzani S, Berlin YA, Schatz GC, Siebbeles LDA, Ratner MA (2009) J Am Chem Soc 131:14204
287. Kubař T, Kleinekathöfer U, Elstner M (2009) J Phys Chem B 113:13107
288. Kubař T, Elstner M (2009) J Phys Chem B 113:5653
289. Keinan S, Venkatramani R, Balaeff A, Beratan DN (2010) J Phys Chem C 114:20496
290. Woiczikowski PB, Kubař T, Gutiérrez R, Cuniberti G, Elstner M (2010) J Chem Phys 133:035103
291. Gutiérrez R, Caetano R, Woiczikowski PB, Kubař T, Elstner M, Cuniberti G (2010) New J Phys 12:023022
292. Woiczikowski PB, Steinbrecher T, Kubař T, Elstner M (2011) J Phys Chem B 115:9846
293. Wolter M, Woiczikowski PB, Elstner M, Kubař T (2012) Phys Rev B 85:075101
294. Berlin YA, Voityuk AA, Ratner MA (2012) ACS Nano 6:8216
295. Renaud N, Berlin YA, Ratner MA (2013) Proc Natl Acad Sci USA 110:14867
296. Renaud N, Berlin YA, Lewis FD, Ratner MA (2013) J Am Chem Soc 135:3953
297. Wolter M, Elstner M, Kubař T (2013) J Chem Phys 139:125102
298. Kubař T, Elstner M (2013) Phys Chem Chem Phys 15:5794
299. Schuster GB (ed) (2004) Long-range charge transfer in DNA II, vol 237, Topics in current chemistry. Springer, Berlin
300. Schuster GB (ed) (2004) Long-range charge transfer in DNA I, vol 236, Topics in current chemistry. Springer, Berlin
301. Chakraborty T (ed) (2007) Charge migration in DNA. Springer, Berlin
302. Rösch N, Voityuk AA (2004) In: Schuster GB (ed) Long-range charge transfer in DNA II, vol 237, Topics in current chemistry. Springer, Berlin, p 37
303. Siriwong K, Voityuk AA (2012) WIREs Comput Mol Sci 2:780
304. Venkatramani R, Keinan S, Balaeff A, Beratan DN (2011) Coord Chem Rev 255:635
305. Starikov EB, Cuniberti G, Tanaka S (2009) J Phys Chem B 113:10428
306. Chen J, Thazhathveetil AK, Lewis FD, Kohler B (2013) J Am Chem Soc 135:10290
307. Pan Z, Chen J, Schreier WJ, Kohler B, Lewis FD (2012) J Phys Chem B 116:698
308. Sobolewski AL, Domcke W (2004) Phys Chem Chem Phys 6:2763
309. Sobolewski AL, Domcke W, Hättig C (2005) Proc Natl Acad Sci USA 102:17903
310. Schwalb NK, Temps F (2007) J Am Chem Soc 129:9272
311. Abo-Riziq A, Grace L, Nir E, Kabelac M, Hobza P, de Vries MS (2005) Proc Natl Acad Sci USA 102:20
312. Yamazaki S, Taketsugu T (2012) Phys Chem Chem Phys 14:8866
313. de La Harpe K, Crespo-Hernández CE, Kohler B (2009) J Am Chem Soc 131:17557
314. Groenhof G, Schäfer LV, Boggio-Pasqua M, Goette M, Grubmüller H, Robb MA (2007) J Am Chem Soc 129:6812
315. Sauri V, Gobbo JP, Serrano-Pérez JJ, Lundberg M, Coto PB, Serrano-Andrés L, Borin AC, Lindh R, Merchán M, Roca-Sanjuán D (2013) J Chem Theory Comput 9:481

316. Crespo-Hernández CE, de La Harpe K, Kohler B (2008) J Am Chem Soc 130:10844
317. Rak J, Makowska J, Voityuk AA (2006) Chem Phys 325:567
318. Sadowska-Aleksiejew A, Rak J, Voityuk AA (2006) Chem Phys Lett 429:546
319. Ko C, Hammes-Schiffer S (2013) J Phys Chem Lett 4:2540
320. Law YK, Azadi J, Crespo-Hernández CE, Olmon E, Kohler B (2008) Biophys J 94:3590
321. Schreier WJ, Schrader TE, Koller FO, Gilch P, Crespo-Hernández CE, Swaminathan VN, Carell T, Zinth W, Kohler B (2007) Science 315:625
322. Kwok W-M, Ma C, Phillips DL (2008) J Am Chem Soc 130:5131
323. Billinghurst BE, Loppnow GR (2006) J Phys Chem A 110:2353
324. Yarasi S, Brost P, Loppnow GR (2007) J Phys Chem A 111:5130
325. Boggio-Pasqua M, Groenhof G, Schäfer LV, Grubmüller H, Robb MA (2007) J Am Chem Soc 129:10996
326. Blancafort L, Migani A (2007) J Am Chem Soc 129:14540
327. Yuan S, Zhang W, Liu L, Dou Y, Fang W, Lo GV (2011) J Phys Chem A 115:13291
328. Roca-Sanjuán D, Olaso-González G, González-Ramírez I, Serrano-Andrés L, Merchán M (2008) J Am Chem Soc 130:10768
329. Marguet S, Markovitsi D (2005) J Am Chem Soc 127:5780
330. Friedberg EC, Walker GC, Siede W (1995) DNA repair and mutagenesis. ASM Press, Washington
331. McCullagh M, Hariharan M, Lewis FD, Markovitsi D, Douki T, Schatz GC (2010) J Phys Chem B 114:5215
332. Hariharan M, McCullagh M, Schatz GC, Lewis FD (2010) J Am Chem Soc 132:12856
333. Johnson AT, Wiest O (2007) J Phys Chem B 111:14398
334. Pan Z, Hariharan M, Arkin JD, Jalilov AS, McCullagh M, Schatz GC, Lewis FD (2011) J Am Chem Soc 133:20793
335. Pan Z, McCullagh M, Schatz GC, Lewis FD (2011) J Phys Chem Lett 2:1432
336. Kundu LM, Linne U, Marahiel M, Carell T (2004) Chem Eur J 10:5697
337. Holman MR, Ito T, Rokita SE (2007) J Am Chem Soc 129:6
338. Cannistraro VJ, Taylor JS (2009) J Mol Biol 392:1145
339. Tuteja N, Tuteja R (2001) Crit Rev Biochem Mol Biol 36:261
340. Harrison CB, O'Neil LL, Wiest O (2005) J Phys Chem A 109:7001
341. Essen LO, Klar T (2006) Cell Mol Life Sci 63:1266
342. Kao Y-T, Saxena C, Wang L, Sancar A, Zhong D (2007) Cell Biochem Biophys 48:32
343. Liu Z, Tan C, Guo X, Kao Y-T, Li J, Wang L, Sancar A, Zhong D (2011) Proc Natl Acad Sci USA 108:14831
344. Faraji S, Dreuw A (2014) Annu Rev Phys Chem 65:275
345. Masson F, Laino T, Rothlisberger U, Hutter J (2009) ChemPhysChem 10:400
346. Harbach PHP, Borowka J, Bohnwagner M-V, Dreuw A (2010) J Phys Chem Lett 1:2556
347. Faraji S, Dreuw A (2012) J Phys Chem Lett 3:227
348. Faraji S, Groenhof G, Dreuw A (2013) J Phys Chem B 117:10071
349. Tachikawa H, Kawabata H (2008) J Phys Chem B 112:7315
350. Doorley GW, McGovern DA, George MW, Towrie M, Parker AW, Kelly JM, Quinn SJ (2009) Angew Chem Int Ed 48:123
351. de La Harpe K, Crespo-Hernández CE, Kohler B (2009) ChemPhysChem 10:1421
352. Miyahara T, Nakatsuji H, Sugiyama H (2013) J Phys Chem A 117:42
353. Wan C, Fiebig T, Kelley SO, Treadway CR, Barton JK, Zewail AH (1999) Proc Natl Acad Sci USA 96:6014
354. Kelley SO, Barton JK (1999) Science 283:375
355. Wan C, Fiebig T, Schiemann O, Barton JK, Zewail AH (2000) Proc Natl Acad Sci USA 97:14052
356. Tamulis A, Tamulis V, Graja A (2006) J Nanosci Nanotech 6:965
357. McCullagh M, Franco I, Ratner MA, Schatz GC (2011) J Am Chem Soc 133:3452
358. McCullagh M, Franco I, Ratner MA, Schatz GC (2012) J Phys Chem Lett 3:689

Top Curr Chem (2015) 356: 123–164
DOI: 10.1007/128_2013_499

Published online: 6 February 2014

Photosynthesis and Photo-Stability of Nucleic Acids in Prebiotic Extraterrestrial Environments

Scott A. Sandford, Partha P. Bera, Timothy J. Lee, Christopher K. Materese, and Michel Nuevo

Abstract Laboratory experiments have shown that the UV photo-irradiation of low-temperature ices of astrophysical interest leads to the formation of organic molecules, including molecules important for biology such as amino acids, quinones, and amphiphiles. When pyrimidine is introduced into these ices, the products of irradiation include the nucleobases uracil, cytosine, and thymine, the informational sub-units of DNA and RNA, as well as some of their isomers. The formation of these compounds, which has been studied both experimentally and theoretically, requires a succession of additions of OH, NH_2, and CH_3 groups to pyrimidine. Results show that H_2O ice plays key roles in the formation of the nucleobases, as an oxidant, as a matrix in which reactions can take place, and as a catalyst that assists proton abstraction from intermediate compounds. As H_2O is also the most abundant icy component in most cold astrophysical environments, it probably plays the same roles in space in the formation of biologically relevant compounds. Results also show that although the formation of uracil and cytosine from pyrimidine in ices is fairly straightforward, the formation of thymine is not.

Chapter 14 for the book *PHOTOINDUCED PHENOMENA IN NUCLEIC ACIDS* – Mario Barbatti, Antonio C. Borin, Susanne Ullrich (eds.)

S.A. Sandford (✉), T.J. Lee and C.K. Materese
Space Science and Astrobiology Division, NASA Ames Research Center, MS 245-6, Moffett Field, CA 94035, USA
e-mail: Scott.A.Sandford@nasa.gov

P.P. Bera
Space Science and Astrobiology Division, NASA Ames Research Center, MS 245-6, Moffett Field, CA 94035, USA

Bay Area Environmental Research Institute, 596 1st St. W, Sonoma, CA 95476, USA

M. Nuevo
Space Science and Astrobiology Division, NASA Ames Research Center, MS 245-6, Moffett Field, CA 94035, USA

SETI Institute, 189 N. Bernardo Ave., Suite 100, Mountain View, CA 94043, USA

This is mostly due to the fact that methylation is a limiting step for its formation, particularly in H_2O-rich ices, where methylation must compete with oxidation. The relative inefficiency of the abiotic formation of thymine to that of uracil and cytosine, together with the fact that thymine has not been detected in meteorites, are not inconsistent with the RNA world hypothesis. Indeed, a lack of abiotically produced thymine delivered to the early Earth may have forced the choice for an RNA world, in which only uracil and cytosine are needed, but not thymine.

Keywords Astrochemistry · Extraterrestrial abiotic nucleobase synthesis · Ice irradiation · Nucleobases · UV irradiation

Contents

1 Introduction

The processes by which life on Earth originated are not well understood and have been the subject of considerable speculation. While numerous pathways for the emergence of life have been suggested, it was presumably preceded by some sort of prebiotic chemical evolution that set the stage. In this chapter we will concentrate on only one aspect of this potential prebiotic chemistry, namely, the synthesis of nucleobases in extraterrestrial environments.

1.1 Prebiotic Synthesis of the Building Blocks of Life

It is generally assumed that, before life emerged on the primitive Earth, there must have been a period of time during which its basic "building blocks" were synthesized and confined in an environment where they could be protected and interact with each other. There is a priori no requirement for all the building blocks to be synthesized in the same environment, so it cannot be excluded that the individual components in the mixture of materials that led to the emergence of life could have

been formed in different locations and at different times. Indeed, individual classes of components, such as amino acids, could have been made and provided from multiple prebiotic environments. Presumably newly forming life had no concern about the different origins of these compounds and instead used whatever was available in the surrounding environment.

1.1.1 Abiotic Chemistry and the Origin of Life

The chemical steps that progressively led to life are still unknown, but they were probably driven by the inventory of molecules that were present on the primitive Earth and/or the astrophysical environment where they took place. All of these ingredients, together with the principles of thermodynamics, may have played an important role in the processes changing non-living molecules into living entities.

The origin of the building blocks of life has been extensively debated since the 1950s, at which time Miller produced small quantities of amino acids and other organic molecules of prebiotic interest in his famous experiment, from the spark-induced chemistry of a gas mixture that was assumed to simulate the primitive atmosphere of the Earth [1]. However, more recent studies suggest that this was probably not the most relevant model because the actual primitive atmosphere was not as reducing as the gas mixture used by Miller [2]. The discovery in the 1960s and 1970s of a rich variety of organic molecules such as amino acids, carboxylic acids, hydrocarbons, sugar-related compounds, as well as puric and pyrimidic bases in carbonaceous meteorites like Murchison (e.g., [3–8]) supported an extraterrestrial delivery of the building blocks of life rather than an indigenous production of these molecules on the primitive Earth. In particular, the amino acids and nucleobases found in the Murchison meteorite were shown to be of extraterrestrial origin, as they display enrichments in ^{13}C relative to standard terrestrial values [9–11]. This scenario of an extraterrestrial delivery of the building blocks of life to the primitive Earth via meteorites, originating from comets and asteroids, is strengthened by the fact that meteoritic bombardment was significantly heavier during the first hundreds of millions of years of the Earth's history [12–17].

A few chemical mechanisms were proposed for the formation of prebiotic molecules under abiotic conditions. For example, amino acids are usually thought to have formed via the Strecker synthesis in the meteorites' parent bodies during phases of aqueous alteration or in a primitive ocean. This synthesis involves an aldehyde that reacts with hydrogen cyanide (HCN) and ammonia (NH_3) to form an aminonitrile that can be hydrolyzed into the corresponding amino acid [18, 19]. Other chemical pathways to the formation of amino acids involve the formation of *N*-carboylamino acids as intermediate species via the Bücherer–Bergs reaction from an aldehyde, HCN, NH_3, and CO_2, also leading to amino acids via subsequent hydrolysis [19, 20]. The polymerization and/or oligomerization of HCN in H_2O is another potential pathway to the formation of both amino acids and nucleobases, as HCN is abundant in comets [21–28] and can also be found in interstellar ices [29–34]. However, while this chemical route has been extensively

studied both in the laboratory [35–39] and more recently from a theoretical point of view [40], it has also been strongly debated. A similar mechanism involving cyanoacetylene (HC_3N) reacting with either the cyanide anion (OCN^-) or water in the presence of urea (NH_2CONH_2) may also lead to the formation of the nucleobases cytosine and uracil [41], which are of great interest in this chapter. Finally, sugars, in particular glucose, ribose, and deoxiribose, as well as their derivatives, could be formed via the formose reaction, i.e., a polymerization of formaldehyde (H_2CO) [42–46].

The final step from a collection of non-living molecules to those capable of self-replication and evolution is probably the least understood of all. Indeed, even if the primitive Earth contained an abundance of all the molecules required for life, constituting the so-called "primordial soup" [12, 13], it was also probably supplied with an abundance of compounds that did not have the right properties for self-replication and evolution that may have inhibited the emergence of life. The reactions that led to self-replication and evolution are believed to have occurred in a solvent, most probably H_2O, to allow molecules to meet and react under favorable thermodynamic conditions [47]. In addition, H_2O probably played an important role in the formation of prebiotic membranes, as shown by some experiments in which organic molecules produced from the UV irradiation of simple ices spontaneously led to the formation of vesicles, a phenomenon also observed with organic extracts of the Murchison meteorite [48]. Membranes provide considerable advantages for chemical evolution, as they can protect molecules inside the vesicles from external lethal radiation, and because enclosed molecules can evolve under specific chemical conditions (solvent, temperature, pH) that can be different from the outside medium. Reactions inside a membrane-enclosed vesicle can occur under conditions of non-thermodynamic equilibrium, which, when coupled to prebiotic reactions and exchange of entropy with the external medium, can lead to complex reactions including polymerization of amino acids and sugars. Finally, exothermic reactions between organic compounds, in particular polymerizations, may also have occurred on the surface of minerals [49–53], which can play the role of a third body capable of absorbing the excess reaction energy and preventing the dissociation of newly formed products. Clays, in particular montmorillonite, are often cited as one of the minerals likely to have played such a role because of their chemical and physical properties [54, 55].

1.1.2 Potential Environments for Prebiotic Synthesis

While numerous environments for prebiotic chemistry have been suggested, most fall into one of two main categories, namely, extraterrestrial environments and environments found on the early Earth. We briefly comment on both of these environments below, although the bulk of the discussion in this chapter will be devoted to prebiotic chemistry that occurred prior to incorporation of the material into the Earth. Within this category, we will comment on the abiotic synthesis of a

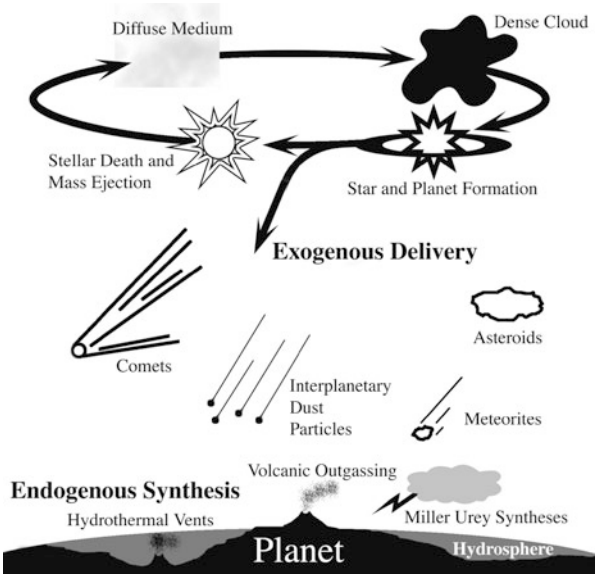

Fig. 1 The life cycle of matter in galaxies. New atoms and molecules formed in stars are ejected into the diffuse interstellar medium (ISM). Some of these materials can subsequently be gathered into dense molecular clouds, the formation sites of new stars and planets. During the formation of new stellar systems these materials can be modified, and new materials made, as they are incorporated into small objects such as asteroids, comets, and planetesimals. Organic matter contained in asteroids and comets can then be delivered to telluric planets such as the Earth via meteorites and interplanetary dust particles (IDPs). Those organic compounds may constitute an inventory of prebiotic molecules that subsequently play a role in the emergence of life if favorable chemical and physical conditions are available (from [48])

number of classes of compounds of astrobiological interest, but will specifically concentrate on the prebiotic extraterrestrial synthesis of the nucleobases.

Extraterrestrial Environments: ISM Dense Clouds, Protosolar Nebula, Comets, and Asteroids

Prior to the middle of the last century it was generally assumed that the conditions found in space were hostile to molecules, that chemistry could not proceed efficiently in space, and that most of the material in space would exist as either atoms or amorphous dust grains. The advent of radio and infrared telescopes, detectors, and spectrometers ultimately showed this to be untrue. We now know that much of the material in circumstellar and interstellar space is in molecular form, and that a variety of chemical processes occur as these materials cycle through a range of astrophysical environments (Fig. 1). In the paragraphs below we describe several environments in which chemistry is observed to occur in space.

Many stars, late in their life cycles, undergo phases in which they lose significant portions of their mass through either gradual (stellar winds) or explosive (nova and

supernova) processes. Where the outflow conditions allow, these materials can form molecules and dust grains. Depending on the local C/O ratios in the ejectae, the main products can be minerals (O-rich ejecta) or carbonaceous molecules and grains (C-rich ejecta) [56, 57].

Much of the material ejected from stars is subsequently destroyed or modified in the diffuse interstellar medium (ISM) where it is subjected to shock waves from supernova, sputtering, photo-destruction, etc. However, there are several lines of evidence that some of these materials survive transit through the diffuse ISM. Indeed, astronomical observations clearly indicate that the diffuse ISM contains silicate grains and solid organic materials that contain both aromatic and aliphatic components [56, 58–60]. Most individual molecules are unable to survive in the gas phase in the diffuse ISM, with the notable exception of polycyclic aromatic hydrocarbons (PAHs) and related species. These molecules are seen in the outflows of dying stars and are sufficiently robust to resist complete photolytic destruction in the diffuse ISM. As a result, they are the dominant form of molecular carbon found in many astrophysical environments [61–64].

Perhaps the most compelling and interesting proof that at least some material survives the trip from stellar synthesis through the diffuse ISM is the existence of presolar grains in meteorites. Presolar grains having a number of different compositions (aluminum oxides, silicates, SiC, graphite, etc.) have been identified and their circumstellar formation is demonstrated by the presence of non-solar isotopic ratios that indicate formation in a variety of nucleosynthetic environments.

However, from the perspective of prebiotic chemistry and astrobiology, the most interesting type of extraterrestrial environment is that of dense interstellar molecular clouds. Such clouds contain enough material to be optically thick so that they screen out much of the stellar radiation that destroys most molecules in the diffuse ISM. The large optical depths of these clouds allow their interiors to cool to temperatures as low as 10–15 K. At these temperatures, most gas phase species other than H, H_2, He, and Ne will condense out onto dust grains in the form of ice mantles (Fig. 2). Little "normal" chemistry of the sorts we are familiar with on Earth can take place under such conditions, but chemical reactions occur nonetheless.

Some chemistry occurs via gas–grain reactions in which individual gas-phase atoms like H, C, N, and O collide with grains, react with resident surface species on the grains, and form new compounds [65]. None of the species made in this manner are particularly complex. In dense cloud environments where $H > H_2$, these reactions simply tend to create hydrides like CH_4, CH_3OH, NH_3, and H_2O, and this process is thought to be the principle source of interstellar H_2 via reactions between two H atoms on the surface of cold dust grains. When $H < H_2$, reactions involving heteroatoms become important and species like N_2 and O_2 predominate.

More complex species can be created when ionizing radiation is present (Fig. 2). The large optical depth of dense clouds screens out most stellar radiation, but cosmic rays and the energetic photons they create when colliding with interstellar matter produce some ionization, even in the densest clouds [66]. Newly forming stars within dense interstellar clouds can also irradiate nearby materials. Ionizing radiation produces ions and radicals that are able to react even at the low

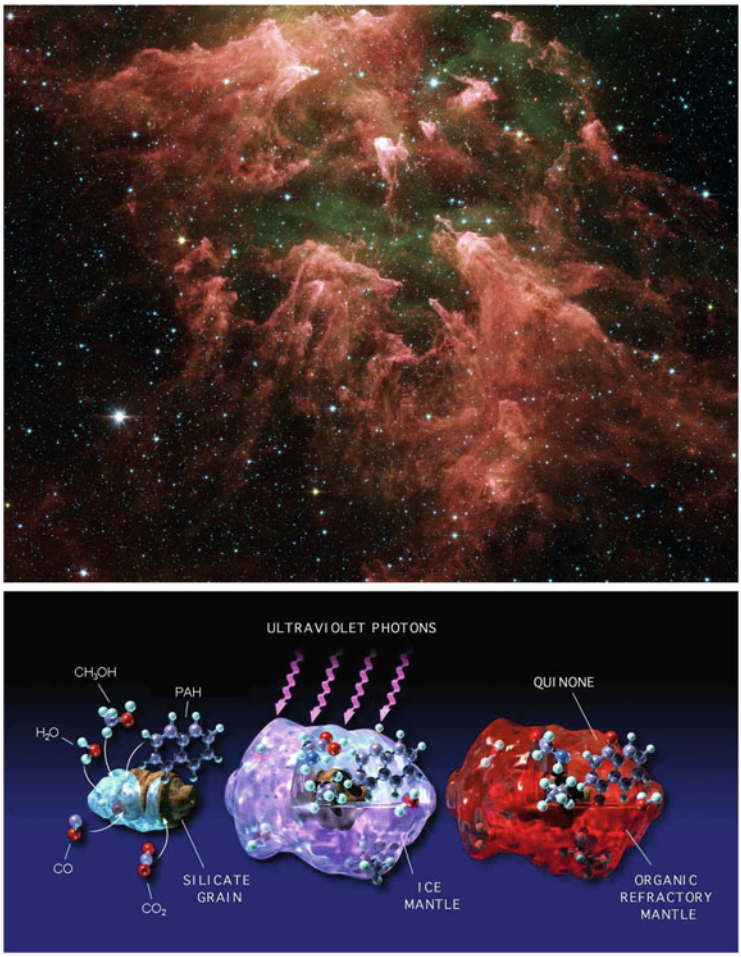

Fig. 2 *Top:* Spitzer telescope image of the Eta Carinae molecular cloud. *Bottom:* Schematic of a cold interstellar dust grain. Volatiles such as H_2O, CO, CO_2, CH_3OH, and larger molecules such as polycyclic aromatic hydrocarbons (PAHs) can condense on the surface of cold dust grains in interstellar clouds. Such ice mantles can be processed by ionizing radiation, including UV photons, leading to the formation of more complex, refractory molecules (adapted from [197])

temperatures common in these clouds. Ions created in the gas phase can react in an extensive chain of ion-molecule reactions that can lead to numerous gas-phase species [67, 68]. To date more than 175 specific molecules have been identified in the gas phase in such clouds [69], although most are relatively small (<7–8 atoms). However, the majority of the material other than H and He in dense clouds is trapped in the dust grains and their icy mantles, and it is in these ices that ionizing radiation likely produces the most complex molecular species [65, 70–72]. Such a

radiation process will be the subject of much of the discussion in this chapter, particularly in the context of the abiotic formation of the nucleobases.

Because of their biological significance, astronomers have sought to confirm the presence of small *N*-heterocycles, including pyrimidine, purine, and their derivatives, in the gas phase of the ISM. To date, none of these compounds have been detected [73–77]. Nonetheless, PAHs are known to be ubiquitous in galactic and extragalactic interstellar/circumstellar environments, and polycyclic aromatic nitrogen heterocycles (PANHs) are expected to be present as well [61–64]. It is therefore reasonable to assume that *N*-heterocycles, including pyrimidine-based species, may be present in space where they can condense on the surfaces of cold, icy grains, such as those found in dense molecular clouds [78, 79]. These materials are therefore expected to participate in the types of ice irradiation process mentioned above.

Delivery of Extraterrestrial Organics to the Early Earth

Of course, the creation of organics in extraterrestrial environments is somewhat inconsequential, at least with regards to the origin of life, if these materials are unable to survive incorporation into planetary environments. Organics incorporated into the early Earth during its initial molten accretion were presumably destroyed – arriving organics would do little beyond contributing part of the inventory of important elements like C, N, O, and H. The actual delivery and survival of astrobiologically important compounds would have had to wait for the surface of the Earth to become a more hospitable place. It is therefore likely that the majority of complex organics delivered intact to the surface of the early Earth were first incorporated into small bodies like comets and asteroids and only delivered to the Earth at a later stage [80].

The efficiency of successful delivery of extraterrestrial organics to the surfaces of planets depends critically on the nature of the body that delivers them [17]. While comets and asteroids can contain large amounts of organics, as whole bodies they are not a very efficient way to deliver organics intact to planetary surfaces. The enormous energy releases that occur during hypervelocity impact of such large objects is likely to destroy or modify much of their organic molecule content, not to mention mediating the destruction, alteration, and creation of compounds on the planet. However, over the course of their orbital evolution, bodies like asteroids can shed material in the form of smaller meteoroids or dust particles generated by impacts with other asteroidal bodies. Comets can also shed rocks and dust through collisions as well as lose dust during outgassing that occurs when cometary volatiles sublime during warming.

These smaller meteoroids and cosmic dust particles can deliver organics much more efficiently than their cometary and asteroidal parent bodies. When smaller bodies like meteorites and cosmic dust collide with the Earth, they are slowed to terminal velocity high in the atmosphere and can deliver organics to the surface of the planet with far less degradation [81, 82]. For example, while the exterior of a meteoroid suffers serious heating and ablation during atmospheric entry, the interiors

of meteorites experience little or no changes in temperatures during the entire infall process because ablation removes their surface faster than heat can thermally conduct into the interior of the meteorite. For a typical meteorite that makes it to the surface of the Earth, atmospheric entry only affects the outer few millimeters of the surviving material. Meteorites typically land on the surface of the Earth with their interior temperatures largely unchanged from what they were in space and can therefore preserve and deliver their initial organic contents (e.g., [3–8]).

The Early, Prebiotic Earth

Since the focus of this chapter is on the possible extraterrestrial abiotic formation of nucleobases, we will not go into great detail regarding the possible synthesis of these compounds in terrestrial environments. Nonetheless, the origin of life would almost certainly have occurred in an environment in which compounds of both extraterrestrial and terrestrial origin could have been present. While the issue of terrestrial synthesis is not central to the subject of this chapter, the possible importance of extraterrestrial delivery of nucleobases (as well as many other molecules of biological importance, for that matter) should be assessed in context with terrestrial sources. There are a number of excellent papers that address prebiotic chemistry on the early Earth, including extensive discussions of the nucleobases, and the reader is invited to examine them for informative reviews (e.g., [83–86] and references therein).

Note that we are not concerned here with the formation of RNA and DNA in their macromolecular forms. While it is the ultimate formation of RNA and DNA that motivates much of the interest in the abiotic formation of nucleobases, it is likely that this advance in chemical complexity occurred in a planetary environment, which falls outside the purview of our discussion here. Indeed, it has even been suggested that the formation of RNA and DNA need not have required the preexistence of nucleobases [87].

1.2 Abiotic Extraterrestrial Chemistry and the Origin of Life

There are several lines of evidence that suggest abiotic extraterrestrial chemistry may have resulted in the delivery of numerous compounds of biological importance to the early Earth. Some of this evidence comes from astronomical observations of dense clouds and forming planetary systems, but the main lines of evidence come from laboratory simulation experiments and the detection of biologically important species in the organic materials found in primitive meteorites.

1.2.1 Evidence from Astronomical Observations and Laboratory Simulations

Astronomical spectral observations of the ISM at infrared and longer wavelengths have demonstrated that the molecular composition of interstellar dense clouds is dominated by simple species. For example, absorption spectra taken along lines of

sight towards embedded and background stars show that the ices in most dense clouds are dominated by H_2O along with varying amounts of other simple molecules like CH_3OH, CO, CO_2, CH_4, NH_3, HCN, etc. [59, 88–93]. These ices are exposed to doses of ionizing radiation in the form of cosmic rays and high-energy photons that can create ions and radicals in the ices that can ultimately react to form more complex molecules (Fig. 2). Evidence that interstellar ices are truly processed by ionizing radiation in this manner comes from the observation of a broad absorption feature near 4.62 μm (2165 cm^{-1}) in the infrared spectra of the ices in many clouds [59, 88, 89, 91, 94, 95]. This feature is reliably reproduced in virtually all laboratory experiments involving the irradiation of ices containing sources of O, C, N, and H, and is due to the C≡N stretching mode in what is most likely OCN^- [96–98].

Numerous laboratory studies have demonstrated that irradiation of astrophysically relevant ices dominated by simple molecules like those listed above results in the production of numerous ions and radicals within the ices that can then combine as the ice warms to form a wide variety of new molecular species that are considerably more complex than those seen in the gas phase in dense clouds [72]. Many of these species are of astrobiological interest and include amino acids [99–102], amphiphiles [48], urea, glycerol, glyceric acid, hydantoin [103, 104], and, if aromatic species are present in the ices, quinones, ethers [105–109], and nucleobases [110–112].

This chemistry appears to be very "robust" in the sense that the types of organic materials that are produced are relatively insensitive to many of the experimental parameters of the irradiation. For example, the temperature of the ice during irradiation is relatively unimportant; all that is required is that the ice be cold enough that the starting materials remain condensed during irradiation. Since H_2O is the dominant species in many astrophysical ices, this means that ice irradiation processes yield similar products over the entire 10–150 K temperature range [71]. This processing is similarly insensitive to the source of the ionization: identical ices will yield very similar products independent of whether they are irradiated by energetic protons or UV photons [108, 113–115]. Indeed, the basic suite of products is even relatively insensitive to the composition of the ices themselves provided they contain fragmentable sources of C, H, O, and N. For instance, ices containing widely different relative abundances of the same starting molecules will produce much the same set of products, although their relative and total abundances may vary. Similarly, laboratory experiments performed with ices in which the initial sources of C, H, O, and N are different will still often yield similar products. For example, irradiation of ices yields amino acids independent of whether the initial carrier of C in the ices is CH_3OH, CH_4, or CO_2 [99–102], and whether the initial carrier of N is NH_3 or HCN [116].

Of particular interest is the radiation processing of ices that contain aromatic molecules like PAHs and related aromatic species that contain heterocycles. In dense molecular clouds, they should be largely condensed out onto grains [78, 79]. As previously stated, these molecules are relatively robust against photo-destruction in the gas phase in the ISM, but they can also participate in a

rich chemistry when irradiated in mixed molecular ices. One of the chief outcomes of the irradiation of PAHs in ices is the addition of side groups to the aromatic rings of the PAHs. Since most interstellar ices are dominated by H_2O, this largely results in O and H addition reactions that make aromatic ketones, alcohols, ethers [105–109], and hydrogenated PAHs (H_n-PAHs [117]); however, additional side groups like $–NH_2$, $–CH_3$, $–OCH_3$, $–C{\equiv}N$, etc. can be added if other molecules are present in the starting ice [105, 107]. As we will see, this process is likely to play an important role in the abiotic production of nucleobases in astrophysical environments.

1.2.2 Evidence from Meteorites

Meteorites that fall on the Earth are divided into a wide variety of classes having different compositions and evolutionary histories [118, 119]. Among these classes, carbonaceous chondrites are of the most interest for studies of extraterrestrial organics. These meteorites typically contain a few weight percent carbon [120]. Much of the carbon is in the form of insoluble organic matter (IOM), a material that consists of small aromatic moieties interlinked by a complex variety of bridging units [121, 123]. Meteoritic IOM has a number of interesting properties, for example, it is the carrier of components having large D/H and $^{15}N/^{14}N$ isotopic anomalies [122, 123]. However, other than being a major carrier of carbon in meteorites, it is of limited interest in astrobiology because it is chemically intractable.

Of more interest in astrobiology are the soluble carbonaceous components of these meteorites. A wide variety of soluble compounds are found in carbonaceous meteorites, including aliphatic and aromatic hydrocarbons, carboxylic and dicarboxylic acids, amines, and amides [120]. These individual classes of compounds are typically present at concentration falling in the range from a few ppm to a few hundred ppm.

A number of compounds are of clear astrobiological interest, including amino acids [4, 10, 124–127], amphiphiles [48], and *N*-heterocycles [11, 128–135], which are the building blocks of proteins, membranes, and nucleic acids, respectively. There is ample evidence that many of these materials are truly extraterrestrial, and not terrestrial contamination. For example, the extraterrestrial nature of the many amino acids detected in meteorites is supported by the presence of (1) amino acids not used by biological systems on Earth, (2) amino acids that are largely (but not entirely) racemic, and (3) amino acids having non-terrestrial isotopic ratios [9, 10, 124, 136–140].

Of particular relevance to the discussion in this chapter are *N*-heterocyles. To date, a series of pyrimidines, quinolines, isoquinolines, benzoquinolines, and several of their methyl isomers have been identified in meteorites ([120] and references therein). Purine- and pyrimidine-based compounds have so far been detected in the carbonaceous chondrites Orgueil, Murchison, Murray, and Lonewolf Nunataks 94102 [128–135, 143]. The extraterrestrial origin of these compounds has been

confirmed in many cases by isotopic analysis [11], lending further credence to their extraterrestrial formation via at least one astrophysical, non-biological process.

Uracil is, to date, the only pyrimidine-based nucleobase that has been unequivocally identified in meteorites [11, 132]. The extraterrestrial nature of uracil in the Murchison meteorite is supported by $\delta^{13}C$ measurements by Martins et al. [11], although it has been suggested that coeluting compounds could be confusing the issue [134]. The lack of detection of cytosine in meteorites might be explained by its conversion into uracil via hydrolysis when the organics are extracted from the meteorite, as cytosine was shown to be easily hydrolyzed in the laboratory [141, 142]. Thus, the presence of cytosine in meteorites cannot currently be ruled out.

So far, studies of the Allende, Orgueil, Murchison, and Murray have only managed to establish upper limits on the presence of thymine in these meteorites, but these upper limits are an order of magnitude *lower* than those for uracil [132]. The non-detection of thymine cannot be explained by the same conversion process that may be limiting the detection of meteoritic cytosine. This suggests that there must be another reason for its lower abundance in meteorites relative to uracil. We will return to this point later in this chapter.

Several purines have been identified in meteorites, including xanthine, hypoxanthine, and the nucleobases guanine and adenine [128–135, 143]. The presence of pre-terrestrial pyrimidine and purine-based compounds in meteorites clearly indicates that some extraterrestrial abiotic processes are capable of making at least some of the nucleobases in space. In the sections that follow we will discuss some of the extraterrestrial environment in which these processes may occur.

2 The Synthesis/Stability of Nucleobases in Extraterrestrial Environments

The primary environments of interest for chemistry in the interstellar medium are dominated by materials in the gas phase and, in dense clouds and protostellar disks, in solids and ices. Chemistry in the liquid phase is largely restricted to planetary environments and, for brief periods in the early history of the Solar System, to some asteroids, and is therefore not considered in any detail here. In the sections that follow we will thus concentrate on gas- and solid-phase photochemistry.

2.1 Synthesis/Stability in the Gas Phase

A few mechanisms for the formation of both pyrimidine- and purine-based nucleobases have been proposed and tested experimentally and theoretically. Among them, the most popular is probably the formation of purine-based

compounds from the polymerization or oligomerization of HCN in the gas phase. HCN is a common component of astrophysical ices; in particular it is found in comets [21–28], but also in interstellar and circumstellar sources [29–34]. In the 1960s, Matthews noticed that adenine, one of the purine-based biological nucleobases found in DNA and RNA, was a pentamer of HCN, i.e., that it could be obtained from the combination of five molecules of HCN. This mechanism was tested experimentally by his team and independently by Ferris' and Toupance's teams, but none of them could find a pathway that could lead to an efficient production yield of adenine [35–39]. However, the probability for five molecules of HCN to encounter one another in low-density astrophysical gas phase environments is small, so such a process would not be very efficient in space. The formation of adenine from the pentamerization of HCN in the gas phase has also been studied theoretically via density functional theory (DFT) and singles and doubles coupled-cluster with perturbational triples [CCSD(T)] computations, which showed that such a process is energetically favored [40, 144], and thus that adenine could be formed abiotically. Similarly, ab initio CCSD(T) quantum chemical computations indicate that pyrimidine could be formed in the gas phase via an ion–molecule mechanism through a structural isomer of vinyl cyanide ion [145].

Another mechanism, involving the reaction between cyanoacetylene (HC_3N) and the cyanate anion (OCN^-), could lead to the formation of the pyrimidine-based nucleobases uracil and cytosine [146]. HC_3N is abundant in comets [147–149], circumstellar disks [150–153], as well as in the atmosphere of Titan [154–157], the largest satellite of Saturn, known to house a very complex chemistry that may be in some points similar to what existed on the primitive Earth several billions of years ago [158–162]. OCN^- has been observed in the solid phase (ice) in several astrophysical sources [59, 88, 89, 91, 94, 95], and is often considered to be the proof that photo-induced chemical reactions do occur at the surface of icy cold grains, since it can be formed from the irradiation of H_2O, CO, CO_2, and NH_3 [96, 97]. However, to date, OCN^- has not yet been observed in the gas phase. Alternatively, HC_3N could also react with H_2O to form an intermediate species, cyanoacetaldehyde ($N{\equiv}CCH_2CHO$), which, by reacting with urea (NH_2CONH_2), could lead to the formation of uracil and cytosine [146, 163].

In dense environments, such as molecular clouds or Titan's atmosphere, *N*-heterocycles such as pyridine and pyrimidine may be formed in the gas phase via copolymerization of HCN and acetylene (C_2H_2), believed to be one of the precursors of PAHs in space [164, 165]. Acetylene and ethylene could also react with protonated hydrogen cyanide ($HCNH^+$), considered to be a major ion in Titan's ionosphere due to its high concentration, that could lead to synthesis of cyclic molecules involving nitrogen, and possible precursors of nucleobases [166]. $HCNH^+$ is also known to exist in the gas phase in interstellar clouds, where it plays a role in the conversion of HCN to HNC [167]. Once formed, *N*-heterocycles and PAHs could condense on small, cold grains in the ISM [78, 79] and be photo-processed together with other ices present, such as H_2O, CH_3OH, CO, CO_2, CH_4, and NH_3 [59, 88–93], to form subsequently complex

molecules of prebiotic and biological interest such as quinones [105, 107] and nucleobases [110–112].

Once formed in astrophysical environments, nucleobases, like other gas-phase and ice components, will be subjected to strong ionizing radiation. While radiation can affect the chemical composition of a medium by breaking bonds, creating ions and radicals, and drive the formation of new, more complex products after recombination, it can also destroy these same compounds. Because of this, studying the photo-stabilities of compounds of interest is also important. Peeters et al. [168] studied the photo-stability of pyridine, pyrimidine, and triazine in an argon matrix under astrophysically relevant conditions. Their results show that these molecules, if isolated in the gas phase and subjected to UV radiation, would have half-lives of 2–20 years in the optically thin diffuse ISM, and up to 2 Myr in the dense ISM, which is mostly opaque to UV photons but subjected to cosmic-ray radiation and their secondary electrons as well as UV photons produced from the interaction between cosmic rays and grains [168]. Because of higher UV fluxes, these numbers drop to 4–30 min in the Solar System. All these values are smaller than those expected for small PAHs irradiated in astrophysical environments [61, 169–171], probably due to the smaller bond energies and the polarization of the C–N bonds in heterocyclic compounds. The stability of nucleobases under UV irradiation, and the processes of radical and ion formation on them, were also studied both experimentally [172, 173] and theoretically [174].

2.2 Synthesis of Pyrimidine-Based Nucleobases in Extraterrestrial Ices

Laboratory and theoretical work has been done on the ice-phase photochemistry of pyrimidine, leading to the synthesis of all three pyrimidine-based nucleobases. In the sections that follow, we summarize the results of this work separately for uracil, cytosine, and thymine (Fig. 3). We use the discussion of uracil to provide a general overview of the approaches that have been used for this kind of work. The subsequent discussions about cytosine and thymine are largely restricted to details unique to these individual molecules.

2.2.1 Synthesis of Uracil

Uracil (2,4-dihydroxypyrimidine) is a doubly oxidized pyrimidine derivative. It is one of the five biologically relevant nucleobases, and is found only in RNA. The "RNA world" hypothesis proposes that RNA served as the original genetic material and as biological catalysts [175–177]. Under this paradigm, understanding the abiotic formation of uracil is of great importance.

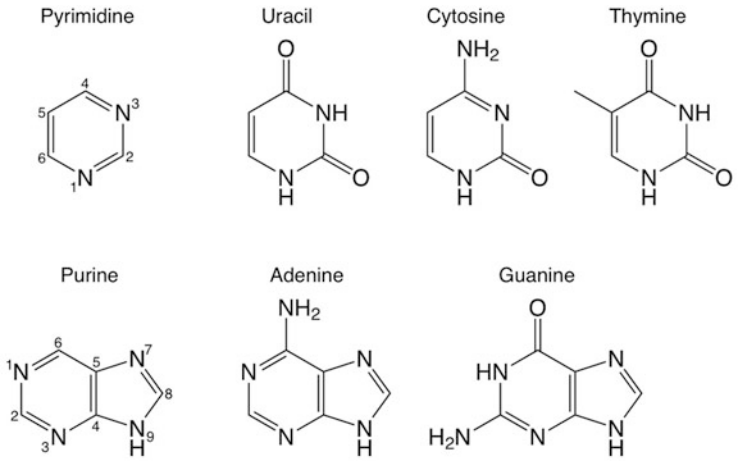

Fig. 3 The molecular structures of pyrimidine, purine, and the five biological nucleobases whose backbones are based on these compounds: uracil (2,4-dihydroxypyrimdine), cytosine (4-amino-2-hydroxypyrimidine), and thymine (2,4-dihydroxy-5-methylpyrimidine) for pyrimidine, and adenine (6-aminopurine) and guanine (2-amino-6-hydroxypurine) for purine

As mentioned earlier, the detection of pyrimidine- and purine-based nucleobases in meteorites suggests that such molecules may be present on the surfaces of cold grains in astrophysical environments and mixed into ices. If this is so, then biologically relevant molecules such as nucleobases might be formed via photo-processing of pyrimidine in ices, the same way other organic compounds such as amino acids are probably formed in similar environments [99–102].

The formation of uracil via the photo-irradiation of pyrimidine mixed with simple ices requires an oxygen source. Among the catalog of compounds present in interstellar ices, H_2O is by far the most abundant [90–93], and can be a strong oxidant. Consequently, H_2O:pyrimidine ices subjected to UV photon irradiation are simple, relevant models to simulate the oxidation of pyrimidine under astrophysical conditions in the laboratory.

Laboratory Synthesis of Uracil

In these laboratory experiments, H_2O:pyrimidine mixtures prepared in the gas phase are deposited in a controlled fashion onto a substrate cooled to temperatures as low as 15–20 K inside a cryogenic vacuum chamber evacuated to a pressure of a few 10^{-8} mbar. During deposition, the growing ice films are simultaneously irradiated with UV photons emitted by a microwave-powered H_2 discharge lamp. Such a lamp provides UV photons mainly at 121.6 nm (Lyman-α) and a continuum

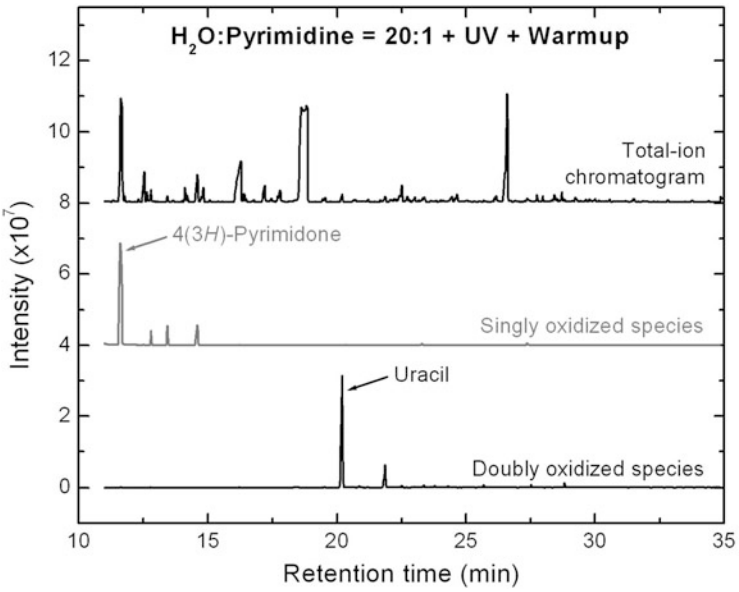

Fig. 4 Total-ion chromatogram (*top trace*) of a residue produced from the UV photo-irradiation of an H_2O:pyrimidine = 20:1 ice mixture at low temperature followed by a subsequent warmup to room temperature. The *middle* and *bottom* traces show the single-ion chromatograms of the same residue corresponding to the masses for the singly and doubly oxidized pyrimidine derivatives, respectively, and show the identification of 4(3*H*)-pyrimidone and uracil in this sample (from [110])

centered around 160 nm, with a flux of about 2×10^{15} photons cm^{-2} s^{-1} [178] that simulates the UV radiation field observed in many astrophysical environments [66, 179, 180].

Following the simultaneous deposition and radiation process, each ice sample is warmed to 220 K to allow the original ice components to sublime away, at which temperature the resulting refractory residue material is extracted from the vacuum chamber for further analysis with high-performance liquid chromatography (HPLC) and gas chromatography coupled with mass spectrometry (GC-MS).

Two of the major compounds successfully identified in these residues include 4(3*H*)-pyrimidone (or 4-hydroxypyrimidine), a singly oxidized pyrimidine derivative and precursor of uracil, and uracil itself (Fig. 4; [110]). It should be noted that 2-hydroxypyrimidine, another singly oxidized variant of pyrimidine and a uracil precursor, is only detected in very small quantities in this series of experiments, indicating that oxygen addition to pyrimidine occurs in a regioselective manner [110, 111]. These experiments also show that UV photons can break the pyrimidine ring, leading to the formation of small aliphatic molecules such as urea and the amino acid glycine in measurable quantities [111]. As previously observed in other simple ice mixtures, for example ices in which amino acids are formed [99–102],

the list of products formed is relatively insensitive to the ratios of the starting H_2O and pyrimidine, though their relative abundances vary.

Since data regarding the composition of the residues are obtained ex post facto, it is difficult to know at which point during the irradiation and/or subsequent warm-up products the likes of 4(3*H*)-pyrimidone, uracil, and their isomers are actually formed. However, it is known that the formation of uracil does not occur as a result of exposure to the aqueous phase while awaiting analysis, since its presence is confirmed in samples that were kept free of exposure to liquid water [110]. While this does not answer the question of when uracil is produced, it shows that such compounds can form in the absence of liquid water.

There are limited experimental data related to the reaction mechanisms for the formation of oxidized pyrimidines and their derivatives. Such issues can be addressed with theoretical computations and are discussed in the next section. Nevertheless, experiments reveal that the formation of these compounds is relatively insensitive to temperature and wavelength, which suggests a radical and/or ion chemistry driven by the photo-decomposition of H_2O. Given this hypothesis, the unstable radicals and/or ions engage in a chemistry of opportunity that is not bound by thermodynamic favorability.

Theory of Uracil Synthesis in the Condensed Phase

Detailed quantum mechanical theoretical computations have been conducted to understand the process of photo-oxidation of pyrimidine in a pure H_2O ice matrix [181]. B3LYP DFT, which contains Becke's three-parameter exchange functional (B3) [182], and the correlation functional of Lee, Yang, and Parr (LYP) [183], were used in conjunction with Pople's 6-31G(d,p) split valence basis set [184]. Structures were optimized to obtain the lowest energy minima on the potential energy surfaces of the reactants, intermediates, and products, and were confirmed by a subsequent harmonic frequency calculation. Energy differences were then obtained using second-order Møller-Plesset (MP2) perturbation theory for closed shell species and second-order Z-averaged perturbation theory (ZAPT2) [185, 186] for the open shell species, in conjunction with Dunning's correlation consistent polarized valence triple zeta basis set (cc-pVTZ) [187]. The Q-Chem 3.1 and 3.2 suites of ab initio and DFT quantum mechanical codes were used for all computations [188].

H_2O possesses a large photo-dissociation cross-section in the UV wavelength range [189]. Hydroxyl ($^{\bullet}OH$) radicals are therefore readily produced in the ices by the following process:

$$H_2O + h\nu \rightarrow H^{\bullet} + {}^{\bullet}OH$$

It is therefore reasonable to assume that the chemistry in these ices is dominated by reactions of $^{\bullet}OH$ radicals with pyrimidine and its derivatives. Other radicals and ions can also be generated from the pyrimidine itself via the following processes:

$$\mathrm{Py} + \mathrm{h}\nu \rightarrow [\mathrm{Py}]^{+\bullet} + \mathrm{e}^{-}$$
$$\mathrm{Py} + \mathrm{h}\nu \rightarrow [\mathrm{Py/H}]^{\bullet} + \mathrm{H}^{\bullet}$$

where $[\mathrm{Py}_{/\mathrm{H}}]^{\bullet}$ designates a radical formed from the cleavage of a C–H bond on the pyrimidine ring. $^{\bullet}$OH radicals can react with either neutral pyrimidine molecules or pyrimidine cations to form cations and radicals of oxidized pyrimidines.

An important step in these mechanisms is the loss of either a proton or a hydrogen atom from the intermediates to form the final products. Reactions involving a pyrimidine cation and an $^{\bullet}$OH radical (first oxidation step) are presented in Fig. 5a. Oxidation products of pyrimidine can be further oxidized by $^{\bullet}$OH radicals, and produce doubly oxidized products:

$$[\mathrm{Py-OH}]^{+\bullet} + {}^{\bullet}\mathrm{OH} \rightarrow \left[\mathrm{Py}(-\mathrm{OH})_2\right]^{+}$$
$$\mathrm{Py-OH} + {}^{\bullet}\mathrm{OH} \rightarrow \left[\mathrm{Py}(-\mathrm{OH})_2\right]^{\bullet}$$

The above reactions are ion–molecule or radical–molecule type in nature, and are typically barrierless and fast. Neutral–neutral reactions between H_2O and pyrimidine can also occur but, because of their high activation barriers, should be several orders of magnitude slower than reactions involving radicals or cations, particularly in cold ices.

Computations show that an ionic mechanism in which a pyrimidine cation reacts with an $^{\bullet}$OH radical is energetically favorable and can lead to the formation of intermediate species followed by the subsequent loss of a proton to form the final products [181]. Among all possible products, 4-hydroxypyrimidine and its tautomer 4(3*H*)-pyrimidone are the most favored singly oxidized products, followed by 2-hydroxypyrimidine and its tautomer 2(1*H*)-pyrimidone (Fig. 5b). This result is important since any of these singly oxidized compounds can be further oxidized, leading to the formation of uracil. Additionally, computations show that a purely gas-phase proton loss from the ionic intermediate species is unfavorable, as illustrated in the energy diagram (Fig. 5b). The presence of several H_2O molecules in the ice matrix, acting as proton acceptors, allows this reaction to become favorable towards the formation of the products. In other words, a condensed-phase environment is critically important for these mechanisms to be viable. Oxidation of neutral pyrimidine via a reaction with an $^{\bullet}$OH radical is also shown to be energetically favorable and leads to the expected products, although this mechanism is not as energetically favorable as that of an ionic mechanism according to the ab initio MP2/ZAPT2 calculations.

As illustrated in Fig. 6a, Bera et al. [181] showed that oxidation of 4(3*H*)-pyrimidone (and its tautomer 4-hydroxypyrimidine) via an ionic mechanism follows a similar path as that described for the first oxidation step via an ionic mechanism. That is, the initial hydroxylation step is highly exothermic and should be barrierless, and the subsequent proton loss is energetically favorable in the presence of the surrounding H_2O molecules (i.e., a condensed-phase environment

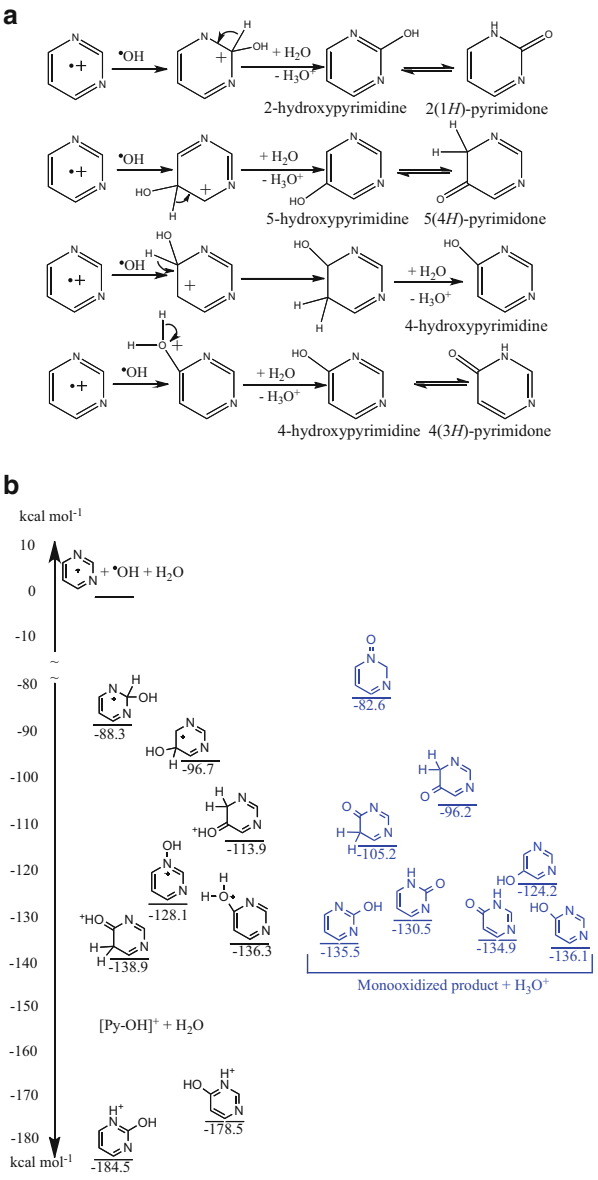

Fig. 5 (**a**) Mechanistic routes of pyrimidine cation reaction with hydroxyl radicals. The first step is a nucleophilic attack of a hydroxyl radical to pyrimidine cation. The second step is the loss of a proton assisted by H_2O. The third step is a tautomerization. (**b**) Energy diagram of the first oxidation step (energies are in kcal mol^{-1}). On the left hand side are the energies of intermediates + H_2O, and on the right hand side are the energies of singly oxidized products + H_3O^+ (see [181])

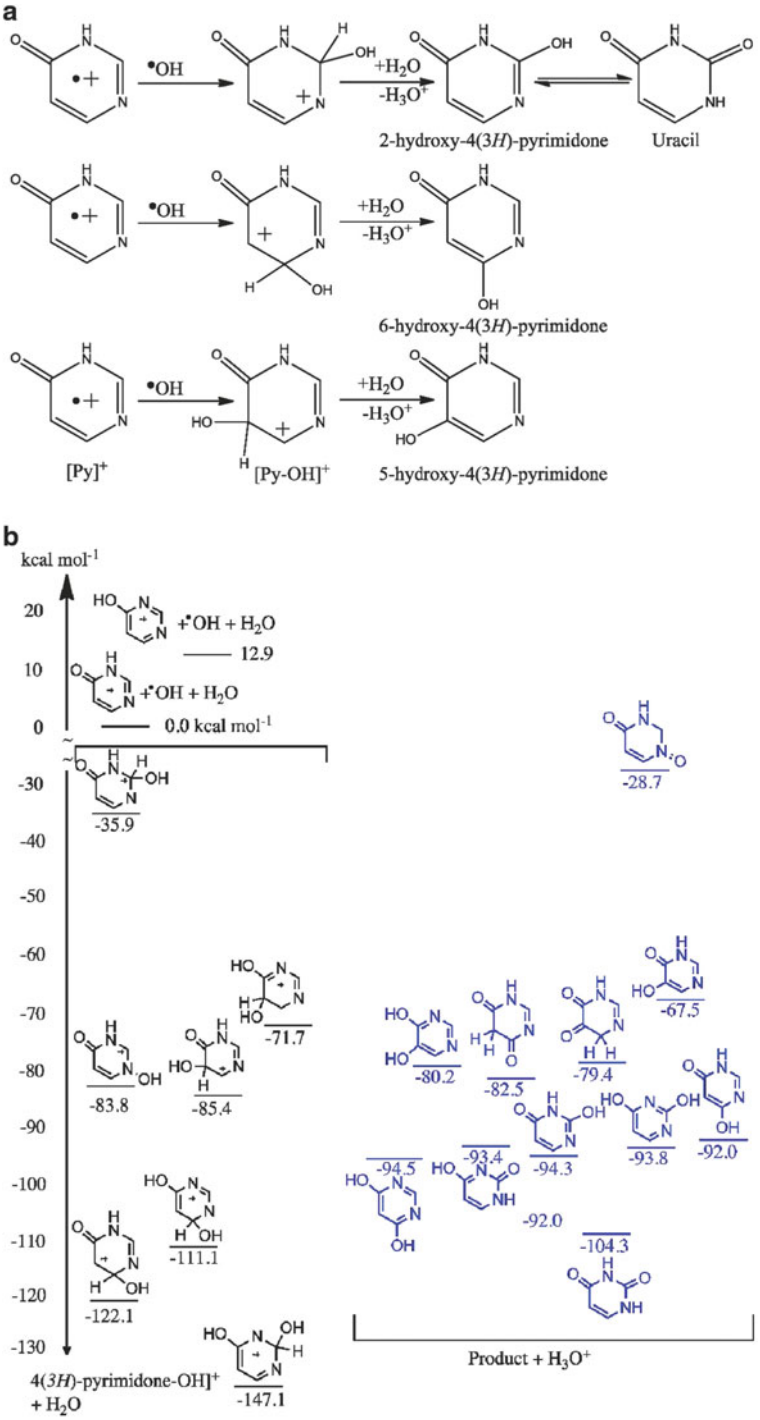

Fig. 6 (**a**) Mechanistic routes of hydroxyl radical attacking the 4(3*H*)-pyrimidone cation. The first step is a nucleophilic attack of a hydroxyl radical to pyrimidine cation. The second step is the

is again required for the deprotonation step). From the energetic order of the formed intermediate species and products (Fig. 6b), it is evident that the formation of *uracil* is favored over that of other doubly oxidized products. Additionally, the reaction between an $^{\bullet}OH$ radical and a neutral 4-hydroxypyrimidine molecule, which requires a neutral–radical intermediate species, is also a viable route for the formation of uracil and other doubly oxidized pyrimidine derivatives.

Another route for the formation of uracil is via the oxidation of 2-hydroxypyrimidine or its tautomer 2(1*H*)-pyrimidone. The reaction schemes for an ionic mechanism reaction are shown in Fig. 7a, and the associated energies are shown in Fig. 7b. It is interesting to note that 2,4-dihydroxypyrimidine, the dienol tautomer of uracil, is found to be the most stable doubly oxidized product. Again, the presence of H_2O molecules to abstract a proton from the intermediate is essential for the oxidation reaction to proceed via an ionic mechanism. A similar result was found for a neutral–radical oxidation mechanism, which showed that the formation of uracil is still favored over that of other products.

Therefore, theoretical computations are in agreement with laboratory studies of the UV photo-irradiation of H_2O:pyrimidine ice mixtures at low temperature [110], in which 4(3*H*)-pyrimidone was found to be the most abundant singly oxidized pyrimidine. The detection of only small quantities of 2-hydroxypyrimidine in laboratory samples favor a route for the formation of uracil in which 4(3*H*)-pyrimidone is its main precursor, though computations show that the oxidation of 2-hydroxypyrimidine towards the formation of uracil is also energetically favored in an H_2O ice matrix [181]. Similarly, uracil was found to be the most abundant doubly oxidized pyrimidine in laboratory samples [110], as well as the most favorable product in the ab initio quantum calculations, regardless of its singly oxidized precursors, i.e., 4-hydroxypyrimidine, 2-hydroxypyrimidine, or their tautomers. Finally, both experimental and theoretical results show a clear regioselectivity for the oxidation of pyrimidine, favoring position 4 of the ring over position 2 for the first oxidation, and the formation of uracil as the most stable doubly oxidized product.

Perhaps the single most important conclusion from these quantum mechanical computations is that the oxidation of pyrimidine is not expected to be energetically favorable in the gas phase, whereas it is feasible in an ice matrix. The presence of several H_2O molecules surrounding the reactants in the condensed phase is absolutely necessary to assist the proton abstractions leading to the formation of the final products for both oxidation steps of pyrimidine and its derivatives. This important result indicates that the formation of uracil, as well as other pyrimidine derivatives, via the oxidation of pyrimidine under astrophysical conditions is likely to be viable

Fig. 6 (continued) loss of a proton. (**b**) Energy diagram of the second oxidation step starting from 4(3*H*)-pyrimidone (energies are in kcal mol^{-1}). On the *left hand side* are the energies of intermediates + H_2O, and on the *right hand side* are the energies of singly oxidized products + H_3O^+ (see [181])

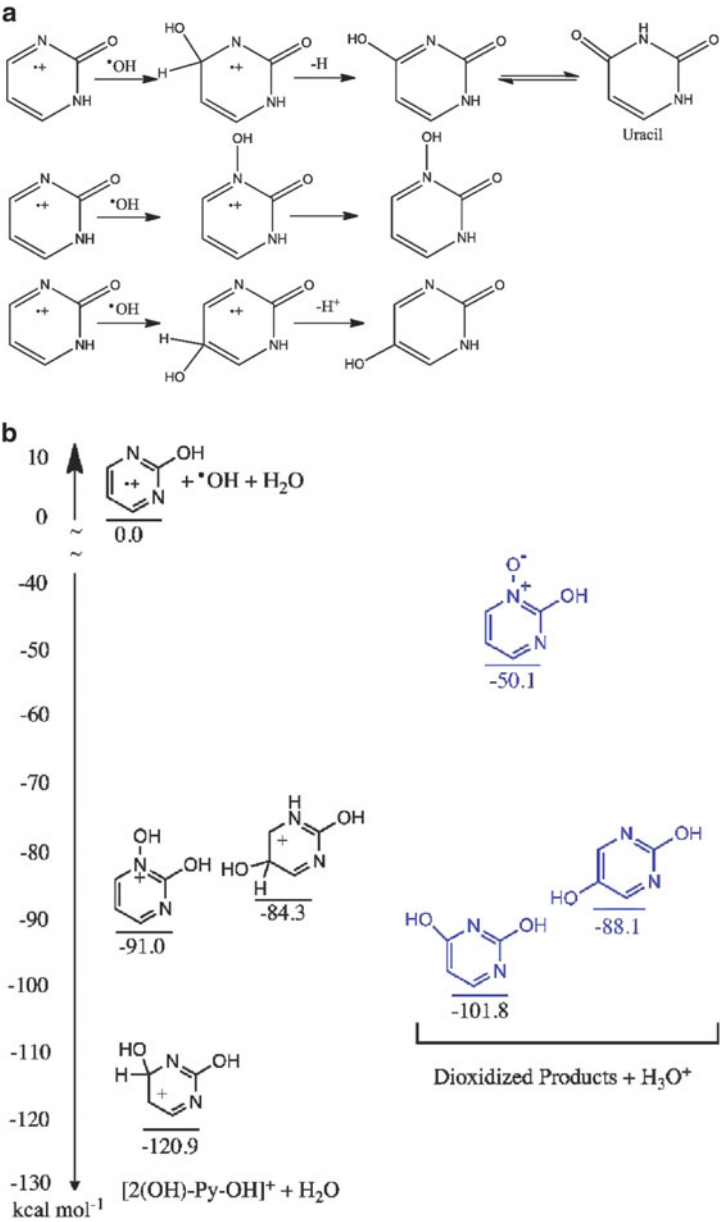

Fig. 7 (**a**) Mechanistic routes for the oxidation of starting from 2(1*H*)-pyrimidone towards the formation of uracil and its isomers. The first step is a nucleophilic attack of a hydroxyl radical to the 2(1*H*)-pyrimidone cation. The second step is the loss of a proton. (**b**) Energy diagram of 2 (1*H*)-pyrimidone cation and hydroxyl radical (energies are in kcal mol^{-1}). On the *left hand side* are the energies of intermediates + H_2O, and on the *right hand side* are the energies of doubly oxidized products + H_3O^+ (see [181])

only in icy mantles, such as those observed at the surface of cold grains in the ISM, and in the presence of ionizing radiation [181].

2.2.2 Synthesis of Cytosine

Cytosine (4-amino-2-hydroxypyrimidine) is another biologically relevant pyrimidine-based nucleobase, which is found in both DNA and RNA. Like uracil, this compound is a doubly substituted pyrimidine derivative, but has an amino (NH_2) group replacing the OH group on position 4 (Fig. 3). Therefore, the abiotic production of cytosine from the irradiation of pyrimidine requires the addition of both one OH group to position 2 of the pyrimidine ring and one NH_2 group to position 4. $^{\bullet}OH$ and $^{\bullet}NH_2$ radicals are nucleophilic species that are readily formed from the photo-dissociation of H_2O and NH_3, respectively, both in laboratory ices and cold astrophysical environments such as diffuse clouds, protostellar disks, circumstellar sources, and comets [90–93]. Because of the low NH_2–H and HO–H dissociation energies of 4.60 eV [190] and 5.10 eV [191], respectively, both $^{\bullet}OH$ and $^{\bullet}NH_2$ radicals are expected to react with pyrimidine in a similar way under these experimental conditions.

Laboratory Synthesis of Cytosine

The irradiation of pyrimidine mixed with H_2O and NH_3 ices in the laboratory is thus expected to lead to the formation of cytosine, uracil, and a suite of other oxidized and/or aminated pyrimidine derivatives. Experiments in which H_2O:NH_3:pyrimidine ice mixtures with different relative proportions are irradiated following the same protocol as for the formation of uracil show that cytosine can be formed efficiently under similar conditions, and with a comparable yield to uracil [111]. As was observed for the oxidation of pyrimidine, the addition of amino groups is regioselective and favors the amination of position 4 of the ring over the other positions to form 4-aminopyrimidine (one of cytosine's precursors), though small quantities of other isomers such as 2-aminopyrimidine are also formed.

However, even if 4-aminopyrimidine is a logical precursor of cytosine, its formation in H_2O+NH_3 is in competition with the formation of 4(3*H*)-pyrimidone via oxidation of pyrimidine ([110, 111]; Sect. 2.2.1). The amination of 4(3*H*)-pyrimidone leads to the formation of isocytosine (2-amino-4-hydroxypyrimidine), an isomer of cytosine that has been detected in most of the residues produced from the UV photo-irradiation of H_2O:NH_3:pyrimidine ice mixtures [111].

Finally, it is interesting to note that, although both OH and NH_2 groups have similar nucleophilic properties and are expected to react with pyrimidine in a similar manner, these experiments indicate that the presence of H_2O in the starting ice mixtures enhances the addition of NH_2 groups, in particular to increase the formation yield of products such as 2-aminopyrimidine, whose formation in an H_2O-poor ice matrix is not favored for regioselective reasons [111].

Theory of Cytosine Synthesis in the Condensed Phase

Investigating reaction mechanisms in mixed ices such as H_2O+NH_3 is more complicated than in separate pure H_2O or pure NH_3 ices. In order to perform theoretical computations aimed at understanding such processes, one needs to identify the most probable sequence of reactions in these ices. Since $^{\bullet}OH$ and $^{\bullet}NH_2$ radicals are known to be readily formed from the photo-degradation of H_2O and NH_3, respectively, it appears logical that the two main types of reactions that will affect pyrimidine in these systems are oxidation (i.e., hydroxyl group addition) and amination (i.e., amino group addition).

Following what is known about the oxidation of pyrimidine from both the experimental and theoretical studies of uracil formation, it is reasonable to assume that functional group additions on pyrimidine (neutral, cation, or radical) take place one after the other rather than simultaneously. Because $^{\bullet}OH$ and $^{\bullet}NH_2$ radicals have a reasonably similar probability to react with pyrimidine, the most important factor concerning which groups is most likely to be added first will largely depend on the relative abundance of their respective parent molecules (H_2O and NH_3) in the ices. For most astrophysical ices and the studies described here, where H_2O is generally the dominant ice component, oxidation will be favored over amination.

When oxidation takes place first, it favors the formation of 4(3*H*)-pyrimidone over that of 2-hydroxypyrimidine for regioselective reasons ([110, 181]; Sect. 2.2.1). The subsequent amino group addition, if it occurs at position 2 of the pyrimidine ring, will lead to the formation of isocytosine (2-amino-4-hydroxypyrimidine), an isomer of the nucleobase cytosine. Of course, 4(3*H*)-pyrimidone and its isomers can also undergo further oxidation, towards the formation of uracil and its isomers, as shown for pyrimidine in a pure H_2O ice ([110, 181]; Sect. 2.2.1).

In the case where amination takes place first, the most favored product may be 4-aminopyrimidine, similar to the oxidation step, which may then be either aminated to form doubly aminated pyrimidine derivatives or oxidized to form cytosine and its isomers. Similar to what happens for the oxidation of 4(3*H*)-pyrimidone, the oxidation of 4-aminopyrimidine may favor the 2 position on the ring, resulting in the formation of cytosine. The formation of other isomers will likely also be exothermic, although they may be less abundant than cytosine if the formation of cytosine follows that of uracil.

The detailed ab initio quantum chemical calculations describing these reactions for three types of mechanisms, namely, ionic, neutral–radical, and radical–radical, are currently in progress [192].

2.2.3 Synthesis of Thymine

Thymine (2,4-dihydroxy-5-methylpyrimidine) is the third and last biologically relevant pyrimidine-based nucleobase. Thymine is found only in DNA and thus is not necessary for the emergence of an RNA world [175–178]. The formation of this

tri-substituted pyrimidine derivative requires a double oxidation in the same positions on the ring as uracil, and the addition of a methyl (CH_3) group to position 5. Therefore, the abiotic production of thymine from pyrimidine requires both a source of oxygen and a source of methyl groups.

Since H_2O is by far the most abundant component of interstellar ices, its presence in any starting ice mixtures to be studied is essential. On the other hand, possible sources of methyl groups in interstellar ices could include both methanol and methane, as both are widely observed in cold astrophysical environments, although methanol is usually observed with abundances that are an order of magnitude larger than those of methane [90–93]. Thus, H_2O:CH_3OH:pyrimidine and H_2O:CH_4:pyrimidine mixtures appear to be the simplest relevant ice analogs to be studied both experimentally and theoretically for the formation of thymine through photo-irradiation. Experiments in which H_2O-free ice mixtures (CH_3OH:pyrimidine and CH_4:pyrimidine) are irradiated have also been performed in order to evaluate better the methylation efficiency of CH_3OH and CH_4, as well as the role of H_2O in these experiments.

Laboratory Synthesis of Thymine

Experimental protocol and analysis techniques employed in the study of the formation of thymine are similar to those previously employed for studying the formation of uracil and cytosine [112]. One notable exception, however, is that laboratory experiments on thymine formation also included experiments that employed higher UV photon doses than needed for the formation of uracil and cytosine.

Experimental results indicate that ice mixtures containing CH_3OH as a methyl group source do not yield measurable quantities of pure methylpyrimidines, although they may still produce small quantities of thymine. The lack of methylpyrimidines may be partially explained by the fact that the photo-dissociation of pure CH_3OH is known to lead to branching ratios from which only 1 in 7 photolytic reactions will result in the production of a CH_3 group [193].

In contrast, methane is a much better source of CH_3 groups than methanol. Experiments on the irradiation of CH_4:pyrimidine ice mixtures do lead to the production of 4-methylpyrimidine, although no other methylpyrimidine isomers were detected [112]. It is interesting to note that similar HPLC analysis of residues produced from experiments involving quinoline rather than pyrimidine yielded similar results for the non-detection and detection of methyl addition in CH_3OH- and CH_4-containing ices, respectively [194]. The addition of H_2O to CH_4:pyrimidine mixtures results in the production of both 4- and 5-methylpyrimidine, once again highlighting the role H_2O can play as a catalyst for the formation of other less abundant methylpyrimidine isomers such as 5-methylpyrimidine, as is also observed for the formation of aminopyrimidines from H_2O:NH_3:pyrimidine ice mixtures [111].

While the production of thymine has been observed in these experiments, its overall abundance is relatively low in comparison to uracil or cytosine in similar previous experiments. One likely cause for this difference is the fact that thymine formation requires three substitutions, while both uracil and cytosine only require two each. This means that more photons are required, and this puts further constraints on the makeup of the surrounding ice to ensure that the proper radicals and/or ions are available. Additionally, since the formation of thymine via UV processing of pyrimidine in ices requires more photons than would be required for either uracil or cytosine, there are more opportunities to derail its formation with an alternative substitution or through further modification of the final product or its precursors.

Theory of Thymine Synthesis in the Condensed Phase

Detailed quantum chemical methods have been used to study the formation of thymine in a system where pyrimidine is surrounded by H_2O molecules, OH radicals, and $^{\bullet}CH_3$ radicals, using the same computational methods as described in Sect. 2.2.1 for uracil [195]. As mentioned earlier, the formation of thymine from pyrimidine requires the addition of three groups, two OH groups (positions 2 and 4 on the ring) and one CH_3 group (position 5).

As in the case of cytosine, investigating the reaction mechanisms of thymine formation is complicated because the process occurs in mixed ices in which the addition of different groups can be carried out in several different orders (Fig. 8). The two main types of reactions in these systems are oxidation and methylation. Three different routes have been explored: (1) the double oxidation of pyrimidine followed by a methylation, (2) the methylation of pyrimidine followed by a double oxidation, and (3) the oxidation of pyrimidine, followed by a methylation, followed by a second oxidation. As in the case of uracil, Bera et al. [195] studied each of these routes for three types of mechanisms, namely, ionic, neutral–radical, and radical–radical.

In the first case, reactions will lead to the formation of uracil via the same route as described for pyrimidine in pure H_2O ice ([110, 181]; Sect. 2.2.1). The subsequent reaction is the methylation of uracil, which can lead to thymine as well as to its isomers. Computations show no clear preference for the product of methylation of uracil, indicating that thymine has the same, or a smaller, probability to be formed relative to its isomer 6-methyluracil. In the second case, pyrimidine is first methylated and then oxidized to form thymine and its isomers. Interestingly, 5-methylpyrimidine, which is the methylated pyrimidine precursor of thymine, is not the most energetically favored product among all possible methylpyrimidine isomers. The oxidation steps have much more favorable reaction energies compared to the methylation steps, which is the key reason why oxidation is overwhelmingly favored. Moreover, although the addition of methyl groups to pyrimidine is energetically favorable, in an H_2O-rich ice methylation will compete unfavorably against oxidation for two main reasons: (1) because $^{\bullet}OH$ radicals

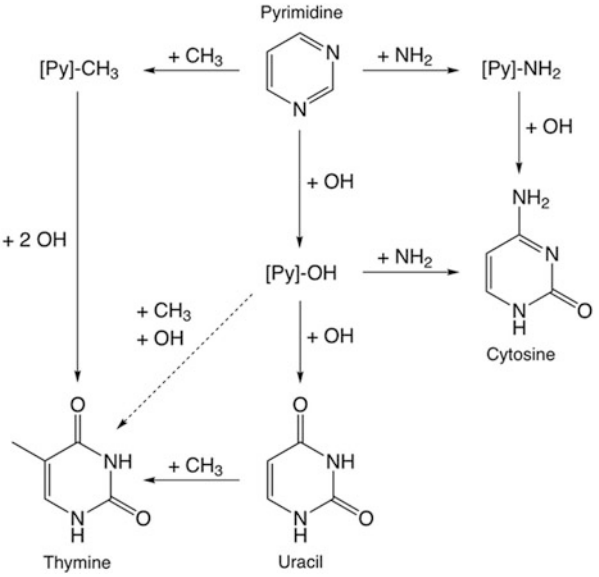

Fig. 8 Pathways leading to the formation of the three nucleobases uracil, cytosine, and thymine from the UV photo-irradiation of pyrimidine in H_2O, NH_3, CH_3OH, and/or CH_4 ices, via the successive addition of OH, NH_2, and CH_3 groups

outnumber $^{\bullet}CH_3$ radicals in these ice mixtures, and (2) because calculations show that the oxidation step is significantly more exothermic and thus favored. It was also shown experimentally that 5-methylpyrimidine deposited in an H_2O ice and UV irradiated can lose its CH_3 group to form pyrimidine, which can then be oxidized to form 4(3*H*)-pyrimidone ([112]). All these results are in agreement with what was seen experimentally, namely, methylation is the limiting step in the formation of thymine.

The theoretical investigations of Bera et al. [195] also revealed two very interesting points. First, following the reactions of a hydroxyl radical with the pyrimidine cation and its derivatives, their results show that, as is the case for uracil, the formation of thymine is not energetically favorable in the gas phase, and only becomes feasible in the condensed phase, where the H_2O ice matrix plays two roles, both as an oxidant and as a solvent for proton abstraction in both oxidation and methylation steps. Second, computations confirm that the oxidation of pyrimidine is significantly favored over its methylation. By combining all these results, it appears that the most probable pathway for the formation of thymine from pyrimidine is via the formation of 4(3*H*)-pyrimidone as a first step, then the formation of uracil after a second oxidation, and finally the methylation of uracil [195]. The fact that methyl addition is the limiting step in this process, and that the formation of thymine in this route is not particularly favored over those of its isomers, could explain the very low quantities of thymine detected in laboratory samples [112] compared to what is seen for uracil and cytosine [110, 111].

The Interesting Difference of Thymine

Experiments showed that thymine is not efficiently produced from the UV photo-irradiation of pyrimidine in ices containing H_2O and a methyl source such as the interstellar icy components CH_3OH and CH_4. This result may be attributed to the fact that the formation of thymine requires three substitutions, and thus higher doses of photons compared with the formation of uracil and cytosine, and to the fact that in an H_2O-rich ice mixture, as is the case in the ISM, methylation becomes the limiting step to forming thymine. From a theoretical point of view, quantum chemical computations do not show any clear thermodynamic preference for the formation of thymine over other competing products; indeed, the methylation of uracil actually slightly favors the formation of 6-methyluracil over that of thymine (5-methyluracil). In an environment where methylation competes with oxidation, oxidation is expected to dominate by virtue of its significantly larger reaction energies compared to methylation. Even if methylation takes place before oxidation in the process leading to the formation of thymine, experiments starting with 5-methylpyrimidine in H_2O ice clearly showed that the CH_3 groups can be easily cleaved off to form pyrimidine, which subsequently will most probably be oxidized to uracil.

The fact that thymine is not formed as easily as the other two pyrimidine-based nucleobases under astrophysical conditions, as demonstrated by both experimental and theoretical studies, and the fact that thymine has not been detected in carbonaceous meteorites, raise an interesting question about its role in the origins of life. If we assume that photo-processing of icy grains plays an important role in the formation of nucleobases in astrophysical environments (Fig. 2), we can imagine a scenario in which the pyrimidine-based nucleobases are formed in space, preserved in small objects such as asteroids and comets during the formation of the Solar System, and subsequently delivered to the early Earth and other telluric planets [12, 13, 17]. However, since (1) methylation is an important step in the formation of thymine, (2) this reaction appears inefficient in CH_3OH-rich ices like those seen in many interstellar dense clouds, and (3) the formation of thymine requires at least three substitutions as opposed to two for uracil and cytosine, it is possible that thymine was not formed in the ISM as efficiently as the other pyrimidine-based nucleobases.

Therefore, the abundance of thymine in the comets and asteroids which seeded the primitive Earth may have been significantly smaller than those of uracil and cytosine. It is interesting to consider these results and assumptions in light of the fact that terrestrial thymine is only found in DNA, but not in RNA. Indeed, several scenarios for the emergence of life involve a period of time during which RNA was the molecule dominating biological reactions as a catalyst and storage for a primitive genetic information [175–177]. It should be mentioned, however, that the RNA world hypothesis is still debated and alternative mechanisms involving small organic molecules which interact with each other via catalyzed reaction cycles driven by a flow of available free energy have also been proposed [196].

Nonetheless, in the hypothesis that such an RNA world did lead to the origin of life, a paucity of thymine among the building blocks that were delivered to Earth could potentially have forced the emergence of replicable systems involving uracil rather than thymine, such as RNA. In such a scenario, the emergence of DNA, and thus the use of thymine, as a more stable, robust molecule to store genetic information, may have appeared at a later stage in the complexity of life, in part because it was not effectively delivered to the early Earth.

2.3 Synthesis of Purine-Based Nucleobases in Extraterrestrial Ices

Although the formation of pyrimidine-based nucleobases under extraterrestrial abiotic conditions has been extensively studied, the same cannot be said about the formation of purine-based nucleobases and their derivatives. Purine is the backbone of the two other biological nucleobases that constitute the genetic material of DNA and RNA, namely, adenine and guanine. There are also a wide variety of biological and non-biological molecules based on the backbone of purine, such as xanthine, hypoxanthine, and caffeine. Most of these compounds have been detected in meteorites [11, 128–135], and it appears that meteoritic purine based compounds are always more abundant than pyrimidine-based compounds.

Therefore, the study of the formation and photo-stability of purine-based compounds is important from both astrochemical and astrobiological points of view. Unfortunately, to date there have been no experimental or theoretical studies of the photolytic formation of such purine-based compounds in ices under astrophysically relevant conditions. However, numerous experimental results have been obtained for radiation-induced functional group addition to small polycyclic aromatic hydrocarbons (PAHs; [99, 105–109]) and small PANHs [194], including pyrimidine-based compounds [110–112], and these allow us to comment on what might be expected for purine.

Given the fact that purine-based species are more stable to UV radiation than are pyrimidine-based species, it is reasonable to predict that experiments in which purine is mixed in ices of astrophysical interest containing compounds like H_2O, NH_3, CH_3OH, and CH_4 will lead to the formation of mostly purine-based compounds, including adenine and guanine, as opposed to pyrimidine, whose ring can be broken by UV radiation to form smaller, aliphatic compounds [111]. Indeed, the abiotic formation of adenine from the UV irradiation of purine in ices would only require the addition of a single NH_2 group, while that of guanine would require the addition of only one OH group and one NH_2 group (Fig. 9). Since previous irradiation studies of small PAHs and pyrimidine have shown that the addition of OH and NH_2 groups to aromatic cyclic molecules is an efficient process, the formation of adenine and guanine from purine ought to be straightforward. Furthermore, since the needed functional group additions involve only OH and NH_2,

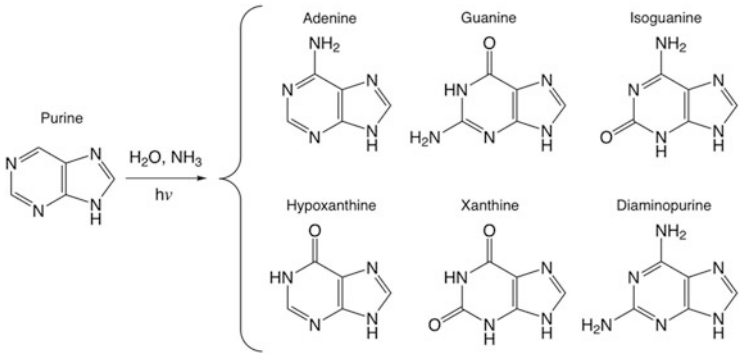

Fig. 9 Schematic showing how the UV photo-irradiation of purine in simple ices consisting of H_2O and/or NH_3 can be expected to lead to the formation of the biological nucleobases adenine and guanine, as well as several other derived compounds of astrobiological interest such as xanthine (2,6-dihydroxypurine) and hypoxanthine (6-hydroxypurine)

and not CH_3, one might expect production yields comparable or higher to those for uracil and cytosine under similar conditions, rather than the lower yields seen for thymine.

Finally, since astrophysical ices contain not only H_2O and NH_3 but also a variety of carbon sources such as CO, CO_2, CH_3OH, or CH_4, it will be interesting to (1) understand the effect of these compounds on the formation of adenine, guanine, and other purine-based nucleobases such as xantine and hypoxantine, (2) verify whether the inclusion of carbonaceous species leads to the methylation of purine, known to be the limiting reaction for the formation of methylated pyrimidine derivatives when formed in an H_2O-rich ice matrix, and (3) verify whether carbon sources have any inhibiting effects on the addition of OH and/or NH_2 groups.

2.4 Photo-Stability of the Nucleobases in Ices

Although there is no extensive body of research examining the photo-stability of pyrimidine-based nucleobases in ices, we can make some general observations. Little work has been done to quantify the effect, but it is clear from the synthesis work that products are not simply made and left alone, but are continuously susceptible to further photolytic reactions, i.e., the abundance of any given species in the ices is the result of the competition between "creation" and "destruction", where this latter term can include complete disruption of the molecule or alteration of the functional groups to form other pyrimidine-based molecules. It is not currently established what radiation exposures are needed to bring the competing creation–destruction processes into quasi-equilibrium, but true equilibrium is never likely to be attained since irradiation will steadily drive H from the ices [198].

In most experimental mixtures, much of the original pyrimidine survives and is detected in HPLC chromatograms of the resulting residues [111, 112], with the exception of H_2O:pyrimidine ice mixtures in which pyrimidine is nearly fully consumed by either photo-destruction or the formation of new products [110]. Having said that, these experiments show that the pyrimidine ring is susceptible to photolytic destruction and rearrangement in ices, and photo-products that could not have been produced from any other source have been detected. For example, in experiments examining the formation of uracil, cytosine, and thymine, acyclic compounds including urea, glycine, *N*-formylglycine, and alanine are also detected [110–112]. Experiments starting with only H_2O, CH_3OH/CH_4, and pyrimidine, where the only source of available nitrogen is from the destruction of pyrimidine itself, also show the presence of aminopyrimidines [112]. Hydantoin, an oxidized carbon and nitrogen heterocyclic molecule with a five-membered ring, is also detected in many of these experiments. It is therefore clear that photolytic destruction of the pyrimidine ring occurs in these ices.

In addition to the destruction of the ring itself, we know that side groups can be cleaved from pyrimidine rings. A good example to demonstrate this is a series of experiments starting with H_2O:5-methylpyrimidine ice mixtures that were designed to test the efficiency of the conversion of the latter into thymine in the presence of H_2O. In these experiments, oxidized pyrimidines, such as 4(3*H*)-pyrimidone, that lacked any methyl group, are found among the products. The formation of these oxidized pyrimidines lacking any methyl side group requires that the initial CH_3 group in 5-methylpyrimidine is cleaved from the ring [112]. Though in this case 5-methylpyrimidine is one of the initial ice components, we can expect to observe the same effect in molecules formed during the UV photolysis, further demonstrating the interaction of creation and destruction processes.

We are currently unaware of any data regarding the photolytic stability of purines in these types of ices. On the basis of irradiation experiments of normal PAHs and pyrimidine in similar ices [99, 106, 107, 109], we would expect that substitutions or rearrangement of side groups should occur. The degree to which the purine ring system is susceptible to photolytic destruction is less clear. In the case of PAHs, ring destruction is greatly diminished with an increasing number of rings. The extent to which this trend can be extended from pyrimidine to purine is unknown because of the heterocyclic nature of the rings.

3 Conclusions

Numerous studies have demonstrated that the radiation processing of astrophysically relevant ices can lead to the production of a host of organic molecules of astrobiological interest, including amino acids, quinones, and amphiphiles. Recent experimental and theoretical work has demonstrated that the presence of pyrimidine in such ices is expected to lead to the formation of the three pyrimidine-based nucleobases uracil, cytosine, and thymine, along with a number of their isomers.

Formation of the pyrimidine-based nucleobases requires various combinations of oxidation, amination, and methylation, all of which are observed experimentally. However, theoretical work makes it clear that the presence of condensed phase H_2O in the ice matrices plays a key role in formation of the nucleobases. Its most obvious role is as a source of oxygen for the oxidation reactions needed to make all of the pyrimidine-based nucleobases. However, it also plays a key role in the addition of hydroxyl, amino, and methyl groups by mediating the abstraction of either a proton or a hydrogen atom from intermediaries to form the final products. Since H_2O is the most abundant component observed in most astrophysical ices, this critical compound is likely to be available to play these roles in most cold astrophysical environments.

The relative abundances of uracil, cytosine, and thymine produced during ice photolysis depend on both the composition of the ices and on the photon dose. In general, larger photon doses will lead to greater degrees of ice processing, but do not necessarily lead to greater yields of any particular photo-product. This is because the abundance of any given photo-product is the result of competing creation and destruction reactions, where "destruction" includes both the rupture of the pyrimidine ring and the replacement of a previously added functional group with a different group. Thymine represents a good example of this issue. While experiments show that photolysis of pyrimidine in CH_4-rich ices can lead to methylation of the pyrimidine, and that thymine can be made in H_2O:CH_4:pyrimidine ices, thymine is generally seen to be produced in far lower abundances than uracil, presumably because relevant astrophysical ices are dominated by H_2O, not CH_4, methylation is less energetically favorable, and the formation of thymine requires the addition of three functional groups instead of the two required for uracil or cytosine. Understanding the true range of relative production efficiencies of uracil, cytosine, and thymine will require the completion of studies of pyrimidine photolysis in more complex, realistic astrophysical ice analogs.

It is interesting to note that the lower production efficiency of thymine relative to uracil is consistent with what is seen in the organics in meteorites. A paucity of abiotically produced thymine delivered to, and available on, the early Earth is also of interest because it is consistent with the idea that modern DNA-based life may have been preceded by an earlier "RNA world" that did not involve any thymine.

While a growing body of work exists for the photoprocessing of pyrimidine in ices, little comparable work has been done for purine in ices. As a result, it is not known whether similar ice photolysis processes can produce the two purine-based nucleobases adenine and guanine. However, based on the earlier work on pyrimidine, as well as ice photolysis experiments on PAHs and other aromatic heterocycles, it is anticipated that such processing should create both adenine and guanine. Since the only reactions needed to make these two nucleobases involve the addition of a few hydroxyl and amino groups, and no methyl groups, these two nucleobases are expected to be formed with efficiencies similar to those seen for uracil, rather than the lower efficiencies associated with the production of thymine.

Acknowledgements The authors are grateful for support from the NASA Origins of Solar Systems, Exobiology, and Astrophysics Research and Analysis, and Astrobiology Programs. Much of the work reported in this chapter also benefited from support of postdoctoral researchers under the NASA Postdoctoral Program. PPB and TJL would like to acknowledge financial support from NASA to investigate the formation and evolution of carbon-based material in the universe. This manuscript benefited from the helpful comments of an anonymous reviewer.

References

1. Miller SL (1953) A production of amino acids under possible primitive Earth conditions. Science 117:528–529
2. Levine JS, Augustsson TR, Natarajan M (1982) The prebiological paleoatmosphere: stability and composition. Orig Life 12:245–259
3. Hayes JM (1967) Organic constituents of meteorites – a review. Geochim Cosmochim Acta 31:1395–1440
4. Kvenvolden K, Lawless J, Pering K, Peterson E, Flores J, Ponnamperuma C (1970) Evidence for extraterrestrial amino-acids and hydrocarbons in the Murchison meteorite. Nature 228:923–926
5. Mullie F, Reisse J (1987) Organic matter in carbonaceous chondrites. Top Curr Chem 139:85–117
6. Cronin JR, Chang S (1993) Organic matter in meteorites: molecular and isotopic analyses of the Murchison meteorite. NATO Advanced Study Institute and International School of Space Chemistry: The chemistry of life's origins. Kluwer Academic Publisher; Springer, The Netherlands, pp 209–258
7. Irvine WM (1998) Extraterrestrial organic matter: a review. Orig Life Evol Biosph 28:365–383
8. Cooper G, Kimmich N, Belisle W, Sarinana J, Brabham K, Garrel L (2001) Carbonaceous meteorites as a source of sugar-related organic compounds for the early Earth. Nature 414:879–883
9. Pizzarello S, Huang Y (2003) Carbon isotopic analyses of individual Murchison amino acids. Geochim Cosmochim Acta Suppl 67:380
10. Martins Z, Alexander CMO'D, Orzechowska GE, Fogel ML, Ehrenfreund P (2007) Indigenous amino acids in primitive CR meteorites. Meteor Planet Sci 42:2125–2136
11. Martins Z, Botta O, Fogel ML, Sephton MA, Glavin DP, Watson JS, Dworkin JP, Schwartz AW, Ehrenfreund P (2008) Extraterrestrial nucleobases in the Murchison meteorite. Earth Planet Sci Lett 270:130–136
12. Oró J (1961) Comets and the formation of biochemical compounds on the primitive Earth. Nature 190:389–390
13. Oró J (1961) Mechanisms of synthesis of adenine from hydrogen cyanide under possible primitive Earth conditions. Nature 191:1193–1194
14. Delsemme AH (1998) Cosmic origin of the biosphere. In: Brack A (ed) The molecular origin of life. Cambridge University Press, Cambridge
15. Prinn RG, Fegley B Jr (1987) Bolide impacts, acid rain, and biospheric traumas at the Cretaceous-Tertiary boundary. Earth Planet Sci Lett 83:1–15
16. Chyba CF (1990) Impact delivery and erosion of planetary oceans in the early inner solar system. Nature 343:129–133
17. Chyba C, Sagan C (1992) Endogenous production, exogenous delivery and impact-shock synthesis of organic molecules: an inventory for the origins of life. Nature 355:125–132
18. Strecker A (1850) Über die künstliche Bildung der Milchsäure und einen neuen, dem Glycocoll homologen Körper. Justus Liebigs Ann Chem 75:27–45 (In German)

19. Taillades J, Beuzelin I, Garrel L, Tabacik V, Bied C, Commeyras A (1998) *N*-Carbamoyl-α-amino acids rather than free α-amino acids formation in the primitive hydrosphere: a novel proposal for the emergence of prebiotic peptides. Orig Life Evol Biosph 28:61–77
20. Bücherer HT, Fischbeck HTJ (1934) Prakt Chem Adv Synth Catal 140:69–89
21. Schloerb FP, Kinzel WM, Swade DA, Irvine WM (1986) HCN production from comet Halley. Astrophys J 310:L55–L60
22. Ip W-H, Balsiger H, Geiss J, Goldstein BE, Kettmann G, Lazarus AJ, Meier A, Rosenbauer H, Schwenn R, Shelley E (1990) Giotto IMS measurements of the production rate of hydrogen cyanide in the coma of Comet Halley. Ann Geophys 8:319–325
23. Jones PA, Sarkissian JM, Burton MG, Voronkov MA, Filipović MD (2006) Radio observations of Comet 9P/Tempel 1 with the Australia Telescope facilities during the Deep Impact encounter. Month Not R Astron Soc 369:1995–2000
24. Biver N, Bockelée-Morvan D, Boissier J, Crovisier J, Colom P, Lecacheux A, Moreno R, Paubert G, Lis DC, Sumner M, Frisk U, Hjalmarson Å, Olberg M, Winnberg A, Florén H-G, Sandqvist A, Kwok S (2007) Radio observations of Comet 9P/Tempel 1 before and after Deep Impact. Icarus 191:494–512
25. Disanti MA, Villanueva GL, Bonev BP, Magee-Sauer K, Lyke JE, Mumma MJ (2007) Temporal evolution of parent volatiles and dust in Comet 9P/Tempel 1 resulting from the Deep Impact experiment. Icarus 191:481–493
26. Lis DC, Bockelée-Morvan D, Boissier J, Crovisier J, Biver N, Charnley SB (2008) Hydrogen isocyanide in Comet 73P/Schwassmann-Wachmann (Fragment B). Astrophys J 675:931–936
27. Jehin E, Bockelée-Morvan D, Dello Russo N, Manfroid J, Hutsemékers D, Kawakita H, Kobayashi H, Schulz R, Smette A, Stüwe J, Weiler M, Arpigny C, Biver N, Cochran A, Crovisier J, Magain P, Rauer H, Sana H, Vervack RJ, Weaver H, Zucconi J-M (2009) A multi-wavelength simultaneous study of the composition of the Halley family Comet 8P/Tuttle. Earth Moon Planets 105:343–349
28. Gibb EL, Bonev BP, Villanueva G, DiSanti MA, Mumma MJ, Sudholt E, Radeva Y (2012) Chemical composition of comet C/2007 N3 (Lulin): another "Atypical" comet. Astrophys J 750:102 (14 pp)
29. Loren RB, Wootten HA (1978) Star formation in the bright-rimmed molecular cloud IC 1848 A. Astrophys J 225:L81–L84
30. Zuckerman B, Dyck HM (1986) Dust grains and gas in the circumstellar envelopes around luminous red giant stars. Astrophys J 311:345–359
31. McMullin JP, Mundy LG, Blake GA (1994) The circumstellar environment of IRAS 05338-0624. Astrophys J 437:305–316
32. Jørgensen JK, Hogerheijde MR, van Dishoeck EF, Blake GA, Schöier FL (2004) The structure of the NGC 1333-IRAS2 protostellar system on 500 AU scales. An infalling envelope, a circumstellar disk, multiple outflows, and chemistry. Astron Astrophys 413:993–1007
33. Thi W-F, van Zadelhoff G-J, van Dishoeck EF (2004) Organic molecules in protoplanetary disks around T Tauri and Herbig Ae stars. Astron Astrophys 425:955–972
34. Decin L, De Beck E, Brünken S, Müller HSP, Menten KM, Kim H, Willacy K, de Koter A, Wyrowski F (2010) Circumstellar molecular composition of the oxygen-rich AGB star IK Tauri. II. In-depth non-LTE chemical abundance analysis. Astron Astrophys 516:23 id. A69
35. Matthews CN, Moser RE (1967) Peptide synthesis from hydrogen cyanide and water. Nature 215:1230–1234
36. Toupance G, Sebban G, Buvet R (1970) Etape initiale de la polymérisation de l'acide cyanhydrique et synthèses prébiologiques. J Chim Phys 67:1870–1874 (In French)
37. Matthews CN (1979) HCN did not condense to give heteropolypeptides on the primitive Earth (reply to Ferris 1979). Science 16:1136–1137
38. Ferris JP (1979) HCN did not condense to give heteropolypeptides on the primitive Earth. Science 16:1135–1137

39. Ferris JP, Hagan WJ (1984) HCN and chemical evolution: the possible role of cyano compounds in prebiotic synthesis. Tetrahedron 40:1093–1120
40. Roy D, Najafian K, von Ragué Schleyer P (2007) Chemical evolution: the mechanism of the formation of adenine under prebiotic conditions. Proc Natl Acad Sci 104:17272–17277
41. Ferris JP, Sanchez RA, Orgel LE (1968) Studies in prebiotic synthesis – III. Synthesis of pyrimidine from cyanoacethylene and cyanate. J Mol Biol 33:693–704
42. Butlerow A (1961) Formation synthétique d'une substance sucrée. C R Acad Sci 53:145–147 (In French)
43. Müller D, Pitsch S, Kittaka A, Wagner E, Wintner CE, Eschenmoser A (1990) Chemie von α-Aminonitrilen. Aldomerisierung von Glycolaldehyd-Phosphat zu racemischen Hexose-2,4,6-triphosphaten und (in Gegenwart von Formaldehyd) racemischen Pentose-2,4-diphosphaten: *rac*-Allose-2,4,6-triphosphat und *rac*-Ribose-2,4,-diphosphat sind die Reaktionshauptprodukte. Helv Chim Acta 73:1410–1468 (In German)
44. Weber AL (1998) Prebiotic amino acid thioester synthesis: thiol-dependent amino acid synthesis from formose substrates (formaldehyde and glycolaldehyde) and ammonia. Orig Life Evol Biosph 28:259–270
45. Jalbout AF (2008) Prebiotic synthesis of simple sugars by an interstellar formose reaction. Orig Life Evol Biosph 38:489–497
46. Jalbout AF, Abrell L, Adamowicz L, Polt R, Apponi AJ, Ziurys LM (2007) Sugar synthesis from a gas-phase formose reaction. Astrobiology 7:433–442
47. Ben-Naim A (1980) Hydrophobic interactions. Plenum Press, New York
48. Dworkin JP, Deamer DW, Sandford SA, Allamandola LJ (2001) Self-assembling amphiphilic molecules: synthesis in simulated interstellar/precometary ices. Proc Natl Acad Sci 98: 815–819
49. Nissenbaum A (1976) Scavenging of soluble organic matter from the prebiotic oceans. Orig Life 7:413–416
50. Siegel BZ, Siegel SM (1981) Enzyme-mimicking properties of silicates and other minerals. Adv Space Res 1:27–36
51. Maurette M (1998) Carbonaceous micrometeorites and the origin of life. Orig Life Evol Biosph 4/6:385–412
52. Schulte M, Blake D, Hoehler T, McCollom T (2006) Serpentinization and its implications for life on the early Earth and Mars. Astrobiology 6:364–376
53. Vázquez-Mayagoitia Á, Horton SR, Sumpter BG, Sponer J, Sponer JE, Fuentes-Cabrera M (2011) On the stabilization of ribose by silicate minerals. Astrobiology 11:115–121
54. Ertem G (2004) Montmorillonite, oligonucleotides, RNA and origin of life. Orig Life Evol Biosph 34:549–570
55. Arribas M, de Vicente A, Arias A, Lázaro E (2005) Effect of metallic cations on the efficiency of DNA amplification. Implications for nucleic acid replication during early stages of life. Int J Astrobiol 4:115–123
56. Tielens AGGM, Allamandola LJ (1987) Composition, structure, and chemistry of interstellar dust. In: Hollenbach D, Thronson H (eds) Interstellar processes. D. Reidel, Dordrecht, pp 397–469
57. Dorschner J, Henning T (1995) Dust metamorphosis in the galaxy. Astron Astrophys Rev 6:271–333
58. Sandford SA, Allamandola LJ, Tielens AGGM, Sellgren K, Tapia M, Pendleton Y (1991) The interstellar C-H stretching band near 3.4 μm: constraints on the composition of organic material in the diffuse interstellar medium. Astrophys J 371:607–620
59. d'Hendecourt L, Jourdain de Muizon M, Dartois E, Breitfellner M, Ehrenfreund P, Bénit J, Boulanger F, Puget JL, Habing HJ (1996) ISO-SWS observations of solid state features towards RAFGL 7009S. Astron Astrophys 315:L365–L368
60. Pendleton YJ, Allamandola LJ (2002) The organic refractory material in the diffuse interstellar medium: mid-infrared spectroscopic constraints. Astrophys J Suppl Ser 138:75–98

61. Allamandola LJ, Tielens AGGM, Barker JR (1989) Interstellar polycyclic aromatic hydrocarbons – the infrared emission bands, the excitation/emission mechanism, and the astrophysical implications. Astrophys J Suppl Ser 71:733–775
62. Puget JL, Léger A (1989) A new component of the interstellar matter – small grains and large aromatic molecules. Ann Rev Astron Astrophys 27:161–198
63. Roelfsema PR, Cox P, Tielens AGGM, Allamandola LJ, Baluteau JP, Barlow MJ, Beintema D, Boxhoorn DR, Cassinelli JP, Caux E, Churchwell E, Clegg PE, de Graauw T, Heras AM, Huygen R, van der Hucht KA, Hudgins DM, Kessler MF, Lim T, Sandford SA (1996) SWS observations of IR emission features towards compact HII regions. Astron Astrophys 315:L289–L292
64. Galliano F, Madden SC, Tielens AGGM, Peeters E, Jones AP (2008) Variations of the mid-IR aromatic features inside and among galaxies. Astrophys J 679:310–345
65. d'Hendecourt LB, Allamandola LJ, Greenberg JM (1985) Time dependent chemistry in dense molecular clouds. I – Grain surface reactions, gas/grain interactions and infrared spectroscopy. Astron Astrophys 152:130–150
66. Shen CJ, Greenberg JM, Schutte WA, van Dishoeck EF (2004) Cosmic ray induced explosive chemical desorption in dense clouds. Astron Astrophys 415:203–215
67. Millar TJ, Roueff E, Charnley SB, Rodgers SD (1995) The chemistry of complex molecules in interstellar clouds. Int J Mass Spectrom Ion Proc 149/150:389–402
68. Charnley S (1997) On the nature of interstellar organic chemistry. In: Cosmovici CB, Bowyer S, Werthimer D (eds) Astronomical and biochemical origins and the search for life in the universe, proceeding of the 5th international conferece on bioastronomy, IAU Coll. #161. Kluwer Academic, Dordrecht, pp 89–96
69. Müller HSP, Endres CP, Stutzki J, Schlemmer S (2013) Molecules in space. Physikalisches Institut, Universität zu Köln. http://www.astro.uni-koeln.de/cdms/molecules. Accessed 10 June 2013
70. Greenberg MJ (1984) The structure and evolution of interstellar grains. Sci Am 250:96–107
71. Bernstein MP, Sandford SA, Allamandola LJ, Chang S, Scharberg MA (1995) Organic compounds produced by photolysis of realistic interstellar and cometary ice analogs containing methanol. Astrophys J 454:327–344
72. Dworkin JP, Gillette JS, Bernstein MP, Sandford SA, Allamandola LJ, Elsila JE, McGlothlin DR, Zare RN (2004) An evolutionary connection between interstellar ices and IDPs? Clues from mass spectroscopy measurements of laboratory simulations. Adv Spa Res 33:67–71
73. Simon MN, Simon M (1973) Search for interstellar acrylonitrile, pyrimidine, and pyridine. Astrophys J 184:757–762
74. Kuan Y-J, Yan C-H, Charnley SB, Kisiel Z, Ehrenfreund P, Huang H-C (2003) A search for interstellar pyrimidine. Month Not R Astron Soc 345:650–656
75. Kuan Y-J, Charnley SB, Huang H-C, Kisiel Z, Ehrenfreund P, Tseng W-L, Yan C-H (2004) Searches for interstellar molecules of potential prebiotic importance. Adv Space Res 33:31–39
76. Charnley SB, Kuan Y-J, Huang H-C, Botta O, Butner HM, Cox N, Despois D, Ehrenfreund P, Kisiel Z, Lee Y-Y, Markwick AJ, Peeters Z, Rodgers SD (2005) Astronomical searches for nitrogen heterocycles. Adv Space Res 36:137–145
77. Brünken S, McCarthy MC, Thaddeus P, Godfrey PD, Brown RD (2006) Improved line frequencies for the nucleic acid base uracil for a radioastronomical search. Astron Astrophys 459:317–320
78. Sandford SA, Bernstein MP, Allamandola LJ (2004) The mid-infrared laboratory spectra of naphthalene ($C_{10}H_8$) in solid H_2O. Astrophys J 607:346–360
79. Bernstein MP, Sandford SA, Allamandola LJ (2005) The mid-infrared absorption spectra of neutral polycyclic aromatic hydrocarbons in conditions relevant to dense interstellar clouds. Astrophys J Suppl Ser 161:53–64

80. Chyba CF, Thomas PJ, Brookshaw L, Sagan C (1990) Cometary delivery of organic molecules to the early Earth. Science 249:366–373
81. Baldwin B, Sheaffer Y (1971) Ablation and breakup of large meteoroids during atmospheric entry. J Geophys Res Space Phys 76(#19):4653–4668
82. Fraundorf P (1980) The distribution of temperature maxima for micrometeorites decelerated in the Earth's atmosphere without heating. Geophys Res Lett 10:765–768
83. Deamer DW, Fleischaker GR (1994) Origins of life: the central concepts. Jones & Bartlett Publisher, Boston
84. Lazcano A, Miller SL (1996) The origin and early evolution of life: prebiotic chemistry, the pre-RNA world, and time. Cell 85:793–798
85. Orgel LE (2004) Prebiotic chemistry and the origin of the RNA world. Crit Rev Biochem Mol Biol 39:99–123
86. Miller SL, Cleaves HJ (2006) Prebiotic chemistry on the primitive Earth. In: Rigoutsos I, Stephanopoulos G (eds) Systems biology, genomics, vol I. Oxford University Press, Oxford, pp 4–56
87. Powner MW, Sutherland JD, Szostak JW (2010) Chemoselective multicomponent one-pot assembly of purine precursors in water. J Am Chem Soc 132:16677–16688
88. Whittet DCB, Schutte WA, Tielens AGGM, Boogert ACA, de Graauw T, Ehrenfreund P, Gerakines PA, Helmich FP, Prusti T, van Dishoeck EF (1996) An ISO SWS view of interstellar ices: first results. Astron Astrophys 315:L357–L360
89. Lacy JH, Faraji H, Sandford SA, Allamandola LJ (1998) Unraveling the 10 micron "silicate" feature of protostars: the detection of frozen interstellar ammonia. Astrophys J Lett 501: L105–L109
90. Ehrenfreund P, Charnley SB (2000) Organic molecules in the interstellar medium, comets, and meteorites: a voyage from dark clouds to the early Earth. Ann Rev Astron Astrophys 38:427–483
91. Gibb EL, Whittet DCB, Schutte WA, Boogert ACA, Chiar JE, Ehrenfreund P, Gerakines PA, Keane JV, Tielens AGGM, van Dishoeck EF, Kerkhof O (2000) An inventory of interstellar ices toward the embedded protostar W33A. Astrophys J 536:347–356
92. Gibb EL, Whittet DCB, Boogert ACA, Tielens AGGM (2004) Interstellar ice: the infrared space observatory legacy. Astrophys J Suppl Ser 151:35–73
93. Dartois E (2005) The ice survey opportunity of ISO. Space Sci Rev 119:293–310
94. Lacy JH, Baas F, Allamandola LJ, van de Bult CEP, Persson SE, McGregor PJ, Lonsdale CJ, Geballe TR (1984) 4.6 Micron absorption features due to solid phase CO and cyano group molecules toward compact infrared sources. Astrophys J 276:533–543
95. Thi W-F, van Dishoeck EF, Dartois E, Pontoppidan KM, Schutte WA, Ehrenfreund P, d'Hendecourt L, Fraser HJ (2006) VLT–ISAAC 3-5 μm spectroscopy of embedded young low-mass stars. III. Intermediate-mass sources in Vela. Astron Astrophys 449:251–265
96. Schutte WA, Greenberg JM (1997) Further evidence for the OCN^- assignment to the XCN band in astrophysical ice analogs. Astron Astrophys 317:L43–L46
97. Demyk K, Dartois E, d'Hendecourt L, Jourdain de Muizon M, Heras AM, Breitfellner M (1998) Laboratory identification of the 4.62 μm solid state absorption band in the ISO-SWS spectrum of RAFGL 7009S. Astron Astrophys 339:553–560
98. van Broekhuizen FA, Keane JV, Schutte WA (2004) A quantitative analysis of OCN^- formation in interstellar ice analogs. Astron Astrophys 415:425–436
99. Bernstein MP, Dworkin JP, Sandford SA, Cooper GW, Allamandola LJ (2002a) Racemic amino acids from the ultraviolet photolysis of interstellar ice analogues. Nature 416:401–403
100. Muñoz Caro GM, Meierhenrich UJ, Schutte WA, Barbier B, Arcones Segovia A, Rosenbauer H, Thiemann WH-P, Brack A, Greenberg JM (2002) Amino acids from ultraviolet irradiation of interstellar ice analogues. Nature 416:403–406
101. Nuevo M, Chen Y-J, Yih T-S, Ip W-H, Fung H-S, Cheng C-Y, Tsai H-R, Wu C-YR (2007) Amino acids formed from the UV/EUV irradiation of inorganic ices of astrophysical interest. Adv Space Res 40:1628–1633

102. Nuevo M, Auger G, Blanot D, d'Hendecourt L (2008) A detailed study of the amino acids produced from the vacuum UV irradiation of interstellar ice analogs. Orig Life Evol Biosph 38:37–56
103. Nuevo M, Bredehöft JH, Meierhenrich UJ, d'Hendecourt L, Thiemann WH-P (2010) Urea, glycolic acid, and glycerol in an organic residue produced by ultraviolet irradiation of interstellar/pre-cometary ice analogs. Astrobiology 10:245–256
104. de Marcellus P, Bertrand M, Nuevo M, Westall F, Le Sergeant d'Hendecourt L (2011) Prebiotic significance of extraterrestrial ice photochemistry: detection of hydantoin in organic residues. Astrobiology 11:847–854
105. Bernstein MP, Sandford SA, Allamandola LJ, Gillette JS, Clemett SJ, Zare RN (1999) UV irradiation of polycyclic aromatic hydrocarbons in ices: production of alcohols, quinones, and ethers. Science 283:1135–1138
106. Bernstein MP, Dworkin JP, Sandford SA, Allamandola LJ (2001) Ultraviolet irradiation of naphthalene in H_2O ice: implications for meteorites and biogenesis. Meteorit Planet Sci 36:351–358
107. Bernstein MP, Elsila JE, Dworkin JP, Sandford SA, Allamandola LJ, Zare RN (2002) Side group addition to the PAH coronene by UV photolysis in cosmic ice analogs. Astrophys J 576:1115–1120
108. Bernstein MP, Moore MH, Elsila JE, Sandford SA, Allamandola LJ, Zare RN (2003) Side group addition to the PAH coronene by proton irradiation in cosmic ice analogs. Astrophys J 582:L25–L29
109. Ashbourn SFM, Elsila JE, Dworkin JP, Bernstein MP, Sandford SA, Allamandola LJ (2007) Ultraviolet photolysis of anthracene in H_2O interstellar ice analogs: potential connection to meteoritic organics. Meteorit Planet Sci 42:2035–2041
110. Nuevo M, Milam SN, Sandford SA, Elsila JE, Dworkin JP (2009) Formation of uracil from the ultraviolet photo-irradiation of pyrimidine in pure H_2O ices. Astrobiology 9:683–695
111. Nuevo M, Milam SN, Sandford SA (2012) Nucleobases and prebiotic molecules in organic residues produced from the ultraviolet photo-irradiation of pyrimidine in NH_3 and H_2O+NH_3 ices. Astrobiology 12:295–314
112. Materese CK, Nuevo M, Bera PP, Lee TJ, Sandford SA (2013) Thymine and other prebiotic molecules produced from the ultraviolet photo-irradiation of pyrimidine in simple astrophysical ice analogs. Astrobiology 13:948–962
113. Gerakines PA, Moore MH, Hudson RL (2000) Carbonic acid production in H_2O:CO_2 ices. UV photolysis vs. proton bombardment. Astron Astrophys 357:793–800
114. Gerakines PA, Moore MH, Hudson RL (2001) Energetic processing of laboratory ice analogs: UV photolysis versus ion bombardment. J Geophys Res 106:33381–33386
115. Gerakines PA, Moore MH, Hudson RL (2004) Ultraviolet photolysis and proton irradiation of astrophysical ice analogs containing hydrogen cyanide. Icarus 170:202–213
116. Elsila JE, Dworkin JP, Bernstein MP, Martin MP, Sandford SA (2007) Mechanisms of amino acid formation in interstellar ice analogs. Astrophys J 660:911–918
117. Sandford SA, Bernstein MP, Materese CK (2013) The infrared spectra of polycyclic aromatic hydrocarbons with excess peripheral H atoms (H_n-PAHs) and their relation to the 3.4 and 6.9 μm PAH emission features. Astrophys J Suppl 205:30 id 8
118. Dodd RT (1981) Meteorites: a petrologic-chemical synthesis. Cambridge University Press, Cambridge
119. Lauretta DS, McSween HY Jr (eds) (2006) Meteorites and the early Solar System II. University Arizona Press, Tucson
120. Pizzarello S, Cooper GW, Flynn GJ (2006) The nature and distribution of the organic material in carbonaceous chondrites and interplanetary dust particles. In: Lauretta DS, McSween HY Jr (eds) Meteorites and the early Solar System II. University of Arizona Press, Tucson, pp 625–651

121. Cody GD, Alexander CMO'D, Tera F (2002) Solid-state (^{1}H and ^{13}C) nuclear magnetic resonance spectroscopy of insoluble organic residue in the Murchison meteorite: a self-consistent quantitative analysis. Geochim Cosmochim Acta 66:1851–1865
122. Alexander CMO'D, Fogel M, Yabuta H, Cody GD (2007) The origin and evolution of chondrites recorded in the elemental and isotopic compositions of their macromolecular organic matter. Geochim Cosmochim Acta 71:4380–4403
123. Kerridge JF, Chang S, Shipp R (1987) Isotopic characterization of kerogen-like material in the Murchison carbonaceous chondrite. Geochim Cosmochim Acta 51:2527–2540
124. Cronin JR, Pizzarello S (1997) Enantiomeric excesses in meteoritic amino acids. Science 275:951–955
125. Sephton MA, Wright IP, Gilmour I, de Leeuw JW, Grady MM, Pillinger CT (2002) High molecular weight organic matter in Martian meteorites. Planet Space Sci 50:711–716
126. Glavin DP, Dworkin JP, Aubrey A, Botta O, Doty JH, Martins Z, Bada JL (2006) Amino acid analyses of Antarctic CM2 meteorites using liquid chromatography-time of flight-mass spectrometry. Meteorit Planet Sci 41:889–902
127. Burton AS, Elsila JE, Hein JE, Glavin DP, Dworkin JP (2013) Extraterrestrial amino acids identified in metal-rich CH and CB carbonaceous chondrites from Antarctica. Meteorit Planet Sci 48:390–402
128. Hayatsu R (1964) Orgueil meteorite: organic nitrogen contents. Science 146:1291–1293
129. Folsome CE, Lawless J, Romiez M, Ponnamperuma C (1971) Heterocyclic compounds indigenous to the Murchison meteorite. Nature 232:108–109
130. Hayatsu R, Anders E, Studier MH, Moore LP (1975) Purines and triazines in the Murchison meteorite. Geochim Cosmochim Acta 39:471–488
131. van der Velden W, Schwartz AW (1977) Search for purines and pyrimidines in the Murchison meteorite. Geochim Cosmochim Acta 41:961–968
132. Stoks PG, Schwartz AW (1979) Uracil in carbonaceous meteorites. Nature 282:709–710
133. Stoks PG, Schwartz AW (1981) Nitrogen-heterocyclic compounds in meteorites – significance and mechanisms of formation. Geochim Cosmochim Acta 45:563–569
134. Callahan MP, Smith KE, Cleaves HJ II, Ruzicka J, Stern JC, Glavin DP, House CH, Dworkin JP (2011) Carbonaceous meteorites contain a wide range of extraterrestrial nucleobases. Proc Natl Acad Sci 108:13995–13998
135. Folsome CE, Lawless J, Romiez M, Ponnamperuma C (1973) Heterocyclic compounds recovered from carbonaceous chondrites. Geochim Cosmochim Acta 37:455–465
136. Engel MH, Macko SA (1997) Isotopic evidence for extraterrestrial non-racemic amino acids in the Murchison meteorite. Nature 389:265–268
137. Cronin JR, Pizzarello S (1999) Amino acid enantiomer excesses in meteorites: origin and significance. Adv Space Res 23:293–299
138. Pizzarello S, Zolensky M, Turk KA (2003) Nonracemic isovaline in the Murchison meteorite: chiral distribution and mineral association. Geochim Cosmochim Acta 67:1589–1595
139. Glavin DP, Elsila JE, Burton AS, Callahan MP, Dworkin JP, Hilts RW, Herd CDK (2012) Unusual nonterrestrial L-proteinogenic amino acid excesses in the Tagish Lake meteorite. Meteorit Planet Sci 47:1347–1364
140. Callahan MP, Burton AS, Elsila JE, Baker EM, Smith KE, Glavin DP, Dworkin JP (2013) A search for amino acids and nucleobases in the Martian meteorite Roberts Massif 04262 using liquid chromatography-mass spectrometry. Meteorit Planet Sci 48:786–795
141. Shapiro R (1999) Prebiotic cytosine synthesis: a critical analysis and implications for the origin of life. Proc Natl Acad Sci 96:4396–4401
142. Nelson KE, Robertson MP, Levy M, Miller SL (2001) Concentration by evaporation and prebiotic synthesis of cytosine. Orig Life Evol Biosph 31:221–229
143. Callahan MP, Stern JC, Glavin DP, Whelley KE, Martin MG, Dworkin JP (2010) Distribution of nucleobases in CM and CR carbonaceous chondrites. Astrobiology science conference 2010: evolution and life: surviving catastrophes and extremes on Earth and beyond, April 26–30, 2010 in League City, LPI Contribution No. 1538, p 5160

144. Boulanger E, Anoop A, Nachtigallova D, Thiel W, Barbatti M (2013) Photochemical steps in the prebiotic synthesis of purine precursors from HCN. Angew Chem Int Ed 52:8000–8003
145. Bera PP, Lee TJ, Schaefer HF III (2009) Are isomers of vinyl cyanide missing links of interstellar pyrimidine formation? J Chem Phys 131:7, id. 074303
146. Raulin F (1991) Bioastronomy: the search for extraterrestial life—the exploration broadens, vol 390, Lecture Notes in Physics. Springer, Berlin, Heidelberg, pp 141–148
147. Lis DC, Mehringer DM, Benford D, Gardner M, Phillips TG, Bockelée-Morvan D, Biver N, Colom P, Crovisier J, Despois D, Rauer H (1997) New molecular species in Comet C/1995 O1 (Hale-Bopp) observed with the Caltech Submillimeter Observatory. Earth Moon Planets 78:13–20
148. Biver N, Bockelée-Morvan D, Colom P, Crovisier J, Paubert G, Weiss A, Wiesemeyer H (2011) Molecular investigations of comets C/2002 X5 (Kudo-Fujikawa), C/2002 V1 (NEAT), and C/2006 P1 (McNaught) at small heliocentric distances. Astron Astrophys 528 (A142):19
149. Dello Russo N, Vervack RJ Jr, Lisse CM, Weaver HA, Kawakita H, Kobayashi H, Cochran AL, Harris WM, McKay AJ, Biver N, Bockelée-Morvan D, Crovisier J (2011) The volatile composition and activity of Comet 103P/Hartley 2 during the EPOXI closest approach. Astrophys J Lett 734:6, pp. id. L8
150. Jewell PR, Snyder LE (1982) New circumstellar cyanoacetylene sources. Astrophys J 255: L69–L73
151. Jewell PR, Snyder LE (1984) Observations and analysis of circumstellar cyanoacetylene. Astrophys J 278:176–185
152. Huang H-C, Kuan Y-J, Charnley SB, Hirano N, Takakuwa S, Bourke TL (2005) Organic molecules in the hot corinos and circumstellar disks of IRAS 16293-2422. Adv Space Res 36:146–155
153. Pardo JR, Cernicharo J, Goicoechea JR (2005) Observational evidence of the formation of cyanopolyynes in CRL 618 through the polymerization of HCN. Astrophys J 628:275–282
154. Kunde VG, Aikin AC, Hanel RA, Jennings DE, Maguire WC, Samuelson RE (1981) C_4H_2, HC_3N and C_2N_2 in Titan's atmosphere. Nature 292:686–688
155. Coustenis A, Bézard B, Gautier D, Marten A, Samuelson R (1991) Titan's atmosphere from Voyager infrared observations. III – Vertical contributions of hydrocarbons and nitriles near Titan's north pole. Icarus 89:152–167
156. Bénilan Y, Andrieux D, Khlifi M, Bruston P, Raulin F, Guillemin J-C, Cossart-Magos C (1996) Temperature dependence of HC_3N, C_6H_2, and C_4N_2 mid-UV absorption coefficients. Application to the interpretation of Titan's atmospheric spectra. Astrophys Space Sci 236:85–95
157. Khanna RK (2005) Condensed species in Titan's stratosphere: confirmation of crystalline cyanoacetylene (HC_3N) and evidence for crystalline acetylene (C_2H_2) on Titan. Icarus 178:165–170
158. Chang S, Scattergood T, Aronowitz S, Flores J (1979) Organic chemistry on Titan. Rev Geophys Space Phys 17:1923–1933
159. Capone LA, Prasad SS, Huntress WT, Whitten RC, Dubach J, Santhanam K (1981) Formation of organic molecules on Titan. Nature 293:45–46
160. Gupta SK, Ochiai E, Ponnamperuma C (1981) Organic synthesis in the atmosphere of Titan. Nature 293:725–727
161. Raulin F, Coll P, Coscia D, Gazeau M-C, Sternberg R, Bruston P, Israël G, Gautier D (1998) An exobiological view of Titan and the Cassini–Huygens mission. Adv Space Res 22:353–362
162. Vuitton V, Yelle RV, Lavvas P, Klippenstein SJ (2012) Rapid association reactions at low pressure: impact on the formation of hydrocarbons on Titan. Astrophys J 744(11):7
163. Horn A, Møllendal H, Guillemin J-C (2008) A quantum chemical study of the generation of a potential prebiotic compound, cyanoacetaldehyde, and related sulfur containing species. J Phys Chem A 112:11009–11016

164. Frenklach M, Feigelson ED (1989) Formation of polycyclic aromatic hydrocarbons in circumstellar envelopes. Astrophys J 341:372–384
165. Ricca A, Bauschlicher CW, Bakes ELO (2001) A computational study of the mechanisms for the incorporation of a nitrogen atom into polycyclic aromatic hydrocarbons in the Titan haze. Icarus 154:516–521
166. Bera PP, Head-Gordon M, Lee TJ (2011) Initiating molecular growth in the interstellar medium via complexes of observed ions and molecules. Astron Astrophys 535:12
167. McElroy D, Walsh C, Markwick AJ, Cordiner MA, Smith K, Millar TJ (2013) The UMIST database for astrochemistry 2012. Astron Astrophys 550(A36):13
168. Peeters Z, Botta O, Charnley SB, Kisiel Z, Kuan Y-J, Ehrenfreund P (2005) Formation and photostability of N-heterocycles in space. I. The effect of nitrogen on the photostability of small aromatic molecules. Astron Astrophys 433:583–590
169. Hudgins DM, Sandford SA (1998) Infrared spectroscopy of matrix-isolated polycyclic aromatic hydrocarbons 1. PAHs containing 2 to 4 rings. J Phys Chem A 102:329–343
170. Hudgins DM, Sandford SA (1998) Infrared spectroscopy of matrix-isolated polycyclic aromatic hydrocarbons 2. PAHs containing 5 or more rings. J Phys Chem A 102:344–352
171. Ruiterkamp R, Peeters Z, Moore MH, Hudson RL, Ehrenfreund P (2005) A quantitative study of proton irradiation and UV photolysis of benzene in interstellar environments. Astron Astrophy 440:391–402
172. Satzger H, Townsend D, Zgierski MZ, Patchkovskii S, Ullrich S, Stolow A (2006) Primary processes underlying the photostability of isolated DNA bases: adenine. Proc Natl Acad Sci 103:10196–10201
173. Fondren LD, McLain J, Jackson DM, Adams NG, Babcock LM (2007) Studies of reactions of a series of ions with nitrogen containing heterocyclic molecules molecules using a selected ion flow tube. Int J Mass Spectrom 265:60–67
174. Bera PP, Schaefer HF III (2006) Lesions in DNA subunits: the nucleic acid bases. In trends and perspectives in modern computational science, vol 6. Brill Academic Publishers, Boston, pp 254–264
175. Gilbert W (1986) Origin of life: the RNA world. Nature 319:618
176. Joyce GF (1989) RNA evolution and the origin of life. Nature 338:217–224
177. Joyce GF (2002) The antiquity of RNA-based evolution. Nature 418:214–221
178. Warnek P (1962) A microwave-powered hydrogen lamp for vacuum ultraviolet photochemical research. Appl Optics 1:721–726
179. Mathis JS, Mezger PG, Panagia N (1983) Interstellar radiation field and dust temperatures in the diffuse interstellar matter and in giant molecular clouds. Astron Astrophys 128:212–229
180. Prasad SS, Tarafdar SP (1983) UV radiation field inside dense clouds—its possible existence and chemical implications. Astrophys J 267:603–609
181. Bera PP, Nuevo M, Milam SN, Sandford SA, Lee TJ (2010) Mechanism for the abiotic synthesis of uracil via UV-induced oxidation of pyrimidine in pure H_2O ices under astrophysical conditions. J Chem Phys 133(10):104303
182. Becke AD (1993) Density functional thermochemistry. III. The role of exact exchange. J Chem Phys 98(7):5648–5652
183. Lee CT, Yang WT, Parr RG (1988) Development of the Colle-Salvetti correlation-energy formula into a functional of the electron density. Phys Rev B 37:785–789
184. Hehre WJ, Ditchfield R, Pople JA (1972) Self-consistent molecular orbital methods. XII. Further extensions of Gaussian-type basis sets for use in molecular orbital studies of organic molecules. J Chem Phys 56:2257–2261
185. Lee TJ, Jayatilaka D (1993) An open-shell restricted Hartree–Fock perturbation theory based on symmetric spin orbitals. Chem Phys Lett 201:1–10
186. Lee TJ, Rendell AP, Dyall KG, Jayatilaka D (1994) Open-shell restricted Hartree–Fock perturbation theory: some considerations and comparisons. J Chem Phys 100:10 id. 7400
187. Dunning TH (1989) Gaussian-basis sets for use in correlated molecular calculations. 1. The atoms boron through neon and hydrogen. J Chem Phys 90:1007–1024

188. Shao Y, Molnar LF, Jung Y, Kussmann J, Ochsenfeld C, Brown ST, Gilbert ATB, Slipchenko LV, Levchenko SV, O'Neill DP, DiStasio RA, Lochan RC, Wang T, Beran GJO, Besley NA, Herbert JM, Lin CY, Van Voorhis T, Chien SH, Sodt A, Steele RP, Rassolov VA, Maslen PE, Korambath PP, Adamson RD, Austin B, Baker J, Byrd EFC, Dachsel H, Doerksen RJ, Dreuw A, Dunietz BD, Dutoi AD, Furlani TR, Gwaltney SR, Heyden A, Hirata S, Hsu CP, Kedziora G, Khalliulin RZ, Klunzinger P, Lee AM, Lee MS, Liang W, Lotan I, Nair N, Peters B, Proynov EI, Pieniazek PA, Rhee YM, Ritchie J, Rosta E, Sherrill CD, Simmonett AC, Subotnik JE, Woodcock HL, Zhang W, Bell AT, Chakraborty AK, Chipman DM, Keil FJ, Warshel A, Hehre WJ, Schaefer HF, Kong J, Krylov AI, Gill PMW, Head-Gordon M (2006) Advances in methods and algorithms in a modern quantum chemistry program package. Phys Chem Chem Phys 8:3172–3191
189. Engel V, Staemmler V, van der Wal RL, Crim FF, Sension RJ, Hudson B, Anderson P, Hennig S, Weide K, Shinke R (1992) Photodissociation of water in the first absorption band: a protoype for dissociation in a repulsive potential energy surface. J Phys Chem 96:3201–3213
190. Mordaunt DH, Dixon RN, Ashfold MNR (1996) Photodissociation dynamics of $\tilde{A}$ state ammonia molecules. II. The isotopic dependence for partially and fully deuterated isotopomers. J Chem Phys 104:6472–6481
191. Woon DE (2002) Pathways to glycine and other amino acids in ultraviolet irradiated astrophysical ices determined via quantum chemical modeling. Astrophys J 571:177–180
192. Rice J, Bera PP, Lee TJ (2013) Ab initio quantum chemical study of formation of cytosine under astrophysical conditions. J Chem Phys, in preparation
193. Öberg KI, Garrod RT, van Dishoeck EF, Linnartz H (2009) Formation rates of complex organics in UV irradiated CH_3OH-rich ices. I. Experiments. Astron Astrophys 504:891–913
194. Elsila JE, Hammond MR, Bernstein MP, Sandford SA, Zare RN (2006) UV photolysis of quinoline in interstellar ice analogs. Meteorit Planet Sci 41:785–796
195. Bera PP, Nuevo M, Mataerese CK, Sandford SA, Lee TJ (2013) The formation of thymine under astrophysical conditions constrains its role in the origin of life: theoretical study. Astrobiology, in preparation
196. Shapiro R (2006) Small molecule interactions were central to the origin of life. Q Rev Biol 81:105–126
197. Bernstein MP, Sandford SA, Allamandola LJ (1999) Life's far-flung raw materials [interstellar organic molecules]. Sci Am 281:26–33
198. Sandford SA, Allamandola LJ (1993) H2 in interstellar and extragalactic ices: infrared characteristics, UV production, and implications. Astrophys J Lett 409:L65–L68

Top Curr Chem (2015) 356: 165–182
DOI: 10.1007/128_2013_525

Published online: 28 February 2014

Photoinduced Charge-Separation in DNA

Kiyohiko Kawai and Tetsuro Majima

Abstract DNA site-specifically modified with a photosensitizer (Sens) was synthesized and the charge-separation and charge-recombination dynamics in DNA were studied. We specifically focused on the formation of the long-lived charge-separated state whose lifetime (τ) is longer than 0.1 μs. The quantum yields of the formation of the charge-separated states (Φ) upon the photoexcitation of the Sens, and the τ were measured using the laser flash photolysis technique. We utilized naphthalimide (NI), naphthaldiimide (ND), and anthraquinone (AQ) as a Sens to investigate the mechanism of the formation of the charge-separated state in DNA via rapid positive charge (hole) transfer between adenine and thymine (A-T) base-pairs. By replacing some T bases in the A-T stretch with 5-bromouracil (^{br}U), the charge-separation was shown to occur via the photoinduced charge-injection into the second and further neighboring As to the Sens. On the other hand, the generation of a hole on A nearest to Sens ends up with the rapid charge-recombination within a contact ion pair. A long-lived charge-separated state was also generated in DNA when a commonly used fluorophore such asTAMRA, Alexa 532, and ATTO 655, which can only oxidize guanine-cytosine (G-C) base-pair, but not A-T, was used as a Sens. These results suggested that the charge-separation in DNA is a general phenonmenon for fluorescent dyes which fluorescence is quenched only by G-C.

Keywords Charge-separation · DNA · Electron transfer · Hole transfer

K. Kawai (✉) and T. Majima (✉)
The Institute of Scientific and Industrial Research, Osaka University, Mihogaoka 8-1, Ibaraki, Osaka 567-0047, Japan
e-mail: kiyohiko@sanken.osaka-u.ac.jp; majima@sanken.osaka-u.ac.jp

Contents

Abbreviations

Acr^+	9-Alkylamino-6-chloro-2-methoxyacridine
AQ	Anthraquinone
ND	Naphthaldiimide
NI	Naphthalimide
Sens	Photosensitizer
^{br}U	Bromouridine
τ	Lifetime of the long-lived charge-separated state
Φ	Quantum yields of the formation of the charge-separated states

1 Introduction

Formation of a long-lived charge-separated state, which allows the efficient conversion of photon energy into chemical potentials, is desired in molecular-scale optoelectronics and nano-technology [1–7]. Even when the photoinduced electron transfer takes place efficiently, it often ends up with a rapid charge-recombination. Therefore, in order to achieve a long-lived charge-separated state with a high Φ, it is important to prevent this energy-wasting charge-recombination. The charge transfer rate constant usually follows an exponential dependence on the donor–acceptor distance. The charge transfer rate exponentially decreases with increasing distance between the donor and acceptor. In natural photosynthesis, while the single-step photoinduced electron transfer from the special pair to the final quinone is very inefficient due to the large distance between the special pair and final quinone acceptor, a high Φ is achieved by forming the final state via a series of short range, fast charge transfer processes [5]. This has also proved to be the case in the formation of the long-lived charge-separated states in DNA.

Duplex DNA forms a one-dimensional π-stacked array of nucleobases, and the possibility of charge transfer along a one-dimensional π-array of nucleobases was suggested not long after the discovery in 1952 of its double-helical structure. The self-assembly of hundreds of well-designed oligonucleotides, the so-called DNA origami method, recently enabled the creation of a variety of two- and

three-dimensional nanostructures of defined sizes [8–11]. This renders DNA an interesting bottom-up material for the design of nanoelectronic sensors and devices. DNA is one of the extensively studied organic molecules, and there are plenty of reports on the synthesis of artificial nucleobase analogs. Therefore, DNA can be used to assemble natural and various artificial nucleobases of different redox potentials within a defined double-helical structure and provides a unique system to study the charge-separation mechanism.

DNA consists of two building blocks, A-T and G-C base pairs; HOMO localizes on the purine bases G and A, and the former has lower oxidation potential, i.e., higher HOMO energy [12, 13]. The photoirradiation of DNA-bound Sens triggers electron transfer from nucleobases to the excited Sens to produce the radical anion of Sens ($Sens^{\cdot -}$) and the radical cation of the nucleobase (hole) in a charge-separated state. We have shown that when Sens is attached to the A-T stretch, photoinduced electron transfer from an A-T base-pair to a Sens leads to the formation of a long-lived charge-separated state in DNA [14–22]. The subsequent sequential hole transfer process between the A-T base-pairs help to separate a hole from $Sens^{\cdot -}$ before trapping at the G-C base-pair to form the G radical cation ($G^{\cdot +}$). Since the back hole transfer from $G^{\cdot +}$ to the A-T stretch is energetically unfavorable and thus inefficient, the charge-recombination mainly proceeds by a single-step mechanism between $Sens^{\cdot -}$ and $G^{\cdot +}$. Thus, the charge-recombination rate significantly decreases with the increasing number of A-T base pairs between Sens and the nearest G, and a long-lived charge-separated state can be generated for DNA having a long A-T stretch between Sens and G.

In this chapter we will overview the formation of the long-lived charge-separated state in DNA triggered by the photoinduced charge-injection into the A-T stretch by utilizing NI, ND, and AQ as a Sens [23]. The mechanism was investigated in detail by utilizing a series of NI and 5-bromouracil (^{br}U) modified DNAs. The ^{br}U increases the oxidation potential of its complementary A through hydrogen bonding and then changes the hole transfer rates between As. The Φ was modulated by the incorporation site of ^{br}U. The results were explained by the charge-separation via the initial charge transfer between NI in the singlet excited state and second and further neighboring As to the NI, while the generation of a hole on A nearest to NI ends up with the rapid charge-recombination within a contact ion pair [24]. These results suggested that the charge-separation process can be refined to increase the Φ by putting a redox inactive spacer base-pair between a photosensitizer and an A-T stretch. We also describe how a long-lived charge-separated state can be generated in DNA when a Sens which can only oxidize a G-C base-pair was used as a Sens. In this case A-T base-pairs serve as a redox inactive spacer that prevents the formation of a contact ion pair. A long-lived charge-separated state was formed in DNA modified with a commonly used fluorophore such as TAMRA, Alexa 532, and ATTO 655, suggesting that other fluorescent dyes of which fluorescence is quenched only by G may also produce a long-lived charge-separated state in DNA upon the photoirradiation [25, 26].

2 Charge-Separation via Sequential Hole Transfer Between A-Ts

2.1 *Redox Properties of Sens and the Length of the A-T Stretch*

We chose NI, ND, and AQ as a Sens, and a series of DNAs having varying numbers of A-T base-pairs between Sens and neighboring G-C base-pair were synthesized (Fig. 1). The reduction potentials (E_{red}) [27, 28] as well as the singlet (E_S) and triplet (E_T) energies [28, 29] of NI, ND, and AQ reported in the literature are also shown in Fig. 1. NI, ND, and AQ can oxidize both G (1.31 V vs NHE) and A (1.63 V vs NHE) [30] upon photoexcitation [14, 19, 28, 31–43]. Since the nucleobases do not absorb at 355 nm, the 355 nm laser flash irradiation allows the selective excitation of Sens, which triggers electron transfer from the nucleobase to the excited Sens to inject a hole into DNA. Transient absorption spectra with a peak maximum at around 400 nm, 495 nm [28, 44], and 530 nm [42, 43] were observed using NI5, ND5, and AQ5, which were assigned to $Sens^{\cdot-}$; $NI^{\cdot-}$, $ND^{\cdot-}$, and $AQ^{\cdot-}$, respectively (Fig. 2). The Φ and τ for Sens-modified DNA were measured by monitoring the formation and decay of $NI^{\cdot-}$, $ND^{\cdot-}$, and $AQ^{\cdot-}$ (Fig. 3). For NI- and ND-modified DNA, the Φ and τ followed similar trends [14, 19, 31]. Formation of the charge-separated state was not observed in the nanosecond time scale when the G-C base-pair was too close to Sens ($n < 3$). While a hole was injected into DNA, rapid charge-recombination occurs due to the close distance between $Sens^{\cdot-}$ and $G^{\cdot+}$. An exponential increase in τ and gradual decrease in Φ was observed with increasing numbers of intervening A-T base-pairs ($n \geq 3$) between Sens and the neighboring G-C base-pair. These results show that the charge-separation occurs via multi-step charge transfer between A-T base-pairs which proceeds by a random-walk process. Thus, Φ will not sharply decrease with increasing distance between Sens and G. On the other hand, the charge-recombination between $Sens^{\cdot-}$ and $G^{\cdot+}$ proceeds by single-step mechanism which rate exponentially decreases with the increasing distance between the donor and acceptor. In the case of AQ-modified DNA, the formation of the charge-separated state was observed in the nanosecond time scale even when the G-C base-pair was located close to AQ. In addition, when the distance between AQ and the G-C base-pair became long ($n \geq 5$), the Φ_{CS} did not changed any more. Thus, the charge-separation mechanism for AQ-modified DNA differed from that for NI- and ND-modified DNA.

In the case of NI- and ND-modified DNA, hole-injection occurs via Sens in the singlet excited state. While the charge-separation yields ($\Phi_{CS} < 3\%$) are moderate due to the rapid charge-recombination between $NI^{\cdot-}$ and $A^{\cdot+}$, a positive charge escaped from the initial charge-recombination migrates through DNA by a multistep hole-transfer process between A-T base-pairs to be trapped at G to form $G^{\cdot+}$. When the Sens locates close to the G-C base-pair ($n < 3$), charge-recombination between $Sens^{\cdot-}$ and $G^{\cdot+}$ proceeds faster than the time resolution of our nanosecond laser experimental setup ($\tau < 50$ ns). Formation and fast decay of $Sens^{\cdot-}$ were observed for NI3 and ND3, and the formation of the long-lived

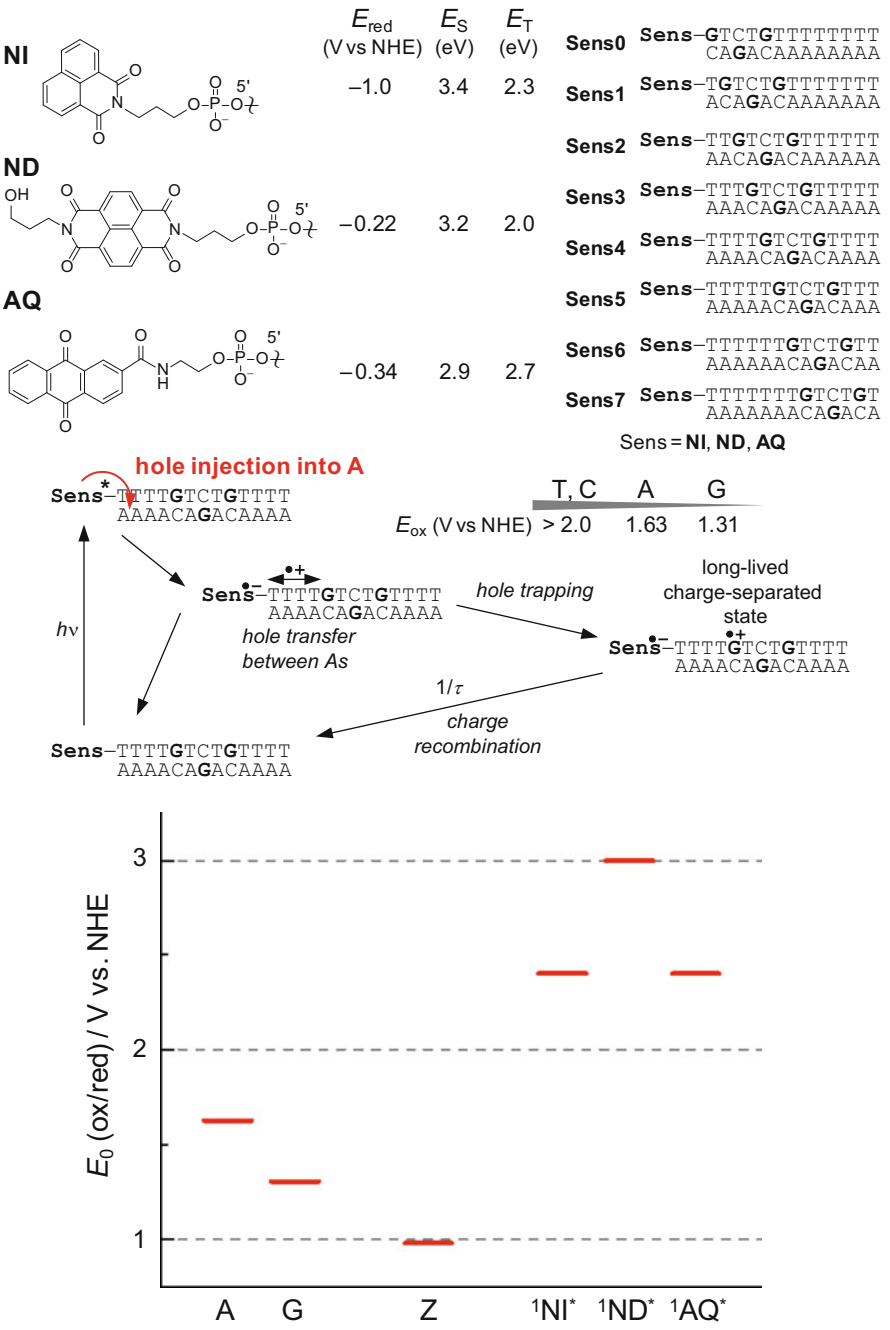

Fig. 1 Chemical structures of Sens NI, ND, and AQ attached at the 5′-end of DNA, sequences of Sens-modified DNA, and kinetic scheme for hole-injection, charge-separation, and charge-recombination in Sens-modified DNA. Schematic comparison between the reduction potentials of excited photosensitizers and the oxidation potentials of nucleobases

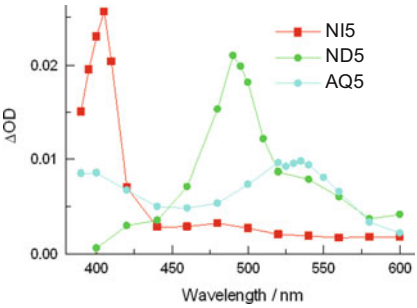

Fig. 2 The transient absorption spectra of NI5, ND5, and AQ5 obtained at 1 μs after the 355-nm laser flash excitation

charge-separated state became obvious for DNA having longer A-T base-pairs between Sens and the neighboring G-C base-pair ($n \geq 4$). The observed charge-separation and charge-recombination dynamics for NI- and ND-modified DNA were quite consistent with the work reported by Lewis, Wasielewski, and Fiebig using stilbene dicarboxamide as a Sens [45, 46].

In sharp contrast, a unique relation between the τ and number of intervening A-T base-pairs between AQ and the neighboring G-C base-pairs was observed for AQ-modified DNA. Formation and fast decay of $AQ^{\cdot-}$ were observed even when a G-C base-pair was located in the vicinity of AQ ($n = 0 - 2$). It is reported that AQ derivatives undergo rapid intersystem crossing to form AQ in the triplet excited states capable of oxidizing A and G forming the spin-forbidden triplet ion-pairs [42, 43]. Thus, the relatively slow charge-recombination observed for AQn ($n = 0 - 2$) compared to corresponding NIn and NDn ($n = 0 - 2$) may be explained by the charge-separation via AQ in the triplet excited state. Lewis and Wasielewski have reported that charge-injection via AQ in the singlet excited states ($^1AQ^*$) competes with the intersystem crossing [42], which may explain the undramatic increase in the Φ_{CS} compared with NI- and ND-modified DNA [34]. They also reported that yield of the formation of AQ in the triplet excited state increases with increasing distance between AQ and G. This is because the electron transfer proceeds faster between $^1AQ^*$ and G than between $^1AQ^*$ and A. The Φ_{CS} becomes almost constant for AQ-modified DNA having more than five A-T base-pairs between AQ and the nearby G, suggesting that once the distance between AQ and G becomes long enough the yield of AQ in the triplet excited state become constant because the electron transfer between $^1AQ^*$ and G becomes negligible and charge transfer between As proceeds faster than the charge-recombination via $AQ^{\cdot-}$ and $A^{\cdot+}$ triplet ion-pairs.

2.2 *Charge-Separation Triggered by Hole-Injection into the Second and Further Neighboring As to the NI*

In order to gain further insights into the charge-separation via sequential hole transfer between A-Ts, the charge-separation process was examined for a series

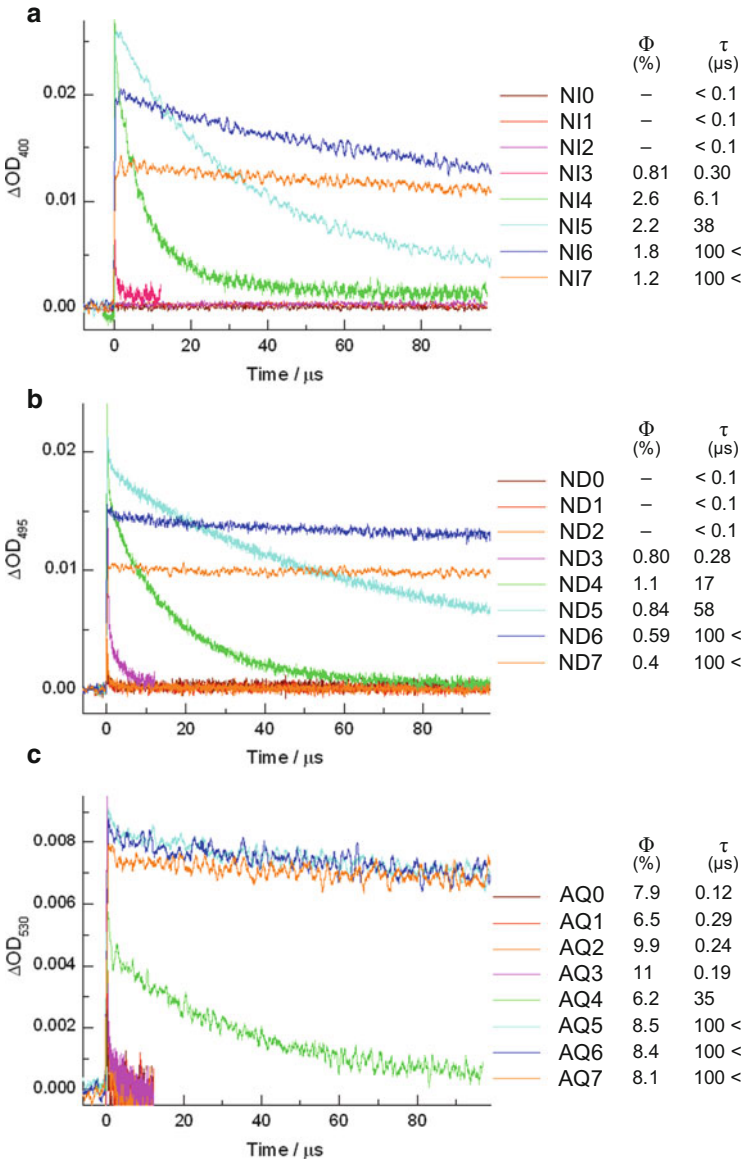

Fig. 3 Time profiles of the transient absorption of (**a**) $NI^{\cdot -}$, (**b**) $ND^{\cdot -}$, and (**c**) $AQ^{\cdot -}$ monitored at 400, 495, and 530 nm, respectively, during the 355-nm laser flash photolysis of Sens-modified DNA

of DNAs in which the oxidation potential of each A base in an A-T stretch between Sens and a hole trap G-C base-pair is systematically increased. The DNA structure should not change upon altering the oxidation potential of A. Previously, we demonstrated that the oxidation potential of G can be controlled through hydrogen

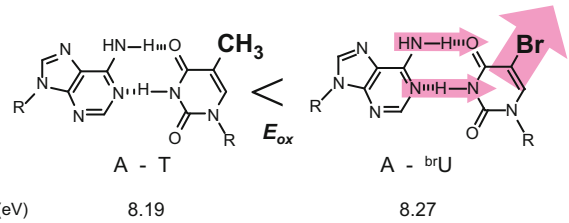

Fig. 4 Estimated ionization potentials of A-T and A-^{br}U base-pairs calculated at the 3-21G(*) level

bonding by introducing a substituent on the base pairing cytosine. A bromine substitution of the cytosine C5 hydrogen in the C-G base-pair caused a 24-mV increase in the oxidation potential of G [20, 47]. The electron-withdrawing effect of 5-bromo substituent of cytosine can be transmitted to its complementary base G through hydrogen bonding to increase the oxidation potential of G. We expected that, the oxidation potential of A in the A-T base-pair can be similarly increased by replacing the C5 methyl group of T with a bromine group (A-^{br}U). The theoretical calculations of ionization potentials of A-T, and A-^{br}U base-pairs at the 3-21G(*) level (Fig. 4) demonstrated that the oxidation potential of A can be increased by introducing the electron-withdrawing group bromine on its base pairing T. Since the van der Waals radius of bromine is similar to that of a methyl group, the oxidation potential of the A-^{br}U base-pair can be increased from that of the A-T base-pair without substantially alternating the global DNA double helical structure.

We synthesized a series of NI-modified DNAs in which the A-T base-pair in an A-T stretch was systematically changed to the A-^{br}U base-pair (Fig. 5).[1] The presence of an A-^{br}U base-pair was expected to attenuate the hole-passing through it because of the slower hole transfer rate from $A^{\cdot+}$-T to A-^{br}U compared to that between two A-T base-pairs. Especially, when the A-T base-pair nearest to NI was changed to the A-^{br}U base-pair, the A-^{br}U base-pair serves as a barrier for a hole residing on the second A (A_2), avoiding going back to the first A (A_1), and therefore the Φ of **Nbr1** is expected to increase compared to that of **N1** which does not have an A-^{br}U base-pair. As expected, the Φ value was higher for **Nbr1** than that for **N1**. For the other A-T base-pairs, the change to the A-^{br}U base-pair is likely to decrease the Φ value because an A-^{br}U base-pair attenuates the hole-passing through it, and a decrease in the Φ was observed for **Nbr3**, **Nbr4**, and **Nbr5**. However, of special interest, substitution of an A-^{br}U base-pair at the second nearest position to NI (**Nbr2**) unexpectedly resulted in an increase in the Φ value.

We next prepared a series of DNAs in which each A-T base-pair was inverted to form a T-A base-pair. Since a hole moves much faster through a consecutive A-T sequence rather than through an A-T/T-A repeat sequence due to the closer distance and direct stacking between As [18], the inversion of the A-T base-pair in an A-T stretch was expected to decrease the Φ. Interestingly, the inversion of the A-T base-pair adjacent to NI led to an increase in Φ (**NTA1**) in spite of the unfavorable

[1] The electron transfer from NI radical anion to bromouridine dose not takes place in less than 100 μs (see [58]).

		Φ (%)
N1	NI–T–T–T–T–T –GCGCGT A–A–A–A–A –CGCGCA	3.1
Nbr1	NI–**U**–T–T–T–T –GCGCGT A–A–A–A–A –CGCGCA	4.0
Nbr2	NI–T–**U**–T–T–T –GCGCGT A–A–A–A–A –CGCGCA	3.9
Nbr3	NI–T–T–**U**–T–T –GCGCGT A–A–A–A–A –CGCGCA	3.1
Nbr4	NI–T–T–T–**U**–T –GCGCGT A–A–A–A–A –CGCGCA	2.5
Nbr5	NI–T–T–T–T–**U** –GCGCGT A–A–A–A–A –CGCGCA	2.8

		Φ (%)
NTA1	NI–**A**–T–T–T–T –GCGCGT **T**–A–A–A–A –CGCGCA	4.4
NTA2	NI–T–**A**–T–T–T –GCGCGT A–**T**–A–A–A –CGCGCA	2.1
NTA4	NI–T–T–T–**A**–T –GCGCGT A–A–A–**T**–A –CGCGCA	0.2
NTA5	NI–T–T–T–T–**A** –GCGCGT A–A–A–A–**T** –CGCGCA	0.8

U = ^{br}U

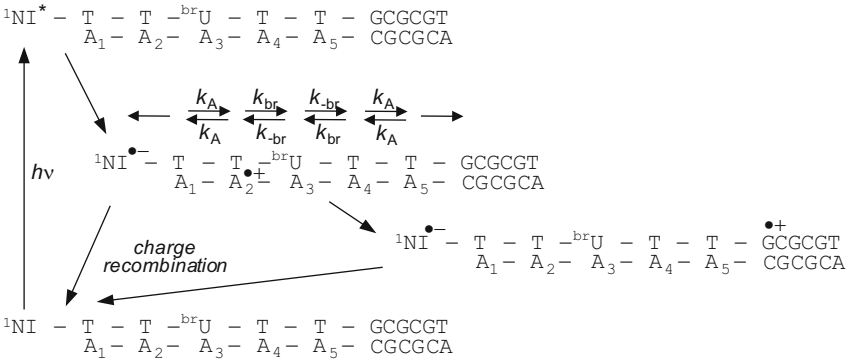

Fig. 5 Sequences of NI and ^{br}U-modified DNA, and kinetic scheme for photoinduced one-electron oxidation of A, hole transfer between two A-T base pairs (k_A), that between A-T base pair and A-^{br}U base pair (k_{br} and k_{-br}), hole trapping, and charge-recombination in DNA

decrease in the hole transfer rate from $A_1^{\cdot+}$ to A_2. On the other hand, the inversion of the other A-T base-pairs resulted in a significant decrease in Φ, as expected (**NTA2**, **NTA4**, and **NTA5**). These results clearly demonstrated that a decrease in the hole transfer rate from $A_1^{\cdot+}$ to A_2 does not affect Φ, while a decrease in the hole transfer rate from $A_2^{\cdot+}$ to A_1 leads to an increase in Φ.

Based on the results, it was strongly suggested that a hole initially generated on A_1 does not lead to the formation of the long-lived charge-separated state, that is, a hole cannot escape from the charge-recombination within a contact ion-pair. Rather, the formation of the charge-separated state is triggered by the electron transfer between A_n ($n \geq 2$) and NI in the singlet excited state ($^1NI^*$). The electron transfer rate between $^1NI^*$ and A (k_{et}), or the yield of the hole initially generated on A, decreases with the distance between $^1NI^*$ and A to be oxidized (Δr) according to (1):

$$\ln k_{et} \propto -\beta \Delta r \tag{1}$$

where the β takes the value between 0.4 and 0.7 $Å^{-1}$ in DNA [48–50]. By assuming the β-value of 0.55 $Å^{-1}$ and that 90% of the absorbed photons leads to the electron transfer between $^{1}NI^{*}$ and A, a hole will be initially generated on A_1, A_2, and A_3 with a Φ-value of 0.77, 0.12, and 0.018, respectively. Therefore, it is possible to explain the formation of the charge-separated state with a quantum yield of 5% or lower observed here according to the hole initially generated on A_n ($n \geq 2$). These results suggested that long-lived charge-separated state is formed through the initial charge generation on the second and further neighboring As to the NI instead of the oxidation of A adjacent to NI. The Φ may be increased by putting a redox inactive spacer base-pair between Sens and an A-T stretch.

3 Charge-Separation via Direct Hole Generation on G-C

While sequential hole transfer between A-Ts is useful to generate a long-lived charge-separated state in DNA, the yield was not sufficiently high ($\Phi < 3.5\%$), mainly due to the initial charge-recombination process within the $Sens^{\cdot -}$ and $A^{\cdot +}$ contact ion pair [19, 51]. To avoid charge-recombination within a contact ion-pair, it is one way to put a redox inactive spacer between Sens and the nucleobase to be oxidized. Sens which can only oxidize G upon photoexcitation may be suitable for this purpose because the A-T base-pair can be used as a spacer to slow down the charge-recombination rate between $Sens^{\cdot -}$ and $G^{\cdot +}$ while maintaining the sufficient hole-injection efficiency. The protonated 9-alkylamino-6-chloro-2-methoxyacridine (Acr^{+}) in the singlet excited state ($^{1}Acr^{+*}$) is reported to be selectively quenched by G (not by A, C, and T) via an electron transfer in a distant dependent manner [25, 52–55]. Thus, we synthesized several Acr^{+}- and PTZ-modified DNAs in which PTZ – which has much lower oxidation potential than G – serves as a final hole acceptor. We also tested several commonly used fluorophores, TAMRA, ATTO 655, and Alexa 532, the fluorescence of which can only be quenched by G in the context of DNA.

DNAs were designed so as to have between zero and five intervening A-T base-pairs between a fluorescent dye and G (Fig. 6). The fluorescent dyes were anchored and buried in DNA to have a π-stacking interaction between neighboring bases by using the amino-linker X. Three consecutive G-C base-pairs were utilized as a pathway of a positive charge to separate further the positive and negative charges ($Sens^{\cdot -}$) to ensure the hole trapping at PTZ leading to the formation of a long-lived charge-separated state. Some Gs within the consecutive G-C base-pairs were replaced with deazaguanine (Z), which have a lower oxidation potential than G (0.98 V vs NHE) [30, 56–58], to refine the charge-separation process to achieve a larger Φ. Hence, DNAs were designed so as to have an $(A\text{-}T)_n$ ($n = 0 - 5$) spacer and an $(X\text{-}C)_3$ (X=G or Z) charge pathway between Sens and PTZ.

The steady-state fluorescence spectra were measured to investigate the photoinduced fluorescence quenching. We first tested Acr^{+} to verify the present system.

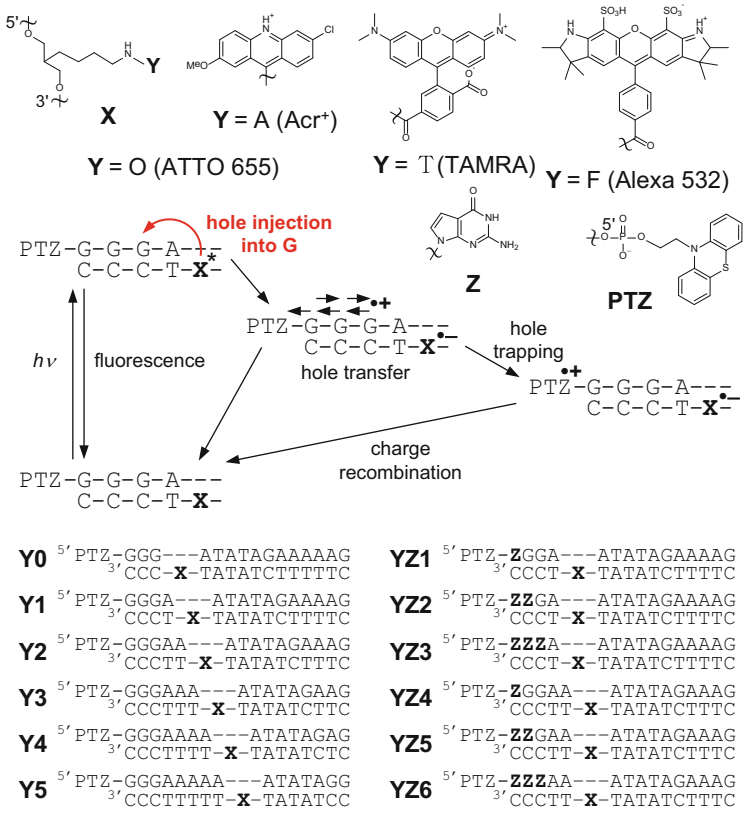

Fig. 6 DNA sequences, chemical structures of an aminolinker (X), Acr^+, TAMRA, Alexa 532, 7-deazaguanine (Z), and phenothiazine (PTZ), and a schematic representation for hole-injection, hole transfer, and charge-recombination in DNA. An additional T was placed as a complementary base of X in the case of Alexa 532 modified DNA

Consistent with previous reports [25, 52–55], the fluorescence intensity increased as the number of intervening A-T base-pairs between Acr^+ and G increased due to the distant-dependent photoinduced charge transfer between $^1Acr^{+*}$ and G (Fig. 7a). Similar trends were observed for TAMRA, ATTO 655, and Alexa 532, suggesting the occurrence of the photoinduced charge transfer between the fluorescent dye in the singlet excited state and G (Fig. 7b–d). The replacement of G close to the fluorescent dye with Z resulted in a further decrease in the fluorescent intensity due to the more efficient fluorescence quenching by Z compared with G, while changes in Gs far from the fluorescent dye caused only small effects on the fluorescence intensity.

Next, the formation of the charge-separated state was investigated. In the case of Acr^+-modified DNA, Acr^+ was excited using the 355-nm laser, and the charge-recombination dynamics were monitored by the formation and decay of $PTZ^{\cdot+}$ and

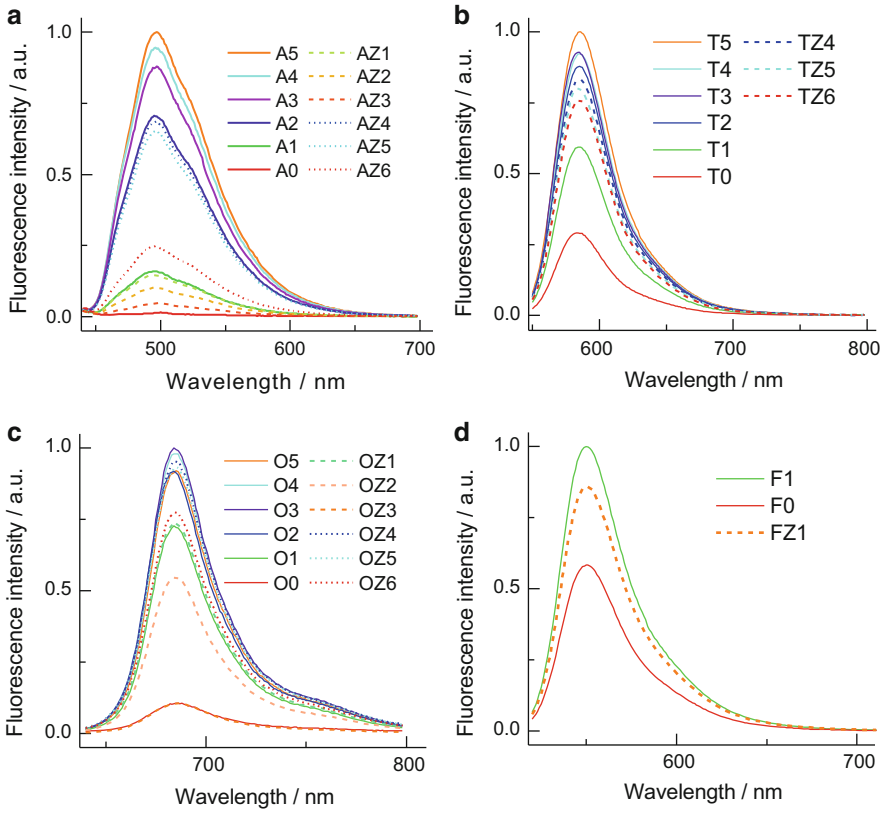

Fig. 7 Fluorescence spectra for (**a**) Acr^+-modified DNA ($\lambda_{ex} = 428$ nm), (**b**) TAMRA-modified DNA ($\lambda_{ex} = 540$ nm), (**c**) ATTO 655-modified DNA ($\lambda_{ex} = 620$ nm), and (**d**) Alexa 532-modified DNA ($\lambda_{ex} = 510$ nm)

$Acr^{\cdot}$, which show absorption with a peak at around 520 nm (Fig. 8a). When there was no A-T spacer between G and Acr^+, the formation of the charge-separated state was not observed because the charge-recombination took place faster than the time resolution of our experimental setup (<50 ns) [25, 52, 53]. The insertion of the A-T base-pair between G and Acr^+ slowed the initial charge-recombination rate between $Acr^{\cdot}$ and $G^{\cdot+}$, resulting in the formation of a long-lived charge-separated state, and the lifetime of the charge-separated state (τ) increased while Φ gradually decreased with increasing numbers of A-T base-pairs (Fig. 8b) [25].

Similarly, charge-recombination dynamics were investigated for TAMRA, ATTO 655, and Alexa 532 modified DNA. Since the absorption of $PTZ^{\cdot+}$ overlaps with the ground state absorption of these fluorescent dyes, and the absorption of the radical anion of these fluorescent dyes have not been reported thus far, charge-recombination dynamics were investigated by monitoring the bleach and recovery of their ground state absorption. The 532-nm laser flash excitation of the fluorescent dye modified DNA caused bleach and recovery of the ground state absorption of

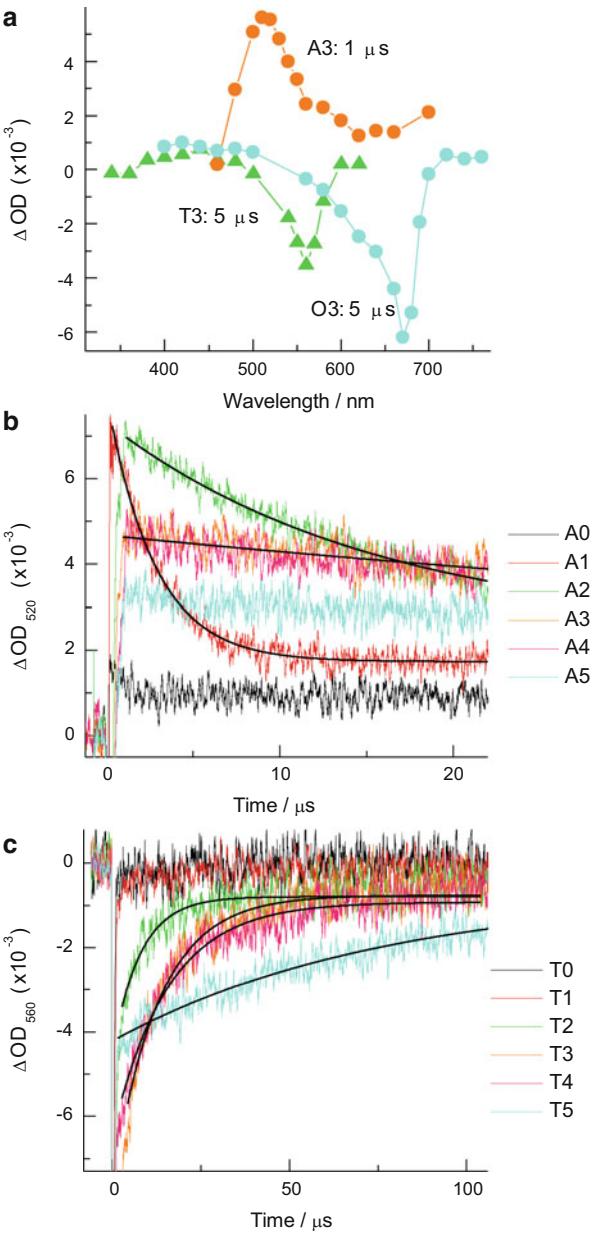

Fig. 8 (**a**) Transient absorption spectra for A3, T3, and O3 observed after the laser flash excitation. (**b**) Time profiles of the transient absorption of $PTZ^{\cdot+}$ and $Acr^{\cdot}$ monitored at 520 nm during the 355-nm laser flash photolysis of A0–A5. (**c**) Time profiles of the bleach and recovery of TAMRA monitored at 560 nm for T0–T5. The *smoothed black curves* superimposed on the experimental data are the single exponential fit from which the lifetime of the charge-separated state (τ) was determined

fluorescent dye, while obvious transient absorption related to the one-electron reduced form of fluorescent dye was not observed in the wavelength range of 350–650 nm (Fig. 8a). Interestingly, all three fluorescent dye modified DNAs showed sequence-dependent bleach and recovery of their ground state absorption consistent with the charge-recombination dynamics observed for Acr^{+}-modified

Table 1 The lifetime (τ) and quantum yield (Φ) of the charge-separated state

DNA	τ (μs)	Φ (%)	DNA	τ (μs)	Φ (%)	DNA	τ (μs)	Φ (%)
A0	<0.5	–	**T0**	<0.5	–	**O0**	<0.5	–
A1	2.7	4.8	**T1**	<0.5	–	**O1**	5.8	0.57
A2	16	4.4	**T2**	7.6	0.36	**O2**	160	0.76
A3	75	2.9	**T3**	13	0.61	**O3**	560	2.4
A4	>200	2.6	**T4**	16	0.52	**O4**	>800	1.5
A5	>200	2.0	**T5**	76	0.34	**O5**	>800	0.90
AZ1	2.4	9.9				**OZ1**	5.4	2.3
AZ2	2.1	13				**OZ2**	4.4	4.0
AZ3	2.0	4.9				**OZ3**	4.2	0.95
AZ4	15	6.5	**TZ4**	7.7	0.43	**OZ4**	220	2.8
AZ5	15	7.6	**TZ5**	8.1	0.51	**OZ5**	210	3.5
AZ6	13	7.3	**TZ6**	5.7	0.51	**OZ6**	100	2.4
F0	<0.5	–						
F1	0.70	1.7						
F1Z	0.96	2.6						

DNA (Fig. 8c, Table 1). These results suggested that charge-recombination dynamics may also be monitored for other fluorescent dyes for which the fluorescence is quenched by G [59, 60].

Gs should be located close to the fluorescent dye for the charge-separation to occur efficiently. However, when G is located too close to the fluorescent dye, the initial charge-recombination between $G^{\cdot+}$ and the reduced fluorescent dye proceeds relatively fast compared with the hole transfer process through consecutive Gs, and only part of a generated positive charge can escape from the initial charge-recombination to produce a long-lived charge-separated state, thus resulting in a moderate value of Φ [25]. In order to increase the Φ, we attempted to increase the hole transfer rate through DNA toward PTZ by replacing some Gs in the G-C tract between the fluorescent dye and PTZ with Z. Since the oxidation potential of Z is lower than that of G, we expected the charge transfer from $G^{\cdot+}$ to Z to proceed faster than that from $G^{\cdot+}$ to G, and at the same time that from $Z^{\cdot+}$ to G to proceed slower than that from $G^{\cdot+}$ to G, resulting in an increase in Φ [24, 61]. Interestingly, for a DNA series having one A-T base-pair between the fluorescent dye and the G-C tract, the replacement of one or two G(s) with Z(s) resulted in a considerable increase in Φ (Fig. 9, Table 1). On the other hand, when all Gs in the G-C tract were replaced with Zs, Φ was only moderately affected, suggesting that charge transfer between $Z^{\cdot+}$ and Z proceeds with a similar rate constant to that between $G^{\cdot+}$ and G, and/or charge-recombination proceeds faster between $Sens^{\cdot-}$ and $Z^{\cdot+}$ compared with that between $Sens^{\cdot-}$ and $G^{\cdot+}$. In the case of DNA having two A-T base-pairs between the fluorescent dye and G-C tract, the effect of the replacement of Gs with Zs on Φ was relatively small compared to those for DNA series with one A-T base-pair between the fluorescent dye and G-C tract. This result was explained by the decrease in the initial charge-recombination rate as a consequence of the increase in the distance between the fluorescent dye and nearest G-C or Z-C.

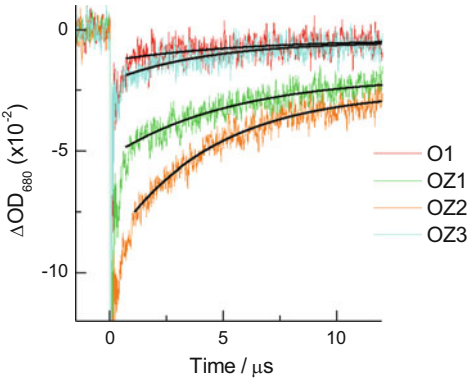

Fig. 9 The effects of replacing G base(s) with Z base(s) on the charge-separation and charge-recombination dynamics in DNA. Time profiles of the bleach and recovery of ATTO 655 monitored at 680 nm for O1, OZ1–OZ3. The *smoothed black curves* superimposed on the experimental data are the single exponential fit from which the lifetime of the charge-separated state (τ) was determined

In contrast to the YZ3 series, an increase in Φ was also observed for the YZ6 series. It may be explained by that the increase in the photoinduced charge transfer efficiency, which is reflected in the increased extent of the florescence quenching, caused the increase in Φ.

4 Conclusions

In this chapter we have described the mechanism of the photoinduced charge-separation in DNA. When Sens is strong enough to oxidize A-T base-pairs, a long-lived charge-separated state in DNA can be formed via sequential hole transfer between consecutive A-Ts. Φ can be increased when the intersystem crossing is fast enough to compete with the photoinduced electron transfer via Sens in the singlet excited state due to the formation of the spin-forbidden triplet ion-pairs. It was also revealed that the charge-separated state is formed through the initial charge generation on the second and further neighboring As to the Sens instead of the oxidation of A adjacent to Sens. These results suggested that the Φ can be increased by putting a redox inactive spacer base-pair between Sens and the base-pair to be oxidized. This is the case for Sens of which fluorescence is quenched only by G among the four natural nucleobases. A long-lived charge-separated state was shown to be formed by widely used fluorescent dyes TAMRA, ATTO 655, and Alexa 532. By utilizing artificial nucleobases, the redox potential gradient of nucleobases, which can be achieved by utilizing the artificial nucleobases, was shown to be effective to increase the Φ. These important fundamental insights about the formation of the long-lived charge-separated state in DNA may aid in the future design of molecular-scale optoelectronics.

References

1. Gust D, Moore TA, Moore AL (2001) Mimicking photosynthetic solar energy transduction. Acc Chem Res 34:40
2. Imahori H, Norieda H, Yamada H, Nishimura Y, Yamazaki I, Sakata Y, Fukuzumi S (2001) Light-harvesting and photocurrent generation by gold electrodes modified with mixed self-assembled monolayers of boron–dipyrrin and ferrocene–porphyrin–fullerene triad. J Am Chem Soc 123:100
3. Akiyama T, Yamada S (2001) Photocurrent generation from self-assembled monolayers of donor-acceptor pairs formed on conductive surfaces. Trends Photochem Photobiol 8:67
4. Guldi DM (2002) Fullerene-porphyrin architectures; photosynthetic antenna and reaction center models. Chem Soc Rev 31:22
5. Lewis NS, Nocera DG (2006) Powering the planet: chemical challenges in solar energy utilization. Proc Natl Acad Sci U S A 103:15729
6. Fukuzumi S (2006) Bioinspired electron-transfer systems and applications. Bull Chem Soc Jpn 79:177
7. Wasielewski MR (2006) Energy, charge, and spin transport in molecules and self-assembled nanostructures inspired by photosynthesis. J Org Chem 71:5051
8. Rothemund PWK (2006) Folding DNA to create nanoscale shapes and patterns. Nature 440:297
9. Wickham SFJ, Endo M, Katsuda Y, Hidaka K, Bath J, Sugiyama H, Turberfield AJ (2011) Direct observation of stepwise movement of a synthetic molecular transporter. Nat Nanotechnol 6:166
10. Kuzuya A, Sakai Y, Yamazaki T, Xu Y, Komiyama M (2011) Nanomechanical DNA origami 'single-molecule beacons' directly imaged by atomic force microscopy. Nat Commun 2:1452/1
11. Stein IH, Steinhauer C, Tinnefeld P (2011) Single-molecule four-color FRET visualizes energy-transfer paths on DNA origami. J Am Chem Soc 133:4193
12. Seidel CAM, Schulz A, Sauer MHM (1996) Nucleobase-specific quenching of fluorescent dyes. 1. Nucleobase one-electron redox potentials and their correlation with static and dynamic quenching efficiencies. J Phys Chem 100:5541
13. Steenken S, Jovanovic SV (1997) How easily oxidizable is DNA? One-electron reduction potentials of adenosine and guanosine radicals in aqueous solution. J Am Chem Soc 119:617
14. Kawai K, Takada T, Nagai T, Cai X, Sugimoto A, Fujitsuka M, Majima T (2003) Long-lived charge-separated state leading to DNA damage through hole transfer. J Am Chem Soc 125:16198
15. Takada T, Kawai K, Cai X, Sugimoto A, Fujitsuka M, Majima T (2004) Charge separation in DNA via consecutive adenine hopping. J Am Chem Soc 126:1125
16. Takada T, Kawai K, Fujitsuka M, Majima T (2004) Direct observation of hole transfer through double-helical DNA over 100 Angstroms. Proc Natl Acad Sci U S A 101:14002
17. Takada T, Kawai K, Fujitsuka M, Majima T (2006) High-yield generation of a long-lived charge-separated state in diphenylacetylene-modified DNA. Angew Chem Int Ed 45:120
18. Takada T, Kawai K, Fujitsuka M, Majima T (2006) Rapid long-distance hole transfer through consecutive adenine sequence. J Am Chem Soc 128:11012
19. Kawai K, Osakada Y, Fujitsuka M, Majima T (2005) Consecutive adenine sequences are potential targets in photosensitized DNA damage. Chem Biol (Cambridge, MA, USA) 12:1049
20. Kawai K, Osakada Y, Takada T, Fujitsuka M, Majima T (2004) Lifetime regulation of the charge-separated state in DNA by modulating the oxidation potential of guanine in DNA through hydrogen bonding. J Am Chem Soc 126:12843
21. Osakada Y, Kawai K, Fujitsuka M, Majima T (2006) Charge transfer through DNA nanoscaled assembly programmable with DNA building blocks. Proc Natl Acad Sci U S A 103:18072
22. Kawai K, Osakada Y, Sugimoto A, Fujitsuka M, Majima T (2007) Hole transfer rates in A-form DNA/2-OMeRNA hybrid. Chem Eur J 13:2386

23. Kawai K, Osakada Y, Matsutani E, Majima T (2010) Charge separation and photosensitized damage in DNA mediated by naphthalimide, naphthaldiimide, and anthraquinone. J Phys Chem B 114:10195
24. Kawai K, Osakada Y, Fujitsuka M, Majima T (2008) Mechanism of charge separation in DNA by hole transfer through consecutive adenines. Chem Eur J 14:3721
25. Kawai K, Osakada Y, Fujitsuka M, Majima T (2008) Charge separation in acridine- and phenothiazine-modified DNA. J Phys Chem B 112:2144
26. Kawai K, Matsutani E, Maruyama A, Majima T (2011) Probing the charge-transfer dynamics in DNA at the single-molecule level. J Am Chem Soc 133:15568
27. Breslin DT, Schuster GB (1996) Anthraquinone photonucleases: mechanisms for GG-selective and nonselective cleavage of double-stranded DNA. J Am Chem Soc 118:2311
28. Rogers JE, Kelly LA (1999) Nucleic acid oxidation mediated by naphthalene and benzophenone imide and diimide derivatives: consequences for DNA redox chemistry. J Am Chem Soc 121:3854
29. van Ramesdonk HJ, Bakker BH, Groeneveld MM, Verhoeven JW, Allen BD, Rostron JP, Harriman A (2006) Ultrafast intersystem crossing in 9,10-anthraquinones and intramolecular charge separation in an anthraquinone-based dyad. J Phys Chem A 110:13145
30. Dohno C, Saito I (2005) In: Wagenknecht H-A (ed) Charge transfer in DNA. Wiley-VCH, Weinheim, p 153
31. Kawai K, Osakada Y, Fujitsuka M, Majima T (2006) Effects of reaction rate of radical anion of a photosensitizer with molecular oxygen on the photosensitized DNA damage. Chem Commun 3918
32. Kawai K, Osakada Y, Fujitsuka M, Majima T (2007) Hole transfer in DNA and photosensitized DNA damage: importance of adenine oxidation. J Phys Chem B 111:2322
33. Henderson PT, Jones D, Hampikian G, Kan YZ, Schuster GB (1999) Long-distance charge transport in duplex DNA: the phonon-assisted polaron-like hopping mechanism. Proc Natl Acad Sci U S A 96:8353
34. Sanii L, Schuster GB (2000) Long-distance charge transport in DNA: sequence-dependent radical cation injection efficiency. J Am Chem Soc 122:11545
35. Liu C-S, Hernandez R, Schuster GB (2004) Mechanism for radical cation transport in duplex DNA oligonucleotides. J Am Chem Soc 126:2877
36. Joseph J, Schuster GB (2009) Oxidatively damaged nucleobases in duplex DNA oligomers: reaction at thymine-thymine mispairs. J Am Chem Soc 131:13904
37. Kanvah S, Joseph J, Schuster GB, Barnett RN, Cleveland CL, Landman U (2010) Oxidation of DNA: damage to nucleobases. Acc Chem Res 43:280
38. Dohno C, Ogawa A, Nakatani K, Saito I (2003) Hole trapping at N6-cyclopropyldeoxyadenosine suggests a direct contribution of adenine bases to hole transport through DNA. J Am Chem Soc 125:10154
39. Williams TT, Dohno C, Stemp EDA, Barton JK (2004) Effects of the photooxidant on DNA-mediated charge transport. J Am Chem Soc 126:8148
40. Leung EKY, Sen D (2007) Electron hole flow patterns through the RNA-cleaving 8-17 deoxyribozyme yield unusual information about its structure and folding. Chem Biol (Cambridge, MA, USA) 14:41
41. Huang YC, Sen D (2010) A contractile electronic switch made of DNA. J Am Chem Soc 132:2663
42. Lewis FD, Thazhathveetil AK, Zeidan TA, Vura-Weis J, Wasielewski MR (2010) Dynamics of ultrafast singlet and triplet charge transfer in anthraquinone-DNA conjugates. J Am Chem Soc 132:444
43. Armitage B, Yu C, Devadoss C, Schuster GB (1994) Cationic anthraquinone derivatives as catalytic DNA photonucleases: mechanisms for DNA damage and quinone recycling. J Am Chem Soc 116:9847
44. Rogers JE, Weiss SJ, Kelly LA (2000) Photoprocesses of naphthalene imide and diimide derivatives in aqueous solutions of DNA. J Am Chem Soc 122:427

45. Lewis FD, Zhu H, Daublain P, Fiebig T, Raytchev M, Wang Q, Shafirovich V (2006) Crossover from superexchange to hopping as the mechanism for photoinduced charge transfer in DNA hairpin conjugates. J Am Chem Soc 128:791
46. Vura-Weis J, Wasielewski MR, Thazhathveetil AK, Lewis FD (2009) Efficient charge transport in DNA diblock oligomers. J Am Chem Soc 131:9722
47. Kawai K, Wata Y, Hara M, Tojo S, Majima T (2002) Regulation of one-electron oxidation rate of guanine by base pairing with cytosine derivatives. J Am Chem Soc 124:3586
48. Lewis FD, Wu TF, Zhang YF, Letsinger RL, Greenfield SR, Wasielewski MR (1997) Distance-dependent electron transfer in DNA hairpins. Science 277:673
49. Lewis FD, Wu Y, Hayes RT, Wasielewski MR (2002) DNA-mediated electron transfer across synthetic T:A.T triplex structures. Angew Chem Int Ed 41:3485
50. Kawai K, Takada T, Tojo S, Ichinose N, Majima T (2001) Observation of hole transfer through DNA by monitoring the transient absorption of pyrene radical cation. J Am Chem Soc 123:12688
51. Takada T, Kawai K, Fujitsuka M, Majima T (2005) Contributions of the distance-dependent reorganization energy and proton-transfer to the hole-transfer process in DNA. Chem Eur J 11:3835
52. Davis WB, Hess S, Naydenova I, Haselsberger R, Ogrodnik A, Newton MD, Michel-Beyerle M-E (2002) Distance-dependent activation energies for hole injection from protonated 9-amino-6-chloro-2-methoxyacridine into duplex DNA. J Am Chem Soc 124:2422
53. Hess S, Goetz M, Davis WB, Michel-Beyerle M-E (2001) On the apparently anomalous distance dependence of charge-transfer rates in 9-amino-6-chloro-2-methoxyacridine-modified DNA. J Am Chem Soc 123:10046
54. Fukui K, Tanaka K, Fujitsuka M, Watanabe A, Ito O (1999) Distance dependence of electron transfer in acridine-intercalated DNA. J Photochem Photobiol B 50:18
55. Fukui K, Tanaka K (1998) Distance dependence of photoinduced electron transfer in DNA. Angew Chem Int Ed 37:158
56. Kelley SO, Barton JK (1999) Electron transfer between bases in double helical DNA. Science 283:375
57. Nakatani K, Dohno C, Saito I (2000) Modulation of DNA-mediated hole-transport efficiency by changing superexchange electronic interaction. J Am Chem Soc 122:5893
58. Kawai K, Kodera H, Majima T (2010) Photocatalytic formation of I-I bonds using DNA which enables detection of single nucleotide polymorphisms. J Am Chem Soc 132:14216
59. Marras SAE, Kramer FR, Tyagi S (2002) Efficiencies of fluorescence resonance energy transfer and contact-mediated quenching in oligonucleotide probes. Nucleic Acids Res 30: e122/1
60. Torimura M, Kurata S, Yamada K, Yokomaku T, Kamagata Y, Kanagawa T, Kurane R (2001) Fluorescence-quenching phenomenon by photoinduced electron transfer between a fluorescent dye and a nucleotide base. Anal Sci 17:155
61. Conron SMM, Thazhathveetil AK, Wasielewski MR, Burin AL, Lewis FD (2010) Direct measurement of the dynamics of hole hopping in extended DNA G-tracts. An unbiased random walk. J Am Chem Soc 132:14388

Top Curr Chem (2015) 356: 183–202
DOI: 10.1007/128_2013_511

Published online: 23 February 2014

Electronic Excitations in Guanine Quadruplexes

Pascale Changenet-Barret, Ying Hua, and Dimitra Markovitsi

Abstract Guanine rich DNA strands, such as those encountered at the extremities of human chromosomes, have the ability to form four-stranded structures (G-quadruplexes) whose building blocks are guanine tetrads. G-quadruplex structures are intensively studied in respect of their biological role, as targets for anticancer therapy and, more recently, of their potential applications in the field of molecular electronics. Here we focus on their electronic excited states which are compared to those of non-interacting mono-nucleotides and those of single and double stranded structures. Particular emphasis is given to excited state relaxation processes studied by time-resolved fluorescence spectroscopy from femtosecond to nanosecond time scales. They include ultrafast energy transfer and trapping of $\pi\pi^*$ excitations by charge transfer states. The effect of various structural parameters, such as the nature of the metal cations located in the central cavity of G-quadruplexes, the number of tetrads or the conformation of the constitutive single strands, are examined.

Keywords Charge transfer states · DNA fluorescence · Energy transfer · Excitons · Guanine quadruplexes · Molecular electronics · Multi-scale dynamics

Contents

P. Changenet-Barret, Y. Hua, and D. Markovitsi (✉)
CNRS, IRAMIS, LIDYL, Laboratoire Francis Perrin, URA 2453, Gif-sur-Yvette 91191, France
e-mail: dimitra.markovitsi@cea.fr

1 Introduction

In DNA double helices, guanines are paired with cytosines via three Watson–Crick hydrogen bonds (Fig. 1a). However, under certain conditions, guanine derivatives self-associate to form tetrads called G-quartets. These are square planar arrays in which each guanine is connected to two others via Hoogsteen hydrogen bonds (Fig. 1b). The vertical stacking of G-quartets gives rise to G-quadruplex structures [1, 2]. G-quadruplexes may be formed by lipophilic guanosine analogues in non-polar solvents or by guanine rich DNA or RNA strands in aqueous solution; for example, this is the case of telomeric sequences located at the end of the human chromosomes (TTAGGG).

During the past few decades the interest of various scientific communities in G-quadruplexes has been continuously increasing, in connection with the biological, pharmaceutical and technological importance of these structures. As early as in the 1980s it was suggested that G-quadruplex structures may be involved in important biological processes but their formation in human cells was observed only recently [3]. Their possible implication in cancer cell proliferation made them promising targets for the development of new anticancer therapies [4–6]. In the meantime, their potential applications in the field of molecular electronics [7, 8] and nanotechnology [9] have stimulated the design of novel guanine-based supramolecular architectures. Snapshots of the cutting edge research on the G-quadruplexes have recently been published in a specific volume of *Topics in Current Chemistry* [10].

Despite the huge number of publications devoted to G-quadruplexes, only a dozen have addressed their photophysical properties [11–22]. Certainly these studies have benefited from the recent advances in the characterization of the excited states of DNA/RNA building blocks, single strands and double strands, outlined in the present book. Yet it became clear that a number of structural parameters specific to G-quadruplexes play a key role both in photon absorption and in the fate of electronic excitations.

The purpose of this chapter is to highlight the specific behaviour of the G-quadruplexes under UV irradiation by focusing on structures formed by DNA strands. In Sect. 2 we present common features encountered in the photophysical properties of all the G-quadruplexes studied so far. On the one hand we compare their behaviour with that of non-interacting mono-nucleotides in order to reveal collective effects (exciton states, excited charge transfer states, energy transfer. . .).

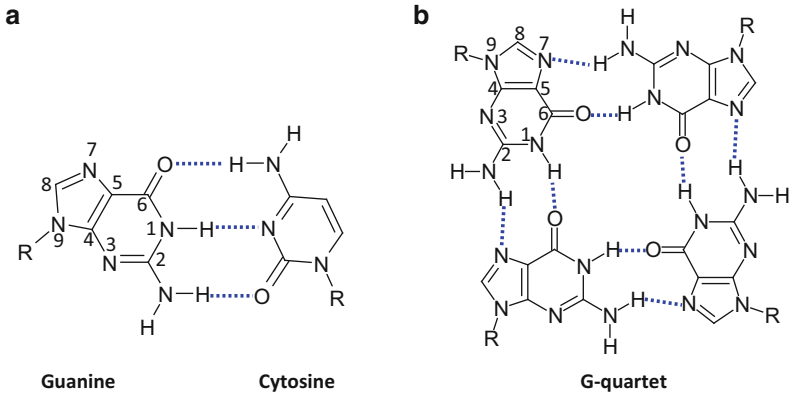

Fig. 1 Watson–Crick (**a**) and Hoogsteen (**b**) hydrogen bonding of guanines in duplexes and G-quadruplexes, respectively

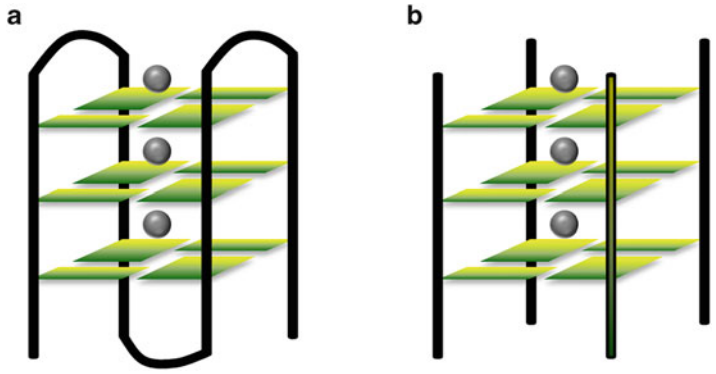

Fig. 2 Schematic representation of monomolecular (**a**) and tetramolecular (**b**) G-quadruplexes; *circles* represent the metal cations located in the central cavity

On the other, we discuss them in relation to single and double strands, emphasizing differences arising from Watson–Crick and Hoogsteen pairing of guanines (Fig. 1).

In Sect. 3 we focus on several structural parameters, specific to G-quadruplex assemblies. We examine how the number of tetrads, which may range from two to several hundreds in the so-called G4-wires [7, 23], affect their electronic excited states. We also tackle the effect of their topology. This is an important point because G-quadruplexes exhibit a remarkable polymorphism. They are usually formed by the folding of a single DNA strand (Fig. 2a) or by the association of two or four different single strands (Fig. 2b) [24, 25]. The number, the base sequence and the polarity of the constitutive strands are known to affect the relative

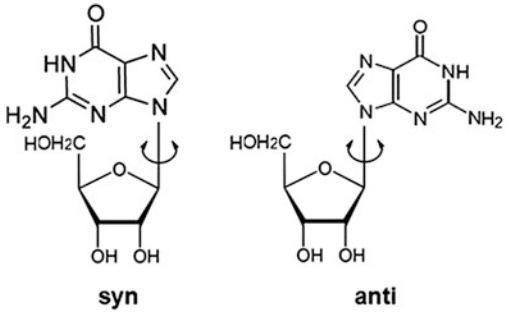

Fig. 3 Guanosine glycosidic *angles* in *syn* and *anti* conformation

orientation of tetrads which depends on the guanosine glycosidic angles (Fig. 3) [24]. Among various factors contributing to the G-quadruplex polymorphism, the metal cations located in their central cavity, essential to their stability, play a key role [1, 2, 26]. Therefore, hereafter we refer to a given G-quadruplex by indicating not only the base sequence of the constitutive strands but also the type of cations present within the structure.

2 General Features

2.1 Franck–Condon Excited States

The absorption spectra of G-quadruplexes differ substantially from those of non-interacting chromophores: the molar absorption coefficient per base decreases around the maximum but increases at the lower energy part of the spectrum. An example is shown in Fig. 4, where the spectrum of $d(TG_4T)_4/K^+$ is compared with that of the stoichiometric mixture of thymidine-5′-monophosphate (TMP) and 2′deoxyguanosine-5′-monophosphate (dGMP) [14, 19].

The hypochromism of DNA duplexes around their absorption maximum is well-known and largely exploited for recording their melting curves. Quantum chemistry calculations carried out for a few bases in single or double stranded arrangement have correlated this effect with charge transfer interactions among stacked bases [27–31]. So far, such calculations have not been performed for four-stranded architectures.

The hyperchromism of the red edge of the absorption spectrum, which may exceed 200%, is a typical feature of G-quadruplex structures. Hence, it was proposed to monitor their formation and their dissociation by following the absorbance at 295 nm [32]. This phenomenological effect was rationalized in a theoretical study performed on $d(G_3)_4/Na^+$ in the frame of the exciton theory combined to molecular dynamics simulations [16]. It was shown that the electronic coupling among dipolar electronic transitions of guanines gives rise to low-energy exciton states which are absent in model duplexes studied by the same methodology [33, 34]. Although the calculated

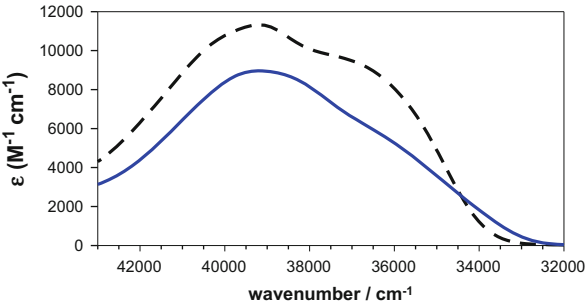

Fig. 4 Comparison of the absorption spectrum of the tetramolecular quadruplex d $(TG4T)_4/K^+$ (*solid line*) with that of the stoichiometric mixture of dGMP and TMP (*dashes*). The molar absorption coefficient ε is given per base

oscillator strength associated with the low-energy exciton states is very weak, it may however increase via vibronic coupling.

Another important conclusion drawn from the above-mentioned theoretical study [16] concerns the degree of delocalization of the exciton states. On average, those of $d(G_3)_4$ extent over 57% of the guanine residues, whereas only 28–29% of bases are coupled in the duplexes $d((GC)_5)\cdot d((GC)_5)$, $d(A_{10})\cdot d(T_{10})$ and $d((AT)_5)\cdot(d(AT)_5)$.

The exciton theory was also used to interpret circular dichroism (CD) spectra of G-quadruplexes [35, 36]. This approach provided evidence that their CD signals arise mainly from the chiral orientation of the adjacent quartets, depending on the glycosidic bond angles (*syn* or *anti*, Fig. 3), regardless of the orientation of the DNA strands.

2.2 Energy Transfer

The occurrence of energy transfer in G-quadruplexes was demonstrated by measuring their fluorescence anisotropy $r(t)$ on the femtosecond time scale [14, 19, 20]. As in the case of duplexes [37–40], the G-quadruplex anisotropy is lower than that of the stoichiometric mixture of non-interacting mono-nucleotides. This difference already appears in the initial $r(t)$ values and is continuously amplified on the examined time-domain.

An example is illustrated in Fig. 5a, b, where the fluorescence anisotropy traces recorded for $d(TG_4T)_4/K^+$ [20] and highly purified calf thymus DNA at 330 nm [40], close to the fluorescence maximum, are compared. Interestingly, at ca. 0.4 ps, the quadruplex anisotropy becomes lower than that of dGMP (0.16), showing that the $r(t)$ decrease is not simply due to the decay of thymine fluorescence whose anisotropy is close to 0.4 [41]. Molecular motions are too slow to account for such loss of anisotropy. In contrast, internal conversion among exciton states (intraband scattering), leading to excitation transfer among the various chromophores composing supramolecular systems, can be an ultrafast process [42–44]. We stress

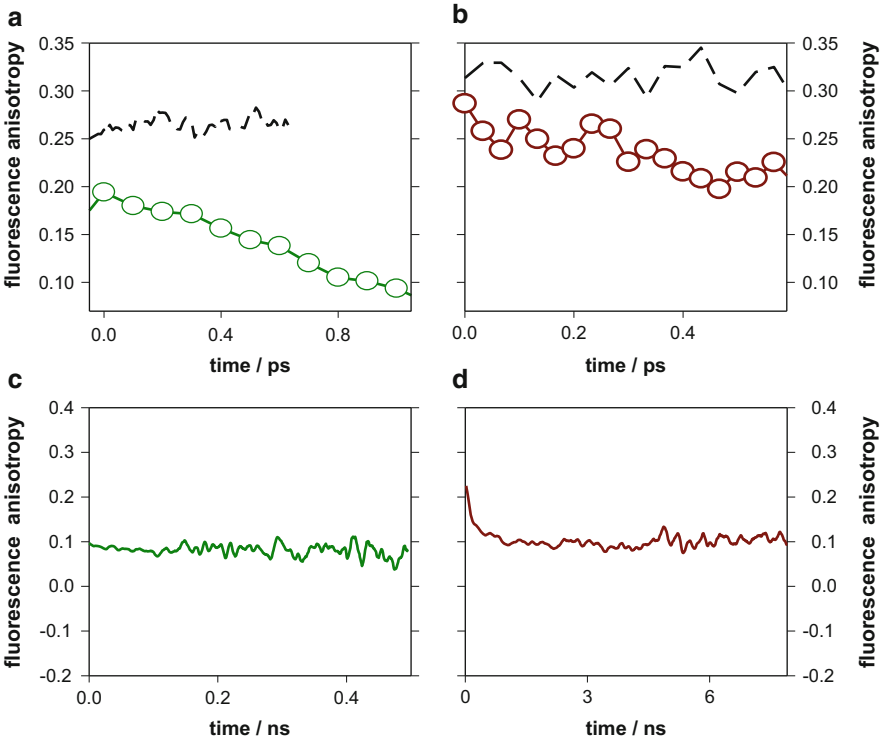

Fig. 5 Fluorescence anisotropy recorded at 330 nm for $d(TG_4T)_4/K^+$ (**a**, **c**) and highly purified calf thymus DNA (**b**, **d**), by fluorescence upconversion (**a**, **b**) and time-correlated single photon counting (**c**, **d**). *Dashes* correspond to stoichiometric mixtures of mono-nucleotides whose fluorescence lifetime does not exceed 0.5 ps. Excitation wavelength: 267 nm

that, given the very large Stokes shift characterizing the DNA mono-nucleotides [41], Förster energy transfer cannot take place on the femtosecond time scale.

At longer time scales the fluorescence anisotropy of both $d(TG_4T)_4/K^+$ [19] and calf thymus DNA [40] reaches a plateau close to 0.1 (Fig. 5c, d). This $r(t)$ value is consistent with in-plane depolarization of the fluorescence, i.e. absorption and emission transition dipoles randomly distributed perpendicular to an axis [45]. As the $\pi\pi^*$ transition vectors of the DNA bases are orthogonal to the G-quadruplex axis or the duplex axis, in-plane depolarization of their fluorescence suggests that the energy transfer process is completely randomized. The randomization process is much faster in G-quadruplexes (ca. 1 ps) [20] than in natural DNA (ca. 800 ps) [46]. This discrepancy is due to different mechanisms leading to energy transfer, as discussed in Sect. 2.3.

In addition to the time-resolved studies, energy transfer was also evidenced by probing the steady-state fluorescence of 8-(2-pyridyl)-deoxyguanosine, a strongly fluorescent guanosine derivative incorporated in G-quadruplex structures [17].

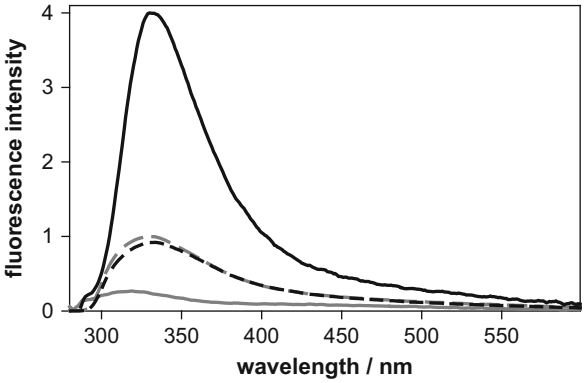

Fig. 6 Fluorescence spectra of $d(TG_4T)_4/K^+$ (*black*) and $d((GC)_3)\cdot d((GC))_3$ (*dark grey*). The spectra of the corresponding mixtures of mono-nucleotides are shown in *dashes*. Intensities are representative of the fluorescence quantum yields. Excitation wavelength: 267 nm

2.3 Emitting States

A common feature of all the G-quadruplexes studied so far is that the quantum yield (ϕ) of the $\pi\pi^*$ fluorescence in these structures is higher and its lifetime is longer than those of non-interacting mono-nucleotides. Such behaviour strongly contrasts with that observed upon Watson–Crick pairing of guanine with cytosine [47]. In GC double-stranded structures, $\pi\pi^*$ fluorescence is quenched [48–50], as shown in Fig. 6, where the emission spectrum of the G-quadruplex $d(TG_4T)_4/K^+$ [19] is compared to that of the duplex $d((GC)_3)\cdot d((GC)_3)$ [50]. From the fluorescence quantum yield and the fluorescence decays recorded by time-correlated single photon counting, where all the emitted photons are taken into account, it was concluded that the quenching efficiency in GC polymers exceeds two orders of magnitude. Gas phase ab initio calculations predicted that the relaxation of $\pi\pi^*$ excitations to the ground state should be accelerated in GC pairs, the process being promoted by electron coupled proton transfer involving the central hydrogen bond of Watson–Crick pairs [51, 52]. In contrast, TD-DFT studies performed for GC pairs in chloroform show the formation of low energy charge transfer states [53]. According to fluorescence measurements, if low energy charge transfer states are also formed in the case of GC duplexes in aqueous solution, their fluorescence quantum yield should be much lower than 10^{-5} [50].

The fluorescence spectra of GC double-stranded structures may exhibit a high energy band decaying on the nanosecond time scale [48]. Its maximum, its spectral width and the fluorescence lifetime vary with the number of base-pairs [50], suggesting that the emitting states are affected by the electronic coupling. As the fluorescence anisotropy is too low for $\pi\pi^*$ excitons, this emission band has been correlated with excited charge transfer states. The fingerprint of charge transfer states was also detected in the fluorescence spectra of G-quadruplexes (for details

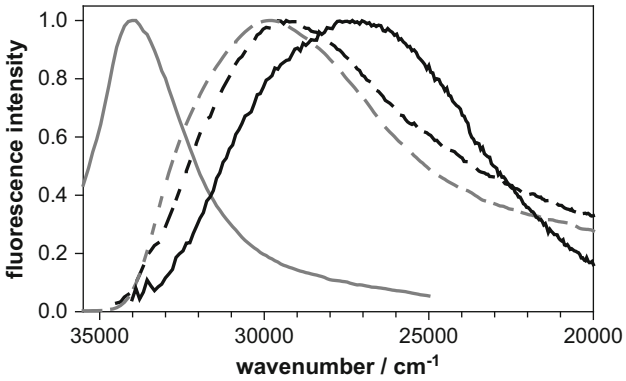

Fig. 7 Normalized fluorescence spectra of G4-wires/Na^+ (*black*) and duplexes polyd(GC)·polyd (GC) (*dark grey*) composed of 800–1,000 tetrads and base-pairs, respectively. The spectra of the corresponding non-interacting mono-nucleotides are shown in *dashes*. Excitation wavelength: 267 nm

see Sect. 3) but it appears at lower energy than that of the ππ* states. These opposite trends can be observed in Fig. 7, where the spectra of G-quadruplexes [16] and GC duplexes [48], composed of 800–1,000 tetrads and base pairs, respectively, are presented together with those of the stoichiometric mixtures of monomeric chromophores.

While emission of ππ* excitations is quenched in GC double-stranded structures, it is enhanced in homopolymeric AT duplexes [54], as well as in highly purified calf thymus DNA [46]. For both double-stranded structures, the steady-state fluorescence spectra are located in the same spectral domain as those of the constitutive mono-nucleotides and this is also the case for the G4-wires/K^+ [19] (Fig. 8).

The fluorescence quantum yield of poly(dA)·poly(dT) (3×10^{-4}) is three times higher and its fluorescence lifetime longer than those of an equimolar mixture of 2′-deoxyadenosine-5′-monophosphate (dAMP) and TMP. However, most of the duplex photons are still emitted at times shorter than 10 ps (Fig. 8). Similar trends are also observed for G4-wires/K^+ but they are much more pronounced: the fluorescence quantum yield is about one order of magnitude higher than that of dGMP and most of the photons are emitted on the sub-nanosecond time scale. The average radiative lifetimes, 7 and 91 ns for poly(dA)·poly(dT) and G4-wires/K^+, respectively, are longer than those of mono-nucleotides (2–3 ns [41]). The increase in the radiative lifetime of ππ* excited states suggests contribution to the fluorescence from exciton states with weak oscillator strength. This behaviour, much stronger for the G4-wires/K^+ compared to poly(dA)·poly(dT), is in line with the more important delocalization of the Franck–Condon excited states of G-quadruplexes compared to those of duplexes [16]. Thus, it appears that the rigidity of four-stranded structures should preserve exciton coherence for a longer time.

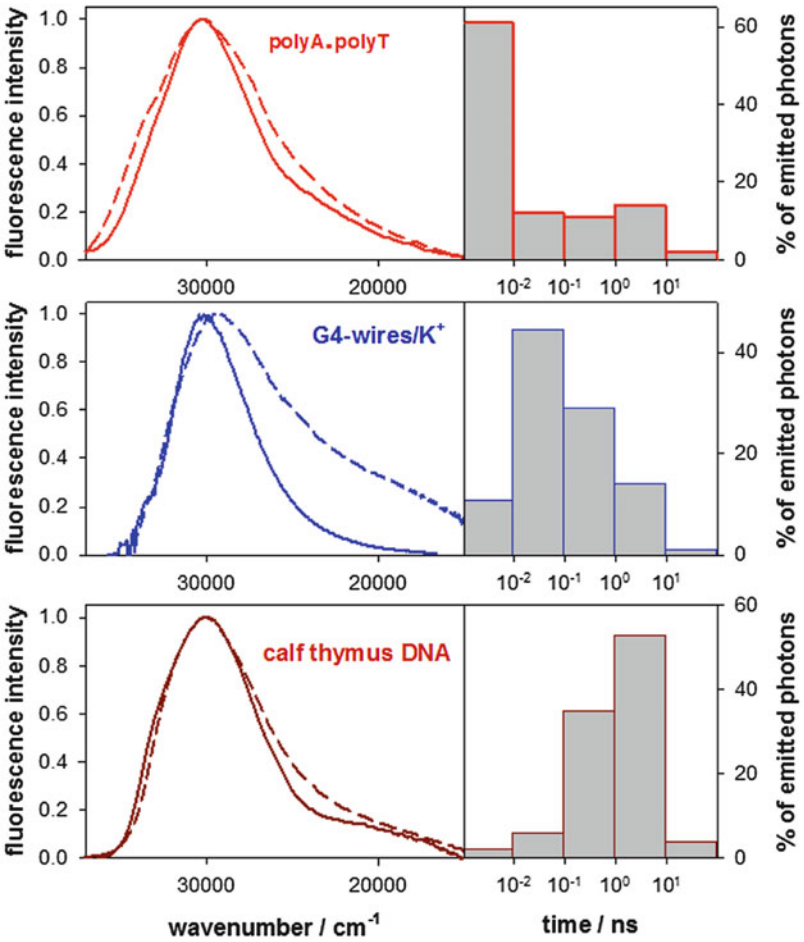

Fig. 8 *Left panels*: normalized fluorescence spectra of poly(dA)·poly(dT), G4-wires/K^+ and highly purified calf thymus DNA (*solid lines*). The spectra of the stoichiometric mixtures of mono-nucleotides are shown in *dashes*. *Right panels*: percentage of photons emitted by each polymer per decade of time at 330 nm. Excitation wavelength: 267 nm

Although the fluorescence quantum yield of natural DNA is the same as that of poly(dA)·poly(dT), we note that in Fig. 8 the largest portion of photons, accounting for the steady-state fluorescence spectrum, is emitted on a much longer time scale, in the nanosecond regime [46]. This implies that the mechanism underlying photon emission in natural DNA is quite different to that proposed for poly(dA)·poly (dT) and G4-wires/K^+[16, 55]. A complex pathway, involving trapping of $\pi\pi^*$ excitations by charge transfer states, followed by charge separation and charge recombination to excited $\pi\pi^*$ states, leading to delayed fluorescence, was invoked to explain the long-lived monomer-like fluorescence of calf thymus DNA [40]. The

overall process corresponds to energy transfer among bases which, due to its complexity, is much slower than energy transfer via exciton diffusion operative in G-quadruplexes (Fig. 8). This picture is supported by the temperature dependence of the fluorescence decays which are fitted with stretched exponentials associated with one-dimensional energy transfer [40].

3 Role of Structural Parameters

3.1 Size

The size effect on the electronic excitations in G-quadruplexes was systematically studied for a series of thymine capped tetramolecular structures $d(TG_nT)_4/K^+$ composed of three, four and five tetrads, whose fluorescence is largely dominated by emission from ππ* states [20]. The divergence of various spectral and dynamical parameters related to photon absorption and photon emission from those of the corresponding stoichiometric mixtures of mono-nucleotides was found to increase with the quadruplex size. It was therefore concluded that the presence of additional tetrads reinforces the collective nature of ππ* excitations. This concerns not only the Franck–Condon but also the emitting excited states, whose decay slows down when additional tetrads are present in the structure (Fig. 9).

The lengthening of the fluorescence lifetime of G-quadruplexes in comparison with that of non-interacting mono-nucleotides could simply originate from hindered intra-chromophore motions. Such motions are responsible for the ultrafast internal conversion to the ground state [56, 57]. In the case of guanine chromophores in aqueous solution, a key role is played by the flipping of the amino group at position 2 [58, 59], which corresponds precisely to Hoogsteen bonding (Fig. 1b). Yet this steric effect alone cannot explain the ensemble of fluorescence properties. In particular, the increase of the average radiative lifetime from 3 ns for dGMP to 10 ns for $d(TG_5T)_4/K^+$ shows a change in the nature of the emitting ππ* states, consistent with emission from exciton states, as previously mentioned for G4-wires/K^+.

One of the G-quadruplex properties whose deviation from the behaviour of non-interacting chromophores is amplified with increasing number of tetrads is the width (fwhm) of the fluorescence spectrum. For instance, a striking spectral narrowing larger than 40% is observed for G4-wires/K^+ (Fig. 8) [19, 20]. Numerous theoretical studies have focussed on the spectral shape of exciton states in H- or J-aggregates [60, 61]. Since G-quadruplexes display features of both types of aggregates, giving rise to intra-tetrad and inter-tetrad interactions, specific calculations devoted to these structures are needed in order to perform detailed spectral analysis.

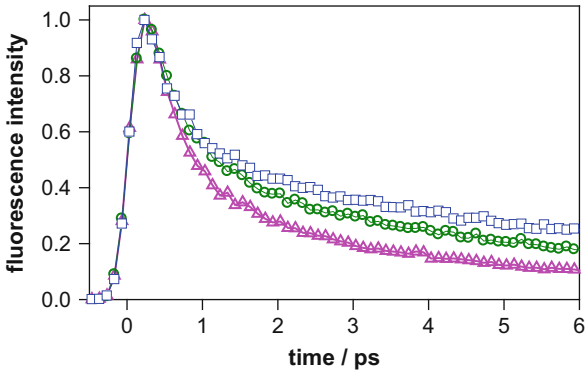

Fig. 9 Fluorescence decays recorded at 360 nm by fluorescence upconversion for $d(TG_3T)_4/K^+$ (*triangles*), $d(TG_4T)_4/K^+$ (*circles*) and $d(TG_5T)_4/K^+$ (*squares*). Excitation wavelength: 267 nm

3.2 Topology

Despite the qualitative agreement regarding the collective behaviour of ππ* excitations in $d(TG_nT)_4/K^+$ on the one hand and in G4-wires/K^+ on the other, a quantitative comparison of their properties is difficult. In addition to their different size, the topology of these two systems is not expected to be the same because the former are all composed of four parallel DNA strands whereas the latter are formed by folding of a single strand. As mentioned in Sect. 2.1, differences in the relative orientation between neighbouring tetrads should affect the strength of the electronic coupling and, consequently, the properties of the exciton states [62].

The effect of topology on the photophysical properties of G-quadruplexes was explicitly examined for mono-molecular structures formed by the human telomeric sequence d(GGGTTAGGGTTAGGGTTAGGG), denoted as Tel21 [63]. CD spectroscopy provided evidence that Tel21 displays topology similar to other relative telomeric sequences [64, 65] depending on the nature of cations. In the presence of Na^+, each tetrad contains two guanosines in *syn* conformation and another two in *anti* conformation (Fig. 3), giving rise to an "antiparallel basket" structure [66]. In the presence of K^+ cations, one tetrad contains three guanosines in *anti* conformation whereas the two other tetrads contain three guanines in *syn* conformation, resulting in equilibrium between two structures called "hybrid 1" and "hybrid 2" [67, 68].

The absorption spectra of Tel21/Na^+ and Tel21/K^+ exhibit subtle differences. They are better visualized by comparing the difference between the spectra recorded at 23°C and 96°C in the presence of each type of cation (Fig. 10). Heating up to 96°C leads to the complete dissociation of quadruplex structures. Thus, the differential absorbance spectra shown in Fig. 10 display the fingerprint of electronic coupling among ππ* transitions in the considered quadruplex structures. Both differential spectra exhibit a maximum around 34,000 cm^{-1} and a minimum at 37,500 cm^{-1} but their amplitude is larger in the case of Tel21/Na^+, suggesting that the basket topology favours delocalization of the Franck–Condon states.

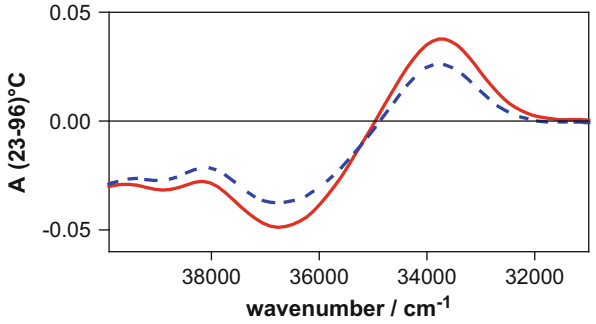

Fig. 10 Difference between the absorption spectra recorded at 23°C and 96°C for Tel21/Na^+ (*solid line*) and Tel21/K^+ (*dashed line*)

Based on the effect of topology on the Franck–Condon states, Webba da Silva and *coll*. proposed a classification of mono-molecular G-quadruplexes in three families exhibiting specific CD patterns [62, 69]. As the UV absorption spectra of each family also display specific features, these authors suggested using UV spectroscopy, which is easily accessible, for the determination of the quadruplex topology [62].

The fluorescence quantum yields of Tel21/K^+ (6.8×10^{-4}) and Tel21/Na^+ (8.7×10^{-4}) are higher than those of tetra-molecular G-quadruplexes with the same number of tetrads, d$(TG_3T)_4$/K^+ (3.2×10^{-4}). In addition, their fluorescence spectra, peaking at 340 nm (Tel21/K^+) and 360 nm (Tel21/Na^+), are clearly red-shifted in respect to that of non-interacting chromophores whose maximum is located at 330 nm (Fig. 11). Time-resolved experiments associated with theoretical studies are needed in order to elucidate whether this behaviour is related to emission from exciton states and/or charge transfer states (see Sect. 3.3). In any case, the presence of short loops holding together the tetrads is expected to increase the rigidity of the system, which favours the collective behaviour of ππ* states. The effect of the sequence and the length of the loops on the intrinsic fluorescence properties of mono-molecular G-quadruplexes were pointed out by Kwok et al. [22].

3.3 Metal Cations

Charge transfer in DNA is known to be influenced by metal ions [70]. Those located in the central cavity of G-quadruplexes were shown to intervene in the population of charge transfer states during excited state relaxation. The latter point was illustrated in the case of the tetra-molecular G-quadruplexes d$(TG_4T)_4$/K^+ and d$(TG_4T)_4$/Na^+ [19]. Two-dimensional NMR experiments performed for these structures could not detect any difference in the relative positions of their guanine residues [71]. In agreement with this finding, no difference was found either in the shape or in the intensity of their absorption spectra, which partly correspond to

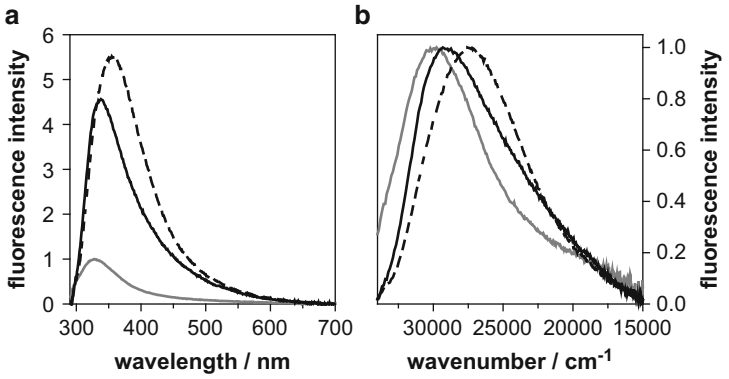

Fig. 11 Fluorescence spectra Tel21/K^+ (*solid lines*), Tel21/Na^+ (*dashed lines*) and the stoichiometric mixture of mono-nucleotides (*dark grey lines*). The spectra in (**a**) are representative of the fluorescence quantum yields whereas in (**b**) spectra are normalized. Excitation wavelength: 255 nm

exciton states, and, therefore, are sensitive to the arrangement of the monomeric chromophores.

Despite the similarity of the excited Franck–Condon states, the emitting states of $d(TG_4T)_4/K^+$ and $d(TG_4T)_4/Na^+$ exhibit important differences (Figs. 12 and 13). As mentioned before, the fluorescence spectrum of $d(TG_4T)_4/K^+$ is dominated by emission from ππ* states (Fig. 6). The intensity of the ππ* emission is substantially reduced in the $d(TG_4T)_4/Na^+$ spectrum where a shoulder around 420 nm is present (inset in Fig. 12).

Fluorescence upconversion measurements showed that the lifetime of the ππ* states is shorter in the presence of Na^+ compared to K^+ (Fig. 12a). The opposite trend is observed in the fluorescence decays recorded, in the red part of the spectrum by time correlated single photon counting (Fig. 12b).

As the photons associated with the low energy emission band of $d(TG_4T)_4/Na^+$ are emitted on the sub-nanosecond timescale, further information was obtained by measuring the wavelength dependence of the fluorescence anisotropy in the 100–500 ps range (Fig. 13). For both systems, $r(t)$ decreases with increasing wavelengths, but significantly larger variations are observed in the presence of Na^+ cations [19]. At the red edge of the fluorescence spectrum the anisotropy of $d(TG_4T)_4/Na^+$ becomes negative, whereas that of $d(TG_4T)_4/K^+$, although lower than that observed at 330 nm (Fig. 5), remains positive.

A mechanism involving motion of metal cations within the central cavity of G-quadruplexes was proposed to interpret the photophysical properties of $d(TG_nT)_4/K^+$ and $d(TG_nT)_4/Na^+$. The trapping of ππ* excitations by low energy charge transfer states would be facilitated by the presence of Na^+ cations, which, are smaller and, therefore, more mobile than K^+ cations. Larger shifts in the Na^+ position compared to that of K^+ during the excited state relaxation were indeed predicted by quantum chemistry calculations performed for two stacked guanine

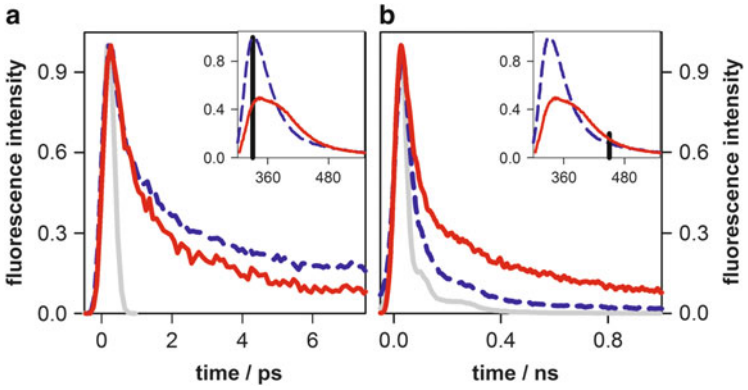

Fig. 12 Fluorescence decays recorded at 330 nm by fluorescence upconversion (**a**) and at 450 nm by time-correlated single photon counting (**b**) for $d(TG_4T)_4/Na^+$ (*solid lines*) and $d(TG_4T)_4/K^+$ (*dashed lines*). The steady-state fluorescence spectra are shown in the *insets*; the *vertical arrows* indicate the probed fluorescence wavelengths. Excitation wavelength: 267 nm

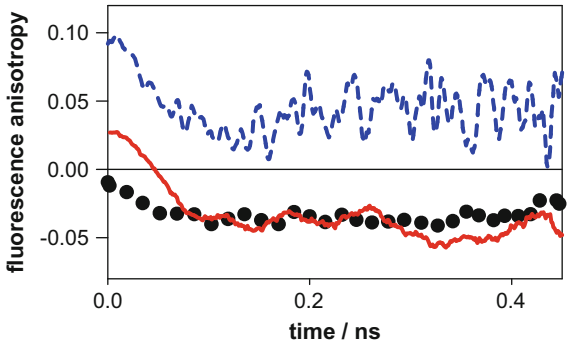

Fig. 13 Fluorescence anisotropy recorded by time-correlated single photon counting at 450 nm for $d(TG_3T)_4/K^+$ (*dashed line*), $d(TG_3T)_4/Na^+$ (*solid line*) and the single strand $d(A_{20})$ (*dotted line*)

tetrads [19]. We stress that no difference in the fluorescence properties of single and double strands is detected when Na^+ or K^+ cations are present in solution [48, 72].

Interestingly, in this spectral region, the fluorescence anisotropy of the single strand $d(A_{20})$, whose fluorescence also contains a band peaking at 420 nm [73], exhibits the same negative anisotropy as $d(TG_nT)_4/Na^+$ (Fig. 13). Negative anisotropy observed upon excitation of $\pi\pi^*$ states has been associated with charge transfer transitions involving orbital overlap among stacked bases whose polarization is located out of the aromatic plane of the bases [19, 73].

The nature of metal ions is known to affect the topology of mono-molecular G-quadruplexes and, therefore, the properties of their Franck–Condon excited states. It is thus difficult to assign their role in the excited state relaxation of such quadruplex structures. Yet it is worth-noting that the fluorescence spectra of G4-wires/Na^+ and Tel21/Na^+ are red-shifted compared to those of G4-wires/K^+ and Tel21/K^+, respectively.

4 Conclusions and Outlook

The collective behaviour of electronic excitations in G-quadruplexes formed by DNA strands is more pronounced than in DNA duplexes. This is due to the specific architecture of G-quadruplexes structures, consisting of a vertical stacking of guanine tetrads, and the resulting rigidity. Both in double- and four-stranded structures, the population of exciton states gives rise to ultrafast energy transfer, but only in G-quadruplexes is the transfer process completely randomized within 1 ps, as attested by the in-plane depolarization of the fluorescence. In contrast to Watson–Crick pairing of guanines with cytosines, which leads to quenching of ππ* fluorescence, the self-association of guanines in G-quadruplexes slows down the non-radiative decay processes of ππ* states. The concomitant increase of the average radiative lifetime indicates the contribution of exciton states to the ππ* fluorescence. This effect is particularly strong for mono-molecular G-quadruplexes with short side loops. The relaxation of ππ* states toward lower energy charge transfer states involving guanines on different tetrads depends on the nature cations in the central cavity; it is facilitated by Na^+ ions, which are smaller and more mobile compared to K^+ ions.

The picture described above was derived from a relatively small number of photophysical studies. Yet it became clear, despite some features shared by all G-quadruplex structures, that their rich polymorphism does affect the properties of their excited states. Detailed examination of key factors, such as the base sequence in the loops, is necessary in order to obtain a better understanding of the process involved. Evidently, experimental studies need to be accompanied by theoretical work. Modelling the fate of electronic excitations in G-quadruplexes constitutes a real challenge.

From the biological point of view, it would be interesting to explore the direct damage generated in G-quadruplexes upon absorption of UV radiation. In this respect, Brash and colleagues reported hypersensitivity of telomeres regarding the formation of UV-induced cyclobutane dimers and evoked possible correlation with four-stranded structures [74]. Furthermore, Taylor and colleagues detected cyclobutane dimers with unusual conformations in quadruplex structures formed by the human telomeric sequence TTAGGG [75]. However, these reactions concern thymines, which are present in the loops, and probably arise more from steric factors than electronic ones. The photoreactivity proper to guanines, whose excited states are greatly modified within four-stranded structures, has not been tackled so far. Moreover, the photoinduced oxidative damage of guanines, expected to be facilitated by stacking, deserves particular attention [76, 77].

The properties of the electronic excited states reported here concern quadruplexes formed by natural DNA bases. Their replacement by guanine analogues absorbing at longer wavelengths may be required in order to explore their potential applications in the field of molecular electronics or optoelectronics. In this perspective, the findings on “natural” quadruplexes provide some rules for the design of similar supramolecular architectures. For example, tuning between ππ* and charge transfer states by an appropriate choice of the cations in the

central cavity whose aperture could be modulated so as to enhance or reduce cation mobility.

Acknowledgment The French National Agency for Research (ANR-12-BS08-0001-01) is acknowledged for financial support.

References

1. Huppert JL (2008) Four-stranded nucleic acids: structure, function and targeting of G-quadruplexes. Chem Soc Rev 37:1375–1384
2. Neidle S (2009) The structures of quadruplex nucleic acids and their drug complexes. Curr Opin Struct Biol 19:239–250
3. Biffi G, Tannahill D, McCafferty J, Balasubramanian S (2013) Quantitative visualization of DNA G-quadruplex structures in human cells. Nat Chem 5:182–186
4. De Cian A, Lacroix L, Douarre C, Temime-Smaali N, Trentesaux C, Riou JF, Mergny JL (2008) Targeting telomeres and telomerase. Biochimie 90:131–155
5. Ruden M, Puri N (2013) Novel anticancer therapeutics targeting telomerase. Cancer Treat Rev 39:444–456
6. Neidle S, Parkinson G (2002) Telomere maintenance as a target for anticancer drug discovery. Nat Rev Drug Discov 1:383–393
7. Borovok N, Iram N, Zikich D, Ghabboun J, Livshits GI, Porath D, Kotlyar AB (2008) Assembling of G-strands into novel tetra-molecular parallel G4-DNA nanostructures using avidinbiotin recognition. Nucleic Acids Res 36:5050–5060
8. Liu SP, Weisbrod SH, Tang Z, Marx A, Scheer E, Erbe A (2010) Direct measurement of electrical transport through G-quadruplex DNA with mechanically controllable break junction electrodes. Angew Chem Int Ed 49:3313–3316
9. Lee JB, Campolongo MJ, Kahn JS, Roh YH, Hartman MR, Luo D (2010) DNA-based nanostructures for molecular sensing. Nanoscale 2:188–197
10. Chaires BJ, Graves D (eds) (2013) Quadruplex nucleic acids, vol 330. Top Curr Chem Springer
11. Markovitsi D, Gustavsson T, Sharonov A (2004) Cooperative effects in the photophysical properties of self-associated triguanosine diphosphates. Photochem Photobiol 79:526–530
12. McGovern DA, Quinn S, Doorley GW, Whelan AM, Ronayne KL, Towrie M, Parker AW, Kelly JM (2007) Picosecond infrared probing of the vibrational spectra of transients formed upon UV excitation of stacked G-tetrad structures. Chem Commun 5158–5160
13. Gepshtein R, Huppert D, Lubitz I, Amdursky N, Kotlyar AB (2008) Radiationless transitions of G4 wires and dGMP. J Phys Chem C 112:12249–12258
14. Miannay FA, Banyasz A, Gustavsson T, Markovitsi D (2009) Excited states and energy transfer in G-quadruplexes. J Phys Chem C 113:11760–11765
15. Mendez MA, Szalai VA (2009) Fluorescence of unmodified oligonucleotides: a tool to probe G-quadruplex DNA structure. Biopolymers 91:841–850
16. Changenet-Barret P, Emanuele E, Gustavsson T, Improta R, Kotlyar AB, Markovitsi D, Vaya I, Zakrzewska K, Zikich D (2010) Optical properties of guanine nanowires: experimental and theoretical study. J Phys Chem C 114:14339–14346
17. Dumas A, Luedtke NW (2010) Cation-mediated energy transfer in G-quadruplexes revealed by an internal fluorescent probe. J Am Chem Soc 132:18004–18007
18. Dao NT, Haselsberger R, Michel-Beyerle ME, Phan AT (2011) Following G-quadruplex formation by its intrinsic fluorescence. FEBS Lett 585:3969–3977
19. Hua Y, Changenet-Barret P, Improta R, Vayá I, Gustavsson T, Kotlyar AB, Zikich D, Šket P, Plavec J, Markovitsi D (2012) Cation effect on the electronic excited states of guanine

nanostructures studied by time-resolved fluorescence spectroscopy. J Phys Chem C 116:14682–14689
20. Hua Y, Changenet-Barret P, Gustavsson T, Markovitsi D (2013) The effect of size on the optical properties of guanine nanostructures: a femtosecond to nanosecond study. Phys Chem Chem Phys 15:7396–7402
21. Dao NT, Haselsberger R, Michel-Beyerle ME, Phan AT (2013) Excimer formation by stacking G-Quadruplex blocks. ChemBioChem 1–5
22. Kwok CK, Sherlock ME, Bevilacqua PC (2013) Effect of loop sequence and loop length on the intrinsic fluorescence of G-quadruplexes. Biochemistry 52:3019–3021
23. Kotlyar AB, Borovok N, Molotsky T, Cohen H, Shapir E, Porath D (2005) Long, monomolecular guanine-based nanowires. Adv Mater 17:1901–1905
24. Burge S, Parkinson GN, Hazel P, Todd AK, Neidle S (2006) Quadruplex DNA: sequence, topology and structure. Nucleic Acids Res 34:5402–5415
25. Mergny JL, Gros J, De Cian A, Bourdoncle A, Rosu F, Sacca B, Guitatat L, Amrane S, Mills M, Alberti P, Takasugi M, Lacroix L (2006) Energetics, kinetics and dynamics of quadruplex folding. In: Neidle S, Balasubramanian S (eds) Quadruplex nucleic acids. RSC Publishing, Cambridge
26. Qin Y, Hurley LH (2008) Structures, folding patterns, and functions of intramolecular DNA G-quadruplexes found in eukaryotic promoter regions. Biochimie 90:1149–1171
27. Starikov EB (2004) Importance of charge transfer excitations in DNA electron spectrum: a ZINDO semiempirical quantum-chemical study. Mod Phys Lett B 18:825–831
28. Varsano D, Di Felice R, Marques MAL, Rubio A (2006) A TDDFT study of the excited states of DNA bases and their assemblies. J Phys Chem B 110:7129–7138
29. Santoro F, Barone V, Improta R (2009) Excited states decay of the A-T DNA: a PCM/TD-DFT study in aqueous solution of the (9-methyl-adenine) 2 (1-methyl-thymine) 2 stacked tetramer. J Am Chem Soc 131:15232–15245
30. Lange AW, Herbert JM (2009) Both intra- and interstrand charge-transfer excited states in aqueous B-DNA are present at energies comparable to, or just above, the $^1\pi\pi^*$ excitonic bright states. J Am Chem Soc 131:3913–3922
31. Plasser F, Aquino AJA, Hase WL, Lischka H (2012) UV absorption spectrum of alternating DNA duplexes. Analysis of excitonic and charge transfer interactions. J Phys Chem A 116:11151–11160
32. Mergny JL, Phan AT, Lacroix L (1998) Following G-quartet formation by UV-spectroscopy. FEBS Lett 435:74–78
33. Bouvier B, Dognon JP, Lavery R, Markovitsi D, Millié P, Onidas D, Zakrzewska K (2003) Influence of conformational dynamics on the exciton states of DNA oligomers. J Phys Chem B 107:13512–13522
34. Emanuele E, Zakrzewska K, Markovitsi D, Lavery R, Millie P (2005) Exciton states of dynamic DNA double helices: alternating dCdG sequences. J Phys Chem B 109:16109–16118
35. Masiero S, Trotta R, Pieraccini S, De Tito S, Perone R, Randazzo A, Spada GP (2010) A non-empirical chromophoric interpretation of CD spectra of DNA G-quadruplex structures. Org Biomol Chem 8:2683–2692
36. Randazzo A, Spada GP, Webba da Silva M (2013) Circular dichroism of quadruplex structures. Top Curr Chem 330:67–86
37. Markovitsi D, Onidas D, Gustavsson T, Talbot F, Lazzarotto E (2005) Collective behavior of Franck–Condon excited states and energy transfer in DNA double helices. J Am Chem Soc 127:17130–17131
38. Miannay FA, Banyasz A, Gustavsson T, Markovitsi D (2007) Ultrafast excited state deactivation and energy transfer in guanine-cytosine DNA double helices. J Am Chem Soc 129:14574–14575
39. Onidas D, Gustavsson T, Lazzarotto E, Markovitsi D (2007) Fluorescence of the DNA double helices $(dAdT)_n$. $(dAdT)_n$ studied by femtosecond spectroscopy. Phys Chem Chem Phys 9:5143–5148
40. Vayá I, Gustavsson T, Douki T, Berlin Y, Markovitsi D (2012) Electronic excitation energy transfer between nucleobases of natural DNA. J Am Chem Soc 134:11366–11368

41. Onidas D, Markovitsi D, Marguet S, Sharonov A, Gustavsson T (2002) Fluorescence properties of DNA nucleosides and nucleotides: a refined steady-state and femtosecond investigation. J Phys Chem B 106:11367–11374
42. Sundstrom V, Pullerits T, van Grondelle R (1999) Photosynthetic light-harvesting: reconciling dynamics and structure of purple bacterial LH2 reveals function of photosynthetic unit. J Phys Chem B 103:2327–2346
43. Kennis JTM, Gobets B, van Stokkum IHM, Dekker JP, van Grondelle R, Fleming GR (2001) Light harvesting by chlorophylls and carotenoids in the photosystem I core complex of Synechococcus elongatus: a fluorescence upconversion study. J Phys Chem B 105:4485–4494
44. Zigmantas D, Read EL, Mancal T, Brixner T, Gardiner AT, Cogdell RJ, Fleming GR (2006) Two-dimensional electronic spectroscopy of the B800-B820 light-harvesting complex. Proc Natl Acad Sci U S A 103:12672–12677
45. Albrecht AC (1961) Polarizations and assignments of transitions – method of photoselection. J Mol Spectrosc 6:84–108
46. Vayá I, Gustavsson T, Miannay FA, Douki T, Markovitsi D (2010) Fluorescence of natural DNA: from the femtosecond to the nanosecond time-scales. J Am Chem Soc 132:11834–11835
47. Schwalb N, Temps F (2007) Ultrafast electronic excitation in guanosine is promoted by hydrogen bonding with cytidine. J Am Chem Soc 129:9272–9273
48. Vayá I, Miannay FA, Gustavsson T, Markovitsi D (2010) High energy long-lived excited states in DNA double strands. ChemPhysChem 11:987–989
49. Vayá I, Changenet-Barret P, Gustavsson T, Zikich D, Kotlyar A, Markovitsi D (2010) Long-lived fluorescence of homopolymeric guanine-cytosine DNA duplexes. Photochem Photobiol Sci 9:1193–1195
50. Brazard J, Thazhathveetil A, Vayá I, Lewis F, Gustavsson T, Markovitsi D (2013) Electronic excited states of guanine-cytosine hairpins and duplexes studied by fluorescence spectroscopy. Photochem Photobiol Sci 12:1453–1459
51. Sobolewski AL, Domcke W, Hattig C (2005) Tautomeric selectivity of the excited-state lifetime of guanine/cytosine base pairs: the role of electron-driven proton-transfer processes. Proc Natl Acad Sci U S A 102:17903–17906
52. Groenhof G, Schäfer LV, Boggio-Pasqua M, Goette M, Grubmüller H, Robb MA (2007) Ultrafast decactivation of an excited cytosine guanine base pair in DNA. J Am Chem Soc 129:6812–6819
53. Biemann L, Kovalenko SA, Kleinermanns K, Mahrwald R, Markert M, Improta R (2011) Excited state proton transfer is not involved in the ultrafast deactivation of guanine-cytosine pair in solution. J Am Chem Soc 133:19664–19667
54. Onidas D, Gustavsson T, Lazzarotto E, Markovitsi D (2007) Fluorescence of the DNA double helix (dA)20. (dT)20 studied by femtosecond spectroscopy – effect of the duplex size on the properties of the excited states. J Phys Chem B 111:9644–9650
55. Markovitsi D, Gustavsson T, Talbot F (2007) Excited states and energy transfer among DNA bases in double helices. Photochem Photobiol Sci 6:717–724
56. Gustavsson T, Improta R, Markovitsi D (2010) DNA/RNA: building blocks of life under UV irradiation. J Phys Chem Lett 1:2025–2030
57. Kleinermanns K, Nachtigallová D, de Vries MS (2013) Excited state dynamics of DNA bases. Int Rev Phys Chem. doi:10.1080/0144235X.0142012.0760884
58. Karunakaran V, Kleinermanns K, Improta R, Kovalenko SA (2009) Photoinduced dynamics of guanosine monophosphate in water from broad-band transient absorption spectroscopy and quantum-chemical calculations. J Am Chem Soc 131:5839–5850
59. Miannay FA, Gustavsson T, Banyasz A, Markovitsi D (2010) Excited state dynamics of deoxy-guanosine monophosphate dGMP measured by steady-state and femtosecond fluorescence spectroscopy. J Phys Chem A 114:3256–3263
60. Kasha M, Rawls HR, El-Bayoumi MA (1965) The exciton model in molecular spectroscopy. Pure Appl Chem 11:371–392
61. Spano FC (2010) The spectral signatures of Frenkel polarons in H- and J-aggregates. Acc Chem Res 43:429–439

62. Karsisiotis AI, Hessari NM, Novellino E, Spada GP, Randazzo A, da Silva MW (2011) Topological characterization of nucleic acid G-quadruplexes by UV absorption and circular dichroism. Angew Chem Int Ed 50:10645–10648
63. Hua Y (2013) Self-associated gunanine structures studied by time-resolved optical spectroscopy. Université de Paris Sud, Orsay
64. Viglasky V, Tluckova K, Bauer L (2011) The first derivative of a function of circular dichroism spectra: biophysical study of human telomeric G-quadruplex. Eur Biophys J 40:29–37
65. Manet I, Manoli F, Zambelli B, Andreano G, Masi A, Cellai L, Monti S (2011) Affinity of the anthracycline antitumor drugs Doxorubicin and Sabarubicin for human telomeric G-quadruplex structures. Phys Chem Chem Phys 13:540–551
66. Wang Y, Patel DJ (1993) Solution structure of the human telomeric repeat d[$AG_3(T_2AG_3)_3$] G-tetratraplex. Structure 1:263–282
67. Luu KN, Phan AT, Kuryavyi V, Lacroix L, Patel DJ (2006) Structure of the human telomere in K^+ solution: an intramolecular (3+1) G-quadruplex scaffold. J Am Chem Soc 128:9963–9970
68. Phan AT, Kuryavyi V, Luu KN, Patel DJ (2007) Structure of two intramolecular G-quadruplexes formed by natural human telomere sequences in K^+ solution. Nucleic Acids Res 35:6517–6525
69. da Silva MW, Trajkovski M, Sannohe Y, Hessari NM, Sugiyama H, Plavec J (2009) Design of a G-quadruplex topology through glycosidic bond angles. Angew Chem Int Ed 48:9167–9170
70. Barnett RN, Cleveland CL, Joy A, Landman U, Schuster GB (2001) Charge migration in DNA: ion-gated transport. Science 294:567–571
71. Sket P, Plavec J (2010) Tetramolecular DNA quadruplexes in solution: insights into structural diversity and cation movement. J Am Chem Soc 132:12724–12732
72. Banyasz A, Vayá I, Changenet-Barret P, Gustavsson T, Douki T, Markovitsi D (2011) Base-pairing enhances fluorescence and favors cyclobutane dimer formation induced upon absorption of UVA radiation by DNA. J Am Chem Soc 133:5163–5165
73. Banyasz A, Gustavsson T, Onidas D, Changenet-Barret P, Markovitsi D, Importa R (2013) Multi-pathway excited state relaxation of adenine oligomers in aqueous solution: a joint theoretical and experimental study. Chem Eur J. doi:10.1002/chem.201202741
74. Rochette P, Brash D (2010) Human telomers are hypersensitive to UV-induced DNA damage and refractory to repair. PLoS Genet 6:e1000926
75. Su DGT, Fang HF, Gross ML, Taylor JSA (2009) Photocrosslinking of human telomeric G-quadruplex loops by anti cyclobutane thymine dimer formation. Proc Natl Acad Sci U S A 106:12861–12866
76. Colson AO, Sevilla MD (1995) Elucidation of primary radiation damage in DNA through Application of ab initio molecular orbital theory. Int J Radiat Biol 67:627–645
77. Kim NJ, Jeong G, Sung J, Kim YS, Park YD (2000) Resonant two-photon ionization and laser induced fluorescence spectroscopy of jet cooled adenine. J Chem Phys 113:10051–10055

Top Curr Chem (2015) 356: 203–248
DOI: 10.1007/128_2014_531

Published online: 3 April 2014

Physiological Aspects of UV-Excitation of DNA

Richa, Rajeshwar P. Sinha, and Donat-P. Häder

Abstract Solar ultraviolet (UV) radiation, mainly UV-B (280–315 nm), is one of the most potent genotoxic agents that adversely affects living organisms by altering their genomic stability. DNA through its nucleobases has absorption maxima in the UV region and is therefore the main target of the deleterious radiation. The main biological relevance of UV radiation lies in the formation of several cytotoxic and mutagenic DNA lesions such as cyclobutane pyrimidine dimers (CPDs), 6-4 photoproducts (6-4PPs), and their Dewar valence isomers (DEWs), as well as DNA strand breaks. However, to counteract these DNA lesions, organisms have developed a number of highly conserved repair mechanisms such as photoreactivation, excision repair, and mismatch repair (MMR). Photoreactivation involving the enzyme photolyase is the most frequently used repair mechanism in a number of organisms. Excision repair can be classified as base excision repair (BER) and nucleotide excision repair (NER) involving a number of glycosylases and polymerases, respectively. In addition to this, double-strand break repair, SOS response, cell-cycle checkpoints, and programmed cell death (apoptosis) are also operative in various organisms to ensure genomic stability. This review concentrates on the UV-induced DNA damage and the associated repair mechanisms as well as various damage detection methods.

Keywords Cyclobutane-pyrimidine dimers · Excision repair · Photoreactivation · Recombinational repair · Ultraviolet radiation

Richa and R.P. Sinha
Laboratory of Photobiology and Molecular Microbiology, Centre of Advanced Study in Botany, Banaras Hindu University, Varanasi 221005, India

D.-P. Häder (✉)
Emeritus from Dept. Biology, Friedrich-Alexander University, Erlangen, Germany
e-mail: donat@dphaeder.de

Contents

Abbreviations

6-4PPs	Pyrimidine (6-4) pyrimidone photoproducts
8-AIA	8-(5-Aminoimidazol-4-yl)adenine
8-HDF	8-Hydroxy-5-deaza-riboflavin
8-oxo-Ade	8-Oxo-7,8-dihydroadenine
8-oxoGua	8-Oxo-7,8-dihydroguanine
ATM protein	Ataxia telangiectasia mutated protein
BER	Base excision repair
CAT	Catalase
CCs	Chlorocarbons
CFCs	Chlorofluorocarbons
CPDs	Cyclobutane pyrimidine dimers
DEWs	Dewar valence isomers
DGPY	4,6-Diamino-5-guanidinopyrimidine
DP	DNA polymerase
dRPase	Deoxyribophosphodiesterase
DSB	Double strand break
FAD	Flavin-adenine dinucleotide
FADU	Fluorometric analysis of DNA unwinding
FapyGua	2,6-Diamino-4-hydroxy-5-formamidopurine
FEN	1-Flap endonuclease-1
FISH	Fluorescence in situ hybridization
GG-NER	Global genome NER
HR	Homologous recombination
IC-PCR	Immunocoupled polymerase chain reaction
LP-BER	Long-patch BER
MMR	Mismatch repair
MTHF	5,10-Methenyltetrahydrofolate
NADPH	Nicotinamide adenine dinucleotide phosphate
NER	Nucleotide excision repair

NHEJ	Non-homologous end joining
OBs	Organobromides
PIKKs	Phosphatidylinositol-3 (PI3)-kinase related kinases
POD	Peroxidase
RAPD	Random amplified polymorphic DNA
RIA	Radio-immunoassay
ROS	Reactive oxygen species
RPA	Replication protein A
SINE	Short interspersed DNA element
SOD	Superoxide dismutase
SP-BER	Short-patch BER
SSB	Single strand break
TBP	TATA-box binding protein
TC-NER	Transcription-coupled NER
TD-PCR	Terminal transferase-dependent PCR
TFIIH	Transcription factor-IIH
Top1	Topoisomerase I
TRCF	Transcription-repair coupling factor
UV-DDB	UV-damaged DNA binding protein
UVR	Ultraviolet radiation
XPV	Xeroderma pigmentosum variant

1 Introduction

The effect of harmful ultraviolet radiation (UVR; 280–400 nm) particularly ultraviolet-B (UV-B; 280–315 nm) at the Earth's surface atmosphere has increased in the past few decades due to depletion of the stratospheric ozone layer caused by increased release of atmospheric pollutants such as chlorofluorocarbons (CFCs), chlorocarbons (CCs), and organobromides (OBs). It has been shown that substantial amounts of reactive nitrogen species (RNS) such as nitric oxide, nitrous oxide, and peroxynitrite, produced naturally or from anthropogenic sources such as biomass or fuel burnings, may also contribute to the depletion of the ozone layer [1]. Solar UV radiation is responsible for a wide range of biological effects including alteration in the structure of proteins, DNA, and many other biologically important molecules, chronic depression of key physiological processes, and acute physiological stress leading either to reduction in growth and cell division, pigment bleaching, N_2 fixation, and energy production, or to photoinhibition of photosynthesis in several organisms [2, 3]. It has been documented that UV-B severely affects survival, fecundity, and sex-ratio in several intertidal copepods [4].

The high-energetic UV-B radiation constituting $<1\%$ of the total solar irradiance may affect normal states of life either through direct effects on cellular DNA or indirectly by the production of reactive oxygen species (ROS) [5, 6] in various living systems including bacteria [7], cyanobacteria [8], phytoplankton [9],

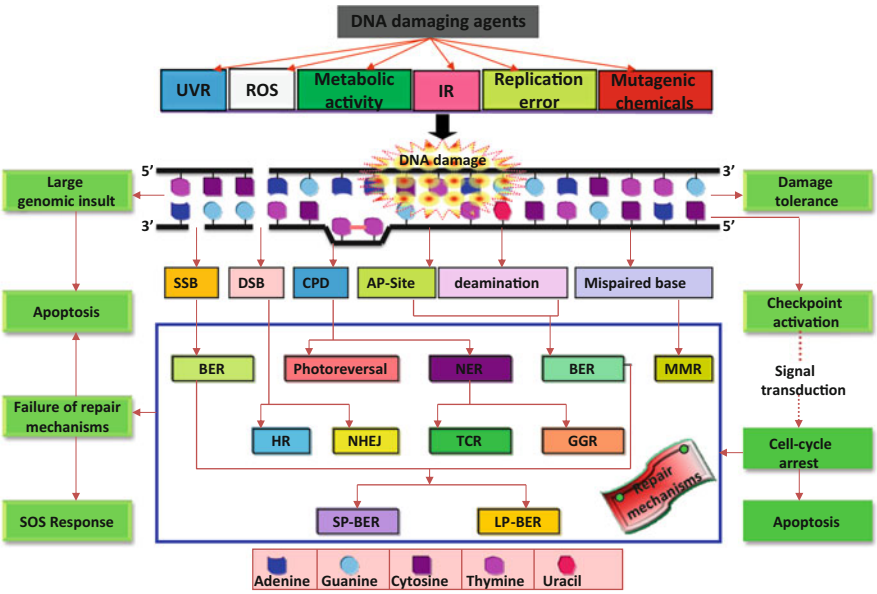

Fig. 1 DNA lesions produced by different damaging agents and the possible repair mechanisms to ensure genomic stability

macroalgae [10], plants [11], animals, and humans. In contrast, UV-A (315–400 nm) radiation, which is not absorbed directly by the native DNA, can still induce DNA damage either by producing a secondary photoreaction of existing DNA photoproducts or via indirect photosensitizing reactions [12].

To counteract the deleterious effects of UVR, mainly UV-B, a number of organisms have evolved certain defensive mechanisms such as avoidance, scavenging of reactive oxygen species (ROS) by enzymatic and non-enzymatic antioxidants like catalase (CAT), superoxide dismutase (SOD), peroxidase (POD), carotenoids, etc. and synthesis of UV-absorbing/screening compounds (mycosporine-like amino acids, scytonemin, parietin, melanin, etc.) [13–16]. However, these mitigating strategies are not highly efficient in completely preventing deleterious UV-B from reaching the DNA in the superficial tissue layers [17]. However, the emergence of certain highly specific and conserved repair and resynthesis mechanisms like, photoreactivation, excision repair, mismatch repair (MMR), double strand break (DSB) repair, and certain other mechanisms like damage tolerance (dimer bypass), SOS (save our soul) response, checkpoint activation, and programmed cell death (PCD) or apoptosis (Fig. 1) that efficiently remove DNA lesions make it possible to ensure genomic integrity [18–20].

2 UV-Induced DNA Damage

DNA damage is induced by a number of endogenous factors such as free radicals as well as exogenous factors like UV radiation, ionizing radiations, and genotoxic chemicals, thereby affecting the normal life processes of all living organisms. Several types of DNA damage that have been identified result in misincorporation of bases during the replication process and hydrolytic damage, resulting in deamination of bases, depurination, and depyrimidination [21]. DNA can be oxidatively damaged [22] by direct interaction with ionizing radiation (IR) or by UV radiation-induced free radicals or reactive oxygen species [23]. Alkylating agents may also modify DNA bases, resulting in DNA damage [21, 24]. DNA damage as a result of UVR exposure is known to be one of the initiating factors in photocarcinogenesis [25]. In irradiated cells, DNA acts as a chromophore, directly absorbing photons of UVR, thereby resulting in the formation of mutagenic DNA lesions [26]. The highly energetic UV-B radiation induces three major cytotoxic and lethal pyrimidine photoproducts such as cyclobutane pyrimidine dimers (CPDs), pyrimidine (6-4) pyrimidone photoproducts (6-4PPs), and their Dewar isomers [20, 27, 28]. The generation of pyrimidine (6-4) pyrimidone photoproducts (6-4PPs) is rationalized in terms of a Paternò–Büchi reaction by a [2 + 2] cycloaddition between the C5–C6 double bond of the 5′-end base and the C4 carbonyl group of a 3′-end pyrimidine. CPD, the most abundant and cytotoxic DNA lesion, is a four-membered rigid ring structure involving C5 and C6 of the adjacent bases, whereas 6-4PPs are formed by a noncyclic bond between C6 (of the 5′-end) and C4 (of the 3′-end) of the involved pyrimidines via spontaneous rearrangement of the oxetane (when the 3′-end is thymine) or azetidine (when the 3′-end is cytosine) intermediates [29]. The 6-4PPs are photoisomerized into their Dewar valence isomers (DEWs) upon exposure to wavelengths greater than 290 nm, i.e., by UV-B or UV-A radiation that may further undergo reversion to the 6-4PPs [30] upon exposure to short wavelength UV radiation (Fig. 2). The secondary transformation of 6-4PPs into DEWs results due to the presence of a pyrimidone moiety, and this mechanism has been described in detail by Cadet et al. [31]. The presence of two adjacent cytosine bases is considered as mutation hotspots for short wavelength UV radiation [28]. Courdavault et al. [32] reported the higher photoreactivation capacity of T–T and T–C sequences than C–T and C–C sequences. The cytotoxic CPD lesions are generally *cis-syn* configured, whereas the frequency of occurrence of *trans-syn* configured lesions is low. The flexibility of single-stranded and denatured DNA commonly favors the incidence of *trans-syn* isomers. Bastien et al. [33] reported that cytosine containing dipyrimidine sites are the hotspots for CPD formation following UV-B exposure.

The rates of CPD formation throughout the genome determine in part the overall genotoxic burden. The CPD yield depends on several variables like nature of adjacent sequence, sequence specificity [34, 35], and the irradiation wavelength and absorbed dose. Matallana-Surget et al. [36] found that the distribution of bipyrimidine photoproducts within UVB-irradiated DNA is greatly affected by

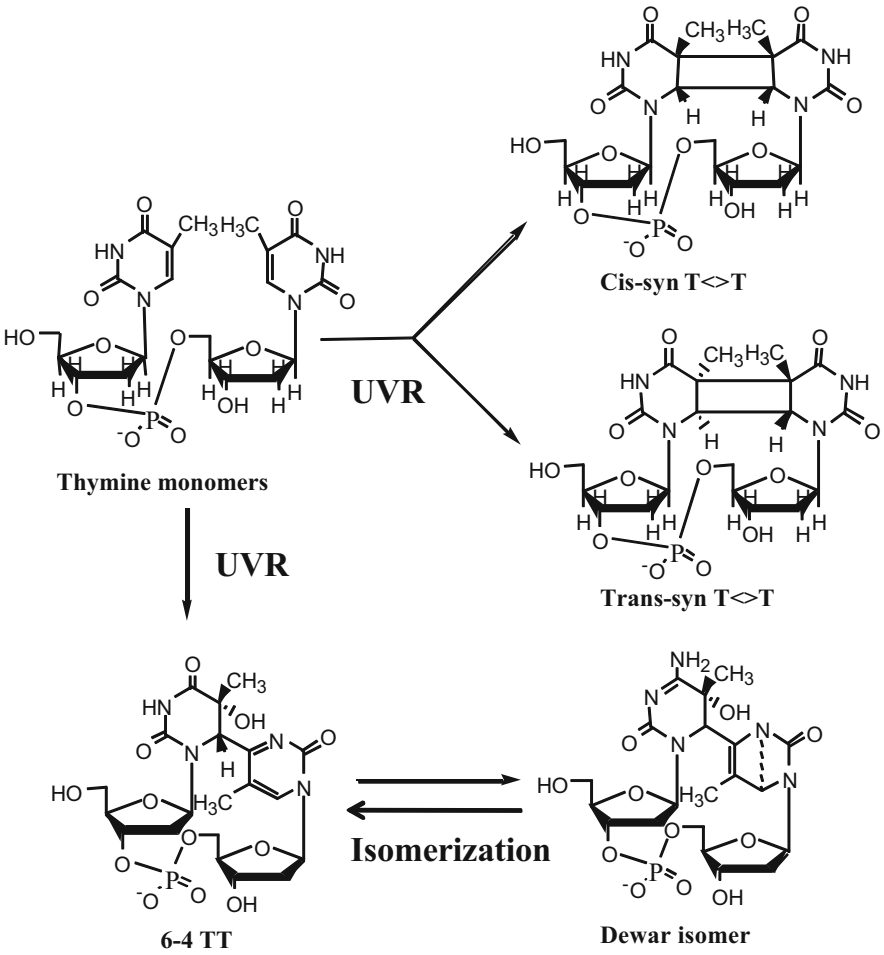

Fig. 2 Formation of UV-induced cytotoxic CPD, 6-4PP and their Dewar valence isomer

the content in GC base pairs of the genome. The yield of CPDs under UV-C irradiation at a given site in isolated DNA decreases in the order TT > TC > CT > CC [37]. In bacterial spores, irradiation with UV-B and UV-C leads to the formation of a spore photoproduct, a dimeric lesion involving two thymines [38].

The CPDs and 6-4PPs, constituting around 75% and 25% of the UV-induced DNA damage products, induce a bend or kink of 7–9° and 44°, respectively [39, 40]. UV-mediated DNA damage mainly depends upon the flexibility of the DNA, nature and position of the bases. CPDs form at higher yields in single-stranded DNA by the cycloaddition of two pyrimidine bases and at the flexible ends of poly(dA)-(dT) tracts, but not in their rigid center [41, 42]. CPD formation is less frequent when there is bending of the DNA towards the minor groove [43]. TATA-box binding protein (TBP), one of the major transcriptional factors, directly influences DNA damage and

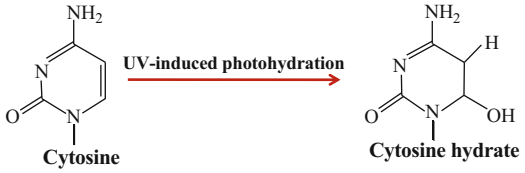

Fig. 3 Formation of cytosine hydrate. For details see the text

repair and has been found to induce the formation of 6-4PPs in the TATA-box, where the DNA is bent, but CPDs are formed at the edge of the TATA-box and outside, where the DNA is not bent [44]. You et al. [45] reported the formation of CPDs at the major p53 mutational hotspot in UV-B induced mouse skin tumors. In addition to UV-B, UV-A has also been reported to induce the formation of CPDs in bacteria, eukaryotic cells, and whole skin [46, 47]. Detailed information on the distribution of cyclobutane pyrimidine dimers (CPDs), pyrimidine (6-4) pyrimidone photoproducts (6-4PPs), and their Dewar valence isomers in isolated cells and human skin is available [48–50].

The irradiation of human skin cells and rodents by UV-A results in higher yields of CPDs than 8-oxo-7, 8-dihydroguanine and DNA strand breaks [51, 52]. Cytosine undergoes photohydration reaction to form monomeric pyrimidine photoproduct "cytosine photohydrate" (6-hydroxy-5,6-dihydrocytosine) [53] (Fig. 3) but at a very low efficiency, since it could not be detected in UV-C-irradiated cells using a highly sensitive HPLC-Tandem mass spectrometry method [54]. There is little information concerning the formation of cytosine hydrates in UV-irradiated DNA due to instability of the resulting photoproduct [55]. The oxidation product of pyrimidine bases such as pyrimidine glycols is also formed by means of a hydration reaction [28]. In fact, oxidized pyrimidine bases that are likely to include thymine and cytosine glycols may be generated upon UV-A irradiation via the generation of a hydroxyl radical and not through the transient formation of a pyrimidine radical cation. CPDs have been reported to inhibit the progress of DNA polymerases. Mammalian RNA polymerase II has been reported to stall at both CPDs and 6-4PPs [56, 57]. If unrepaired, a single CPD is sufficient to eliminate completely the expression of a transcriptional unit and finally results in mutation [58].

Indirect damage to DNA by UV-A radiation is mediated by endogenous photosensitizers, such as flavins, nicotinamide adenine dinucleotide phosphate (NADPH) oxidase, heme groups, porphyrins, melanin, and cytochromes [59, 60], which absorb the UV radiation, resulting in excited molecules. The formation of DSBs is a hallmark of the molecular effects of ionizing radiation due to the multiplicity of radical and excitation events that are created along the radiation track. It has been reported that UV-A is capable of generating single (SSBs) and double strand breaks (DSBs) in DNA, which, if persistent, can cause chromosomal aberrations and tumorigenic transformation in keratinocytes [61]. However, more recently, it has been clearly established that DSBs are not produced by UV-B and UV-A radiation, either through a direct photochemical reaction or indirectly through biochemical processes of bulky bipyrimidine photoproducts at the replication fork [62–64]. It

seems that γ-H2Ax has become a surrogate of DSBs. However, evidence is now growing, showing that not all γ-H2Ax foci represent DSBs and that a significant fraction of DNA repair of DSBs may occur without functional implication of γ-H2Ax. Therefore, the specificity of γ-H2Ax has recently been questioned, in particular in the case of UV-B-induced formation of DNA damage [63, 65]. It has been recently proposed that DSBs could originate from the biochemical processing of oxidatively UV-induced clustered lesions [66].

In spite of the poor UV-A absorption capacity of DNA, 6-4PPs seem to be generated, but in much lower quantities than CPDs. Moreover, the amount of CPDs is higher after exposure to UV-B radiation compared to UV-A radiation, considering equimutagenic doses [67]. Therefore, DNA photoproducts induced by UV-A are considered potentially more mutagenic than those formed by UV-B, most likely due to less effective cell cycle arrest, weak p53 and p95 activation, and an ineffective cell cycle check point, which leads to the progression of DNA replication and the accumulation of mutations [67].

3 UV-Induced Purine Adducts

UV-B radiation has been found to modify the purine bases of the DNA [68]. The purine photoproducts involve at least one adenine residue that undergoes photocycloaddition reactions with contiguous adenine or thymine upon exposure to UV-B radiation [69, 70] (Fig. 4). The frequency of mutagenic adenine-containing photoproduct (A-T) is very low (1×10^{-5} in native DNA) [71]. Adenine residues are photodimerized into very unstable azetidine intermediates by the cycloaddition of N7–C8 double bonds of the 5′-A across the C6 and C5 positions of the 3′-A [70]. This intermediate photoproduct finally results in two distinct adenine photoproducts such as adenine dimer (A=A) and Pörschke photoproduct [72] (Fig. 4). In fact the earlier proposals concerning the UV-induced generation of the adenine photoadducts have never been confirmed [73, 74]. Evidence has been provided for the UV-induced formation, albeit with very low efficiency, of a thymine-adenine addition product [75–77]. A minor photoadduct between 5-methylcytosine and adenine has also been characterized [78].

The conversion of both these photoproducts into 4,6-diamino-5-guanidinopyrimidine (DGPY) and 8-(5-aminoimidazol-4-yl)adenine (8-AIA), respectively, can be detected from individual acid hydrolyzates of UV-irradiated polynucleotides and DNA [74]. It has been found that complexing of UV-irradiated poly(dA)-poly (dT) effectively reduces the formation of A=A photoproduct [74]. Complementary base pairing in the DNA greatly suppresses the photoreactivity of adjoining adenine bases [41]. UV-B radiation is a very poor inducer of oxidized bases and DNA strand breaks. It has been established that UV-A radiation is a more efficient generator of oxidatively produced damage to cellular components, mostly through the initial formation of singlet oxygen according to type II photosensitization mechanisms [27, 79]. UV-induced generation of ROS can cause oxidatively generated damage of

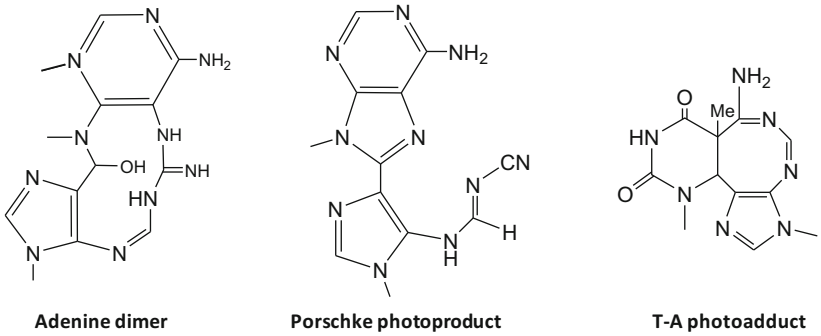

Fig. 4 Structure of purine photoproducts

the DNA, and the most common oxidation products are 8-oxo-7,8-dihydroguanine (8-oxoGua), 8-oxo-7,8-dihydroadenine (8-oxo-Ade), 2,6-diamino-4-hydroxy-5-formamidopurine (FapyGua), 4,6-diamino-5-formamidopyrimidine (FapyAde), and 2,2,5-triamino-4-(2*H*)oxazolone [80]. However, interaction of UV-A photons with DNA that give rise to CPDs constitutes the main degradation pathway [38, 52, 81–83]. Thus, it can be concluded that UV-induced DNA damage, such as cytotoxic lesions, abasic sites (although very poorly generated by UV radiation), strand breaks, and oxidatively generated damage, distorts the structural integrity of DNA and thus the normal cellular processes of replication and transcription, ultimately resulting in mutagenesis, cancer, and finally death of the organisms [19–21].

4 UV-Induced Double Strand Breaks in DNA

UV-radiation is responsible for generation of double strand breaks in replicating DNA [84]. UV-B-induced ROS [5] as well as DNA lesions (CPDs and 6-4PPs) may cause primary as well as secondary breaks, respectively. These lesions are commonly associated with replication blockage that may lead to production of DNA double-strand breaks (DSBs) at the sites of collapsed replication forks of CPDs-containing DNA [85] (Fig. 5). The role of UV-C radiation in inducing DSBs in the replicating DNA has been worked out by Dunkern and Kaina [86]. It has been assumed that those initial photoproducts are converted into DSBs during replication; hence very low amounts of DSBs have been observed in cells where replication was inhibited. Several reports suggest that DSBs are produced during the replication of unrepaired UV-induced DNA lesions [85] and also in response to the repair of single strand breaks (SSBs) by base excision repair (BER) [87]. UV radiation does not produce the DNA DSBs directly but rather produces pyrimidine dimers and other photoproducts leading to replication arrest and DSBs. UV-induced replication arrest in the xeroderma pigmentosum variant (XPV) followed by the accumulation of Mre11/Rad50/Nbs1 complex and phosphorylated histone H2AX

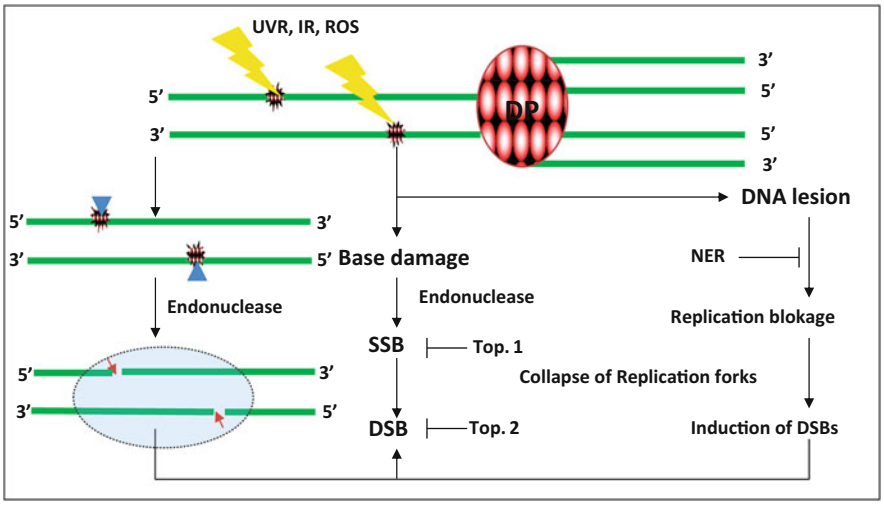

Fig. 5 Schematic illustration of pathways involved in DSBs and their repair by NER. The details of NER mechanisms in prokaryotes and eukaryotes are illustrated in Figs. 8 and 9, respectively

(γ-H2AX) in large nuclear foci at the sites of stalled replication forks also suggests that UV damage leads to the formation of DSBs during the course of replication arrest [87]. Mutagenic agents like epoxides and ROS are also known to induce the DSBs in the DNA [88] that, when left unrepaired, can cause cell death, and if they are misrepaired they may lead to chromosomal translocations and genomic instability [89]. Lottner et al. [90] have reported the role of antioxidants in reducing the number of DSBs in DNA under in vitro conditions.

A number of pathways have been recognized for the formation of DSBs at a stalled replication fork. It was shown that when the DNA replication machinery encounters a replication-blocking lesion, DNA polymerase (DP) enzyme is stalled at the blocked site, resulting in the formation of a Y-shaped DNA structure, which may be recognized by a specific endonuclease that successively makes a nick in the template strand, resulting in the induction of a DSB close to the replication-blocking lesion [91]. Furthermore, replication stresses may trap topoisomerase I (Top1) cleavage complexes, leading to generation of DSBs by preventing Top1-mediated DNA relegation [92]. Free radicals may also cause DSBs [93] by preventing the topoisomerase II (Top2)-mediated DNA relegation [91] (Fig. 5). Recently, Harper et al. [94] have shown that radiation-induced SSBs and non-DSB DNA damage contribute to the formation of replication-induced DSBs. However, extensive experimental evidence is still needed regarding the formation of DSBs.

5 DNA Repair Mechanisms

The accurate transmission of genetic material from parent to offspring is very essential for the survival of organisms. Highly accurate DNA replication, precise chromosome distribution, and the ability to survive spontaneous and induced DNA damage ensure faithful transmission [95]. In order to overcome the effects of DNA lesions, organisms have developed certain DNA repair mechanisms the existence of which in the cell depends on the types and locations of lesions in the genome [96]. Kelner [97] and Dulbecco [98] independently reported the existence of DNA photorepair pathways. Specialized DNA repair proteins scan the genome continuously and encounter the DNA lesions by triggering several distinct repair mechanisms such as photoreactivation, excision repair (BER and NER), and some specialized forms of repair systems such as SOS response, damage tolerance, and apoptosis.

5.1 Photoreactivation

The simplest and the oldest repair system involving the enzyme photolyase is highly conserved in all the three domains of life. The enzyme binds specifically to the CPDs (CPD photolyase) or 6-4PPs (6-4 photolyase) and directly monomerizes the cyclobutane ring of the CPDs, using the energy of a UV-A or blue photon and protects the genome from deleterious effects of UVR [99, 100]. The absorption of every blue-light photon may split approximately one dimer [101]. DNA photolyases having a molecular weight of 50–65 kDa and 420–616 amino acid residues [99] are monomeric flavin-dependent repair enzymes, consisting of two known cofactors, a catalytic cofactor and a light-harvesting cofactor. 5,10-Methenyltetrahydrofolate (MTHF) [102], 8-hydroxy-5-deaza-riboflavin (8-HDF) [103], FMN [104], and riboflavin [105] are known as light-harvesting cofactors, which absorb blue light energy efficiently and transfer it to the catalytic cofactor $FADH^{-}$ [106]. A flavin–adenine dinucleotide ($FADH^{-}$), reduced by two electrons, in its excited state donates an electron to the CPD, splitting the cyclobutane ring, and the electron is transferred back to the flavin concomitantly with the generation of the two canonical bases [100, 107] (Fig. 6). CPD photolyases have been reported in diverse groups such as archaea, bacteria, fungi, viruses, plants, invertebrates, and many vertebrates including aplacental mammals, whereas, 6-4 photolyases have been identified in certain organisms like *Drosophila*, silkworm, *Xenopus laevis*, and rattlesnakes [20] (Table 1). Photolyases seem to be absent or non-functional in humans and other placental mammals [133, 134]. Placental animals have been demonstrated to have lost the photolyase genes, although they keep homologs that are related to circadian rhythms. These proteins do not have any DNA repair activity. However, Sutherland [135] and Harm [136] have reported the photolyase activity in the cell and tissues, including white blood cells of certain placental mammals. Hsu et al. [137] have reported a human photolyase showing homology with plant blue-light receptor, *Cry*

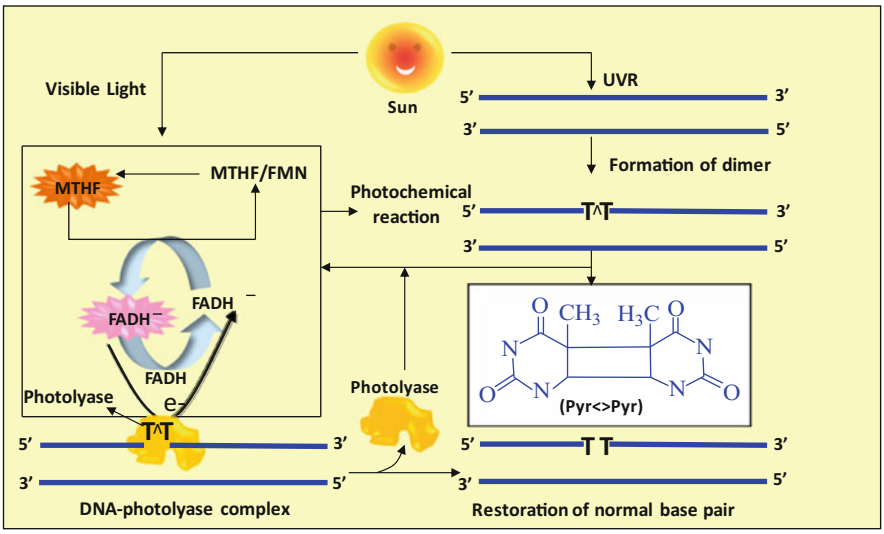

Fig. 6 Mechanism of photoreactivation involving enzyme photolyase

gene, and about 40% significant sequence similarity to the *Drosophila* 6-4 photolyase, but its role in the repair pathway is still to be worked out. DNA photolyases are considered to be ancient repair proteins, which may have helped in the evolution of the organisms on primordial Earth [138]. Photolyase enzyme has been identified from *E. coli* [139], *Streptomyces griseus* [140], and *Salmonella typhimurium* [141]. *S. typhimurium* and *E. coli* photolyases have 80% identity and 88% significant sequence homology in amino acid sequence. The crystal structures of CPD photolyase of *E. coli* and *A. nidulans* suggest that, upon binding to DNA, the enzymes flip the pyrimidine dimer out of the duplex into a hole that contains the catalytic cofactor [142]. CPD photolyases recognize CPDs with a selectivity similar to that of sequence-specific DNA-binding proteins, which suggests that they could compete with histones for DNA accessibility in a manner similar to transcription factors [143]. The first thermostable CPD photolyase was identified in *Thermus thermophilus* by Kato et al. [144]. The absorption of one blue-light photon by photolyases splits approximately one dimer [101]. Photolyase genes have been cloned from a number of bacteria and fungi [145], e.g., in *E. coli* and *Synechocystis* sp. strain PCC 6803 photoreactivating factors *phr* and *phrA* codes for specific DNA photolyases, respectively [146]. Todo et al. [147] reported that the 6-4 photolyase in cell-free extracts of *Drosophila* were able to restore the biological activity of UV-irradiated DNA. Kim et al. [148] reported the conversion of 6-4PPs into unmodified bases by 6-4 photolyase, involving an oxetane intermediate. Mammals, birds, and plants have photolyase-like proteins, called cryptochromes, which have no ability to repair damaged DNA but function as blue-light photoreceptors [149]. In addition to shielding by flavonoids and phenolic compounds [150], photoreactivation mediated by the enzyme photolyases is thought to be the major DNA repair

Table 1 Photolyase enzymes in four different kingdoms (modified from [108])

Kingdom	Organism	CPD photolyase	6-4PP photolyase	References
Viruses	*Fowl pox virus* (FPV)	+	–	[109]
	Melanoplus sanguinipes entomopox virus (MsEPV)	+	–	[110]
	Chrysodeixis chalcites nucleopolyhedrovirus (ChchNPV)	+	–	[111]
Archaebacteria	*Halobacterium halobium*	+	–	[112]
	Methanobacterium thermoautotrophicum	+	–	[113]
	Sulfolobus tokodaii	+	–	[114]
Eubacteria	*Bacillus firmus*	+	–	[242]
	Escherichia coli	+	–	[115]
	Salmonella typhimurium	+	–	[116]
	Anacystis nidulans	+	–	[117]
	Synechocystis sp. PCC 6803	+	–	[118]
	Streptomyces griseus	+	–	[119]
	Myxococcus xanthus	+	–	[120]
	Vibrio cholerae	+	–	[121]
Eukaryotes	*Saccharomyses cerevisiae*	+	–	[116]
	Neurospora crassa	+	–	[122]
	Drosophila melanogaster	+	+	[123]
	Homo sapiens	?	?	[124]
	Carassius auratus	+	–	[125]
	Oryzias latipes	+	–	[124]
	Monodelphis domestica	+	–	[126]
	Potorous tridactylis	+	–	[124]
	Xenopus laevis	+	+	[127]
	Arabidopsis thaliana	+	+	[128]
	Chlamydomonas reinhardtii	+	–	[129]
	Cucumis sativus	+	–	[130]
	Ginkgo biloba	+	–	[131]
	Medicago sativa	+	–	[11]
	Triticum sp.	+	–	[132]

pathway in several higher plants such as rice, *Arabidopsis*, wheat, and maize [151, 152]. Plants grown in the presence of photoreactivating radiation can eliminate the majority of both 6-4PPs and CPD lesions within hours, or in some cases minutes, of their induction [18], whereas 6-4PPs are generally observed to be repaired more quickly than CPDs [153] in the absence of blue light. The apoproteins of the purified blue-light photoreceptors of *Arabidopsis thaliana* [154] and mustard containing folate and flavin chromophores [155] were found to be very similar and structurally related to the microbial CPD photolyase. Todo et al. [156] have shown that the three systems – the CPD photolyase, the 6-4 photolyase, and the plant blue-light photoreceptors – are evolutionary and mechanistically related. The interaction between

CPD lesions and photolyases was studied with the help of X-ray crystallography [157] and nuclear magnetic resonance (NMR) spectroscopy [158]. The precise mechanism of recognition of the lesion by photolyases in the DNA molecule is still unclear. It has been observed that about 240 KJ/mol of energy is captured upon absorption, out of which about 125 KJ/mol energy is consumed during the initial electron transfer from the excited FADH to CPD lesions [159]. The splitting of the CPD lesion proceeds rapidly within 0.6 ns [160]. The back-transfer of electrons from the CPD lesion to the FADH radical takes place only after the completion of cyclobutane ring cleavage [100]. MacFarlane and Stanley [160] have suggested that the photolyase enzyme is indeed left in the semiquinonid state after completion of the repair of the CPD lesion. Kavakli and Sancar [161] have analyzed the role of intraprotein electron transfer in photoreactivation by DNA photolyase. In the absence of photoreactivating light, the enzyme binds to pyr <> pyr in the organisms *Saccharomyces cerevisiae* and *Escherichia coli* and stimulates the removal of UV damage by stimulating the NER system in vivo or in vitro as a defense against DNA damage, even in the absence of light [162].

5.2 Excision Repair

Excision repair is a complex multistep dark pathway, where the damaged DNA is replaced with new, undamaged nucleotides [101, 163] following two subpathways: base excision repair (BER) and nucleotide excision repair (NER).

5.2.1 Base Excision Repair (BER)

BER provides protection against the DNA lesion arising from endogenous factors like hydrolytic deamination, strong alkylating agents, ionizing radiation (IR), intracellular metabolites, and UV-induced ROS [164, 165] and proceeds through a series of repair complexes that act at the site of DNA damage [166]. The most frequently used repair pathway recognizes the damaged base utilizing various forms of DNA glycosylases which removes different types of modified bases (Table 2) by cleaving the *N*-glycosidic bond between the abnormal base and 2-deoxyribose, creating either an abasic site or an SSB [167]. Parsons et al. [168] have reported that the formation of DNA repair complexes on damaged DNA stabilizes BER proteins. In contrast, BER proteins that are not involved in repair are ubiquitylated by the carboxyl terminus of Hsc70 interacting protein (CHIP) and subsequently degraded by the proteasome. The removal of the damaged base results in an apurinic/apyrimidinic (AP) site, that is removed by an AP endonuclease or an AP lyase, which nicks the DNA strand 5′ or 3′ to the AP site, respectively. Bi- and trifunctional DNA glycosylases have AP lyase activity via a β- or β/δ-elimination mechanism using an ε amino group of a lysine residue or α-imino group in addition to DNA glycosylase activity [169]. AP sites are targeted by both AP endonuclease

Table 2 DNA glycosylases in bacteria, yeasts and humans (modified from Sinha and Häder 2002)

Glycosylases	Organisms	Genes	Substrate
1. Uracil DNA glycosylase	*E. coli*	*Ung*	Uracil from ss- and dsDNA
		Dug/mug	U from U:G, ethenocytosine, hypoxanthine and 5-hydroxycytosine
		Dut	?
	S. cerevisiae	*UNG*	Uracil
	Human	*UNG1/UNG2*	Uracil from ss- and ds-DNA
		SMUG1	Uracil from ss-DNA, hydroxymethyluracil, formyluracil
2. 3-Methyl adenine DNA glycosylase	*E. coli*	*tag*	3-Methyladenine
		alkA	3-Methyladenine, 7-methylguanine, 2-methylcytosine, 5-formyluracil
	S. cerevisiae	*MAG1*	3-Methyladenine, 7-methylguanine
	Human	*MPG*	3-Methyladenine
		Aag	Hypoxanthine
3. UV-endonuclease	T4	*den V*	*cis-syn*-Cyclobutane-type pyrimidine dimer
	E. coli	?	?
	Bacillus subtilis	*UVDE*	Pyrimidine dimers
	S. cerevisiae	?	?
	S. pombe	*UVDE*	Pyrimidine dimers
	Human	?	
4. Endonuclease III/thymine glycol DNA glycosylase	*E. coli*	*Nth*	5-Hydroxycytosine, thymine glycol, urea
	S. cerevisiae	*NTG1*	Oxidative DNA damage, thymine glycol and formamido-pyrimidines, oxidized pyrimidines, 2 formamido-pyrimidine-G, Me^7-formamido-pyrimidine-G
		NTG2	Oxidative DNA damage, thymine glycol and formamido-pyrimidines residues, 5-hydroxycytosine, oxidized pyrimidines, Me^7-fapy-G
	Human	*NTH1*	Oxidized guanine lesions
5. Endonuclease VIII	*E. coli*	*nei*	Thymine, thymine glycol, urea, 5-hydroxycytosine, dihydrothymine, and β-ureidoisobutyric acid
	S. cerevisiae	?	?

(continued)

Table 2 (continued)

Glycosylases	Organisms	Genes	Substrate
	Human	*NEIL1*	5-Hydroxyuracil, 5-hydroxycytosine, 5,6-dihydrouracil, thymine glycol, formamido-pyrimidines (FapyA/G)
			5-Hydroxyuracil and 5-hydroxycytosine
		NEIL2	?
		NEIL3	
6. Fapy/8 oxoguanine DNA glycosylase	*E. coli*	*fpg/mutM*	2,6-Diamino-5-formamidopyrimidine 8-oxo-7,8-dihydroguanine, 5-hydroxycytosine
	S. cerevisiae	*OGG1*	2,6-Diamino-5-formamidopyrimidine 8-oxoG, 2 formamidopyrimidine-G, Me^7-formamidopyrimidine-G
	Human	*hOGG1*	8-Hydroxyguanine, Me^7 formamidopyrimidine-G
7. A-G-mismatch DNA glycolsylase	*E. coli*	*mut Y*	Adenine/C
	S. pombe	*spMYH*	2-Aminopurine/G and A/2-aminopurine, Adenine/C
	Human	*MYH*	Adenine from G:A, 8-oxoG:A, 2-hydroxyadenine
8. G-T-mismatch DNA glycosylase	*E. coli*	?	?
	M. thermoautrophicum	*Mig-Mth*	Thymine residues from T–G mismatches
	S. pombe	*thp1*	Uracil from G:U
	Human	*MBD4*	Thymine from T:G
		(≈MED1)	Recognizes a G:T mispair in a CpG sequence
		TDG	
9. Formyluracil DNA glycosylase	*E. coli*	*mug*	Formyluracil mispaired with A&G
		mutM	?
		mutS	Formyluracil mispaired with G
	S. cerevisiae	?	?
	Human	*MBD4*	Formyluracil mispaired with G
		hNTH1	?
10. Hydroxymethyl uracil DNA glycosylase	E. *coli*	?	?
	S. cerevisiae	?	?
	Human	?	5-Hydroxymethyluracil mispaired with G

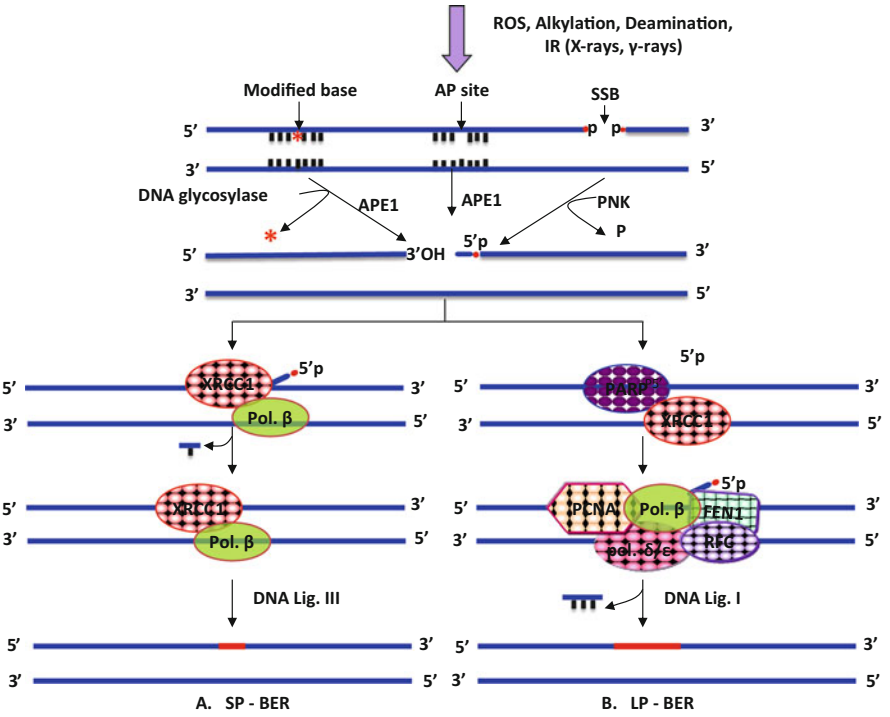

Fig. 7 Schematic representation of mammalian SP-BER (**a**) and LP-BER (**b**). SP-BER is initiated by the activity of various DNA glycosylases and APE1, whereas LP-BER involves PNK

and AP lyase. AP endonuclease nicks an AP site through a hydrolytic reaction to generate a 3′-OH and 5′-deoxyribosephosphate (dRP) [170, 171]. This 5′ block is removed by deoxyribophosphodiesterase (dRPase) or dRP lyase using hydrolytic or lyase (β-elimination) mechanisms, respectively [172, 173]. When the AP lyase incises an AP site, it produces 3′-α,β-unsaturated aldehyde (by β-elimination) or 3′-phosphate (by β/δ-elimination) and 5′-phosphate [174]. These 3′-blocking groups must be removed by 3′-phosphoesterase to allow DNA polymerase activity. DNA having one nucleotide lesion is removed by short-patch BER (SP-BER) whereas two/more nucleotide lesions are repaired by long-patch BER (LP-BER) pathways [175] (Fig. 7). It is assumed that the majority of repairs takes place through SP-BER, initiated either by monofunctional or by bifunctional glycosylase [164]. The pathway of SP-BER after excision of the damaged base involves the recruitment of poly (ADP-ribose) polymerase-1(PARP-1) followed by scaffold protein XRCC1 and DNA pol. β to replace the damaged nucleotide. DNA ligase III (Lig. III) seals the nick and restores the intact DNA. LP-BER involves proliferating cell nuclear antigen (PCNA) coupled with DNA pol. $-\delta/\varepsilon$ or β which extends and fills the gap by inserting 2–13 nucleotide [164]. The replication factor C (RF-C) is required to load PCNA onto the damaged DNA [175]. The flap endonuclease

(Fen1) protein then displaces the ensuing DNA flap, leaving a nick which is ligated by DNA ligase I (Lig. I) [176].

UV-Endonucleases

UV-endonucleases, generally present in the UV resistant organisms [177], cleave the *N*-glycosidic bond of the 5′-pyrimidine of the dimer followed by AP-lyase-mediated strand cleavage. However, a similar enzyme has also been coded by the *denV* gene of the bacteriophage T4 and such activity has been detected in *S. cerevisiae* [178]. UV-endonucleases from eukaryotes have been reported to recognize both CPDs and 6-4PPs and generate an incision immediately 5′ to the lesion [179]. Several workers have partially characterized the endonucleases from plant extracts (120–123). Besides this, a number of glycosylases and endonucleases have recently been identified [20].

Eukaryotic-Specific BER Enzymes

The BER mechanism is highly conserved in both prokaryotes and eukaryotes. Eukaryotes have many functional homologues of bacterial BER enzymes. To date, poly (ADP-ribose) polymerase (PARP) and X-ray cross complementing group 1 (XRCC1) have been identified as eukaryotic-specific enzymes. PARP1 uses NAD to add branched ADP-ribose chains to proteins. PARP1 functions as a DNA nick-sensor in DNA repair and as a negative regulator of the activity of Polβ in LP-BER [180]. XRCC1 interacts with DNA ligase III and PARP through its two BRCT domains and with Polβ through an N-terminal domain. XRCC1 also interacts with many other proteins and forms a large DNA repair complex [181].

5.2.2 Nucleotide Excision Repair

Nucleotide excision repair (NER), the versatile and flexible repair system, is conserved in prokaryotes as well as in higher eukaryotes [182, 183]. The NER system has broader substrate specificity and it sorts out a wide range of structurally unrelated DNA lesions, such as CPDs and 6-4PPs caused by UVR, bulky chemical adducts, DNA-intrastrand crosslinks, and some forms of oxidatively generated damage, that cause helical distortion of the DNA double helix (see Fig. 5) as well as modification of the DNA chemistry and interfere with DNA duplication and transcription [184]. The relative repair efficiency of both of the pyrimidine lesions by NER proteins varies considerably in mammalian cells. It has been reported that in human and hamster cells, the elimination of 6-4PP is at least five times faster than that of CPDs [185].

The NER system was first described in *E. coli*, where about six proteins, UvrA, B, and C (known as ABC-complex, having excinuclease activity), UvrD (helicase II), DNA polymerase I (pol. I), and DNA ligase are recruited to complete

the repair [186]. The eukaryotic NER pathway has been extensively studied at the molecular level in yeast and human cells and it has been found that the eukaryotic pathway is very similar to that of the prokaryotes in terms of the biochemical strategy used but differs widely in the nature and number of proteins used [184]. NER has two regulated subpathways: global genome NER (GG-NER) and transcription-coupled NER (TC-NER) which remove a wide range of UV-induced DNA lesions in a sequential way involving damage recognition, opening of DNA double helix at damage site, and dual incisions on both sides of the lesion followed by resynthesis and ligation [184]. Global genome repair (GGR) refers to the repair of lesions over the entire genome, whereas, repair of transcription-blocking lesions present in transcribed DNA strands is referred to as transcription coupled repair (TCR). In GGR, recognition of DNA lesions by UvrAB initiates the initiation of the repair reaction, whereas, in TCR, stalling of the RNA polymerase is responsible for the initiation of repair [187]. When a transcribing RNA polymerase meets a bulky DNA lesion, the polymerase stalls. Transcription-repair coupling factor (TRCF), an *mfd* gene product in *E. coli* releases the stalled RNA polymerase from the template DNA and then recruits UvrA. After UvrA has bound to the DNA, the subsequent reactions proceed in the same fashion as in GGR. UvrB and DNA form a pre-incision complex, and then UvrC incises both sides of the DNA strand. The displacement of stalled polymerase is brought about by the recruitment of two proteins CSA and CSB. The CSA protein (44 kDa) which belongs to the "WD repeat" family of proteins exhibits structural and regulatory roles and CSB proteins (168 kDa) which belong to the SWI/SNF family of proteins exhibit DNA-stimulated ATPase activity [188]. The CSA and CSB gene products are required for efficient repair only during the elongation stages of RNA pol II transcription, which is a prerequisite for efficient TCR. It is assumed that the CSB protein ubiquitinates the stalled elongating RNA pol II complex at the lesion and enhances the assembly of repair factors [189]. However, the fate and the role of ubiquitylated RNA pol II have yet to be clarified [190]. Recently, Fousteri et al. [191] have revealed that CSB is a prerequisite factor in vivo to assemble NER proteins while it is not essential to recruit TFIIH or NER complex in vitro. Proietti-De-Santis et al. [192] have reported that CSB is required during the first phases of RNA pol II transcription initiation. However, at higher doses of UV radiation, elongation of RNA pol II is greatly impaired, affecting the efficiency of TCR and, thus, at this point GGR controls the TCR pathway [193].

Global Genome NER in Prokaryotes

Bacterial GGR is a multistep process that removes a wide variety of DNA lesions. In solution, UvrA and UvrB form $UvrA_2B$ or $UvrA_2B_2$ that can recognize lesions in DNA and can make a stable complex with the DNA [194].When UvrB detects a lesion, it hydrolyzes ATP to form the pro-preincision complex. After UvrA is released, UvrB binds tightly to DNA and makes a stable UvrB-DNA complex, that is, a preincision complex. In this state, UvrB hydrolyzes ATP and can then specifically recognize damage in the absence of UvrA [195]. UvrB can hydrolyze

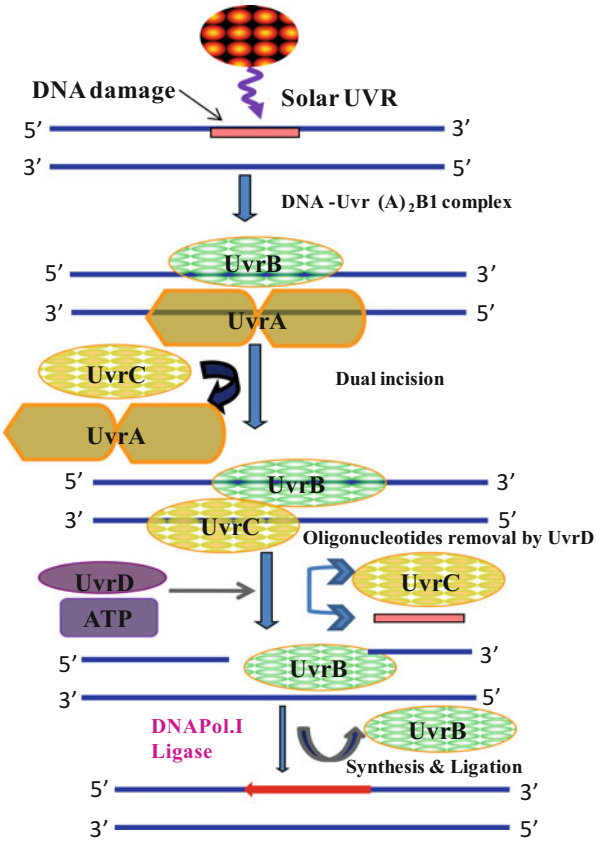

Fig. 8 NER in *E. coli* involving six proteins. $UvrA_2B$ recognizes DNA lesions and forms a stable complex with the DNA. When UvrB detects a lesion, it hydrolyzes ATP to form the pro-preincision complex. After UvrA is released, UvrB binds tightly to DNA and makes a stable UvrB-DNA preincision complex. Binding of UvrC to the pre-incision complex incises both sides of a DNA lesion. Removal of the damaged DNA portion is done by UvrD. Finally, synthesis and sealing is done by PolI and ligase

ATP with the help of UvrA in *E. coli* [196], whereas in *T. thermophilus* HB8 the UvrB protein (ttUvrB; TTHA1892) shows ATPase activity at its physiological temperature, even in the absence of UvrA (ttUvrA; TTHA1440) [197]. UvrC can bind to the pre-incision complex to incise both sides of a DNA lesion. The first incision is made at the fourth or fifth phosphodiester bond on the 3′ side of the lesion and is immediately followed by incision at the eighth phosphodiester bond on the 5′ side [198]. UvrD is a DNA helicase that releases lesion-containing DNA fragments from dsDNA. After removing the nucleotide fragment, PolI synthesizes a new strand with the same sequence as the removed nucleotide fragment. The newly synthesized sequence is ligated to the adjacent strand by DNA ligase, and all the repair steps are completed (Fig. 8).

Global Genome NER in Eukaryotes

In the eukaryotic GG-NER pathway (Fig. 9), lesions produced in transcriptionally silent areas of the genome are recognized by hHR23BXPC protein complex in an energy-independent manner. GGR removes 6-4PPs much faster from the

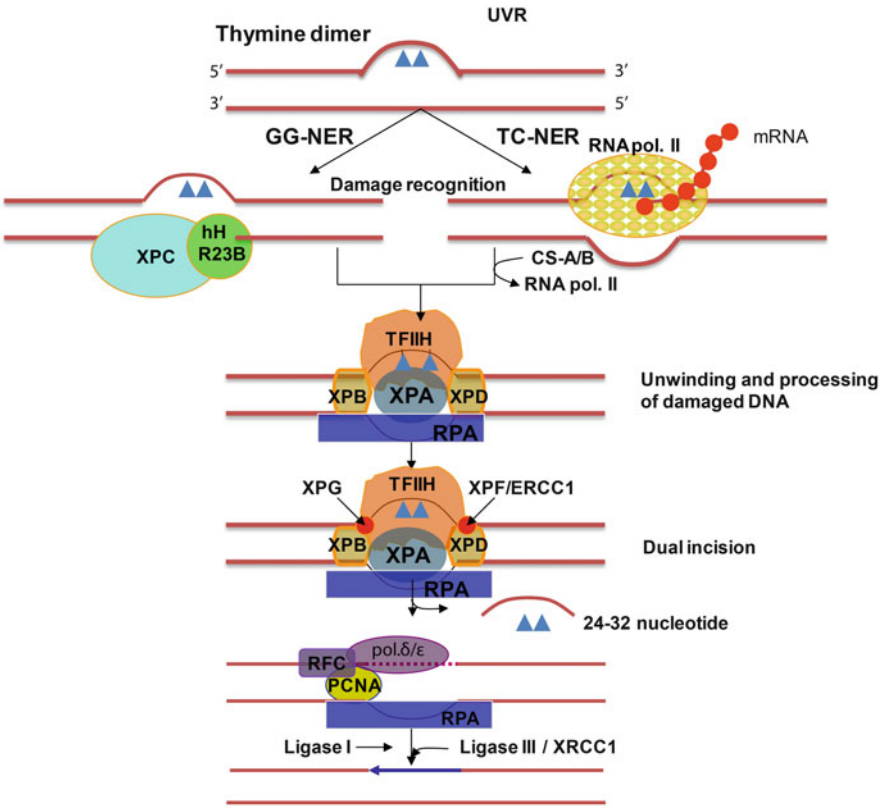

Fig. 9 Schematic representation of NER repair mechanisms in mammals. For details see the text

genome than CPDs, possibly because of disparity in affinity of the damage sensor hHR23B-XPC. XPC is the sole XP factor that is restricted to GGR [185] and binds preferentially to the stretch of ssDNA that occurs in the undamaged strand, opposite to a lesion [199]. However, association of UV-damaged DNA binding protein (UV-DDB) with a cullin-based ubiquitin ligase has revealed novel mechanistic and regulatory aspects of mammalian GG- NER. It was reported that XPC and UV-DDB materialize to assist in the efficient recognition of UV-induced photolesions and that both factors are ubiquitylated [200]. Lesions that cause little distortion can be recognized by the DDB complex which is also part of an E3 ubiquitin (Ub) ligase which poly-ubiquitinates XPC and XPE [201]. It was shown that the DDB complex is recruited first to the lesion (CPD) before the XPC complex, on a little distorted DNA helix; however, in the case of large distortion of the DNA helix caused by 6-4PPs, direct recognition by XPC is also possible for this lesion [201]. Sugasawa et al. [202] showed that hHR23B-XPC attaches directly to DNA damage and alters the DNA conformation around the lesion. The XPC protein (125 kDa) is complexed with hHR23B protein (58 kDa). These two proteins are human homologs of the yeast (*S. cerevisiae*) NER factor Rad4 and Rad23,

Table 3 Role of NER proteins in certain prokaryotes and eukaryotes (modified from [105, 108])

	Organisms				
NER factors	*Escherichia coli*	*Saccharomyces cerevisiae*	*Arabdiopsis thaliana*	*Homo sapiens*	Functions
XPC-hHR23B	–	Rad4	–	XPC	Binds damaged DNA; recruits other NER proteins; works with hHR23B involved only in GGR
	–	Rad23	–	hHR23B	Stimulates XPC activity in vitro; contains ubiquitin domain
	–	Rad23	–	hHR23A	Can substitute for hHR23B in vitro
	–	–	–	CEN2	Stabilizes the XPC-hHR23B complex
TFIIH	–	Rad25/SSL2	XPB2	XPB	$3' \rightarrow 5'$ helicase
	–	Rad3	UVH6	XPD	$5' \rightarrow 3'$ helicase
	–	TFB4	AT1G18340	p34	DNA binding?
	–	SSL1	GTF2H2	p44	DNA binding?
	–	TFB1	AT1G55750	p62	Core TFIIH subunit
	–	TFB2	AT4G17020	p52	Core TFIIH subunit
	–	TFB3	AT4G30820	Mat1	CDK assembly factor; CAK subcomplex
	–	Kin28	CDKD1; 3	Cdk7	CDK, C-terminal domain kinase; (CAK) subcomplex; phosphorylates RNA pol. II and other substrates
	–	CCL1	CYCH; 1	Cyclin H	Cyclin; CAK subcomplex
	–	Tfb5	AT1G12400	TFB5/TTDA (p8)	Stabilizing subunit
XPA	–	Rad14	–	XPA	Binds damaged DNA and facilitates repair complex assembly; affinity for ssDNA
DNA repair (ABC complex)	UvrA	–	–	–	Binds damaged DNA in complex with UvrB
	UvrB	–	–	–	Catalyze unwinding in preincision complex

RPA	SSB	Rfa1	RPA1	RPA70	Stabilizes opened DNA complex; positions nucleases; ssDNA binding
	–	Rfa2	RPA2	RPA32	Stabilizes opened DNA complex; positions nucleases; ssDNA binding
	UvrD	Rfa3	RPA3	RPA14	Stabilizes open complex (with XPA /Rad14)
XPG	–	Rad2	UVH3	XPG	Endonuclease (catalyzes 3′ incision); stabilizes full open complex
ERCC1-XPF	–	Rad10	ERCC1	ERCC1	Part of structure-specific endonuclease; catalyzes 5′ incision; interstrand cross-link repair
	–	Rad1	UVH1	XPF	Part of endonuclease (5′-incision); recombination via single-strand annealing
DDB	–	–	DDB1	DDB1	CPD recognition?
	–	–	DDB2	DDB2	Chromatin remodeling?

respectively (Table 3). In mammalian cells, the quantity of hHR23B is higher than the XPC [203] and in vitro activation of the latter protein is stimulated by hHR23B possibly in a structural rather than catalytic way [204].

After initial steps of damage recognition, the subsequent pathway for both GGR and TCR systems is almost similar. The unwinding of DNA double helix at the site of lesion takes place by the components of multi-subunit transcription factor-IIH (TFIIH). TFIIH is a ten-subunit protein complex composed of a core complex (XPB, XPD, p62, p44, p34, p52, p8) and of a cdk activating kinase (CAK) subunit (Mat1, Cdk7, CyclinH) [205]. Two subunits of TFIIH such as XPB (3′ to 5′ helicase) and XPD (5′ to 3′ helicase) are responsible for the opening of the DNA double helix around the lesion in an energy (ATP) dependent manner. After the opening of the DNA double helix by TFIIH, three proteins such as RPA, XPA, and XPG are recruited. XPA and heterotrimeric replication protein A (RPA) are recruited to confirm the presence of DNA damage and form a more stable preincision complex [206]. XPG, which belongs to the flap endonuclease-1 (FEN-1) family of structure-specific endonucleases [207], is not only involved in performing the 3′ incision in NER but is also required for stabilizing the fully open DNA bubble structure and to permit the 5′ incision by ERCC1-XPF [208]. Dubest et al. [209] have reported Atercc1 as *Arabidopsis* homologue of the Ercc1 (Rad10) protein which is a key component of nucleotide excision repair and cleaves 5′ to UV photoproducts in DNA. Subsequently, the injured part of the DNA is removed by cleaving the damaged strand towards 3′ and 5′ of the lesion by endonuclease XPG and XPF/ERCC1 complexes, respectively, generating a 24–32 base oligonucleotide fragment [165]. Finally, the gap is filled by DNA polymerase δ or ε (along with some accessory proteins like PCNA and RFC) and sealed by DNA ligase.

The presence of NER homologs (with the exception of the XPA protein) in plants has been fully characterized [184, 210]. NER in plants has been studied mainly using *Arabidopsis* [211]. Based on genetic and genomic analysis, it has been found that the NER pathway in plants is homologous to that of mammals and fungi and unrelated to the bacterial system [212, 213]. NER has been reported to occur in several plants such as *Glycine max* and cultivars of *Oryza sativa* [214]. The NER-related genes *UV-DDB*, *FEN-1*, *PCNA*, *DNA polymerase δ*, *RPA*, and *CSB* have been isolated and characterized in rice [210]. CPDs have been found to be excised from the nuclear DNA of *Daucus carota* and *Wolffia microscopia* at rates dependent on damage levels. A UV-specific endonuclease resembling UvrABC nuclease in activity was partially characterized in spinach [215]. Moreover, a plant homologue of the human NER gene of the endonuclease, *ERCC1*, has been cloned from *Lilium longiflorum* which showed a similar role in DNA repair in plants [216]. It seems that the plant NER is not exactly the same as the animal NER, since *XPA* is not present in plants, but multiple homologues of *CSB* have been reported [210]. The orthologs of prokaryotic UvrABC have also been reported in plants [184].

5.3 Recombinational Repair

Recombination is one of the most important processes involved in repair of double-strand breaks (DSBs) and single-strand gaps in damaged DNA, ensuring the transmission of correct genetic information from parents to offspring. DSBs can be caused by ionizing radiation, ROS, nuclease dysfunction, or replication fork collapse [217]. The harmful effects of double strand breaks (DSBs) can be overcome by the existence of two independent pathways, such as homologous recombination (HR) and non-homologous end joining (NHEJ). DSB repair by recombination requires multiple proteins which are conserved among all eukaryotes and deficiencies in this repair mechanism can cause cancer and several other hereditary diseases, e.g., mutation of BRCA1 may lead to hereditary breast cancer [218]. DSB repair through HR process is an error free pathway, since it requires an extensive region of sequence homology between the damaged and template strands, whereas NHEJ is an error prone pathway which joins broken chromosomal ends independent of sequence homology. In most bacteria, the HR pathway is thought to be the major route for repair of DSBs [219, 220].

5.3.1 Homologous Recombination

The genes of "*RAD52* epistasis group" involved in repair of DSBs by HR were first identified in yeast *Saccharomyces cerevisiae* mutants. Homologues of most of the genes are highly conserved among all eukaryotes including human [221], revealing the importance of these genes for cell survival. Thacker [222] demonstrated that *E. coli recA* gene and its eukaryotic homologs *RAD51*s are the best recombination genes. The *recA* gene encodes a DNA-dependent ATPase that binds to ssDNA and promotes strand invasion and exchange between homologous DNA molecules [223]. Among eukaryotes, the yeasts *S. cerevisiae* and *Schizosaccharomyces pombe* have four *RAD51*-like genes [224] whereas vertebrate animals and plants have seven types of *RAD51*-like genes [225]. The eukaryotic *RAD51*s maintains the genomic integrity in both mitotic and meiotic cell cycles [225]. There is 59% identity between *S. cerevisiae,* human, and mouse in the case of Rad51 protein (Rad51p) and 30% identity to RecA protein of bacteria [226], whereas yeast and human proteins are 60% identical in the case of Rad52 proteins (Rad52p) [227]. The recombinational pathway of DSBs seems to be operated in late S- and G2-phases in mammalian cells [228]. Plants have also been reported to have significant recombinational repair [229]. The first step in HR is the resection of 5′ ends to produce a 3′ ssDNA overhang by means of an exonuclease (such as RecBCD in *E. coli*, MRX-complex in *S. cerevisiae*, and MRN-complex in vertebrates). Rad51 [230], a central protein in HR, binds the exposed single-stranded tails, forming a nucleoprotein filament and this early step is promoted by a Rad55/Rad57 protein heterodimer [231] by overcoming the inhibitory effects of the heterotrimeric single-stranded DNA binding protein RPA [232]. It has been found

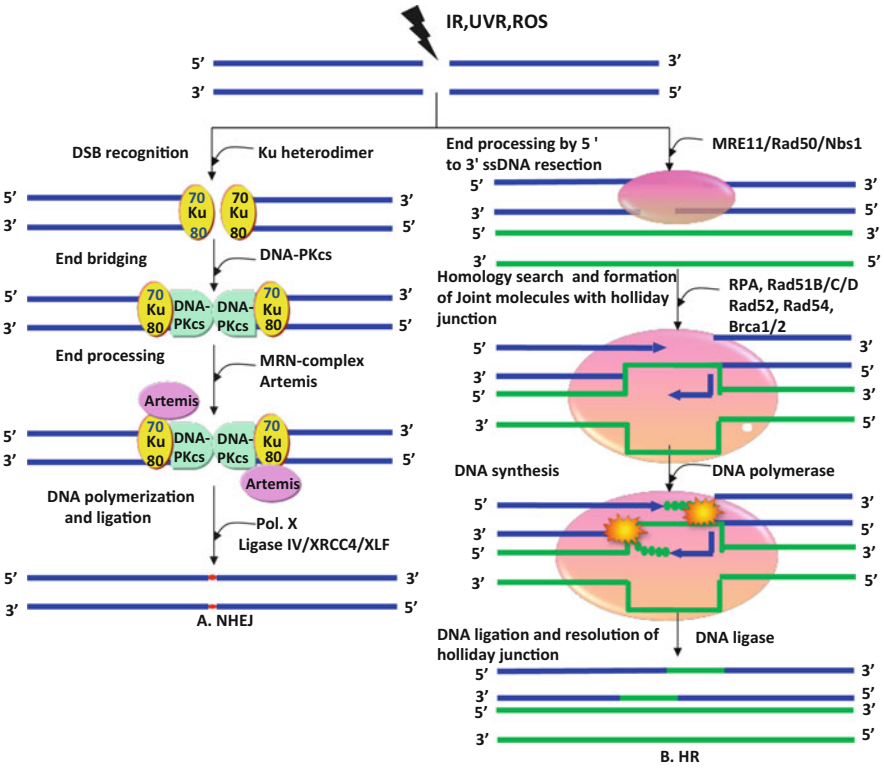

Fig. 10 Schematic overview of recombinational repair by (**a**) non-homologous end joining (NHEJ) and (**b**) homologous recombination (HR)

that the recruitment of Rad51 protein in eukaryotes is assisted by γ-H2AX protein [233]. The Rad51 nucleoprotein filament in association with other repair protein searches the genome for an intact copy of the broken DNA on the sister chromatid to form a heteroduplex of joint molecules or D-loop that is matured into a Holliday junction (HJ) (Fig. 10). HJ is then resolved to give crossover products. In *E. coli*, this HJ is resolved by the positioning of RuvABC resolvasome; however, the mechanism is unclear in eukaryotic cells. The noncrossover product in *S. cerevisiae* does not involve the processing of a double HJ structure. The joint molecule thus formed is followed by extension of the incoming strand by DNA polymerases and branch migration, leading to restoration of the genetic information [221].

5.3.2 Non-homologous End Joining

NHEJ, an alternate pathway, is highly conserved in prokaryotes and mammals and becomes functional when HR is inactivated. Most of the protein factors involved in

NHEJ were initially identified in mammalian cells [234]. The participation of DNA polymerase λ (Pol. λ) and/or polymerase μ (Pol. μ) in the NHEJ process to generate ligatable termini is still a matter of discussion [235]. The NHEJ process is initiated by the binding of a specific protein to the broken ends, which may acts as an end bridging factor [236]. It has been shown that Ku complex (a heterodimer of Ku70/Ku80 [≈86 kDa]) is a major end binding factor in mammalian cells, possessing end bridging activity [237]. The catalytic subunit of DNA protein kinase (DNA-PKcs) is required in mammalian NHEJ to bridge the DNA ends through their protein–protein interactions [238]. Cells lacking functional DNA-PK components are known to have elevated sensitivity toward UV irradiation [239]. Several repair proteins, such as ligaseIV/Xrcc4, Artemis, PNK, and Polymerase X, are then recruited to proceed with the NHEJ repair [234]. Recently, XLF [240] homologous to Xrcc4 have been found to co-associate with the DNA ligaseIV/Xrcc4 complex [241]. Artemis, a member of the β-lactamase superfamily, has $5' \rightarrow 3'$ exonuclease activity. In the presence of DNA-PKcs, Artemis can also function as a $5' \rightarrow 3'$ endonuclease. Artemis-dependent DSB rejoining also involves ATM, Mre11-Rad50-Nbs1 (MRN) complex, 53BP1, and H2AX [112–114]. The yeasts Hdf1/2 and Dnl4/Lif1 have been reported to show functional homology with mammalian Ku and DNA ligaseIV/Xrcc4, respectively. Mre11-Rad50-Xrs2 (MRX) acts as an end bridging factor in yeast NHEJ instead of DNA-PKcs [115, 242]. Aravind et al. [118] have reported the presence of Ku proteins in bacteria in homodimeric forms which exhibit homology with eukaryotic Ku protein to some extent.

UV-induced chromosomal rearrangements including homologous intrachromosomal recombination events have been reported in plants [229]. However, only a few of the plant genes involved in DSB repair have been identified. The sequence of an *Arabidopsis Rad51* homologue has been made available [119]. It has been reported that, as in mammals, breaks are repaired by nonhomologous recombination more frequently than via HR [120].

5.4 SOS Response

The accumulation of large amounts of DNA lesions within the cells under different specific physiological responses [121] may lead to the occurrence of an SOS repair system. SOS repair involving more than 40 genes has been described in *E. coli* [122]. It has been found that the bacterial NER is linked with all DNA damage responses through a network of reactions known as SOS response [243]. The SOS repair system is initiated by interaction of two important proteins, the RecA and the LexA repressors, which curb the expression of SOS genes by binding to their promoters [123] (Fig. 11). The proteolytic activity of RecA protein inactivates the LexA repressor and induces all the genes with which LexA is associated. A number of genes collectively known as din (damage inducible) genes such as *uvrA, uvrB, cho* (*uvrC* homolog), and *uvrD* of *E. coli* NER take part in SOS response [122]. The SOS response is highly mutagenic due to engagement of error-prone

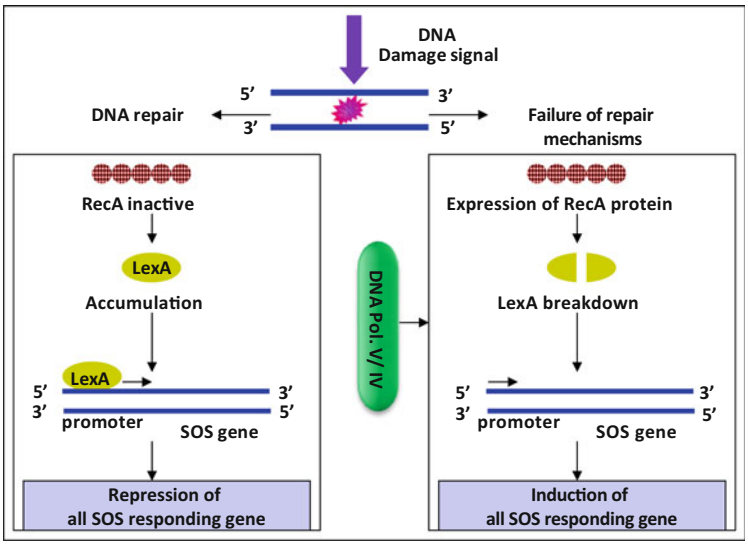

Fig. 11 Mechanism of SOS response involving DNA polymerase V/IV. Expression of RecA proteins activates the auto breakdown of LexA proteins, allowing the induction of all SOS responsible genes

DNA polymerase V (UmuC/UmuD2 complex) [126] and DNA polymerase IV [127] in *E. coli*. DNA polymerase IV (dinB) has been found to be involved in translesion synthesis in *E. coli* [128]. A number of homologous umuD and umuC genes of *E. coli* have been reported in plasmids of various hosts [244]. Majchrzak et al. [121] observed that SOS response genes destabilized the trinucleotide repeat sequences (TRS) tracts in *E. coli* and also altered the superhelical density of the plasmids. Galhardo et al. [129] have reported the role of genes *imuA* and *imuB* in induction of SOS mutagenesis in *Caulobacter crescentus*, but absent in *E. coli*. However, extensive work is needed to investigate the genes of the SOS mechanism.

5.5 *Cell-Cycle Checkpoint Activation*

To overcome the lethal effect of various genotoxic stresses, such as UV radiation, IR, genotoxic chemicals, and by-products of intra-cellular metabolism, organisms have developed several protective mechanisms including processes of DNA repair, cell-cycle checkpoint arrest, and apoptosis (programmed cell death) that ensures genomic integrity [108]. DNA damage may stop the progression of the cell-cycle temporarily to give opportunities to the cell for DNA repair before replication or segregation of the affected chromosome [245], or may induce an apoptotic program to eliminate the damaged cells to avoid their carcinogenic potential [130]. Most of the chromosomal translocations have been shown to work via aberrant processing

of a DNA DSBs. Regulation of cell-cycle checkpoints proceeds through a network of damage sensors, signal transducers, mediators, and various effector proteins [165]. Phosphatidylinositol-3 (PI3)-kinase related kinases (PIKKs), ATM (ataxia telangiectasia mutated) protein, ATR (ATM and Rad3 related) protein, and DNA-PK, with effector proteins mediated cell-cycle checkpoint arrest (at G1/S, G2/M, and intra S-phase), DNA repair, and cell death have been observed in mammalian cells [132]. DSBs activate the ATM and DNA-PK whereas activation of ATR occurs by single strand regions of DNA [131] which results in phosphorylation of Chk2 and Chk1, respectively, causing the transfer of DNA damage signals to the cell-division cycle proteins Cdc25(A-C). Phosphorylation of Cdc25 by Chk1/Chk2 leads to its degradation, resulting in G1 and S-phase arrest.

Lukas et al. [132] suggested that damage response mediated activation of ATM/ATR either directly or via Chk2 phosphorylates p53, which transcriptionally activates the Cdk inhibitor, p21, will arrest the G1/S cell-cycle checkpoint. It has recently been reported that DNA damage caused by UV radiation or ROS such as hydroxyl radicals (˙OH) results in ATM-mediated phosphorylation of BID protein that induces cell-cycle arrest in the S-phase [111]. The occurrence of DNA damage response in the G2-phase leads to checkpoint mediator (claspin)-dependent activation of Chk1/2, followed by SCFβTrcP-mediated degradation of CDK-activating phosphatase Cdc25A [246], resulting in the arrest of multiple cell-cycle transition including the G2 checkpoint [247, 248]. The ubiquitin-mediated destruction of claspin and WEE1 (both proteins have conserved β-TrcP phosphodegrons) eliminates the essential coactivator of Chk1 and CDK inhibitor, respectively, allowing reaccumulation of Cdc25A followed by Cdc25B and C, which results in activation of the cyclin-Cdk (cyclinB-Cdk1) complex [249]. This complex, under normal conditions, promotes G2/M transition and, upon inactivation, blocks the G2 cell-cycle, and, unlike the G1/S checkpoint, this arrest seems to be partly p53/p21 independent [165]. β-TrcP, an adaptor protein, links both WEE1 [250] and claspin [251] with the SCF ubiquitin ligase complex and this SCFβTrcP acts as a trigger to checkpoint initiation where recognition of phosphodegron β-TrcP is exposed after Chk1 mediated phosphorylation of Cdc25A [252], as well as checkpoint recovery, which is linked to Plk1mediated phosphorylation of claspin and WEE1 [251]. However, chronic damage and/or defects in DNA damage response results in malfunctioning of cell-cycle checkpoints which may induce several types of human disorder due to enhanced genomic instability [253].

6 Detection of DNA Damage

A number of methods have been used to determine DNA damage in a variety of organisms [8, 254, 255]. Radioactive methods have been employed in a cyanobacterium *Synechocystis* to detect UV-induced DNA degradation. An alkaline gel method for quantitating single strand breaks (SSBs) in nanogram quantities of nonradioactive DNA was developed by Freeman et al. [256]. Mitchell et al. [255]

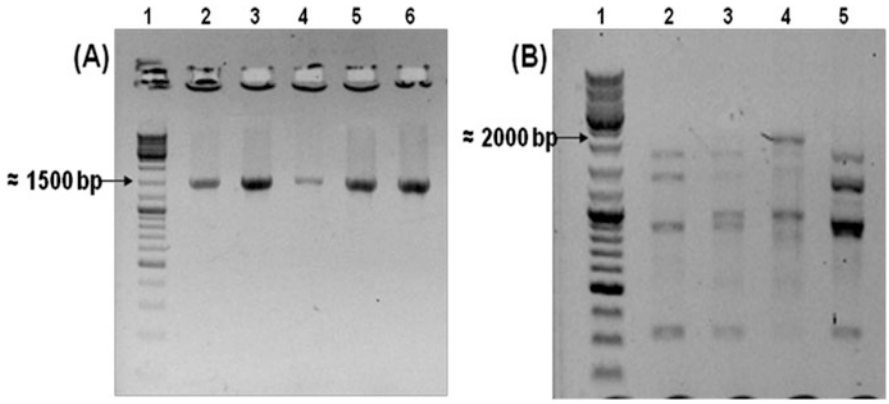

Fig. 12 16S rDNA (**a**) and RAPD (**b**) of *Anabaena variabilis* PCC 7937 after exposure of cultures to simulated solar radiation for 24 h. (**a**) Lane 1 (DNA marker), lane 2 (dark control), lane 3 (light control; without UV-B exposure), lane 4 (PAR + UV-A + UV-B), lane 5 (PAR + UV-A) and lane 6 (PAR only). (**b**) Lane 1, DNA ladder (1 kb); lane 2 (395 nm cut-off filter), lane 3 (320 nm cut-off filter), lane 4 (295 nm cut-off filter), and lane 5 (unirradiated control) (modified from [262])

have developed a method for the detection of CPDs, where DNA is labeled with radioactive substances followed by agarose gel electrophoresis and densitometric analysis and finally digesting with endo.III and endo.V before analyzing on sequencing gels. Wang et al. [257] have reported the detection of UV-B-induced DNA damage in mammalian genome utilizing PCR-based short interspersed DNA element (SINE). Terminal transferase-dependent PCR (TD-PCR) has been used for analyzing 6-4PPs [258]. Hercegová et al. [259] suggested that immunoassay is a simple and efficient method to visualize the CPDs in comparison to the Small and Greimann [260] technique. Kumar et al. [261] demonstrated a UV-induced decrease in template activity of genomic DNA of cyanobacterium *Anabaena* strain BT2 using the PCR-based assays such as random amplified polymorphic DNA (RAPD) and rDNA amplification. Rastogi et al. [262] based his study on RAPD and rDNA amplification and reported that template activity of DNA was affected under both UV-A and UV-B radiation in comparison to unirradiated cultures of *Anabaena variabilis* PCC 7937 (Fig. 12). Formation of thymine dimer (T^T) within human genomic DNA has been detected by immunocoupled PCR (IC-PCR) [258]. Methods for detecting CPDs and 6-4PPs at the nucleotide levels are also available [263–266]. DNA damage such as SSBs, DSBs, and oxidative DNA damage caused by UV-induced ROS, etc., may be detected by Comet assay [267]. Modified Comet and alkaline elution assays have been developed for monitoring the formation and the repair of CPDs in isolated cells using either DNA repair enzymes and/or specific antibodies against DNA lesions [268–271]. Recently, a modified version of Comet assay (apo/necro-Comet assay) has been developed that differentiates viable, apoptotic, and necrotic cells and also correlates the DNA fragmentation pattern [272]. The inability of TUNEL assay to distinguish between various types of cell death arising due to SSBs, DSBs, and apoptosis has led to the development of a new

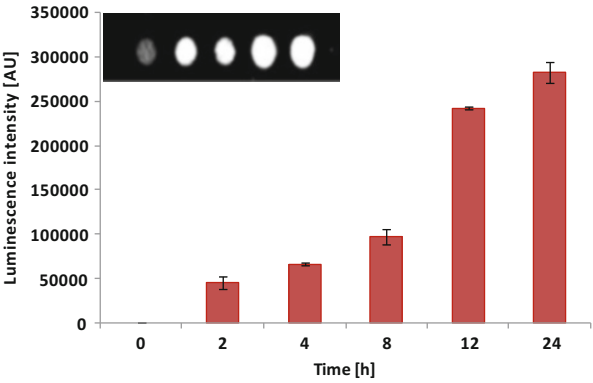

Fig. 13 Induction of thymine cyclobutane dimers in *Anabaena variabilis* PCC 7937 after different durations of UV-B radiation. *Inset* shows the immuno-dot blot pattern of thymine dimer formation (modified from [262])

flow cytometry-based method for detection of apoptosis [273]. HPLC coupled with electrospray ionization-tandem mass spectrometry (HPLC-ESI-MS/MS) is considered as the gold standard method for monitoring the formation of dimeric pyrimidine photoproducts in isolated cells and human skin [37, 274]. FCM assay is useful in detecting chromosomal aberrations, sister chromatid exchange, chemical adducts to DNA, and DNA strand breakage [275]. Nucleotide excision repair (NER) is detected with alkaline unwinding FCM (AU-FCM) [276]. Singh and Farmer [277] reported the use of liquid chromatography coupled with electrospray ionization mass spectrometry as a method for detecting DNA adducts. The changes in DNA organization in the individual cells can be determined by halo assay [278]. UV-B-induced DNA damage was detected in *A. variabilis* PCC7937 and *Rivularia* HKAR-4 by PCR [279]. DNA strand breaks induced by UVR can also be detected by fluorometric analysis of DNA unwinding (FADU) assay, which was first reported by Birnboim and Jevcak [280] to detect X ray-induced DNA damage in mammalian cells. Rastogi et al. [262] utilized FADU assay to detect the UV-induced DNA strand breaks and observed maximum loss in the percentage of dsDNA under UV-B radiation followed by UV-A. Numerical aberrations in chromosomes can be detected efficiently by the fluorescence in situ hybridization (FISH) method [281]. A number of workers have reported numerous applications of immunoassays such as ELISA, dot-blot, etc., involving either polyclonal or monoclonal antibodies against the main classes of dimeric pyrimidine photoproducts [282–286]. The immuno-dot-blot assay, utilizing thymine-dimer specific antibodies, has been developed to detect UV-induced photoproducts in various organisms ranging from prokaryotes to eukaryotes [287]. Rastogi et al. [262] reported the formation of thymine cyclobutane dimers in the cyanobacterium *Anabaena variabilis* PCC 7937 using the immuno-dot-blot technique. He observed that maximum yield of the dimer was under a 280 nm cut-off filter and an induction in the formation of thymine dimer was observed with increasing UV-irradiation times (Fig. 13). Radio-immunoassay (RIA) has been utilized to detect very low amounts of CPDs caused by UVR in bacterioplankton and marine viruses [288]. Kara et al. [289] have studied the electrochemical detection of DNA damage

by direct and indirect irradiation with radioactive technetium (TC-99 m) and iodine (I-131). High-performance liquid chromatography and mass spectrometry were used to detect 5-methylcytosine and adenine [78]. Kumari et al. [254] have made an attempt to dissect various strategies for detection of DNA lesions produced by a number of genotoxic agents.

In addition to the above-mentioned repair mechanisms, several other repair machineries such as lesion bypass and programmed cell death (PCD) or apoptosis may become effective for maintaining genomic stability. However, if for certain reasons the repair mechanisms become botched, it may then cause cellular senescence (permanent cell cycle arrest), oncogenesis, or apoptosis [290]. Apoptosis plays an essential role in the survival of organisms by preventing the multiplication of mutated chromosomes, enabling normal embryonic development, eliminating indisposed cells, and maintaining cell homeostasis. Malfunctioning of any of these repair pathways may lead to several diseases such as cancer, xeroderma pigmentosum, autoimmune disorders, etc.

7 Future Perspectives

The formation and distribution of UVR-induced DNA photoproducts in several organisms has been determined during the last few decades. However, the molecular mechanisms of DNA damage and repair in certain organisms such as cyanobacteria, phytoplankton, and macroalgae are still poorly understood. There is the possibility of the existence of hitherto unknown types of DNA lesions induced by UVR that need to be further explored. Photoreactivation is an efficient and rapid repair mechanism that can be extremely important for organisms living in brightly lit habitats. However, the regulation of photolyase enzymes by several wavebands of light and temperature regimes needs to be explored in various photosynthetic organisms. NER is a versatile and flexible repair system the function of which is to remove UV-induced DNA lesions. Defects in this pathway result in the serious cancer-prone inherited disease Xeroderma pigmentosum (XP). It is notable that humans do not have any backup pathway for this important cellular defense mechanism. Therefore NER-defective individuals are more or less unable to excise pyrimidine dimers from DNA. This situation is unique to placental mammals since lower eukaryotes, plants, and bacteria all have additional defense systems against UV radiation such as DNA photolyases which monomerize dimers or DNA glycosylases or nucleases to incise DNA specifically at pyrimidine dimers. Although there are several methods to detect the DNA damage, their efficiencies need to be improved.

Acknowledgment The work outlined in this review was partially supported by Department of Science and Technology, Government of India under the project No. SR/WOS-A/LS-140/2011 granted to Richa.

References

1. Kramlich JC, Linak WP (1994) Nitrous oxide behavior in the atmosphere, and in combustion and industrial systems. Prog Energy Combust Sci 20:149–202
2. Llabrés M, Agustí S, Alonso-Laita P, Herndl GJ (2010) *Synechococcus* and *Prochlorococcus* cell death induced by UV radiation and the penetration of lethal UVR in the Mediterranean Sea. Mar Ecol Prog Ser 399:27–37
3. Zeeshan M, Prasad SM (2009) Differential response of growth, photosynthesis, antioxidant enzymes and lipid peroxidation to UV-B radiation in three cyanobacteria. South Afr J Bot 75:466–474
4. Chalker-Scott L (1995) Survival and sex ratios of the intertidal copepod, *Tigriopus californicus*, following ultraviolet-B (290–320 nm) radiation exposure. Mar Biol 123:799–804
5. Rastogi RP, Singh SP, Häder D-P, Sinha RP (2010) Detection of reactive oxygen species (ROS) by the oxidant-sensing probe 2′,7′-dichlorodihydrofluorescein diacetate in the cyanobacterium *Anabaena variabilis* PCC 7937. Biochem Biophys Res Commun 397:603–607
6. Vincent WF, Neale PJ (2000) Mechanisms of UV damage to aquatic organisms. In: de Mora SJ, Demers S, Vernet M (eds) The effects of UV radiation on marine ecosystems. Cambridge University Press, Cambridge, pp 149–176
7. Peak MJ, Peak JG (1982) Single-strand breaks induced in *Bacillus subtilis* DNA by ultraviolet light: action spectrum and properties. Photochem Photobiol 35:675–680
8. Sinha RP, Dautz M, Häder D-P (2001) A simple and efficient method for the quantitative analysis of thymine dimers in cyanobacteria, phytoplankton and macroalgae. Acta Protozool 40:187–195
9. Buma AGJ, De Boer MK, Boelen P (2001) Depth distributions of DNA damage in antarctic marine phyto and bacterioplankton exposed to summertime UV radiation. J Phycol 37:200–208
10. Pakker H, Beekman CAC, Breeman AM (2000) Efficient photoreactivation of UVBR-induced DNA damage in the sublittoral macroalga *Rhodymenia pseudopalmata* (Rhodophyta). Eur J Phycol 35:109–114
11. Quaite FE, Sutherland BM, Sutherland JC (1992) Quantitation of pyrimidine dimers in DNA from UVB irradiated alfalfa (*Medicago sativa* L.) seedlings. Appl Theor Electrophor 2:171–175
12. Hargreaves A, Taiwo FA, Duggan O, Kirk SH, Ahmad SI (2007) Near-ultraviolet photolysis of β-phenylpyruvic acid generates free radicals and results in DNA damage. J Photochem Photobiol B Biol 89:110–116
13. Rastogi RP, Richa, Sinha RP, Singh SP, Häder D-P (2010) Photoprotective compounds from marine organisms. J Ind Microbiol Biotechnol 37:537–558
14. Richa, Sinha RP (2013) Biomedical applications of mycosporine-like amino acids. In: Kim SE (ed) Marine microbiology, bioactive compounds and biotechnological applications. Wiley, Germany, pp 509–534
15. Sinha RP, Singh SP, Häder D-P (2007) Database on mycosporines and mycosporine-like amino acids (MAAs) in fungi, cyanobacteria, macroalgae, phytoplankton and animals. J Photochem Photobiol B 89:29–35
16. Xie Z, Wang Y, Liu Y, Liu Y (2009) Ultraviolet-B exposure induces photo-oxidative damage and subsequent repair strategies in a desert cyanobacterium *Microcoleus vaginatus* Gom. Eur J Soil Biol 45:377–382
17. Rastogi RP, Richa, Singh SP, Häder D-P, Sinha RP (2010) Mycosporine-like amino acids profile and their activity under PAR and UVR in a hot-spring cyanobacterium *Scytonema* sp. HKAR-3. Aus J Bot 58:286–293
18. Britt AB (2004) Repair of DNA damage induced by solar UV. Photosynth Res 81:105–112
19. Häder D-P, Sinha RP (2005) Solar ultraviolet radiation-induced DNA damage in aquatic organisms: potential environmental impact. Mutat Res 571:221–233

20. Sinha RP, Häder D-P (2002) UV-induced DNA damage and repair: a review. Photochem Photobiol Sci 1:225–236
21. Lindahl T (1993) Instability and decay of the primary structure of DNA. Nature 362:709–715
22. Cooke MS, Loft S, Olinski R, Evans MD, Bialkowski K, Wagner JR, Dedon PC, Maller P, Greenberg MM, Cadet J (2010) Recommendations for standardized description of and nomenclature concerning oxidatively damaged nucleobases in DNA. Chem Res Toxicol 23:705–707
23. Halliwell B, Gutteridge J (2007) Free radicals in biology and medicine, 4th edn. Oxford University Press, Oxford
24. Dizdaroglu M (1992) Oxidative damage to DNA in mammalian chromatin. Mutat Res 275:331–342
25. Ley RD, Fourtanier A (1997) Sunscreen protection against ultraviolet radiation-induced pyrimidine dimers in mouse epidermal DNA. Photochem Photobiol 65:1007–1011
26. Regan JD, Setlow RB (1974) Two forms of repair in the DNA of human cells damaged by the chemical carcinogens and mutagens. Cancer Res 34:3318–3325
27. Cadet J, Sage E, Douki T (2005) Ultraviolet radiation-mediated damage to cellular DNA. Mutat Res 571:3–17
28. Ravanat J-L, Douki T, Cadet J (2001) Direct and indirect effects of UV radiation on DNA and its components. J Photochem Photobiol B 63:88–102
29. Friedberg EC, Walker GC, Siede W, Wood RD, Schultz RA, Ellenberger T (2006) DNA repair and mutagenesis, 2nd edn. ASM Press, Washington
30. Taylor JS, Lu HF, Kotyk JJ (1990) Quantitative conversion of the (6-4) photoproduct of TpdC to its Dewar valence isomer upon exposure to simulated sunlight. Photochem Photobiol 51:161–167
31. Cadet J, Mouret S, Ravanat JL, Douki T (2012) Photoinduced damage to cellular DNA: direct and photosensitized reactions. Photochem Photobiol 88:1048–1065
32. Courdavault S, Baudouin C, Charveron M, Canguilhem B, Favier A, Cadet J, Douki T (2005) Repair of the three main types of bipyrimidine DNA photoproducts in human keratinocytes exposed to UVB and UVA radiations. DNA Repair (Amst) 4:836–844
33. Bastien N, Therrien J-P, Drouin R (2013) Cytosine containing dipyrimidine sites can be hotspots of cyclobutane pyrimidine dimer formation after UV-B exposure. Photochem Photobiol Sci 12:1544–1554
34. Hariharan M, Lewis FD (2008) Context-dependent photodimerization in isolated thymine-thymine steps in DNA. J Am Chem Soc 130:11870–11871
35. Mitchell DL, Jen J, Cleaver JE (1992) Sequence specificity of cyclobutane pyrimidine dimers in DNA treated with solar (ultraviolet B) radiation. Nucleic Acids Res 20:225–229
36. Matallana-Surget S, Meador JA, Joux F, Douki T (2008) Effect of the GC content of DNA on the distribution of UVB-induced bipyrimidine photoproducts. Photochem Photobiol Sci 7:794–801
37. Douki T, Cadet J (2001) Individual determination of the yield of the main UV-induced dimeric pyrimidine photoproducts in DNA suggests a high mutagenicity of CC photolesions. Biochemistry 40:2495–2501
38. Desnous C, Guillaume D, Clivio P (2010) Spore photoproduct: a key to bacterial eternal life. Chem Rev 110:1213–1232
39. Kim JK, Patel D, Choi BS (1995) Contrasting structural impacts induced by *cis-syn* cyclobutane dimer and (6-4) adduct in DNA duplex decamers: implication in mutagenesis and repair activity. Photochem Photobiol 62:44–50
40. Wang CI, Taylor JS (1991) Site-specific effect of thymine dimer formation on dAn.dTn tract bending and its biological implications. Proc Natl Acad Sci USA 88:9072–9076
41. Becker MM, Wang Z (1989) Origin of ultraviolet damage in DNA. J Mol Biol 210:429–438
42. Lyamichev V (1991) Unusual conformation of (dA)n.(dT)n-tracts as revealed by cyclobutane thymine-thymine dimer formation. Nucleic Acids Res 19:4491–4496

43. Pehrson JR, Cohen LH (1992) Effects of DNA looping on pyrimidine dimer formation. Nucleic Acid Res 20:1321–1324
44. Aboussekhra A, Thoma F (1999) TATA-binding protein promotes the selective formation of UV-induced (6-4)-photoproducts and modulates DNA repair in the TATA box. EMBO J 18:433–443
45. You HY, Szabo PE, Pfeifer GP (2000) Cyclobutane pyrimidine dimers form preferentially at the major p53 mutational hotspot in UVB-induced mouse skin tumors. Carcinogenesis 21:2113–2117
46. Kvam E, Tyrrell RM (1997) Induction of oxidative DNA base damage in human skin cells by UV and near visible radiation. Carcinogenesis 18:2379–2384
47. Perdiz D, Gróf P, Mezzina M, Nikaido O, Moustacchi E, Sage E (2000) Distribution and repair of bipyrimidine photoproducts in solar UV-irradiated mammalian cells: possible role of Dewar photoproducts in solar mutagenesis. J Biol Chem 275:26732–26742
48. Mouret S, Baudouin C, Charveron M, Favier A, Cadet J, Douki T (2006) Cyclobutane pyrimidine dimers are predominant DNA lesions in whole human skin exposed to UVA radiation. Proc Natl Acad Sci USA 103:13765–13770
49. Mouret S, Charveron M, Favier A, Cadet J, Douki T (2008) Differential repair of UVB-induced cyclobutane pyrimidine dimers in cultured human skin cells and whole human skin. DNA Repair (Amst) 7:704–712
50. Tewari A, Sarkany RP, Young AR (2012) UVA1 induces cyclobutane pyrimidine dimers but not 6-4 photoproducts in human skin in vivo. J Invest Dermatol 132:394–400
51. Courdavault S, Baudouin C, Charveron M, Favier A, Cadet J, Douki T (2004) Larger yield of cyclobutane dimers than 8-oxo-7,8-dihydroguanine in the DNA of UV-A irradiated human skin cells. Mutat Res 556:135–142
52. Douki T, Reynaud-Angelin A, Cadet J, Sage E (2003) Bipyrimidine photoproducts rather than oxidative lesions are the main type of DNA damage involved in the genotoxic effect of solar UVA radiation. Biochemistry 42:9221–9226
53. Wierzchowski KL, Shugar D (1961) Photochemistry of cytosine nucleosides and nucleotides, II. Acta Biochim Pol 8:219–234
54. Douki T, Vadesne-Bauer G, Cadet J (2002) Formation of 2′-deoxyuridine hydrates upon exposure of nucleosides to gamma radiation and UVC-irradiation of isolated and cellular DNA. Photochem Photobiol Sci 1:565–569
55. Boorstein RJ, Hilbert TP, Cunningham RP, Teebor GW (1990) Formation and stability of repairable pyrimidine photohydrates in DNA. Biochemistry 29:10455–10460
56. Mitchell DL, Vaughan JE, Nairn RS (1989) Inhibition of transient gene expression in Chinese hamster ovary cells by cyclobutane dimers and (6-4) photoproducts in transfected ultraviolet-irradiated plasmid DNA. Plasmid 21:21–30
57. Protic-Sabljic M, Kraemer KH (1986) One pyrimidine dimer inactivates expression of a transfected gene in Xeroderma pigmentosum cells. Proc Natl Acad Sci USA 82:6622–6626
58. Britt AB (1995) Repair of DNA damage induced by ultraviolet radiation. Plant Physiol 108:891–896
59. Cadet J, Douki T, Ravanat JL, Di Mascio P (2009) Sensitized formation of oxidatively generated damage to cellular DNA by UVA radiation. Photochem Photobiol Sci 8:903–911
60. Swalwell H, Latimer J, Haywood RM, Birch-Machin MA (2012) Investigating the role of melanin in UVA/UVB- and hydrogen peroxide-induced cellular and mitochondrial ROS production and mitochondrial DNA damage in human melanoma cells. Free Radic Biol Med 52:626–634
61. Wischermann K, Popp S, Moshir S, Kochanek KS, Wlaschek M, de Gruijl F, Hartschuh W, Greinert R, Volkmer B, Faust A, Rapp A, Schmezer P, Boukamp P (2008) UVA radiation causes DNA strand breaks, chromosomal aberrations and tumorigenic transformation in HaCaT skin keratinocytes. Oncogene 27:4269–4280
62. Cadet J, Douki T (2011) Oxidatively generated damage to DNA by UVA radiation in cells and human skin. J Invest Dermatol 131:1005–1007

63. Cleaver JE (2011) γH2Ax: biomarker of damage or functional participant in DNA repair "All that glitters is not gold!". Photochem Photobiol 87:1230–1239
64. Rizzo JL, Dunn J, Rees A, Runger TM (2011) No formation of DNA double-strand breaks and no activation of recombination repair with UVA. J Invest Dermatol 131:1139–1148
65. Revet I, Feeney L, Bruguera S, Wilson W, Dong TK, Oh DH, Dankort D, Cleave JE (2011) Functional relevance of the histone γH2Ax in the response to DNA damaging agents. Proc Natl Acad Sci USA 108:8663–8667
66. Greinert R, Volkmer B, Henning S, Breitbart EW, Greulich KO, Cardoso MC, Rapp A (2012) UVA-induced DNA double-strand breaks result from the repair of clustered oxidative DNA damages. Nucleic Acids Res 40:10263–10273
67. Runger TM, Farahvash B, Hatvani Z, Rees A (2012) Comparison of DNA damage responses following equimutagenic doses of UVA and UVB: a less effective cell cycle arrest with UVA may render UVA-induced pyrimidine dimers more mutagenic than UVB-induced ones. Photochem Photobiol Sci 11:207–215
68. Duker NJ, Gallagher PE (1988) Purine photoproducts. Photochem Photobiol 48:35–39
69. Koning TMG, Davies RJH, Kaptein R (1990) The solution structure of the intramolecular photoproduct of d(TpA) derived with the use of NMR and a combination of distance geometry and molecular dynamics. Nucleic Acids Res 18:277–284
70. Kumar S, Sharma ND, Davies RJ, Phillipson DW, McCloskey JA (1987) The isolation and characterisation of a new type of dimeric adenine photoproduct in UV-irradiated deoxyadenylates. Nucleic Acids Res 15:1199–1216
71. Bose SN, Davies RJ (1984) The photoreactivity of T-A sequences in oligodeoxyribonucleotides and DNA. Nucleic Acids Res 12:7903–7914
72. Porschke D (1973) A specific photoreaction in polydeoxyadenylic acid. Proc Natl Acad Sci USA 70:2683–2686
73. Davies RJH (1997) Purines as targets for DNA photodamage. Biochem Soc Trans 25:323–326
74. Sharma ND, Davies RJH (1989) Extent of formation of a dimeric adenine photoproduct in polynucleotides and DNA. J Photochem Photobiol B 3:247–258
75. Bowden GM, Davies RJ (1997) Thymine-adenine photoadduct formation in UV-irradiated human cells. Biochem Soc Trans 25:130S
76. Davies RJH, Malone JF, Gan Y, Cardin CJ, Lee MPH, Neidle S (2007) High-resolution crystal structure of the intramolecular d(TpA) thymine–adenine photoadduct and its mechanistic implications. Nucleic Acids Res 35:1048–1053
77. Zhao X, Nadji S, Kao JLF, Taylor JS (1996) The structure of d(TpA)*, the major photoproduct of thymidylyl-(3′-5′)-deoxyadenosine. Nucleic Acids Res 24:1554–1560
78. Su DGT, Taylor JSA, Gross ML (2010) A new photoproduct of 5-methylcytosine and adenine characterized by high-performance liquid chromatography and mass spectrometry. Chem Res Toxicol 23:474–479
79. Pouget JP, Douki T, Richard MJ, Cadet J (2000) DNA damage induced in cells by γ and UVA radiation as measured by HPLC/GC–MS and HPLC–EC and comet assay. Chem Res Toxicol 13:541–549
80. Hall DB, Holmlin RE, Barton JK (1996) Oxidative DNA damage through long-range electron transfer. Nature 382:731–735
81. Cadet J, Wagner JR (2013) DNA base damage by reactive oxygen species, oxidizing agents, and UV radiation. Cold Spring Harb Perspect Biol 5:a012559
82. Cortat B, Garcia CCM, Quinet A, Schuch AP, de Lima-Bessa KM, Menck CFM (2013) The relative roles of DNA damage induced by UVA irradiation in human cells. Photochem Photobiol Sci 12:1483–1495
83. Schuch AP, Yagura T, Makita K, Yamamoto H, Schuch NJ, Agnez-Lima LF, MacMahon RM, Menck CFM (2012) DNA damage profiles induced by sunlight at different latitudes. Environ Mol Mutagen 53:198–206
84. Wang TV, Smith KC (1986) Post replication repair in ultraviolet-irradiated human fibroblasts: formation and repair of DNA double-strand breaks. Carcinogenesis 7:389–392

85. Batista LFZ, Kaina B, Meneghini R, Menck CFM (2009) How DNA lesions are turned into powerful killing structures: insights from UV-induced apoptosis. Mutat Res 681:197–208
86. Dunkern TR, Kaina B (2002) Cell proliferation and DNA breaks are involved in ultraviolet light-induced apoptosis in nucleotide excision repair-deficient Chinese hamster cells. Mol Biol Cell 13:348–361
87. Takahashi A, Ohnishi T (2005) Does γH2AX foci formation depend on the presence of DNA double strand breaks? Cancer Lett 229:171–179
88. Mahaney BL, Meek K, Lees-Miller SP (2009) Repair of ionizing radiation-induced DNA double-strand breaks by non-homologous end-joining. Biochem J 417:639–650
89. Povirk LF (2006) Biochemical mechanisms of chromosomal translocations resulting from DNA double-strand breaks. DNA Repair (Amst) 5:1199–1212
90. Lottner S, Shehata M, Hickel R, Reichl F-X, Durner J (2013) Effects of antioxidants on DNA-double strandbreaks in human gingival fibroblasts exposed to methacrylate based monomers. Dent Mater 29:991–998
91. Ohnishi T, Mori E, Takahashi A (2009) DNA doublestrand breaks: their production, recognition, and repair in eukaryotes. Mutat Res 669:8–12
92. Strumberg D, Pilon AA, Smith M, Hickey R, Malkas L, Pommier Y (2000) Conversion of topoisomerase I cleavage complexes on the leading strand of ribosomal DNA into 5′-phosphorylated DNA double-strand breaks by replication runoff. Mol Cell Biol 20:3977–3987
93. Box HC, Dawidzik JB, Budzinski EE (2001) Free radical induced double lesions in DNA. Free Radical Biol Med 31:856–868
94. Harper JV, Anderson JA, O'Neill P (2010) Radiation induced DNA DSBs: contribution from stalled replication forks? DNA Repair (Amst) 9:907–913
95. Zhou BBS, Elledge SJ (2000) The DNA damage response: putting checkpoints in perspective. Nature 408:433–439
96. Essers J, Vermeulen W, Houtsmuller AB (2006) DNA damage repair: anytime, anywhere? Curr Opin Cell Biol 18:240–246
97. Kelner A (1949) Effects of visible light on the recovery of *Streptomyces griseus* conidia from ultraviolet irradiation injury. Proc Natl Acad Sci USA 35:73–79
98. Dulbecco R (1949) Reactivation of ultra-violet-inactivated bacteriophage by visible light. Nature 163:949–950
99. Essen LO, Klar T (2006) Light-driven DNA repair by photolyases. Cell Mol Life Sci 63:1266–1277
100. Kim S-T, Heelis PF, Sancar A (1992) Energy transfer (deazaflavin → $FADH_2$) and electron transfer ($FADH_2$ → T<>T) kinetics in *Anacystis nidulans* photolyase. Biochemistry 31:11244–11248
101. Britt AB (1996) DNA damage and repair in plants. Annu Rev Plant Physiol Plant Mol Biol 47:75–100
102. Johnson JL, Hamm-Alvarez S, Payne G, Sancar GB, Rajagopalan KV, Sancar A (1988) Identification of the second chromophore of *Escherichia coli* and yeast DNA photolyases as 5,10-methenyltetrahydrofolate. Proc Natl Acad Sci 85:2046–2050
103. Eker APM, Kooiman P, Hessels JKC, Yasui A (1990) DNA photoreactivating enzyme from the cyanobacterium *Anacystis nidulans*. J Biol Chem 265:8009–8015
104. Ueda T, Kato A, Kuramitsu S, Terasawa H, Shimada I (2005) Identification and characterization of a second chromophore of DNA photolyase from *Thermus thermophilus* HB27. J Biol Chem 280:36237–36243
105. Morita R, Nakane S, Shimada A, Inoue M, Iino H, Wakamatsu T, Fukui K, Nakagawa N, Masui R, Kuramitsu S (2010) Molecular mechanisms of the whole DNA repair system: a comparison of bacterial and eukaryotic systems. J Nucleic Acids, Article ID 179594. doi:10.4061/2010/179594
106. Saxena C, Sancar A, Zhong D (2004) Femtosecond dynamics of DNA photolyase: energy transfer of antenna initiation and electron transfer of cofactor reduction. J Phys Chem B 108:18026–18033

107. Kao Y-T, Saxena C, Wang L, Sancar A, Zhong D (2005) Direct observation of thymine dimer repair in DNA by photolyase. Proc Natl Acad Sci USA 102:16128–16132
108. Rastogi RP, Richa, Kumar A, Tyagi MB, Sinha RP (2010) Molecular mechanisms of ultraviolet radiation-induced DNA damage and repair. J Nucleic Acids 2010:32. doi:10.4061/2010/592980
109. Shiloh Y (2003) ATM and related protein kinases: safeguarding genome integrity. Nat Rev Cancer 3:155–168
110. Jeggo PA, Löbrich M (2006) Contribution of DNA repair and cell cycle checkpoint arrest to the maintenance of genomic stability. DNA Repair (Amst) 5:1192–1198
111. Zinkel SS, Hurov KE, Ong C, Abtahi FM, Gross A, Korsmeyer SJ (2005) A role for proapoptotic BID in the DNA damage response. Cell 122:579–591
112. Riballo E, Kühne M, Rief N, Doherty A, Smith GC, Recio MJ, Reis C, Dahm K, Fricke A, Krempler A, Parker AR, Jackson SP, Gennery A, Jeggo PA, Lobrich M (2004) A pathway of double strand break rejoining dependent upon ATM, Artemis, and proteins locating to γ-H2AX foci. Mol Cell 16:715–724
113. Lloyd J, Chapman JR, Clapperton JA, Haire LF, Hartsuiker E, Li J, Carr AM, Jackson SP, Smerdon SJ (2009) A supramodular FHA/BRCT-repeat architecture mediates Nbs1 adaptor function in response to DNA damage. Cell 139:100–111
114. Williams RS, Dodson GE, Limbo O, Yamada Y, Williams JS, Guenther G, Classen S, Glover JN, Iwasaki H, Russell P, Tainer JA (2009) Nbs1 is an extended flexible arm binding to Ctp1 and Mre11-Rad50 to coordinate dsDNA break processing. Cell 139:87–99
115. Chen L, Trujillo K, Ramos W, Sung P, Tomkinson AE (2001) Promotion of Dnl4-Catalyzed DNA end-joining by the Rad50/Mre11/Xrs2 and Hdf1/Hdf2 complexes. Mol Cell 8:1105–1115
116. Petersen JL, Lang DW, Small GD (1999) Cloning and characterization of a class II DNA photolyase from *Chlamydomonas*. Plant Mol Biol 40:1063–1071
117. Takahashi S, Nakajima N, Saji H, Kondo N (2002) Diurnal changes of cucumber CPD photolyase gene (CsPHR) expression and its physiological role in growth under UV-B irradiation. Plant Cell Physiol 43:342–349
118. Aravind L, Dixit VM, Koonin EV (2001) Apoptotic molecular machinery: vastly increased complexity in vertebrates revealed by genome comparisons. Science 291:1279–1284
119. Doutriaux M-P, Couteau F, Bergounioux C, White C (1998) Isolation and characterisation of the RAD51 and DMC1 homologs from *Arabidopsis thaliana*. Mol Gen Genet 257:283–291
120. Vergunst AC, Hooykaas PJJ (1999) Recombination in the plant genome and its application in biotechnology. Crit Rev Plant Sci 18:1–31
121. Majchrzak M, Bowater RP, Staczek P, Parniewski P (2006) SOS repair and supercoiling influence the genetic stability of DNA triplet repeats in *Escherichia coli*. J Mol Biol 364:612–624
122. Courcelle J, Khodursky A, Peter B, Brown PO, Hanawalt PC (2001) Comparative gene expression profiles following UV exposure in wild-type and SOS-deficient *Escherichia coli*. Genetics 58:41–64
123. Martins-Pinheiro M, Marques RCP, Menck CFM (2007) Genome analysis of DNA repair genes in the alpha proteobacterium *Caulobacter crescentus*. BMC Microbiol 7:17
124. Eker APM, Yajima H, Yasui A (1994) DNA photolyase from the fungus *Neurospora crassa*. Purification, characterization and comparison with other photolyases. Photochem Photobiol 60:125–133
125. Van Houten B, Eisen JA, Hanawalt PC (2002) A cut above: discovery of an alternative excision repair pathway in bacteria. Proc Natl Acad Sci USA 99:2581–2583
126. Fuchs RP, Fujii S, Wagner J (2004) Properties and functions of *Escherichia coli* Pol IV and Pol V. Adv Protein Chem 69:229–264
127. Goodman MF (2000) Coping with replication 'train wrecks' in *Escherichia coli* using Pol V, Pol II and RecA proteins. Trends Biochem Sci 25:189–195

128. Strauss BS, Roberts R, Francis L, Pouryazdanparast P (2000) Role of the dinB gene product in spontaneous mutation in *Escherichia coli* with an impaired replicative polymerase. J Bacteriol 182:6742–6750
129. Galhardo RS, Rocha RP, Marques MV, Menck CFM (2005) An SOS-regulated operon involved in damage inducible mutagenesis in *Caulobacter crescentus*. Nucleic Acids Res 33:2603–2614
130. Lo H-L, Nakajima S, Ma L, Walter B, Yasui A, Ethell DW, Owen LB (2005) Differential biologic effects of CPD and 6-4PP UV-induced DNA damage on the induction of apoptosis and cell-cycle arrest. BMC Cancer 5:135
131. Mercer J, Mahmoudi M, Bennett M (2007) DNA damage, p53, apoptosis and vascular disease. Mutat Res 621:75–86
132. Lukas J, Lukas C, Bartek J (2004) Mammalian cell cycle checkpoints: signalling pathways and their organization in space and time. DNA Repair (Amst) 3:997–1007
133. Sancar A (1996) No end of history for photolyases. Science 272:48–49
134. Todo T (1999) Functional diversity of the DNA photolyase/blue light receptor family. Mutat Res 434:89–97
135. Sutherland BM (1974) Photoreactivating enzyme from human leukocytes. Nature 248:109–112
136. Harm H (1980) Damage and repair in mammalian cells after exposure to non-ionizing radiations. III. Ultraviolet and visible light irradiation of cells of placental mammals, including humans, and determination of photorepairable damage in vitro. Mutat Res 69:167–176
137. Hsu DS, Zhao X, Zhao S, Kazantsev A, Wang R-P, Todo T, Wei Y-F, Sancar A (1996) Putative human bluelight photoreceptors hCRY1 and hCRY2 are flavoproteins. Biochemistry 35:13871–13877
138. Carell T, Epple R (1998) Repair of UV light induced DNA lesions: a comparative study with model compounds. Eur J Org Chem 1998(7):1245–1258
139. Sancar A, Rupert CS (1978) Cloning of the *phr* gene and amplification of photolyase in *Escherichia coli*. Gene 4:295–308
140. Eker APM, Hessels JKC, Dekker RH (1986) Photoreactivating enzyme from *Streptomyces griseus* - VI. Action spectrum and kinetics of photoreactivation. Photochem Photobiol 44:197–205
141. Li YF, Sancar A (1991) Cloning, sequencing, expression and characterization of DNA photolyase from *Salmonella typhimurium*. Nucleic Acids Res 19:4885–4890
142. Tamada T, Kitadokoro K, Higuchi Y, Inaka K, Yasui A, de Ruiter PE, Eker AP, Miki K (1997) Crystal structure of DNA photolyase from *Anacystis nidulans*. Nat Struct Biol 4:887–891
143. Sancar GB, Smith FW, Reid R, Payne G, Levy M, Sancar A (1987) Action mechanism of Escherichia coli DNA photolyase. I. Formation of the enzyme-substrate complex. J Biol Chem 262:478–485
144. Kato R, Hasegawa K, Hidaka Y, Kuramitsu S, Hoshino T (1997) Characterization of a thermostable DNA photolyase from an extremely thermophilic bacterium, *Thermus thermophilus* HB27. J Bacteriol 179:6499–6503
145. Yajima H, Inoue H, Oikawa A, Yasui A (1991) Cloning and functional characterization of a eukaryotic DNA photolyase gene from *Neurospora crassa*. Nucleic Acids Res 19:5359–5362
146. Ng W-O, Zentella R, Wang Y, Taylor JSA, Pakrasi HB (2000) phrA, the major photoreactivating factor in the cyanobacterium *Synechocystis* sp. strain PCC 6803 codes for a cyclobutanepyrimidine-dimer-specific DNA photolyase. Arch Microbiol 173:412–417
147. Todo T, Takemori H, Ryo H, Ihara M, Matsunaga T, Nikaido O, Sato K, Nomura T (1993) A new photoreactivating enzyme that specifically repairs ultraviolet light-induced (6-4) photoproducts. Nature 361:371–374
148. Kim S-T, Malhotra K, Smith CA, Taylor J-S, Sancar A (1994) Characterization of (6-4) photoproduct DNA photolyase. J Biol Chem 269:8535–8540
149. Müller M, Carell T (2009) Structural biology of DNA photolyases and cryptochromes. Curr Opin Struct Biol 19:277–285

150. Hoerner RS, Weissenböck G (2003) Contribution of phenolic compounds to the UV-B screening capacity of developing barley primary leaves in relation to DNA damage and repair under elevated UV-B levels. Phytochemistry 64:243–255
151. Kaiser G, Kleiner O, Beisswenger C, Batschauer A (2009) Increased DNA repair in *Arabidopsis* plants overexpressing CPD photolyase. Planta 230:505–515
152. Kimura S, Tahira Y, Ishibashi T, Mori Y, Mori T, Hashimoto J, Sakaguchi K (2004) DNA repair in higher plants; photoreactivation is the major DNA repair pathway in non-proliferating cells while excision repair (nucleotide excision repair and base excision repair) is active in proliferating cells. Nucleic Acids Res 32:2760–2767
153. Kang H-S, Hidema J, Kumagai T (1998) Effects of light environment during culture on UV-induced cyclobutyl pyrimidine dimers and their photorepair in rice (*Oryza sativa* L.). Photochem Photobiol 68:71–77
154. Ahmad M, Cashmore AR (1993) The *HY4* gene of *Arabidopsis thaliana* encodes a protein with characteristics of a blue-light receptor. Nature 366:162–166
155. Batschauer A (1993) A plant gene for photolyase: an enzyme catalyzing the repair of UV-light induced DNA damage. Plant J 4:705–709
156. Todo T, Ryo H, Yamamoto K, Toh H, Inui T, Ayaki H, Nomura T, Ikenaga M (1996) Similarity among the *Drosophila* (6-4) photolyase, a human photolyase homology, and the DNA photolyase-blue-light photoreceptor family. Science 272:109–112
157. Mees A, Klar T, Gnau P, Hennecke U, Eker AP, Carell T, Essen LO (2004) Crystal structure of a photolyase bound to a CPD-like DNA lesion after in situ repair. Science 306:1789–1793
158. Torizawa T, Ueda T, Kuramitsu S, Hitomi K, Todo T, Iwai S, Morikawa K, Shimada I (2004) Investigation of the cyclobutane pyrimidine dimer (CPD) photolyase DNA recognition mechanism by NMR analyses. J Biol Chem 279:32950–32956
159. Heelis PF, Hartman RF, Rose SD (1995) Photoenzymic repair of UV-damaged DNA - a chemist's perspective. Chem Soc Rev 24:289–297
160. MacFarlane AW, Stanley RJ (2003) cis-syn Thymidine dimer repair by DNA photolyase in real time. Biochemistry 42:8558–8568
161. Kavakli IH, Sancar A (2004) Analysis of the role of intraprotein electron transfer in photoreactivation by DNA photolyase in vivo. Biochemistry 43:15103–15110
162. Sancar GB, Smith FW (1989) Interactions between yeast photolyase and nucleotide excision repair proteins in *Saccharomyces cerevisiae* and *Escherichia coli*. Mol Cell Biol 9:4767–4776
163. Prakash S, Sung P, Prakash L (1993) DNA repair genes and proteins of *Saccharomyces cerevisiae*. Annu Rev Genet 27:33–70
164. Almeida KH, Sobol RW (2007) A unified view of base excision repair: lesion-dependent protein complexes regulated by post-translational modification. DNA Repair (Amst) 6:695–711
165. Houtgraaf JH, Versmissen J, van der Giessen WJ (2006) A concise review of DNA damage checkpoints and repair in mammalian cells. Cardiovasc Revasc Med 7:165–172
166. Robertson AB, Klungland A, Rognes T, Leiros I (2009) Base excision repair: the long and short of it. Cell Mol Life Sci 66:981–993
167. Barnes DE, Lindahl T (2004) Repair and genetic consequences of endogenous DNA base damage in mammalian cells. Annu Rev Genet 38:445–476
168. Parsons JL, Tait PS, Finch D, Dianova II, Allinson SL, Dianov GL (2008) CHIP-mediated degradation and DNA damage-dependent stabilization regulate base excision repair proteins. Mol Cell 29:477–487
169. Fromme JC, Banerjee A, Verdine GL (2004) DNA glycosylase recognition and catalysis. Curr Opin Str Biol 14:43–49
170. Motta ES, Souza-Santos PT, Cassiano TR, Dantas FJS, Caldeira-De-Araujo A, De Mattos JCP (2010) Endonuclease IV is the main base excision repair enzyme involved in DNA damage induced by UVA radiation and stannous chloride. J Biomed Biotechnol, Article ID 376218, 9 p

171. Mundle ST, Delaney JC, Essigmann JM, Strauss PR (2009) Enzymatic mechanism of human apurinic/apyrimidinic endonuclease against a THF AP site model substrate. Biochemistry 48:19–26
172. Piersen CE, McCullough AK, Lloyd RS (2000) AP lyases and dRPases: commonality of mechanism. Mutat Res 459:43–53
173. Prasad R, Batra VK, Yang X-P, Krahn JM, Pedersen LC, Beard WA, Wilson SH (2005) Structural insight into the DNA polymerase β deoxyribose phosphate lyase mechanism. DNA Repair (Amst) 4:1347–1357
174. McCullough AK, Sanchez A, Dodson ML, Marapaka P, Taylor J-S, Lloyd RS (2001) The reaction mechanism of DNA glycosylase/AP lyases at abasic sites. Biochemistry 40:561–568
175. Fortini P, Dogliotti E (2007) Base damage and single-strand break repair: mechanisms and functional significance of short- and long-patch repair subpathways. DNA Repair (Amst) 6:398–409
176. Gary R, Kim K, Cornelius HL, Park MS, Matsumoto Y (1999) Proliferating cell nuclear antigen facilitates excision in long-patch base excision repair. J Biol Chem 274:4354–4363
177. Dodson ML, Michaels ML, Lloyd RS (1994) Unified catalytic mechanism for DNA glycosylases. J Biol Chem 269:32709–32712
178. Hamilton KK, Kim PMH, Doetsch PW (1992) A eukaryotic DNA glycosylase/lyase recognizing ultraviolet light-induced pyrimidine dimers. Nature 356:725–728
179. Bowman KK, Sidik K, Smith CA, Taylor J-S, Doetsch PW, Freyer GA (1994) A new ATP-dependent DNA endonuclease from *S. pombe* that recognizes cyclobutane pyrimidine dimers and 6-4 photoproducts. Nucleic Acids Res 22:3026–3032
180. Sukhanova M, Khodyreva S, Lavrik O (2009) Poly(ADPribose) polymerase 1 regulates activity of DNA polymerase β in long patch base excision repair. Mutat Res 685:80–89
181. Cuneo MJ, London RE (2010) Oxidation state of the XRCC1 N-terminal domain regulates DNA polymerase β binding affinity. Proc Natl Acad Sci USA 107:6805–6810
182. Sancar A (1996) DNA excision repair. Annu Rev Biochem 65:43–81
183. Van Houten B (1990) Nucleotide excision repair in *Escherichia coli*. Microbiol Rev 54:18–51
184. Costa RMA, Chigancas V, Galhardo RDS, Carvalho H, Menck CFM (2003) The eukaryotic nucleotide excision repair pathway. Biochimie 85:1083–1099
185. van Hoffen A, Venema J, Meschini R, van Zeeland AA, Mullenders LHF (1995) Transcription-coupled repair removes both cyclobutane pyrimidine dimers and 6-4 photoproducts with equal efficiency and in a sequential way from transcribed DNA in xeroderma pigmentosum group C fibroblasts. EMBO J 14:360–367
186. Orren DK, Selby P, Hearst JE, Sancar A (1992) Postincision steps of nucleotide excision repair in *Escherichia coli*. Disassembly of the UvrBC-DNA complex by helicase II and DNA polymerase I. J Biol Chem 267:780–788
187. Selby CP, Sancar A (1993) Molecular mechanism of transcription-repair coupling. Science 259:53–58
188. Matson SW, Bean DW, George JW (1994) DNA helicases: enzymes with essential roles in all aspects of DNA metabolism. BioEssays 16:13–22
189. Ratner JN, Balasubramanian B, Corden J, Warren SL, Bregman DB (1998) Ultraviolet radiation-induced ubiquitination and proteasomal degradation of the large subunit of RNA polymerase II: implications for transcription-coupled DNA repair. J Biol Chem 273:5184–5189
190. Sarasin A, Stary A (2007) New insights for understanding the transcription-coupled repair pathway. DNA Repair (Amst) 6:265–269
191. Fousteri M, Vermeulen W, van Zeeland AA, Mullenders LHF (2006) Cockayne syndrome A and B proteins differentially regulate recruitment of chromatin remodelling and repair factors to stalled RNA polymerase II in vivo. Mol Cell 23(4):471–482
192. Proietti-De-Santis L, Drańe P, Egly J-M (2006) Cockayne syndrome B protein regulates the transcriptional program after UV irradiation. EMBO J 25:1915–1923

193. Balajee AS, Bohr VA (2000) Genomic heterogeneity of nucleotide excision repair. Gene 250:15–30
194. Orren DK, Sancar A (1989) The (A)BC excinuclease of *Escherichia coli* has only the UvrB and UvrC subunits in the incision complex. Proc Natl Acad Sci USA 86:5237–5241
195. Moolenaar GF, Herron MF, Monaco V, Van der Marel GA, van Boom JH, Visse R, Goosen N (2000) The role of ATP binding and hydrolysis by UvrB during nucleotide excision repair. J Biol Chem 275:8044–8050
196. Caron PR, Grossman L (1988) Involvement of a cryptic ATPase activity of UvrB and its proteolysis product, UvrB* in DNA repair. Nucleic Acids Res 16:9651–9662
197. Kato R, Yamamoto N, Kito K, Kuramitsu S (1996) ATPase activity of UvrB protein from *Thermus thermophilus* HB8 and its interaction with DNA. J Biol Chem 271:9612–9618
198. Lin J-J, Sancar A (1992) Active site of (A)BC excinuclease. I. Evidence for 5_ incision by UvrC through a catalytic site involving Asp399, Asp438, Asp466, and His538 residues. J Biol Chem 267:17688–17692
199. Maillard O, Solyom S, Naegeli H (2007) An aromatic sensor with aversion to damaged strands confers versatility to DNA repair. PLoS Biol 5:e79
200. Sugasawa K, Okuda Y, Saijo M, Nishi R, Matsuda N, Chu G, Mori T, Iwai S, Tanaka K, Tanaka K, Hanaoka F (2005) UV-induced ubiquitylation of XPC protein mediated by UV-DDB-ubiquitin ligase complex. Cell 121:387–400
201. Nouspikel T (2009) Nucleotide excision repair: variations on versatility. Cell Mol Life Sci 66:994–1009
202. Sugasawa K, Ng JMY, Masutani C, Iwai S, van der Spek PJ, Eker APM, Hanaoka F, Bootsma D, Hoeijmakers JHJ (1998) Xeroderma pigmentosum group C protein complex is the initiator of global genome nucleotide excision repair. Mol Cell 2:223–232
203. van der Spek PJ, Eker A, Rademakers S, Visser C, Sugasawa K, Masutani C, Hanaoka F, Bootsma D, Hoeijmakers JHJ (1996) XPC and human homologs of RAD23: intracellular localization and relationship to other nucleotide excision repair complexes. Nucleic Acids 24:2551–2559
204. Sugasawa K, Masutani C, Uchida A, Maekawa T, van der Spek PJ, Bootsma D, Hoeijmakers JHJ, Hanaoka F (1996) HHR23B, a human Rad23 homolog, stimulates XPC protein in nucleotide excision repair in vitro. Mol Cell Biol 16:4852–4861
205. Schultz P, Fribourg S, Poterszman A, Mallouh V, Moras D, Egly JM (2000) Molecular structure of human TFIIH. Cell 102:599–607
206. Hitomi K, Iwai S, Tainer JA (2007) The intricate structural chemistry of base excision repair machinery: implications for DNA damage recognition, removal, and repair. DNA Repair (Amst) 6:410–428
207. Lieber MR (1997) The FEN-1 family of structure-specific nucleases in eukaryotic DNA replication, recombination and repair. BioEssays 19:233–240
208. Constantinou A, Gunz D, Evans E, Lalle P, Bates PA, Wood RD, Clarkson SG (1999) Conserved residues of human XPG protein important for nuclease activity and function in nucleotide excision repair. J Biol Chem 274:5637–5648
209. Dubest S, Gallego ME, White CI (2004) Roles of the AtErcc1 protein in recombination. Plant J 39:334–342
210. Kimura S, Sakaguchi K (2006) DNA repair in plants. Chem Rev 106:753–766
211. Kunz BA, Anderson HJ, Osmond MJ, Vonarx EJ (2005) Components of nucleotide excision repair and DNA damage tolerance in *Arabidopsis thaliana*. Environ Mol Mutagen 45:115–127
212. Hefner E, Preuss SB, Britt AB (2003) *Arabidopsis* mutants sensitive to gamma radiation include the homologue of the human repair gene ERCC1. J Exp Bot 54:669–680
213. Liu Z, Hall JD, Mount DW (2001) *Arabidopsis UVH3* gene is a homolog of the *Saccharomyces cerevisiae* RAD2 and human XPG DNA repair genes. Plant J 26:329–338
214. Hidema J, Kumagai T, Sutherland JC, Sutherland BM (1997) Ultraviolet B-sensitive rice cultivar deficient in cyclobutyl pyrimidine dimer repair. Plant Physiol 113:39–44

215. Vonarx EJ, Mitchell HL, Karthikeyan R, Chatterjee I, Kunz BA (1998) DNA repair in higher plants. Mutat Res 400:187–200
216. Xu H, Swoboda I, Bhalla PL, Sijbers AM, Zhao C, Ong E, Hoeijmakers JHJ, Singh MB (1998) Plant homologue of human excision repair gene *ERCC1* points to conservation of DNA repair mechanisms. Plant J 13:823–829
217. Shrivastav M, De Haro LP, Nickoloff JA (2008) Regulation of DNA double-strand break repair pathway choice. Cell Res 18:134–147
218. Friedberg EC (2003) DNA damage and repair. Nature 421:436–440
219. Nowosielska A (2007) Bacterial DNA repair genes and their eukaryotic homologues: 5. The role of recombination in DNA repair and genome stability. Acta Biochim Pol 54:483–494
220. Rocha EPC, Cornet E, Michel B (2005) Comparative and evolutionary analysis of the bacterial homologous recombination systems. PLoS Genet 1:0247–0259
221. Cromie GA, Connelly JC, Leach DRF (2001) Recombination at double-strand breaks and DNA ends: conserved mechanisms from phage to humans. Mol Cell 8:1163–1174
222. Thacker J (2005) The RAD51 gene family, genetic instability and cancer. Cancer Lett 219:125–135
223. McEntee K, Weinstock GM, Lehman IR (1980) recA protein-catalyzed strand assimilation: stimulation by *Escherichia coli* single-stranded DNA-binding protein. Proc Natl Acad Sci USA 77:857–861
224. Bishop DK, Park D, Xu L, Kleckner N (1992) DMC1: a meiosis-specific yeast homolog of *E. coli* recA required for recombination, synaptonemal complex formation, and cell cycle progression. Cell 69:439–456
225. Li W, Ma H (2006) Double-stranded DNA breaks and gene functions in recombination and meiosis. Cell Res 16:402–412
226. Aylon Y, Kupiec M (2004) New insights into the mechanism of homologous recombination in yeast. Mutat Res 566:231–248
227. Park MS (1995) Expression of human RAD52 confers resistance to ionizing radiation in mammalian cells. J Biol Chem 270:15467–15470
228. Jeggo PA (1990) Studies on mammalian mutants defective in rejoining double-strand breaks in DNA. Mutat Res 239:1–16
229. Puchta H, Swoboda P, Hohn B (1995) Induction of intrachromosomal homologous recombination in whole plants. Plant J 7:203–210
230. Ira G, Pellicioll A, Balijja A, Wang X, Fiorani S, Carotenuto W, Liberi G, Bressan D, Wan L, Hollingsworth NM, Haber JE, Foiani M (2004) DNA end resection, homologous recombination and DNA damage checkpoint activation require CDK1. Nature 431:1011–1017
231. Sung P (1997) Yeast Rad55 and Rad57 proteins form a heterodimer that functions with replication protein A to promote DNA strand exchange by Rad51 recombinase. Genes Dev 11:1111–1121
232. Wolner B, Van Komen S, Sung P, Peterson CL (2003) Recruitment of the recombinational repair machinery to a DNA double-strand break in yeast. Mol Cell 12:221–232
233. Sonoda E, Zhao GY, Kohzaki M, Dhar PK, Kikuchi K, Redon C, Pilch DR, Bonner WM, Nakano A, Watanabe M, Nakayama T, Takeda S, Takami Y (2007) Collaborative roles of γH2AX and the Rad51 paralog Xrcc3 in homologous recombinational repair. DNA Repair (Amst) 6:280–292
234. Hefferin ML, Tomkinson AE (2005) Mechanism of DNA double-strand break repair by non-homologous end joining. DNA Repair (Amst) 4:639–648
235. Capp J-P, Boudsocq F, Bertrand P, Lopez BS, Cazaux C, Hoffman J-S, Canitrot Y (2006) The DNA polymerase λ is required for the repair of non-compatible DNA double strand breaks by NHEJ in mammalian cells. Nucleic Acids Res 34:2998–3007
236. Thode S, Schäfer A, Pfeiffer P, Vielmetter W (1990) A novel pathway of DNA end-to-end joining. Cell 60:921–928
237. Cary RB, Peterson SR, Wang J, Bear DG, Bradbury EM, Chen DJ (1997) DNA looping by Ku and the DNA-dependent protein kinase. Proc Natl Acad Sci USA 94:4267–4272

238. Yajima H, Lee K-J, Zhang S, Kobayashi J, Chen BPC (2009) DNA double-strand break formation upon UV-induced replication stress activates ATM and DNA-PKcs kinases. J Mol Biol 385:800–810
239. Muller C, Calsou P, Frit P, Cayrol C, Carter T, Salles B (1998) UV sensitivity and impaired nucleotide excision repair in DNA-dependent protein kinase mutant cells. Nucleic Acids Res 26:1382–1389
240. Hentges P, Ahnesorg P, Pitcher RS, Bruce CK, Kysela B, Green AJ, Bianchi J, Wilson TE, Jackson SP, Doherty AJ (2006) Evolutionary and functional conservation of the DNA non-homologous end-joining protein, XLF/Cernunnos. J Biol Chem 281:37517–37526
241. Ahnesorg P, Smith P, Jackson SP (2006) XLF interacts with the XRCC4-DNA ligase IV complex to promote DNA nonhomologous end-joining. Cell 124:301–313
242. Paull TT, Gellert M (2000) A mechanistic basis for Mre11-directed DNA joining at microhomologies. Proc Natl Acad Sci USA 97:6409–6414
243. Michel B (2005) After 30 years of study, the bacterial SOS response still surprises us. PLoS Biol 3:1174–1176
244. Woodgate R, Sedgwick S (1992) Mutagenesis induced by bacterial UmuDC proteins and their plamid homologues. Mol Microbiol 6:2213–2218
245. Hartwell LH, Weinert TA (1989) Checkpoints: controls that ensure the order of cell cycle events. Science 246:629–634
246. Jin J, Shirogane T, Xu L, Nalepa G, Qin J (2003) SCFβ-TRCP links Chk1 signaling to degradation of the Cdc25A protein phosphatise. Genes Dev 17:3062–3074
247. Mailand N, Falck J, Lukas C, Syljuasen RG, Welcker M, Bartek J, Lukas J (2000) Rapid destruction of human Cdc25A in response to DNA damage. Science 288:1425–1429
248. Mailand N, Podtelejnikov AV, Groth A, Mann M, Bartek J, Lukas J (2002) Regulation of G2/M events by Cdc25A through phosphorylation-dependent modulation of its stability. EMBO J 21:5911–5920
249. Bartek J, Lukas J (2007) DNA damage checkpoints: from initiation to recovery or adaptation. Curr Opin Cell Biol 19:238–245
250. Watanabe N, Arai H, Nishihara Y, Taniguchi M, Watanabe N, Hunter T, Osada H (2004) M-phase kinases induce phospho-dependent ubiquitination of somatic Wee1 by SCFβ-TrCP. Proc Natl Acad Sci USA 101:4419–4424
251. Mailand N, Bekker-Jensen S, Bartek J, Lukas J (2006) Destruction of claspin by SCFβTrCP restrains Chk1 activation and facilitates recovery from genotoxic stress. Mol Cell 23:307–318
252. Busino L, Donzelli M, Chiesa M, Guardavaccaro D, Ganoth D, Dorrello NV, Hershko A, Pagano M, Draetta GF (2003) Degradation of Cdc25A by β-TrCP during S phase and in response to DNA damage. Nature 426:87–91
253. Kastan MB, Bartek J (2004) Cell-cycle checkpoints and cancer. Nature 432:316–323
254. Kumari S, Rastogi RP, Singh KL, Singh SP, Sinha RP (2008) DNA damage: detection strategies. EXCLI Journal 7:44–62
255. Mitchell DL, Jen J, Cleaver JE (1991) Relative induction of cyclobutane dimers and cytosine photohydrates in DNA irradiated in vitro and in vivo with ultraviolet-C and ultraviolet-B light. Photochem Photobiol 54:741–746
256. Freeman SE, Blackett AD, Monteleone DC (1986) Quantitation of radiation-, chemical-, or enzyme-induced single strand breaks in nonradioactive DNA by alkaline gel electrophoresis: application to pyrimidine dimers. Anal Biochem 158:119–129
257. Wang G, Hallberg LM, Saphier E, Englander EW (1999) Short interspersed DNA element-mediated detection of UVB-induced DNA damage and repair in the mouse genome, in vitro, and in vivo in skin. Mutat Res 433:147–157
258. Wang G, Hallberg LM, Saphier E, Englander EW (2006) Pyrimidine (6-4) pyrimidone photoproduct mapping after sub-lethal UVC doses: nucleotide resolution using terminal transferase-dependent PCR. Photochem Photobiol 82:1370–1376
259. Hercegová A, Ševčovičová A, Gálová E (2008) UV light-induced DNA damage detection in the unicellular green alga *Chlamydomonas reinhardtii*. Biologia 63:958–961

260. Small GD, Greimann CS (1977) Repair of pyrimidine dimers in ultraviolet-irradiated *Chlamydomonas*. Photochem Photobiol 25:183–187
261. Kumar A, Tyagi MB, Jha PN (2004) Evidences showing ultraviolet-B radiation-induced damage of DNA in cyanobacteria and its detection by PCR assay. Biochem Biophys Res Commun 318:1025–1030
262. Rastogi RP, Singh SP, Häder D-P, Sinha RP (2011) Ultraviolet-B-induced DNA damage and photorepair in the cyanobacterium *Anabaena variabilis* PCC7937. Env Exp Bot 74:280–288
263. Besaratinia A, Pfeifer GP (2012) Measuring the formation and repair of UV damage at the DNA sequence level by ligation-mediated PCR. Methods Mol Biol 920:189–202
264. Pfeifer GP, Dammann R (1999) Measuring the formation and repair of UV photoproducts by ligation-mediated PCR. Methods Mol Biol 113:213–226
265. Rochette PJ, Bastien N, Todo T, Drouin R (2006) Pyrimidine (6-4) pyrimidone photoproduct mapping after sublethal UVC doses: nucleotide resolution using terminal transferase-dependent PCR. Photochem Photobiol 82:1370–1376
266. Ye N, Bianchi MS, Bianchi NO, Holmquist GP (1999) Adaptive enhancement and kinetics of nucleotide excision repair in humans. Mutat Res 435:43–61
267. Olive PL, Banath JP, Durand RE (1990) Heterogeneity in radiation-induced DNA damage and repair in tumor and normal cells measured using the 'comet' assay. Radiat Res 122:86–94
268. Han P, Clingen PH, Lowe JE, Katsuya A, Arlett CF, Green MHL (1998) Repair of cyclobutane pyrimidine dimers in unstimulated human mononuclear cells is deficient at very low fluencies of ultraviolet B and is not enhanced by addition of deoxyribonucleosides. Mutagenesis 13:353–356
269. Kielbassa C, Roza L, Epe B (1997) Wavelength dependence of oxidative DNA damage induced by UV and visible light. Carcinogenesis 18:811–816
270. Sauvaigo S, Serres C, Signorini N, Emonet N, Richard MJ, Cadet J (1998) Use of the single-cell gel electrophoresis assay for the immunofluorescent detection of specific DNA damage. Anal Biochem 259:1–7
271. Woollons A, Clingen PH, Price ML, Farlett C, Green MHL (1997) Induction of mutagenic DNA damage in human fibroblasts after exposure to artificial tanning lamps. Br J Dermatol 137:687–692
272. Morley N, Rapp A, Dittmar H, Salter L, Gould G, Ko G, Curnow A (2006) UVA-induced apoptosis studied by the new apo/necro-Comet-assay which distinguishes viable, apoptotic and necrotic cells. Mutagenesis 21:105–114
273. Koopman G, Reutelingsperger CP, Kuiiten GA, Keehnen RM, Pals ST (1994) Annexin V for flow cytometric detection of phosphotidylserine expression on B cells undergoing apoptosis. Blood 4:1415–1420
274. Douki T, Court M, Sauvaigo S, Odin F, Cadet J (2000) Formation of the main UV-induced thymine dimeric lesions within isolated and cellular DNA as measured by high performance liquid chromatography-tandem mass spectrometry. J Biol Chem 275:11678–11685
275. Bickham JW (1990) Flow cytometry as a technique to monitor the effects of environmental genotoxins on wild life populations. In: Sandhu SS, Lower WR, De Serres FJ, Suk WA, Tice RR (eds) In situ evaluation of biological hazards of environmental pollutants. Plenum Press, New York, pp 97–108
276. Thyagarajan B, Anderson KE, Lessard CJ et al (2007) Alkaline unwinding flow cytometry assay to measure nucleotide excision repair. Mutagenesis 22:147–153
277. Singh R, Farmer PB (2006) Liquid chromatography-electrospray ionization-mass spectrometry: the future of DNA adduct detection. Carcinogenesis 27:178–196
278. Roti JLR, Wright WD (1987) Visualization of DNA loops in nucleoids from HeLa cells: assays for DNA damage and repair. Cytometry 8:461–467
279. Rastogi RP, Sinha RP (2011) Solar ultraviolet radiation-induced DNA damage and protection/repair strategies in cyanobacteria. Int J Pharma Biosci 2:B271–288
280. Birnboim HC, Jevcak JJ (1981) Fluorometric method for rapid detection of DNA strand breaks in human white blood cells produced by low doses of radiation. Cancer Res 41:1889–1892

281. Murthy SK, Demetrick DJ (2006) New approaches to fluorescence in situ hybridization. Methods Mol Biol 319:237–259
282. Berton TR, Mitchell DL (2012) Quantification of DNA photoproducts in mammalian cell DNA using radioimmunoassay. Methods Mol Biol 920:177–187
283. Kobayashi N, Katsumi S, Imoto K, Nakagawa A, Miyagawa S, Furumura M, Mori T (2001) Quantitation and visualization of ultraviolet-induced DNA damage using specific antibodies: application to pigment cell biology. Pigment Cell Res 14:94–102
284. Mitchell D, Brooks B (2010) Antibodies and DNA photoproducts: applications, milestones and reference guide. Photochem Photobiol 86:2–17
285. Strickland PT (1985) Immunoassay of DNA modified by ultraviolet radiation: a review. Environ Mutagen 7:599–607
286. Yarosh DB, Boumakis S, Brown AB, Canning MT, Galvin JW, Both DM, Kraus E, O'Connor A, Brown DA (2002) Measurement of UVB-induced DNA damage and its consequences in models of immunosuppression. Methods 28:55–62
287. Klisch M, Sinha RP, Helbling EW, Häder D-P (2005) Induction of thymine dimers by solar radiation in natural freshwater phytoplankton assemblages in Patagonia, Argentina. Aqua Sci 67:72–78
288. Jeffrey WH, Aas P, Lyons MM, Coffin RB, Pledger RJ, Mitchell DL (1996) Ambient solar radiation-induced photodamage in marine bacterioplankton. Photochem Photobiol 64:419–427
289. Kara P, Daideviren K, Özsöz M (2007) An electrochemical DNA biosensor for the detection of DNA damage caused by radioactive iodine and technetium. Turkish J Chem 31:243–249
290. Rastogi RP, Richa, Sinha RP (2009) Apoptosis: molecular mechanisms and pathogenicity. EXCLI J 8:155–181

Top Curr Chem (2015) 356: 249–276
DOI: 10.1007/128_2014_553

Published online: 5 November 2014

Solar UV Radiation-Induced DNA Bipyrimidine Photoproducts: Formation and Mechanistic Insights

Jean Cadet, André Grand, and Thierry Douki

Abstract This review chapter presents a critical survey of the main available information on the UVB and UVA bipyrimidine photoproducts which constitute the predominant recipient classes of photo-induced DNA damage. Evidence is provided that UVB irradiation of isolated DNA in aqueous solutions and in cells gives rise to the predominant generation of *cis-syn* cyclobutane pyrimidine dimers (CPDs) and, to a lesser extent, of pyrimidine (6-4) pyrimidone photoproducts (6-4PPs), the importance of which is strongly primary sequence dependent. A notable change in the photoproduct distribution is observed when DNA either in the dry or in desiccated microorganisms is exposed to UVC or UVB photons with an overwhelming formation of 5-(α-thymidyl)-5,6-dihydrothymidine, also called spore photoproduct (dSP), at the expense of CPDs and 6-4PPs. UVA irradiation of isolated and cellular DNA gives rise predominantly to bipyrimidine photoproducts with the overwhelming formation of thymine-containing cyclobutane pyrimidine dimers at the exclusion of 6-4PPs. UVA photons have been shown to modulate the distribution of UVB dimeric pyrimidine photoproducts by triggering isomerization of the 6-4PPs into related Dewar valence isomers. Mechanistic aspects of the

J. Cadet (✉)
Institut Nanosciences et Cryogénie/DSM, CEA-Grenoble, 17 avenue des Martyrs, 38054 Grenoble Cedex 9, France

Département de Médecine Nucléaire et Radiobiologie, Faculté de Médecine, Université de Sherbrooke, Québec, Canada
e-mail: jean.cadet@cea.fr

A. Grand
Universidad Autonoma de Chile, Carlos Antunez, 1920 Providencia, Santiago, Chile

Laboratoire Lésions des Acides Nucléiques, INac/SCIB UMR-E3 CEA-UJF, CEA-Grenoble, CEA-Grenoble, 17 avenue des Martyrs, 38054 Grenoble Cedex 9, France

T. Douki
Laboratoire Lésions des Acides Nucléiques, INac/SCIB UMR-E3 CEA-UJF, CEA-Grenoble, 17 avenue des Martyrs, 38054 Grenoble Cedex 9, France

formation of bipyrimidine photoproducts are discussed in the light of recent photophysical and theoretical studies.

Keywords Cellular DNA photodamage · Cyclobutane pyrimidine dimers · Dewar valence isomers · Pyrimidine (6-4) pyrimidone photoproducts · Spore photoproduct

Contents

Abbreviations

$^{\bullet}$OH	Hydroxyl radical
6-4PPs	Pyrimidine (6-4) pyrimidone photoproducts
8-oxodGuo	8-Oxo-7,8-dihydro-2′-deoxyguanosine
8-oxoGua	8-Oxo-7,8-dihydroguanine
BCCs	Basal cell carcinoma
CMMs	Cutaneous malignant melanoma
CPDs	Cyclobutane pyrimidine dimers
DEW	Dewar valence isomer
DFT	Density functional theory
DNA-PF	DNA protection factor
dSP	5-(α-Thymidyl)-5,6-dihydrothymidine or “spore photoproduct”
HPLC-ESI-MS/MS	High performance coupled to electrospray ionization – tandem mass spectrometry
LM-PCR	Ligation-mediated polymerase chain reaction
^{m}C	5-Methylcytosine
MED	Minimal erythemal dose
SASP	Small, acid-soluble spore protein
SCCs	Squamous cell carcinoma (SCCs
SPF	Sun protection factor
TD-DFT	Time-dependent density functional theory
Th	Thymidine
TTET	Triple-triplet energy transfer

1 Introduction

Chronic exposure to solar radiation through its UVB ($290 < \lambda < 320$ nm) and UVA components ($320 < \lambda < 400$ nm) is the predominant cause of induction of squamous cell carcinoma (SCCs), one of the two main human skin non-melanomas that also include basal cell carcinomas (BCCs) [1, 2]. The situation is not as clear for the etiology of cutaneous malignant melanoma (CMMs) which also implicates UV photons as causative agents [3], while acute intermittent exposure during childhood has also been suggested to be a major risk factor [4, 5]. Evidence was also recently provided that both UVB and UVA radiation have the ability to favor the incidence of CMMs through a direct excitation pathway and melanin photosensitized reactions, respectively [6]. It is well known that DNA is the main cellular target for UVB and UVA radiation-induced cutaneous carcinogenesis. This has received strong support from the similarity of the UVC and UVB action spectra for mutagenic, carcinogenic, and lethal effects with DNA UV absorption [1], the detection of characteristic UV signature mutations including $C \rightarrow T$ transitions at bipyrimidine sites and $CC \rightarrow TT$ tandem base substitutions in key genes [7–9], and the high susceptibility to skin cancer of xeroderma pigmentosum complementary group patients who suffer from deficiencies in nucleotide excision repair pathways [10, 11]. The photochemistry of DNA triggered by UVB photons which is oxygen independent, is dominated by the formation of intrastrand dimeric photoproducts involving adjacent pyrimidine bases (for comprehensive reviews, see [12–22]). Abundant information is now available on the chemical and biological features of the three main classes of bipyrimidine photoproducts thus generated, including lethality [23] and immunosuppression activities [24, 25]. Extensive photophysical studies also have provided relevant insights into the mechanisms of DNA photoreactions [26–30] which are complemented by increasing numbers of theoretical studies [31–33]. The situation is not so straightforward for the molecular effects of deeper penetrating UVA radiation in dermis. There is still weak absorption of DNA bases by UVA photons within the range 320–340 nm, responsible for the formation of dimeric pyrimidine photoproducts consisting exclusively of cyclobutane pyrimidine dimers (CPDs) and the induction of $C \rightarrow T$ base substitution mutations preferentially at pyrimidine-5-methylCpG sites [9]. In addition, photodynamic reactions requiring the presence of endogenous photosensitizers and oxygen give rise to oxidative degradation pathways involving DNA [34, 35] and other key biomolecules including membrane lipids [36] and proteins [37]. It was recently shown that, in cellular DNA and skin, the contribution of CPDs induced by UVA irradiation remains predominant over oxidative reactions involving mostly singlet oxygen and, to a lesser extent, hydroxyl radicals ($^{\bullet}OH$), at least in terms of quantitative effects [38–40]. The main purpose of this review chapter is to survey critically the available experimental data on the UVB- and UVA-induced formation of dimeric pyrimidine photoproducts in isolated and cellular DNA, with emphasis on the most recent aspects. Information is also provided on the generation of 5-(α-thymidylyl)5,6-dihydrothymidine, the so-called spore photoproduct (dSP)

predominantly formed in the dry state and in dehydrated bacterial cells such as spores following either UVC or UVB irradiation [17]. Key theoretical works from recent literature on reaction pathways initiated by excitation of nucleobases leading to bipyrimidine photoproducts are also included in the discussion of mechanistic photochemical pathways.

2 UVC and UVB Radiation-Induced Bipyrimidine Photoproducts

As discussed in a number of contributions in this issue, absorption of UVB and UVC photons by DNA involves essentially purine and pyrimidine bases. However, damage occurs predominantly at bipyrimidine sequences upon excitation of thymine, the most photoreactive base, or, to a lesser extent, of cytosine. The most frequent photoreactions in aqueous solutions involve two types of dimerization of adjacent pyrimidine bases, leading to CPDs and pyrimidine (6-4) photoproducts (6-4PPs) respectively (Fig. 1). In addition, two other bipyrimidine photolesions may be generated, including the Dewar valence isomers (DEWs) as secondary photoproducts and 5-(α-thymidyl)-5,6-dihydrothymidine, also termed "spore photoproduct" (dSP). Evidence has been provided for the formation in very low yields of other DNA photoproducts; most of them, with the exception of 6-hydroxy-5,6-dihydro-2′-deoxycytidine, the so-called "2′-deoxycytidine "photohydrates" [41] and 8-oxo-7,8-dihydro-2′-deoxyguanosine (8-oxodGuo) [38] have not been detected so far in UVB or UVC irradiated cells. As another minor UVB reaction, [2+2] photocycloaddition C5-C6 of either thymidine or 5-methyl-2′-deoxycytidine and C6-C5 of 2′-deoxyadenosine followed by a rearrangement gives rise to TA* [42–45]. Further support for the structure assignment of the 5-methyl-2′-deoxycytidine containing photoadduct was provided by its conversion into TA* through hydrolytic deamination [45]. Another UVC-induced intrastrand adduct which involves the formation of a covalent bond between the 4-amino group of cytosine and C8 of guanine in either d(GpC) or d(CpG) sequence has recently been identified in short DNA fragments and the structure further confirmed by total synthesis [46]. It was hypothesized that C(4-8)G and G(8-4)C lesions arise from initial UVC generation of 4-aminyl cytosine radical which is able to add to vicinal guanine at C8 before a final oxidation step. An alternative mechanism would involve, in the initial step, ionization of guanine, which exhibits the lowest oxidation potential among DNA components. Subsequently, the resulting guanine radical, highly susceptible to nucleophilic additions [47, 48], would react with the 4-amino group of adjacent cytosine, giving rise to either C(4-8)G or G(8-4)C after the O_2-mediated oxidation of the transiently generated radical adduct. This is supported by several known examples of nucleophilic reactions involving either hydroxyl or amino groups to the guanine radical that give rise to 8-oxodGuo

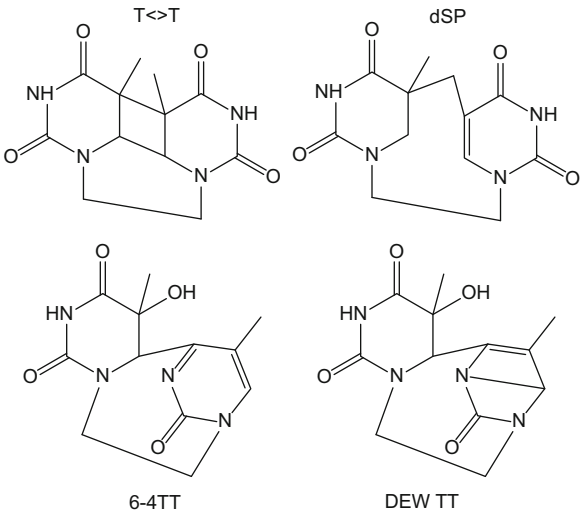

Fig. 1 Structures of the four main classes of thymine containing-bipyrimidine lesions

[47, 49], intrastrand G-T adducts [50], DNA-protein cross-links [51] and interstrand cross-links [48, 52].

2.1 Four Main Classes of Bipyrimidine Photoproducts

Four main classes of dimeric pyrimidine photoproducts that require UVC or UVB excitation of one pyrimidine base in the initial step of the photoreactions have been identified and detected in isolated cells, three of them in human skin.

2.1.1 Cyclobutane Pyrimidine Dimers

The *cis-syn* cyclobutane pyrimidine dimer of thymine (T<>T) was the first bipyrimidine photoproduct isolated and characterized almost 65 years ago [53], giving a very strong impetus to the development of numerous subsequent studies not only in the domain of DNA photochemistry but also in other fields of research including genotoxicity, mutagenicity, photocarcinogenesis, and DNA repair. The formation of cyclobutane pyrimidine dimers (CPDs) that also occurs at the other main T-C, C-T, and C-C bipyrimidine sequences is rationalized in terms of $[2\pi + 2\pi]$ photocycloaddition between the 5,6-pyrimidine bonds of stacked adjacent bases. Recent photophysical and computational studies have shown that the formation of T<>T in thymine strands is an ultrafast process [31], proceeding via bright $^1\pi\pi^*$ excitons along a barrierless path in agreement with a measured constant quantum yield formation within the UVC–UVB range [32, 54]. Four isomers, including *cis-syn, trans-syn, cis-anti* and *trans-anti* CPDs are generated by UVC

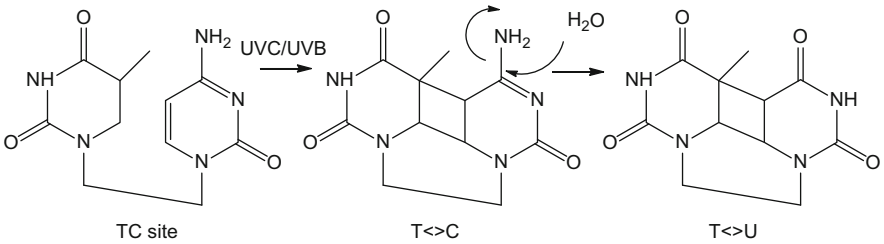

Fig. 2 Photo-induced formation of T<>C and conversion to the uracil derivative (T<>U) through deamination

or UVB irradiation of isolated pyrimidine nucleobases in aqueous solutions [55]. The two implicated bases are on the same or on the opposite sides of the cyclobutane ring, thus defining the *cis*/*trans* isomerism. The *syn*/*trans* isomerism is explained either by the parallel (C5 linked to the other C5, and C6 linked to the other C6) or by the antiparallel orientation of the C5–C6 carbons. CPDs are very stable compounds, at least the cyclobutane ring structure. This has allowed their detection as radiolabeled dimeric base lesions upon strong acidic hydrolysis conditions in early works. However, cytosine-containing CPDs are prone to deamination as the result of the saturation of the 5,6-double bond at a rate increased by several orders of magnitude with respect to cytosine at neutral pH. The hydrolytic process involves the substitution of the exocyclic amino group by a hydroxyl group, converting cytosine into uracil (Fig. 2). The half-life of *cis-syn* cytosine containing CPDs is a few hours whereas related *trans-syn* isomers are slightly more stable. This reaction is likely to play a major biological role when occurring in UV irradiated cells because uracil in CPDs codes for adenine while the initial cytosine coded for guanine. Thus deamination of cytosine-containing CPDs is believed to be the cause of the characteristic T to C transitions at TC sites and CC to TT tandem mutations observed in genes such p53 of UV-induced skin tumors. Major interest is currently shown in the photochemical reactions of 5-methylcytosine (^{m}C), a major epigenetic mark as are the related methyl oxidation products [56–58]. Following initial characterization of the *cis-syn* CPDs formed upon UVC irradiation of d^{m}CpT and Tpd^{m}C) [59, 60], relevant theoretical and experimental information has subsequently been gained regarding the generation and chemical features of ^{m}C-derived CPDs in DNA fragments. Earlier calculations involving the time-dependent density functional theory (TD-DFT) has led to the conclusion that C5-methylation of cytosine does not increase the formation of CPDs [61], in contrast to previous experimental observations [61]. It was later found that the frequency of either ^{m}C<>C or C<>^{m}C formation was dependent on the flanking sequences, often being enhanced by the presence of vicinal adenine [62]. In addition, flanking guanine has a pronounced enhancement effect on the deamination of ^{m}C-containing CPDs. The 5-methyl CpG binding protein 2 (MeCP2) was found to promote the formation of C<>^{m}C at a TC^{m}CG site with almost complete suppression of CPD deamination, whereas no effect was observed on the formation of T<>^{m}C at a

TT^{m}CG site [63]. Flexibility of DNA duplex in nucleosomes has been shown to affect very much the deamination rate of T<>^{m}C at a T^{m}CG site [64]. Evidence was provided from the error-free bypass of *cis-syn* T<>^{m}C-containing template by yeast and human polymerase η that the ^{m}C residue has to deaminate in order to become mutagenic [65].

Direct photoreversal of CPDs is mostly triggered by UVC radiation leading to the splitting of the cyclobutane ring with restitution of starting thymine or uracil if deamination of saturated cytosine has occurred [66]. Evidence has recently been provided that the presence of a vicinal guanine to T<>T does not affect the UVC induced reversal of the CPD, thus ruling out any implication of electron transfer from excited guanine [67]. However, the relevance of direct photo-splitting is very low in cellular DNA because it only takes place for high doses of UVC, in contrast to the efficient enzymatic photoreversal that is mediated by CPD photolyases in microorganisms and yeasts [20, 68, 69] which is a key repair pathway.

2.1.2 Pyrimidine (6-4) Pyrimidone Photoproducts

Pyrimidine (6-4) pyrimidone (6-4PPs) represent the second major class of UVC and UVB bipyrimidine photoproducts in terms of quantitative formation. They are generated via sequence-specific Paternó-Büchi cycloaddition reactions involving the C5–C6 double bond of a pyrimidine base on the 5′-side and either the 4-carbonyl group of a thymine residue or the 4-imine tautomeric group of a cytosine base. In both cases, an unstable four-membered ring intermediate, either an oxetane or an azetidine, is expected to be generated. Indirect support for the cyclic intermediate is provided by the isolation of related stable thietanes upon UVA excitation of 4-thiopyrimidine compounds containing-bipyrimidine sites [70]. The fast rearrangement of either the oxetane or the azetidine intermediates gives rise to an intrastrand adduct through covalent bond formation between C4 of the pyrimidone moiety and C6 of the pyrimidine base. This is accompanied by the stereospecific transfer of the carbonyl oxygen or the amino group to C5 of the pyrimidine base. The mechanism of formation of 6-4TT, which for a long time was supposed to derive from a singlet excited state, has recently been revisited through a wide range of relevant photophysical measurements and theoretical studies. It was proposed that the formation of 6-4TT involves a non-absorbing intermediate in the 300–700 nm spectral range, likely the oxetane compound produced through an excited charge transfer state [32, 54]. A significant energy barrier is associated with the electron transfer from 5′T to 3′T which only occurs when the sugar moieties of the two 2′-deoxyribonucleosides involved in the photocycloaddition reaction adopts the preferential C2′*endo* puckered conformation [32]. A recently performed DFT study of the reaction pathway involved in the UVB formation of 6-4PP in TpT has provided further support to the transient formation of an oxetane intermediate [71]. An interesting feature of 6-4PPs associated with the presence of the pyrimidone moiety is the absorption around 320 nm. This explains, as discussed below, the photo-instability of 6-4PPs and their fluorescence emission properties.

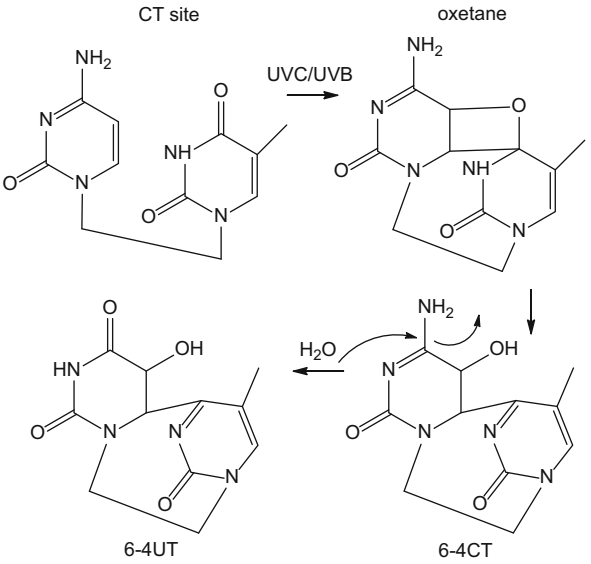

Fig. 3 Photo-induced formation of 6-4CT and conversion to 6-4TU through deamination

The pyrimidine moiety of 6-4CT and 6-4CC is also susceptible to deamination with a rate that is slightly lower than that of cytosine-containing CPDs (Fig. 3). In contrast, 6-4TC, the 4-amino group of which has been transferred to the C5 of the pyrimidine moiety, cannot undergo deamination.

2.1.3 Dewar Valence Isomers

As mentioned in the previous section, 6-4PPs are able to absorb UV radiation at wavelengths around 320 nm with subsequent conversion to related Dewar valence (DEWs) isomers [72, 73]. These recently characterized photoproducts exhibit a β-lactam structure fused to a second four-membered ring through the creation of an intramolecular bond between N3 and C6 of the pyrimidone moiety [74]. Relevant mechanistic insights into the 4π electrocyclization reaction leading to 6-4TT and 6-4TC were gained from a recent detailed time-resolved IR-probe spectroscopy study completed by ab initio calculations [75]. The cyclization process was found to be a slow but highly efficient reaction controlled by the backbone structure of the dinucleoside monophosphate. If UVC and UVB photons are able to convert 6-4PPs efficiently into Dewar valence isomers by irradiation of the isolated precursors, this is not the case in DNA, particularly by low dose irradiations because of strong competition for light absorption by the much stronger normal nucleobases. A specific feature of the Dewar valence isomers not applying to their 6-4PP precursors is their high alkaline lability [73] which, under hot piperidine treatment, leads to specific cleavage of DNA strands at the site of the lesions [76].

2.1.4 Spore Photoproduct

A fourth type of bipyrimidine photoproduct was initially shown to be generated upon UVC-irradiation of bacterial spores [77] and subsequently identified as 5-(α-thymyl)-5,6-dihydrothymine, also called the "spore photoproduct" (SP) [78]. Later efforts have been made to gain insights into the mechanism of formation and structural features of SP. Thus UVC irradiation of thymidine (Th) in either frozen aqueous solutions or in the dry state upon lyophilisation of aqueous solutions gave rise to a pair of diastereomers of 5-(α-thymidyl)-5,6-dihydrothymidine (dSP) [79] the chiral C5 stereochemistry of which has been assigned on the basis of extensive NMR measurements [80]. (5*R*)-and (5S)-dSP could be also generated by pyridopsoralen-mediated photosensitization of thymidine in the dry state [81] or gamma irradiation of frozen aqueous solutions of Th in frozen aqueous solutions [82]. However, only one diastereomer, shown to have the 5*R* stereoconfiguration, is formed in TpT [83] and in DNA [84] via a regio- and stereospecific mechanism produced by steric constraints and specific conformational features [17]. Thus evidence has been provided that SP formation required the DNA to adopt an A-like conformation with bases in an *anti*-orientation and the 2-deoxyribose moieties showing a preferential C′3 *endo* puckered conformation [17]. This is also the case for spores where the presence of α/β type small acid-soluble spore proteins (SASP) coated on DNA favors the formation of an "A-B-DNA" conformation [85, 86]. Interestingly, it was found that UVC irradiation of isolated DNA either in aqueous solution or as dry film in the presence of SASP favored the formation of SP at the expense of CPDs and 6-4PPs [87]. Dipicolinic acid, a major component of *Bacillus subtilis* spores, has been shown to photosensitize the formation of SP in either dry DNA films or frozen aqueous solutions of thymidine upon exposure to UVC radiation [88]. First a consecutive mechanism involving, in the initial stages, the formation of the 5-α-thyminyl radical and 5,6-dihydrothymin-5-yl radical followed by recombination of the two species, was proposed to account for the UVC-induced formation of SP [89]. Later, a concerted mechanism was suggested from the observation of a stereospecific deuterium atom transfer from the deuterated methyl group of thymidine to the C6 of the 5,6-dihydrothymine moiety of dSP [12]. Since then the mechanism has been revisited using [d3]TpT as the target molecule. The kinetic isotope effect observed by using the deuterated dinucleoside monophosphate together with the stereospecific intramolecular transfer of a deuterium atom to 5′T-$_{\text{Hpro-}R}$ moiety in the formation of (5*R*)-SP was rationalized in terms of a consecutive mechanism involving hydrogen atom abstraction of the methyl group of 3′T by the photoexcited adjacent thymine base [90]. This received further support from the consideration of the potential energy profiles of photoexcited TpT using DFT and TD-DFT calculations [91].

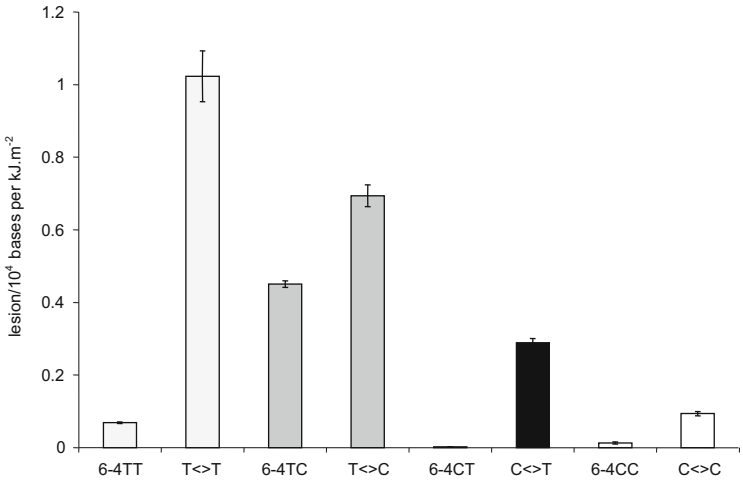

Fig. 4 Bipyrimidine photoproduct distribution in UVB-irradiated isolated DNA

2.2 Isolated DNA

The use of accurate HPLC-ESI-MS/MS assays has made possible the quantitative determination of all possible 12 bipyrimidine lesions and SP induced by exposure of DNA to either UVC or UVB irradiation [59, 92–94]. This contrasts with mostly semi-quantitative information gained on the global formation of classes of either CPDs or 6-4PPs and not individual lesions using more widely applied immunoassays [95–98].

2.2.1 Aqueous Solutions

The product distribution of the main UVC and UVB induced bipyrimidine photoproducts has been determined using the HPLC-MS/MS assay. Only *cis-syn* CPDs are produced in native duplex DNA. However *trans-syn* T<>T has been shown to be generated when large doses of UVC or UVB are applied, probably because of the formation of single-stranded DNA zones [99]. Under mild exposure conditions, TT sequences were found to harbor the largest amount of photoproducts, with CPDs being produced in a tenfold larger yield than 6-4PPs (Fig. 4). TC is second in terms of level of photoproducts but 6-4TC is almost as frequent as the T<>C after exposure to UVC photons and roughly half of it after UVB-irradiation. The level of C<>T is about one-third of that of T<>T and 6-4CT is hardly detectable even after exposure to large doses of UVC radiation. CC sites are less prone to photodimerization, with a large predominance of C<>C. It may be pointed out that 6-4CC is only detected in small amounts in DNA exposed to UVC radiation. The C content of the DNA from microorganisms *Clostridium perfrigens* and

Micrococcus luteus has been shown to modulate the distribution of UVB-induced bipyrimidine photoproducts [100]. There is a significant increase in T<>T at the expense of C<>C in the DNA of *C. perfrigens* where the level of CG content is 28% compared to 42% in calf thymus DNA. An inverse situation is noted for the DNA of *M. luteus* whose content in GC sites is 72% where T<>T is formed in low amounts.

2.2.2 Formation of Anti CPDs in Acidic Aqueous Solutions of DNA and in G-Quadruplex

As already stated, the formation of intrastrand CPDs in native double stranded DNA is controlled by steric constraints giving rise essentially to adjacent *cis-syn* isomers. However, the generation of non-adjacent T<>T with a predominant *cis-syn* stereoconfiguration has been observed in poly[d(G-T)] upon UVC and UVB irradiation as the result of the presence of an extrahelical structure which allows a colinear arrangement of both thymines involved in the photodimerization reaction [101, 102]. Other examples of the formation of non-adjacent CPDs in aqueous solutions have since become available. Thus UVB irradiation of aqueous solution of d(GTATCATGAGGTGC) at pH 5 was found to induce the formation of two isomeric T<>T between T2 and T7 [103]. A *cis-anti* configuration was assigned to the main CPD while the minor T<>T showed a *trans-anti* configuration on the basis of extensive 1D- and 2D-NMR analyses. In addition, a *cis-syn* T<>T is formed from the photocycloaddition reaction involving T2 and T4. The formation of these unusual interstrand-type CPDs was rationalized in terms of efficient crosslink photo-induction in a suitable high order folded DNA structure. Non-adjacent *anti* T<>T photoproducts were found to be specifically generated upon UVB irradiation of the d[AGGG(TTAGGG)$_3$] in the presence of K^+ ions [104]. Under these conditions the human telomere sequence forms G-quadruplex structures consisting of repeated d(TTAAGGG)$_3$] and adopt preferential hybrid-type triple quartet forms. In contrast, *anti* T<>T the formation of which involves either T in loop 1 and central T in loop 3 is not observed when the G-duplex is UV-irradiated in the presence of Na^+ which triggers the formation of a basket structure. This appears to be inconsistent because the basket form is supposed to be more amenable to photo-crosslink formation than the hybrid structures. However, it was recently proposed that the G-quadruplexes in dynamic equilibrium with several conformations are likely to adopt a more photoreactive structure in the presence of K^+ than Na^+ [105].

2.2.3 Dry State

UVC irradiation of either calf DNA or linearized pUC19 DNA in the dry state was shown to gives rise to intrastrand and interstrand bipyrimidine photoproducts differentiated as dinucleoside monophosphates and dinucleosides upon suitable

enzymatic digestion and subsequent analysis by HPLC-MS/MS measurements [79, 87]. The DNA photoproducts consist of CPDs, 6-4PPs and predominant SP with a significant amount of interstrand damage of about 30%. The interstrand CPDs derived from thymidine consist of the four possible stereoisomers – *cis-syn*, *trans-syn*, *cis-anti* and *trans-anti* stereoisomers – with a predominance of the *anti* forms [79]. Similar bipyrimidine photoproduct distribution was observed when calf thymus DNA was exposed to UVC radiation in aqueous solutions in the presence of large amounts of ethanol, promoting a conformation with a high compaction of DNA, thus favoring the photo-induced formation of interstrand crosslink [79].

2.3 Cellular DNA

The presentation of data concerning the formation of bipyrimidine photoproducts in cellular DNA has been restricted to studies where the measurement of the lesions was performed using the sensitive and accurate HPLC-ESI-MS/MS method.

2.3.1 Microorganisms

A large body of information is now available on the UVC- and UVB-induced formation in DNA of several microorganisms including marine bacteria, halophilic archea, microbial organisms (*Escherichia coli*, *Deinococcus radiodurans*), *Acinetobacte*r strains, vegetative *Bacillus subtilis* and related endospores. In contrast to eukyarotic cells, wide variations in the distribution of the DNA bipyrimidine photoproducts were observed among the investigated species with a strong correlation between the relative formation of TT vs CC photoproducts and the GC content as noted in isolated DNA [100]. This is particularly true for *C perfrigens* and *M. luteus* which show the extreme values of GC content with 28% and 72%, respectively. These have to be compared with the 40–42% GC frequency in most mammalian genomes [100]. Accordingly, a closer photoproduct distribution was found in mammalian cells with T<>T and to a lesser extent 6-4TC being predominant being noted in UVC or UVB irradiated vegetative *B. subtilis* and *E. coli* [106]. An inversion in the relative importance of T<>T and 6-4TC was reported for *D. radiodurans* [106, 107]. The trend is even more pronounced for *Natronomonas pharaonis* because 6-4TC represents about 80% of the overall UVC- or UVB-induced bipyrimidine photoproducts in close correlation with the high frequency of TC sites [108]. These results are explained by both the high GC content of DNA and the high doses of UVC irradiation which induced significant photoreversal of CPDs. Relevant information on the enzymatic removal of CPDs and 6-4PPs mediated by photolyases and nucleotide excision repair was obtained

through HPLC-ESI-MS/MS measurements in two marine bacteria [109], *B. subtilis* [110] and *Acinetobacter* strains [111, 112].

A drastic change in bipyrimidine photoproduct distribution is observed upon UVC irradiation of *B. subtilis* [87, 88, 106, 110] and *B. atrophaeus* wild-type spores [110] with the overwhelming formation of the spore photoproduct (about 99%) at the expense of CPDs and 6-4PPs. A significant reduction in the formation of SP was noted in mutant spores lacking either the ability to synthesize dipicolinic acid during sporulation or the two major α/β-type small, acid-soluble spore proteins [88]. The effect was even more pronounced for the double mutant. Another interesting observation deals with the formation in relatively low yields – although significant amounts – of interstrand SP in the spores which were UVC-irradiated in aqueous solutions or in the dry state [87]. This is strongly suggestive of a high compaction of DNA strands in *B. subtilis* spores.

2.3.2 Mammalian Cells

The formation of bipyrimidine photoproducts, with the exception of 6-4CT and the four DEW isomers generated in very low yields, was found to be linear within the dose range 0–2.6 kJ m^{-2} of UVB radiation in the DNA of THP1 human monocytes [59, 93]. Interestingly, the photoproduct distribution (T<>T > 6-4TC > T<>C > C<>T > C<>C > 6-4TT > 6-4CC) in cellular DNA is similar, with the exception of a change of the order of the TC photoproducts, to the distribution observed for UVB-irradiated isolated DNA. This also applied to rodent cell lines [39] and primary cultures of human skin cells, although with a slightly higher yield for T<>C with respect to 6-4TC [40, 113]. Detailed repair kinetics have been examined, showing a more efficient removal of 6-4TT and 6-4TC compared to related CPDs in the DNA of UVB-irradiated keratinocytes [114]. In a subsequent study it was shown that the repair efficiency of CPDs decreases in the order C<>T > C<>T > T<>C and T<>T in both UVB-irradiated human keratinocytes and fibroblasts [115]. Another striking observation was the significant decrease in the excision rate of T<>T and T<>C in keratinocytes upon increasing the UV irradiation dose from 50 J m^2 to 500 J m^2 [114]. This is likely accounted for by a saturation of repair capacities of the cells.

2.4 Human Skin

UVB-irradiation of skin explants from breast tissues of six donors at a dose of 2 kJ m^2 gave rise to six bipyrimidine photoproducts detected by HPLC-ESI-MS/MS. The photoproduct distribution is similar to that observed in isolated and

cellular DNA with a frequency which decreased in the order T<>T > T<>C > 6-4TC > C<>T > C<>C > 6-4TT [113]. It should be noted that a strong attenuation in the formation yield of bipyrimidine by a factor of 22 was found in the whole skin with respect to primary keratinocytes cultured from the skin of the donors. This is likely to be explained by a shielding effect mostly provided by the stratum corneum and melanin against penetration of UVB photons in human skin. It was confirmed in keratinocytes and fibroblasts that 6-4PPs were more rapidly repaired than CPDs in human skin. Furthermore, C<>C, the most detrimental CPDs in terms of mutagenic effects, and C<>T were found to be removed more quickly than T<>T and, to a lesser extent, T<>C [115]. In a recent study, evidence was provided for the existence of a correlation between the levels of UVB-induced bipyrimidine photoproducts in the DNA from biopsies of human donors and their phototypes upon exposure to the minimal exposure dose (MED) [116].

Another relevant investigation achieved using HPLC-ESI-MS/MS measurements of T<>T in a human skin explant dealt with the assessment of DNA protection factor (DNA-PF) provided by three commercial sunscreens [117]. Interestingly, UVB protection afforded by sunscreens assessed using DNA-PF was lower than that inferred from the use of sun protecting factor (SPF) through the measurement of MED. A similar approach based on the global measurement of CPDs based on the determination of the frequency of T4 endo V-sensitive sites in plasmid DNA was recently proposed for the assessment of the protecting effects of sunscreens [118].

3 UVA and Bipyrimidine Photoproducts

The contribution of pyrimidine photoproducts to the genotoxic effects of UVA has long been neglected. Indeed, emphasis was only placed on the oxidative stress induced by photosensitization processes involving endogenous chromophores. Upon excitation these lead to the production of singlet oxygen which specifically induces formation of 8-oxo-7,8-dihydroguanine (8-oxoGua) in DNA [34, 47, 119]. Another photooxidative process involves the release of superoxide radicals which, upon reaction with metal ions, generates hydrogen peroxide and $^{\bullet}$OH. The latter species reacts without specificity with DNA where both purine and pyrimidine bases are oxidized [21, 120]. $^{\bullet}$OH also attacks 2-deoxyribose moieties and leads to single strand breaks [121]. Yet UVA is also involved in the formation of bipyrimidine photoproducts. A first pathway is the well-known photosensitized triplet-triplet energy transfer reaction. Recent findings have also shown that UVA alone could induce CPDs in cellular DNA and play a significant role in the formation of DEWs upon exposure to sunlight.

3.1 *Photosensitized-Formation of Cyclobutane Pyrimidine Dimers*

Pyrimidine dimers are not only produced by direct absorption of UV photons but also by a specific photosensitized reaction, known as triplet-triplet energy transfer (TTET) [122–130]. In this process, a photosensitizer is excited by absorption of a UVA photon and converted into its triplet excited state by intersystem crossing. If the energy of this excited state is high enough, it can be transferred to DNA where the resulting excited triplet state leads to the specific formation of CPDs. No 6-4PPs and DEWs are produced. Several types of molecules have been shown to trigger TTET: aromatic ketones, psoralens and fluoroquinolones. Interestingly, photodegradation products rather than the parent compounds are sometimes responsible for the DNA damaging properties [131]. TTET is not only observed in isolated DNA but also in cells [132, 133]. It explains the phototoxicity of numerous drugs such as fluoroquinolones – which are useful antibacterial agents – and some non-steroidal anti-inflammatory agents exhibiting an aromatic ketone structure.

Thymine has been established as the main target for TTET because its first excited triplet state exhibits the lowest energy among DNA bases [126, 134]. Using a series of sensitizers with known excited triplet state energies ($E_{triplet}$), it was determined that $E_{triplet}$ for thymine in DNA was approximately 267 kJ mol^{-1} [134, 135], representing a drastic stabilization when compared with the monomeric thymidine exhibiting $E_{triplet}$ of 310 kJ mol^{-1} [126]. In agreement with the favored excitation of thymine, T<>T is the predominant photoproduct while T<>C and C<>T are produced in a roughly one order of magnitude lower yield [39, 123, 124, 133, 136, 137]. However, observations that the ratio between T<>T and C<>T/T<>C depends on the photosensitizer and that it cannot be predicted from the proportion of these three dinucleotides in DNA exhibiting different G:C base pairs content throws doubt on the simple scheme of the transfer of triplet energy to an isolated thymine which would then react with the adjacent pyrimidine bases [138]. These results suggest that the target for TTET is larger than the individual base. Local sequence effects previously reported show the importance of the adjacent base in the yield of CPDs generated through TTET [81]. Formation of C<>C, with a roughly three orders of magnitude lower yield than T<>T in calf thymus but only a fivefold lower yield in *M. luteus* DNA also threw doubt on the simple mechanism extrapolated from studies on monomer to double-stranded DNA [138]. At the monomeric level, $E_{triplet}$ for cytosine ranges between 321 and 338 kJ mol^{-1}, depending on the experimental approach used [126, 139–141]. A decrease by 40 kJ mol^{-1} as is the case for thymine would lead to a cytosine $E_{triplet}$ of at least 280 kJ mol^{-1} in DNA. This value is lower than the $E_{triplet}$ of fluoroquinolones, making TTET most unlikely. Yet C<>C lesions are observed in DNA photosensitized by norfloxacin and lomefloxacin ($E_{triplet}$ 290–290 kJ mol^{-1}). It may thus be proposed that TTET in double-stranded DNA involves not only the mechanisms taking place in monomers leading to $^3\pi\pi^*$ excited

states but others leading to delocalized excited states such as those exhibiting a charge transfer character [138].

3.2 Cyclobutane Pyrimidine Dimers and UVA

In contrast to UVB, the first results on the UVA radiation induced formation of CPDs were obtained in cells and then on isolated DNA and model compounds.

3.2.1 Cellular DNA and Skin

Using biochemical assays or radioactive labeling of DNA followed by acidic hydrolysis, a few early works have reported the formation of CPDs upon exposure to UVA. This was, for instance, the case in bacteria [142], cultured mammalian cells [143–146] and even human skin [147, 148]. These observations were not considered until additional data showed that CPDs were actually produced in larger amounts than 8-oxoGua in cultured cells [38, 39] and in human skin [113]. In humans, the formation of CPDs in skin exposed to UVA was dependent on the phototype with more CPDs in fair skin [116]. Interestingly, very good correlation was found for each volunteer between the yield of CPDs and the phototype after exposure to UVA radiation.

The use of accurate HPLC assays for the measurement of DNA damage made possible the collection of quantitative data on the different types of UVA-induced lesions. On average, the ratio between the yield of CPDs and that of 8-oxoGua is around 5. An interesting exception are melanocytes where the level of 8-oxoGua, although lower than that of CPDs, is much higher than in keratinocytes [149]. This observation is in line with results showing that UVA-induced oxidative stress plays a key role in the induction of melanoma in pigmented mice while UVB-induced dimers are responsible for melanoma in albino mice [6]. Use of HPLC-MS/MS showed that the distribution of bipyrimidine photoproducts in cells and skin exposed to UVA was quite different from that induced by UVB [39, 40, 116, 149]. Indeed, neither 6-4PPs nor DEWs were detected upon UVA irradiation even at the highest doses. The latter result was in line with immunological measurements [146]. T<>T is by far the predominant lesion and represents approximately 90% of the photoproducts. The remaining dimeric photoproducts are T<>C and C<>T produced in roughly similar amounts. The amount of C<>C is below the detection limit of the assay. However C<>C was detected in a specific sequence by ligation-mediated polymerase chain reaction (LM-PCR) [150].

The UVA-induction of CPDs has been supported by the results of a series of mutagenicity experiments. A general trend is that T-C transitions at TC sites are the most frequent mutational events after exposure to UVB [150–153]. This shows that, although the oxidative properties of UVA play a significant role even in skin [154],

formation of CPDs is a major event in the onset of mutations leading to tumorogenesis [8].

3.2.2 Isolated DNA

Observation of the formation of CPDs in cellular DNA stimulated work on the underlying photochemical mechanism. The first possibility is the involvement of endogenous sensitizers and TTET-mediated formation of CPDs. However, the observation that CPDs were produced in isolated DNA [155–157] in the absence of photosensitizers showed that a direct photochemical reaction is also possible. Differentiation between the two mechanisms could not be based on the distribution of photoproducts since in both cases only CPDs were produced, with an overwhelming contribution of TT CPDs. However, the observation that the chemical yield of CPDs was similar in isolated DNA and in culture mammalian cells [146, 155, 157] strongly suggested that endogenous photosensitizers do not play a major role.

Involvement of a direct photoreaction requires absorption of UVA photons by DNA. Although often neglected, UVA absorption of DNA was actually established for a series of bacterial genomes [158]. This absorption is three orders of magnitude lower than the maximum in the UVC range but still detectable. UVA absorption is not observed for monomeric DNA components such as nucleotides but becomes significant in double-stranded oligonucleotides, showing the role played by electronic interaction along π-stacked bases [157]. Recent data also explain the difference between the distribution of photoproducts in the UVB and UVA ranges. Spectroscopic measurements strongly suggest that the nature of the excited states involved in the two wavelength ranges are different, with a major contribution of charge-transfer state in the UVA range [159], while $^{1}\pi\pi^{*}$ states are more frequent with UVB radiation. This could explain why the ratio between T<>T and C<>T/T<>C is different after exposure to UVA and UVB. In addition, theoretical calculations have shown the 6-4PPs could be produced from a charge transfer state but with an energy barrier not achievable with UVA photons [54]. As discussed above, charge transfer states could play a role in TTET which could explain the strong similarity between the distributions of photoproducts by the two processes.

3.3 Isomerization of Pyrimidine (6-4) Pyrimidone Photoproducts

As described above, the conversion of 6-4PPs into their DEWs (Fig. 5) was mostly studied in model systems in the UVB range. Indeed, 6-4PPs exhibit a maximum of absorption around 320 nm, reflecting the properties of the pyrimidone ring.

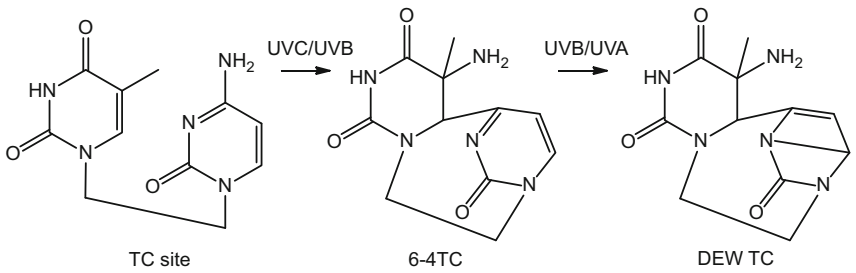

Fig. 5 Photo-induced conversion of 6-4TC into related Dewar valence isomer

However, no DEW is detected in cells or skin exposed to biologically relevant doses of pure UVB [39, 113, 114, 146]. Explanation can be found in the observation that the formation of DEWs in isolated DNA exposed to UVB exhibits a clear quadratic dose response, in agreement with the need for two photons. The formation of DEWs becomes detectable only when the level of damage is approximately a single 6-4PP per 10^4 bases [59], namely far above the amount of DNA damage encountered in living cells. In contrast, DEWs are readily detected when cells are exposed to both UVB and UVA. Under these circumstances, UVB induces the formation of 6-4PPs. UVA is then responsible for photoisomerization since it is efficiently absorbed by 6-4PPs and very poorly by normal bases. Accordingly, DEWs were observed in experiments involving exposure of cultured mammalian cells [39, 146, 160] to simulated sunlight or to sequential exposure to UVB and UVA [114]. DEWs have also been detected in the skin of mice exposed to natural sunlight [161] and in human skin sequentially irradiated with 260 nm and 320 nm radiation [162]. DEWs are also present in bacteria and archaea exposed to UV sources of various spectra [106–108, 110]. Recently, a large fraction of 6-4PPs were also detected as their DEWs in marine microorganisms exposed to natural sunlight [163]. Evidence for the role played by UVA in the formation of DEWs in cellular DNA is that 6-4TT are isomerized in larger yield than 6-4PPs [39, 114, 163], in agreement with the fact that the absorption maximum is 10 nm larger for the former than the latter photoproduct, namely deeper in the UVA range. Altogether, DEWs are likely highly relevant lesions upon exposure of cells to real sunlight.

4 Conclusion and Perspectives

Significant progress has been achieved during the last decade on a better understanding of the photochemical reactions of DNA in isolated cells and human skin because of the development of sensitive and analytical tools such as HPLC-ESI-MS/MS, which is the gold standard method for measuring DNA lesions in general. This has allowed the determination of the repair kinetics of each of the bipyrimidine photoproducts, showing significant differences in the removal rates among CPDs

when the global repair pathway is considered. Another striking finding deals with the elucidation of the mechanism of CPD formation which involves direct UVA excitation and subsequent involvement of singlet excited states with a marked charge transfer characteristic as shown by fluorescence spectroscopy and theoretical studies. The stability of cytosine-containing bipyrimidine photoproducts, particularly C<>C and C<>T in cellular DNA, remains to be established, a critical issue since high mutagenicity of the latter photoproducts is associated with most solar radiation induced skin cancer. Information is expected to be gained on the UVB and UVA mediated formation of 5-methylcytosine bipyrimidine photoproducts in cellular DNA. There is also a strong need for the development of more sensitive methods than the currently available LM-PCR method to map at the nucleotide level the formation of both CPDs and 6-4PPs. It is conceivable that theoretical studies which could be of help to spectroscopic investigations would be able to provide mechanistic explanations of the much lower photosensitivity of cytosine with respect to thymine in relation to the much higher deleterious potential of C<>C and C<>T.

References

1. de Gruijl FR, Rebel H (2008) Early events in UV carcinogenesis – DNA damage, target cells and mutant p53 foci. Photochem Photobiol 84:382–387
2. Narayanan DL, Saladi RN, Fox JL (2010) Ultraviolet radiation and skin cancer. Int J Dermatol 49:978–986
3. Mitchell D, Fernandez A (2012) The photobiology of melanocytes modulates the impact of UVA on sunlight-induced melanoma. Photochem Photobiol Sci 11:69–73
4. Gandini S, Autier P, Boniol M (2012) Reviews on sun exposure and artificial light and melanoma. Prog Biophys Mol Biol 107:362–366
5. Pfeifer GP, Besaratinia A (2012) UV wavelength DNA damage and human non-melanoma and melanoma skin cancer. Photochem Photobiol Sci 11:90–97
6. Noonan F, Zaidi MR, Wolnicka-Glubisz A, Anver MR, Bahn J, Wielgus A, Cadet J, Douki T, Mouret S, Tucker MA, Popratiloff A, Merlino G, De Fabo EC (2012) Nat Commun 3:884
7. Brash DE, Rudolph JA, Simon JA, Lin A, McKenna GJ, Baden HP, Halperin AJ, Pontén J (1991) A role for sunlight in skin cancer: UV-induced p53 mutations in squamous cell carcinoma. Proc Natl Acad Sci U S A 88:10124–11012
8. Sage E, Girard P-M, Francesconi S (2012) Unravelling UVA-induced mutagenesis. Photochem Photobiol Sci 11:74–80
9. Ikehata H, Kumagai J, Ono T, Morita A (2013) Solar-UV-signature mutation prefers TCG to CCG: extrapolative consideration from UVA1-induced mutation spectra in mouse skin. Photochem Photobiol Sci 12:1319–1327
10. Cleaver JE, Crowley E (2002) UV damage, DNA repair and skin carcinogenesis. Front Biosci 7:1024–1043
11. Niedernhofer LJ, Bohr VA, Sander M, Kraemer KH (2011) Xeroderma pigmentosum and other diseases of human premature aging and DNA repair: molecules to patients. Mech Ageing Dev 132:340–347
12. Cadet J, Vigny P (1990) The photochemistry of nucleic acids. In: Morrison H (ed) Bioorganic photochemistry: photochemistry and the nucleic acids, vol 1. Wiley, New York, pp 1–272

13. Cadet J, Anselmino C, Douki T, Voituriez L (1992) Photochemistry of nucleic acids in cells. J Photochem Photobiol B 15:277–298
14. Taylor JS (1994) Unraveling the molecular pathway from sunlight to skin-cancer. Acc Chem Res 27:76–82
15. Ravanat J-L, Douki T, Cadet J (2001) Direct and indirect effects of UV radiation on DNA and its components. J Photochem Photobiol B 63:88–102
16. Cadet J, Sage E, Douki T (2005) Ultraviolet radiation mediated damage to cellular DNA. Mutat Res 571:3–17
17. Desnous C, Guillaume D, Clivio P (2010) Spore photoproduct: a key to bacterial eternal life. Chem Rev 110:1213–1232
18. Heil K, Pearson D, Carell T (2010) Chemical investigation of light induced bipyrimidine damage and repair. Chem Soc Rev 40:4271–4278
19. Cadet J, Mouret S, Ravanat JL, Douki T (2012) Photoinduced damage to cellular DNA: direct and photosensitized reactions. Photochem Photobiol 88:1048–1065
20. Kneuttinger AC, Kashiwazaki G, Prill S, Heil K, Müller M, Carell T (2014) Formation and direct repair of UV-induced DNA pyrimidine lesions. Photochem Photobiol 90:1–14
21. Cadet J, Wagner JR (2013) DNA base damage by reactive oxygen species, oxidizing agents, and UV radiation. Cold Spring Harb Perspect Biol 5:a012559
22. Richa SRP, Häder D-P (2014) Physiological aspects of UV-excitation of DNA. Top Curr Chem. doi:10.1007/128-2014-531
23. Batista LFZ, Kaina B, Meneghini R, Menck CFM (2009) How DNA lesions are turned into powerful killing structures: insights from UV-induced apoptosis. Mutat Res 681:197–208
24. Vink AA, Yarosh DB, Kripke ML (1996) Chromophore for UV-induced immunosuppression: DNA. Photochem Photobiol 63:383–386
25. de Gruijl FR (2008) UV-induced immunosuppression in the balance. Photochem Photobiol 84:2–9
26. Crespo-Hernadez CE, Cohen B, Hare PM, Kohler B (2004) Ultrafast excited-state dynamics in nucleic acids. Chem Rev 104:1977–2020
27. Middleton CT, de la Harpe K, Su C, Law YK, Crespo-Hernandez CE, Kohler B (2009) Annu Rev Phys Chem 60:217–239
28. Markovitsi D, Gustavsson T, Banyasz T (2010) Absorption of UV radiation by DNA: spatial and temporal features. Mutat Res 704:21–28
29. Nielsen LM, Hoffmann SV, Nielsen SB (2013) Electronic coupling between photo-excited stacked bases in DNA and RNA strands with emphasis on the bright states initially populated. Photochem Photobiol Sci 12:1273–1285
30. Changenet-Barret P, Hua Y, Markovitsi D (2014) Electronic excitations in guanine quadruplexes. Top Curr Chem. doi:1007/128_2013_511
31. Schreier WJ, Kubon J, Regner N, Haiser K, Schrader TE, Zinth W, Clivio P, Gilch P (2009) Thymine dimerization in DNA model systems: cyclobutane photolesion is predominantly formed via the singlet channel. J Am Chem Soc 131:5038–5039
32. Improta R (2012) Photophysics and photochemistry of thymine deoxy-dinucleotide in water: a PCM/TD-DFR quantum mechanical study. J Phys Chem B 116:14261–14274
33. Plasser F, Aquino AJA, Lischka H, Nachtigallová D (2014) Electronic excitation processes in single-strand and double-strand DNA: a computational approach. Top Curr Chem. doi:10.1007/128_2013_517
34. Cadet J, Douki T, Ravanat JL, Di Mascio P (2009) Sensitized formation of oxidatively generated damage to cellular DNA by UVA radiation. Photochem Photobiol Sci 8:903–911
35. Epe B (2012) DNA damage spectra induced by photosensitization. Photochem Photobiol Sci 11:98–106
36. Girotti AW (2001) Photosensitized oxidation of membrane lipids: reaction pathways, cytotoxic effects, and cytoprotective mechanisms. J Photochem Photobiol B 63:101–113
37. Pattison DI, Rahmanto AS, Davies MJ (2012) Photo-oxidation of proteins. Photochem Photobiol Sci 11:38–53

38. Douki T, Perdiz D, Grof P, Kulunsics Z, Moustacchi E, Cadet J, Sage E (1999) Oxidation of guanine in cellular DNA by solar UV radiation: biological role. Photochem Photobiol 70:184–190
39. Douki T, Reynaud-Angelin A, Cadet J, Sage E (2003) Bipyrimidine photoproducts rather than oxidative lesions are the main type of DNA damage involved in the genotoxic effect of solar UVA radiation. Biochemistry 42:9221–9226
40. Courdavault S, Baudouin C, Charveron M, Favier A, Cadet J, Douki T (2004) Larger yield of cyclobutane dimers than 8-oxo-7,8-dihydroguanine in the DNA of UV-A irradiated human skin cells. Mutat Res 556:135–142
41. Douki T, Vadesne-Bauer G, Cadet J (2002) Formation of 2'-deoxyuridine hydrates upon exposure of nucleosides to gamma radiation and UVC-irradiation of isolated and cellular DNA. Photochem Photobiol Sci 1:565–569
42. Zhao X, Nadji S, Kao JL, Taylor JS (1996) The structure of d(TpA), the major photoproduct of thymidylyl-(3'5')-deoxyadenosine. Nucleic Acids Res 24:1554–1560
43. Davies RJ, Malone JF, Gan Y, Cardin CJ, Lee MP, Neidle S (2007) High resolution crystal structure of the intramolecular d(TpA) thymine-adenine photoadduct and its mechanistic implications. Nucleic Acids Res 35:1048–1053
44. Asgatay S, Martinez A, Coantic-Castex S, Harakat D, Philippe C, Douki T, Clivio P (2010) UV-induced TA photoproducts: formation and hydrolysis in double-stranded DNA. J Am Chem Soc 132:10260–10261
45. Su DGT, Taylor JSA, Gross ML (2010) A new photoproduct of 5-methylcytosine and adenine characterized by high-performance liquid chromatography and mass spectrometry. Chem Res Toxicol 23:474–479
46. Münzel M, Szeibert C, Glas AF, Globisch D, Carell T (2011) Discovery and synthesis of new UV-induced intrastrand C(4-8)G and G(8-4)C photolesions. J Am Chem Soc 133:5186–5189
47. Cadet J, Douki T, Ravanat J-L (2008) Oxidatively generated damage to the guanine moiety: mechanistic aspects and formation in cells. Acc Chem Res 4:1075–1083
48. Cadet J, Ravanat J-L, TavernaPorro M, Menoni H, Angelov D (2012) Oxidatively generated complex DNA damage: tandem and clustered lesions. Cancer Lett 327:5–15
49. Douki T, Ravanat J-L, Pouget JP, Testard I, Cadet J (2006) Minor contribution of direct ionization to DNA base damage induced by heavy ions. Int J Radiat Biol 82:119–127
50. Madugundu GS, Wagner JR, Cadet J, Kropachev YBH, Geacintov NE, Shafirovich V (2013) Generation of guanine-thymine cross-links in human cells by one-electron oxidation mechanisms. Chem Res Toxicol 26:1031–1033
51. Perrier S, Hau D, Gasparutto D, Cadet J, Favier A, Ravanat J-L (2006) Characterization of lysine-guanine cross-links upon one-electron oxidation of a guanine-containing oligonucleotide in the presence of a trylisine peptide. J Am Chem Soc 128:5703–5710
52. Cadet J, Wagner JR, Shafirovich V, Geacintov NE (2014) One-electron oxidation reactions of purine and pyrimidine bases in cellular DNA. Int J Radiat Biol 90:423–432
53. Beukers R, Berends W (1960) Isolation and identification of the irradiation product of thymine. Biochim Biophys Acta 41:550–551
54. Banyasz A, Douki T, Improta R, Gustavson T, Onidas D, Vayá I, Perron M, Markovitsi D (2012) Electronic excited states responsible for dimer formation upon UV absorption directly by thymine strands: joint experiments and theoretical study. J Am Chem Soc 134:14834–14845
55. Cadet J, Voituriez L, Hruska FE, Kan LS, De Leeuw FAAM, Altona C (1985) Characterization of thymidine ultraviolet photoproducts-cyclobutane dimers and 5,6-dihydrothymidine. Can J Chem 63:2861–2868
56. Branco MR, Ficz G, Reik W (2011) Uncovering the role of 5-hydroxymethylcytosine in the epigenome. Nat Rev Genet 13:7–13
57. Kohli RM, Zhang Y (2013) TET enzymes, TDG and the dynamics of DNA demethylation. Nature 502:472–479

58. Cadet J, Wagner JR (2014) TET oxidation of 5-methylcytosine, 5-hydroxymethylcytosine and 5-formylcytosine. Mutat Res. doi:1016/j.mrgentox.2013.09.001
59. Douki T, Cadet J (1994) Formation of cyclobutane dimers and (6-4) photoproducts upon far-UV photolysis of 5-methylcytosine-containing dinucleoside monophosphates. Biochemistry 33:11942–11950
60. Celewicz L, Mayer M, Shetlar MD (2005) The photochemistry of thymidylyl-(3′-5′)-5-methyl-2′-deoxycytidine in aqueous solution. Photochem Photobiol 81:404–418
61. Li X, Eriksson LA (2005) Influence of C5-methylation of cytosine on the formation of cyclobutane pyrimidine dimer. Chem Phys Lett 401:99–103
62. Cannistraro VJ, Taylor J-S (2009) Acceleration of 5-methylcytosine deamination in cyclobutane dimers by G and its implication for UC-induced C-to-T mutation hotspots. J Mol Biol 392:1145–1157
63. Cannistraro VJ, Taylor J-SA (2010) Methyl CpG binding protein 2 (MeCP2) enhances photodimer formation at methyl-CpG sites but suppresses dimer deamination. Nucleic Acids Res 38:6943–6955
64. Song Q, Cannistraro TJ-S (2011) Rotational position of a 5-methylcytosine-containing cyclobutane pyrimidine dimer in a nucleosome greatly affects its deamination rate. J Biol Chem 286:6329–6335
65. Song Q, Sherrer SM, Suo Z, Taylor J-S (2012) Preparation of site-specific T=^{m}CG cis-syn cyclobutane dimer-containing template and its error-free bypass by yeast and human polymerase η. J Biol Chem 287:8021–8027
66. Garcès F, Dávila CA (1982) Alterations in DNA irradiated with ultraviolet radiation. The formation process of cyclobutylpyrimidine dimers: cross sections, action spectra and quantum yields. Photochem Photobiol 35:9–16
67. Pan Z, Chen J, Schreier WJ, Kohler B, Lewis FD (2012) Thymine dimer photoreversal in purine-containing trinucleotides. J Phys Chem B 116:698–704
68. Sancar A (2000) Enzymatic photoreactivation: 50 years and counting. Mutat Res 451:25–37
69. Brettel K, Byrdin M (2010) Reaction mechanisms of DNA photolyase. Curr Opin Struct Biol 20:693–701
70. Clivio P, Fourrey J-L, Gasche L, Favre A (1991) DNA photodamage mechanistic studies: characterization of a thietane intermediate in a model reaction relevant to "6-4 lesion". J Am Chem Soc 113:5481–5483
71. Labet V, Jorge N, Morell C, Douki T, Grand A, Cadet J, Eriksson LA (2013) UV-induced formation of the thymine-thymine pyrimidone photoproduct – a DFT study of the oxetane intermediate ring opening. Photochem Photophys Sci 12:1509–1516
72. Taylor JS, Lu HF, Kotyk JJ (1990) Quantitative conversion of the (6–4) photoproduct of TpdC to its Dewar valence isomer upon exposure to simulated sunlight. Photochem Photobiol 51:161–167
73. Kan L-S, Voituriez L, Cadet J (1992) The Dewar valence isomer of the (6-4) photoadducts of thymidylyl-(3′-5′)-thymidine monophosphate: formation, alkaline lability and conformational properties. J Photochem Photobiol B 12:339–357
74. Taylor JS, Garett DS, Cohrs MP (1988) Solution-state structure of the Dewar pyrimidinone photoproduct of thymidylyl-(3'-5')-thymidine. Biochemistry 27:7206–7215
75. Haiser K, Fingerhut BP, Heil K, Glas A, Herzog TT, Pilles BM, Schreir ZW, de Vivie-Riedle R, Carell T (2012) Mechanism of UV-induced formation of Dewar lesions in DNA. Angew Chem Int Ed 51:408–411
76. Franklin WA, Lo KM, Haseltine WA (1982) Alkaline lability of fluorescent photoproducts produced in ultraviolet light-irradiated DNA. J Biol Chem 257:13535–13543
77. Donnellan JE, Setlow RB (1965) Thymine photoproducts but not thymine dimers found in ultraviolet-irradiated bacterial spores. Science 149:308–310
78. Varghese AJ (1970) 5-Thyminyl-5,6-dihydrothymine from DNA irradiated with ultraviolet light. Biochem Biophys Res Commun 38:484–490

79. Douki T, Laporte G, Cadet J (2003) Inter-strand photoproducts are produced in high yield within A-DNA exposed to UVC radiation. Nucleic Acids Res 31:3134–3142
80. Chandra T, Silver SC, Zilinskas E, Shepard EM, Broderick WE, Broderick JB (2009) Spore photoproduct lyase catalyzes specific repair of the 5R but not 5S spore photoproduct. J Am Chem Soc 131:2420–2421
81. Moysan A, Viari A, Vigny P, Voituriez L, Cadet J, Moustacchi E, Sage E (1991) Formation of cyclobutane thymine dimers photosensitized by pyridopsoralens: quantitative and qualitative distribution within DNA. Biochemistry 30:7080–7088
82. Shaw AA, Cadet J (1990) Radical combination processes under the direct effects of gamma radiation on thymidine. J Chem Soc Perkin Trans 2:2063–2070
83. Mantel C, Chandor A, Gasparutto D, Douki T, Atta M, Fontecave M, Bayle P-A, Mouesca J-M, Bardet M (2008) Combined NMR and DFT studies for the absolute configuration elucidation of the spore photoproduct, a UV-induced DNA lesion. J Am Chem Soc 130:16978–16984
84. Chandor A, Berteau O, Douki T, Gasparutto D, Sanakis Y, Ollagnier-de-Choudens S, Atta M, Fontecave M (2006) Dinucleotide spore photoproduct, a minimal substrate of the DNA repair spore photoproduct lyase enzyme from *Bacillus subtilis*. J Biol Chem 283:26922–26931
85. Mohr SC, Sokolov NV, He CM, Setlow P (1991) Binding of small acid-soluble spore proteins from Bacillus subtilis changes the conformation of DNA from B to A. Proc Natl Acad Sci U S A 88:77–81
86. Nicholson WL, Setlow B, Setlow P (1991) Ultraviolet irradiation of DNA complexed with alpha/beta-type small, acid-soluble proteins from spores of bacillus or clostridium species makes spore photoproduct but not thymine dimers. Proc Natl Acad Sci U S A 88:8288–8292
87. Douki T, Stelow B, Setlow P (2005) Effects of the binding of alpha/beta-type small, acid-soluble spore proteins on the photochemistry of DNA in spores of Bacillus subtilis and in vitro. Photochem Photobiol 81:163–169
88. Douki T, Setlow B, Setlow P (2005) Photosensitization of DNA by dipicolinic acid, a major component of *Bacillus* species. Photochem Photobiol Sci 4:591–597
89. Varghese AJ (1970) Photochemistry of thymidine in ice. Biochemistry 9:4781–4787
90. Lin G, Li L (2010) Elucidation of spore-photoproduct formation by isotope labeling. Angew Chem Int Ed 49:9926–9929
91. Du Q, Zhao H, Song D, Liu K, Su H (2012) Consecutive reaction mechanism for the formation of spore photoproduct in DNA photolesion. J Phys Chem B 116:11117–11123
92. Douki T, Court M, Cadet J (2000) Electrospray-mass spectrometry characterization and measurement of far-UV-induced thymine photoproducts. J Photochem Photobiol B 54:145–154
93. Douki T, Court M, Sauvaigo S, Odin F, Cadet J (2000) Formation of the main UV-induced thymine dimeric lesions within isolated and cellular DNA as measured by high performance liquid chromatography-tandem mass spectrometry. J Biol Chem 275:11678–11685
94. Douki T (2013) The variety of UV-induced pyrimidine photoproducts in DNA as shown by chromatographic quantification methods. Photochem Photobiol Sci 12:1286–1302
95. Mori T, Nakane M, Hattori T, Ihara M, Nikaido O (1991) Simultaneous establishment of monoclonal antibodies specific for either cyclobutane pyrimidine dimer or (6-4) photoproduct from the same mouse immunized with ultra-violet-irradiated DNA. Photochem Photobiol 54:225–232
96. Mizuno T, Matsunaga T, Ihara M, Nikaido O (1991) Establishment of monoclonal antibody recognizing cyclobutane-type thymine dimer in DNA. A comparative study with 64 M-1 antibody specific for (6-4) photoproducts. Mutat Res 254:175–184
97. Matsunaga T, Hatakeyama Y, Ohta M, Mori T, Nikaido O (1993) Establishment and characterization of a monoclonal antibody recognizing the Dewar isomers of (6-4) photoproducts. Photochem Photobiol 57:934–940
98. Berton TR, Mitchell DL (2012) Quantification of DNA photoproducts in mammalian cell DNA using radioimmunoassay. Methods Mol Biol 920:177–187

99. Kim ST, Malhotra K, Smith CA, Taylor JS, Sancar A (1993) DNA photolyase repairs the trans-syn cyclobutane thymine dimer. Biochemistry 32:7065–7068
100. Matallana-Surget S, Meador JA, Joux F, Douki T (2008) Effect of the GC content of DNA on the distribution of UVB-induced bipyrimidine photoproducts. Photochem Photobiol Sci 7:794–801
101. Nguyen HT, Minton KW (1988) Ultraviolet-induced dimerization of non-adjacent dimerization. A potential mechanism for the targeted -1 frameshift mutation. J Mol Biol 200:681–693
102. Nguyen HT, Minton KW (1989) Extensive photodimerization of non-adjacent pyrimidines. J Mol Biol 210:869–874
103. Su DGT, Kao JL-F, Gross ML, Taylor J-S (2008) Structure determination of an interstrand-type cis-anti cyclobutane dimer produced in high yield by UVB light in an oligodeoxynucleotides at acidic pH. J Am Chem Soc 130:11328–11337
104. Su DGT, Fang H, Gross ML, Taylor J-S (2009) Photocrosslinking of human telomeric G-quadruplex loops by anti cyclobutane thymine dimer formation. Proc Natl Acad Sci U S A 106:12861–12866
105. Smith JE, Lu C, Taylor JS (2014) Effects of sequence and metal ions on UVB-induced anti cyclobutane pyrimidine dimer formation in human telomeric DNA sequences. Nucleic Acids Res 42:5007
106. Moeller R, Douki T, Rettberg P, Reitz G, Cadet J, Nicholson WL, Horneck G (2010) Genomic bipyrimidine nucleotide frequency and microbial reactions to germicidal UV radiation. Arch Microbiol 192:521–529
107. De la Vega UP, Rettberg P, Douki T, Cadet J, Horneck G (2005) Sensitivity to polychromatic UV-radiation of strains of *Deinococcus radiodurans* differing in their DNA repair capacity. Int J Radiat Biol 81:601–611
108. Moeller R, Reitz G, Douki T, Cadet J, Horneck G, Stan-Lotter H (2010) UV photoreactions of the extremely haloalkaliphilic euryarchaeon *Natronomonas pharaonis*. FEMS Microbiol Ecol 73:271–277
109. Matallana-Surget S, Douki T, Cavicchioli R, Joux F (2009) Remarkable resistance to UVB of the marine bacterium *Photobacterium angustum* explained by an unexpected role of photolyase. Photochem Photobiol Sci 8:1313–1320
110. Moeller R, Stackebrandt E, Douki T, Cadet J, Rettberg P, Mollenkopf HJ, Reitz G, Horneck G (2007) DNA bipyrimidine photoproduct repair and transcriptional response of UV-C irradiated *Bacillus subtilis*. Arch Microbiol 188:421–431
111. Albarracin VH, Pathak GP, Douki T, Cadet J, Borsarelli CD, Gärtner W, Farias ME (2012) Extremophilic *Acinetobacter* strains from high-altitude lakes in Argentinean Puna: remarkable UV-B resistance and efficient DNA damage repair. Orig Life Evol Biosph 42:201–221
112. Albarracin VH, Simon J, Pathak GP, Valle L, Douki T, Cadet J, Borsarelli CD, Farias ME, Gärtner W (2014) First characterization of a CPD-class I photolyase from a UV-resistant extremophile isolated from High-Altitude Andean lakes. Photochem Photobiol Sci 13:739–750
113. Mouret S, Baudouin C, Charveron M, Favier A, Cadet J, Douki T (2006) Cyclobutane pyrimidine dimers are predominant DNA lesions in whole human skin exposed to UVA radiation. Proc Natl Acad Sci U S A 103:13765–13770
114. Courdavault S, Baudouin C, Charveron M, Canguilhem B, Favier A, Cadet J, Douki T (2005) Repair of the three main types of bipyrimidine DNA photoproducts in human keratinocytes exposed to UVB and UVA radiations. DNA Repair (Amst) 4:836–844
115. Mouret S, Charveron M, Favier A, Cadet J, Douki T (2008) Differential repair of UVB-induced cyclobutane pyrimidine dimers in cultured human skin cells and whole human skin. DNA Repair (Amst) 7:704–712
116. Mouret S, Leccia M-T, Bourrain J-L, Douki T, Beani JC (2011) Individual photosensitivity of human skin and UVA-induced pyrimidine dimers in DNA. J Invest Dermatol 131:1539–1546

117. Mouret S, Bogdanowicz HMJ, Castex-Rizzi N, Cadet J, Favier A, Douki T (2011) Assessment of the photoprotection properties of sunscreens by chromatographic measurement of DNA damage in skin explants. Photochem Photobiol 87:109–116
118. Schuch AP, Lago JC, Tagura T, Menck CF (2012) DNA dosimetry assessment for sunscreen genotoxic photoprotection. PLoS One 7:e40344
119. Ravanat J-L, Di Mascio P, Martinez GR, Medeiros MH, Cadet J (2000) Singlet oxygen induces oxidation of cellular DNA. J Biol Chem 275:40601–40604
120. Cadet J, Douki T, Ravanat J-L (2010) Oxidatively generated base damage to cellular DNA. Free Radic Biol Med 49:9–21
121. Dedon PC (2008) The toxicology of 2-deoxyribose oxidation in DNA. Chem Res Toxicol 21:206–219
122. Charlier M, Hélène C (1967) Photosensitized dimerization of orotic acid in aqueous solution. Photochem Photobiol 6:501–504
123. Lamola AA (1970) Triplet photosensitization and the photobiology of thymine dimers in DNA. Pure Appl Chem 24:599–610
124. Ben-Ishai R, Ben-Hur E, Hornfeld Y (1968) Photosensitized dimerization of thymine and cytosine in DNA. Isr J Chem 6:769–775
125. Gut IG, Wood PD, Redmond RW (1996) Interaction of triplet photosensitizers with nucleotides and DNA in aqueous solution at room temperature. J Am Chem Soc 118:2366–2373
126. Wood PD, Redmond RW (1996) Triplet state interactions between nucleic acid bases in solution at room temperature: intramolecular energy and electron transfer. J Am Chem Soc 118:4256–4263
127. Marguery MC, Chouini-Lalanne N, Ader JC, Paillous N (1998) Comparison of the DNA damage photoinduced by fenofibrate and ketoprofen, two phototoxic drugs of parent structure. Photochem Photobiol 68:679–684
128. Lhiaubet V, Paillous N, Chouini-Lalanne N (2001) Comparison of DNA damage photoinduced by ketoprofen, fenofibric acid and benzophenone via electron and energy transfer. Photochem Photobiol 74:670–678
129. Cuquerella MC, Lhiaubet-Vallet V, Bosca F, Miranda MA (2011) Photosensitised pyrimidine dimerisation in DNA. Chem Sci 2:1219–1232
130. Cuquerella MC, Lhiiaubet-Vallet V, Cadet J, Miranda MA (2012) Benzophenone photosensitized DNA damage. Acc Chem Res 45:1558–1570
131. Trzcionka J, Lhiaubet-Vallet V, Chouini-Lalanne N (2004) DNA photosensitization by indoprofen – is DNA damage photoinduced by indoprofen or by its photoproducts? Photochem Photobiol Sci 3:226–230
132. Traynor NJ, Gibbs NK (1999) The phototumorigenic fluoroquinolone lomefloxacin photosensitizes pyrimidine dimer formation in human keratinocytes in vitro. Photochem Photobiol 70:957–959
133. Sauvaigo S, Douki T, Odin F, Caillat S, Ravanat J-L, Cadet J (2001) Analysis of fluoroquinolone-mediated photosensitization of 2′-deoxyguanosine, calf thymus and cellular DNA: determination of type-I, type-II and triplet-triplet energy transfer mechanism contribution. Photochem Photobiol 13:230–237
134. Bosca F, Lhiaubet-Vallet V, Cuquerella MC, Castell JV, Miranda MA (2006) The triplet energy of thymine in DNA. J Am Chem Soc 128:6318–6319
135. Lhiaubet-Vallet V, Cuquerella MC, Castell JV, Bosca F, Miranda MA (2007) Triplet excited fluoroquinolones as mediators for thymine cyclobutane dimer formation in DNA. J Phys Chem B 111:7409–7414
136. Varghese AJ (1972) Photochemistry of nucleic acids and their constituents. In: Giese AC (ed) Photophysiology, vol 7. Academic, New York, pp 207–274
137. Patrick MH, Snow JM (1977) Studies on thymine-derived UV photoproducts in DNA-I. A comparative analysis of damage caused by 254 nm irradiation and triplet-state photosensitization. Photochem Photobiol 25:373–384

138. Douki T, Bérard I, Wack A, Andrä S (2014) Contribution of cytosine-containing cyclobutane dimers to DNA damage produced by photosensitized triplet-triplet energy transfer. Chemistry 20:5787–5794
139. Lamola AA, Gueron M, Yamane T, Eisinger J, Shulman RG (1967) Triplet state of DNA. J Chem Phys 47:2210–2217
140. Zuo ZH, Yao SD, Luo JA, Wang WF, Zhang JS, Lin NY (1992) Laser photolysis of cytosine, cytidine and dCMP in aqueous solution. J Photochem Photobiol B 15:215–222
141. Abouaf R, Pommier J, Dunet H, Quan P, Nam PC, Nguyen MT (2004) The triplet state of cytosine and its derivatives: electron impact and quantum chemical study. J Chem Phys 121:11668–11674
142. Tyrrell RM (1973) Induction of pyrimidine dimers in bacterial DNA by 365 nm radiation. Photochem Photobiol 17:69–73
143. Freeman SE, Ryan SL (1990) Wavelength dependence for UV-induced pyrimidine dimer formation in DNA of human peripheral blood lymphocytes. Mutat Res 235:181–186
144. Kielbassa C, Roza L, Epe B (1997) Wavelength dependence of oxidative DNA damage induced by UV and visible light. Carcinogenesis 18:811–816
145. Kvam E, Tyrrell RM (1997) Induction of oxidative DNA base damage in human skin cells by UV and near visible radiation. Carcinogenesis 18:2379–2384
146. Perdiz D, Gróf P, Mezzina M, Nikaido O, Moustacchi E, Sage E (2000) Distribution and repair of bipyrimidine photoproducts in solar UV-irradiated mammalian cells: possible role of Dewar photoproducts in solar mutagenesis. J Biol Chem 275:26732–26742
147. Freeman SE, Hacham H, Gange RW, Maytum DJ, Sutherland JC, Sutherland BM (1989) Wavelength dependence of pyrimidine dimer formation in DNA of human skin irradiated in situ with ultraviolet light. Proc Natl Acad Sci U S A 86:5605–5609
148. Young AR, Potten CS, Nikaido O, Parsons PG, Boenders J, Ramsden JM, Chadmick CA (1998) Human melanocytes and keratinocytes exposed to UVB or UVA in vivo show comparable levels of thymine dimers. J Invest Dermatol 111:936–940
149. Mouret S, Forestier A, Douki T (2012) The specificity of UVA-induced DNA damage in human melanocytes. Photochem Photobiol Sci 11:155–162
150. Rochette PJ, Therrien J-P, Drouin R, Perdiz D, Bastien N, Drobetsky EA, Sage E (2003) UVA-induced cyclobutane pyrimidine dimers form predominantly at thymine-thymine dipyrimidines and correlate with the mutation spectrum in rodent cells. Nucleic Acids Res 31:2786–2794
151. Kappes UP, Luo D, Potter M, Schulmeister K, Rünger TM (2006) Short- and long-wave light (UVB and UVA) induce similar mutations in human skin cells. J Invest Dermatol 126:667–675
152. Rünger TM (2008) C -> T transition mutations are not solely UVB-signature mutations, because they are also generated by UVA. J Invest Dermatol 128:2138–2140
153. Ikehata H, Kawai K, Komura J, Sakatsume K, Wang L, Imai M, Higashi S, Nikaido O, Yamamoto K, Hieda K, Watanabe M, Kasai H, Ono T (2008) UVA1 genotoxicity is mediated not by oxidative damage but by cyclobutane pyrimidine dimers in normal mouse skin. J Invest Dermatol 128:2289–2296
154. Agar NS, Halliday GM, Barnetson ESC, Ananthaswamy HN, Wheeler M, Jones AM (2004) Proc Natl Acad Sci U S A 101:4954–4959
155. Kuluncsics Z, Perdriz D, Brulay E, Muel B, Sage E (1999) Wavelength dependence of ultraviolet-induced DNA damage distribution: involvement of direct or indirect mechanisms and possible artefacts. J Photochem Photobiol B 49:71–80
156. Jiang Y, Rabbi M, Kim M, Ke CH, Lee W, Clark RL, Mieczkowski PA, Marszalek PE (2009) UVA generates pyrimidine dimers in DNA directly. Biophys J 96:1151–1158
157. Mouret S, Philippe C, Gracia-Chantegrel J, Banyasz A, Karpati S, Markovitsi D, Douki T (2010) UVA-induced cyclobutane pyrimidine dimers in DNA: a direct photochemical mechanism? Org Biomol Chem 8:1706–1711

158. Sutherland JC, Griffin KP (1981) Absorption spectrum of DNA for wavelengths greater than 300 nm. Radiat Res 86:399–409
159. Banyasz A, Vaya I, Changenet-Barret P, Gustavsson T, Douki T, Markovitsi D (2011) Base pairing enhances fluorescence and favors cyclobutane dimer formation induced upon absorption of UVA radiation by DNA. J Am Chem Soc 133:5163–5165
160. Clingen PH, Arlett CF, Roza L, Mori T, Nikaido O, Green MHL (1995) Induction of cyclobutane pyrimidine dimers, pyrimidine(6-4)pyrimidone photoproducts, and Dewar valence isomers by natural sunlight in normal human mononuclear cells. Cancer Res 55:2245–2248
161. Qin XS, Zhang SM, Zarkovic M, Nakatsuru Y, Shimizu S, Yamazaki Y, Oda H, Nikaido O, Ishikawa T (1996) Detection of ultraviolet photoproducts in mouse skin exposed to natural sunlight. Jpn J Cancer Res 87:685–690
162. Chadwick CA, Potten CS, Nikaido O, Matsunaga T, Proby C, Young AR (1995) The detection of cyclobutane thymine dimers, (6-4) photolesions and the Dewar photoisomers in sections of UV-irradiated human skin using specific antibodies, and the demonstration of depth penetration effects. J Photochem Photobiol B 28:163–170
163. Meador JA, Baldwin AJ, Pakulski JD, Jeffrey WH, Mitchell DL, Douki T (2014) The significance of the Dewar valence photoisomer as an ultraviolet radiation induced DNA photoproduct in marine microbial communities, Environ Microbiol 16:1808–1820

Index